DESIGN OF CONTROLLED RELEASE FERTILIZERS ON THE BASE OF POLYMERIC, NANOCLAYS AND NANOCOMPOSITE EXCIPIENTS

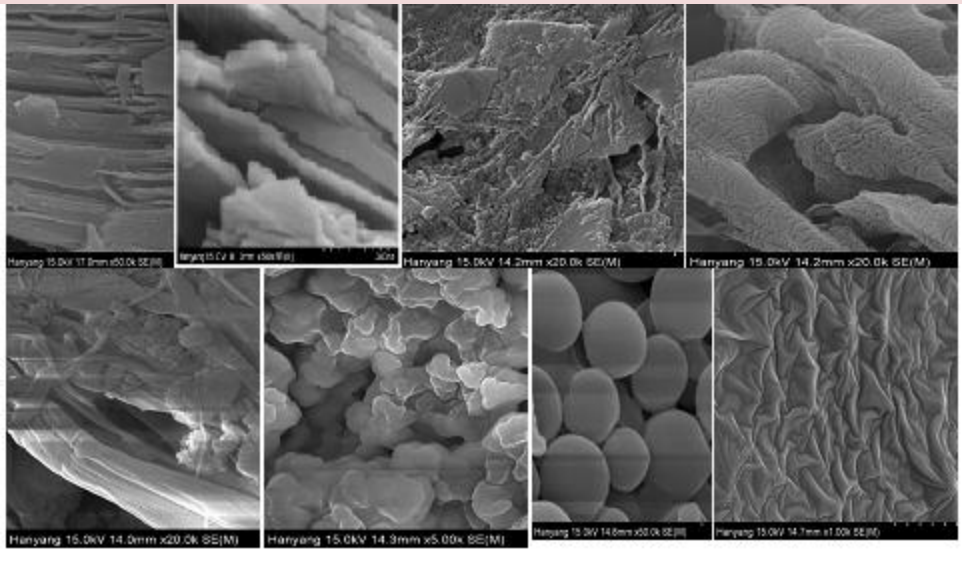

Sempeho Ibahati Siafu

A Dissertation Submitted in Partial Fulfilment of the Requirements for the Degree of Doctor of Philosophy in Materials Sciences and Engineering of the Nelson Mandela African Institution of Science and Technology.

April, 2016

DESIGN OF CONTROLLED RELEASE FERTILIZERS ON THE BASE OF POLYMERIC, NANOCLAYS AND NANOCOMPOSITE EXCIPIENTS

Sempeho Ibahati Siafu

A Dissertation Submitted in Partial Fulfilment of the Requirements for the Degree of Doctor of Philosophy in Materials Sciences and Engineering of the Nelson Mandela African Institution of Science and Technology.

Arusha, Tanzania.

April, 2016

ABSTRACT

It was hypothesised that agronomically suitable controlled release fertilizers (CRFs) can be prepared using synthetic and/or natural biopolymers and polymer-clay nanocomposite excipients. Literature has focused almost exclusively on the urea-CRFs basing on intercalations and/or encapsulations leaving behind a question of the synergy between them which this study endeavoured to answer. Thus, experiments were performed using polyacrylamide (synthetic polymer), kaolinite (layered phyllosilicate), chitosan and gum arabic (natural biopolymers) plus carbonatite volcanic ashes to synthesise and adva

nce knowledge regarding our understanding of preparations of urea CRFs under materials engineering perspectives. The findings revealed the following: (i) application of nanotechnology/materials engineering in agricultural-CRFs synthesis is possible; (ii) physico-chemical properties including, particle sizes, shrinkage, porosity, water-absorption, density and compressive strength exhibited by Pugu kaolinite makes it suitable for urea intercalations; (iii) kaolinite face centred cubic (FCC) Bravais crystal lattices remained unaffected following urea intercalations; (iv) wet-beneficiation effectively eliminated 39.58-0.36% kaolinite impurities; (v) the order of kaolinite intercalation compounds sized 92.5-14.6 nm was: urea intercalated-kaolinite via methanol-dimethysulfoxide (DMSO) route (91.10%), DMSO intercalated-kaolinite (89.20%), methanol intercalated-kaolinite (87.4%); urea intercalated-kaolinite via ferrous-oligomeric route (76.83%), cationic ferrous-oligomeric intercalated-kaolinite (70.41%), hydroxyaluminum-oligomeric intercalated-kaolinite (51.20%), hydroxyaluminum-oligomeric reintercalated-kaolinite (38.40%), naturally oligomerized-Fe^{3+} intercalated-kaolinite (37.53%), urea intercalated-kaolinite via hydroxyaluminum route (32.40%), coarcevated urea-kaolinite nanocomposite (15.30%) and calcined DMSO intercalated-kaolinite (7.0%). Morphological diversity were: overlapping euhedral pseudohexagonal platelets, irregular booklets, vermiform, dispersed euhedral pseudohexagonal platelets, dispersed euhedral pseudohexagonal platelets coexisting with blocky-vermicular booklets, brain-from agglomerations, roundish particulate-mart, stacked vermiform, pustulated forms and self-assembled curled glomeruli-like morphologies. Biocementation produced reinforced urea-ash nanocomposites with nanoropes and nano anvil-hammer structures exhibiting antagonistic atomic/weight percentages of urea'-N

relative to other components detected with EDX. Chitosan-acrylamide co-encapsulation urea-CRF showed crystallinity indices of 50.9-72.1% with-without silicone doping; urea'-N successfully leached from the polymeric excipients within 90 days of diurnal exposure. Wrinkled Nanodunes and Nanoballs 3D-network were observed. Thermo-degradation of the excipients occurred at 48-800 °C; molecular vibrations occurred at 399.42-3998.41 cm^{-1}. Elemental analysis revealed the presence of urea'-N in the produced CRFs. Release profiles showed that 100% of urea can be released in 97 hours from urea-kaolinite nanocomposite while 87% can be released in 150 hours from the encapsulated nanocomposite.

Keywords: Intercalation, Encapsulation, Nanocomposite, Excipient, Coarcevation, Biocementation, Release, Control release fertilizers (CRFs)

DECLARATION

I, **Sempeho Ibahati Siafu** do hereby declare to the Senate of Nelson Mandela African Institution of Science and Technology that this dissertation is my own original work and that it has neither been submitted nor being concurrently submitted for degree award in any other institution.

_____	_____
Name and signature of candidate	**Date**

The above declaration is confirmed

_____	_____
Name and signature of supervisor 1	**Date**
_____	_____
Name and signature of supervisor 2	**Date**
_____	_____
Name and signature of supervisor 3	**Date**

COPYRIGHT

CERTIFICATION

The undersigned certify that they have read and hereby recommend for acceptance by the Nelson Mandela African Institute of Science and Technology a dissertation entitled*: Design of Controlled Release Fertilizers on the Base of Polymeric, Nanoclays and Nanocomposite Excipients*, in fulfillment of the requirements for the degree of Doctor of Philosophy in Materials Sciences and Engineering of the Nelson Mandela African Institution of Science and Technology.

……

Dr. Askwar Hilonga

(**Supervisor**)

Date: ----------

……

Prof. Alexander Pogrebnoi

(**Supervisor**)

Date: ----------

……

Dr. Egid Mubofu

(**Supervisor**)

Date: ----------

ACKNOWLEDGEMENT

Prima facie, I'm grateful to the almighty God and my Lord Jesus Christ for the good health and well being that were necessary to complete this study. Of paramount significance, I would like to express my sincere gratitude to my supervisors, Dr. Askwar Hilonga, Prof. Alexander Pogrebnoi, and Dr. Egid Mubofu for their continuous support in my PhD study both for inspiring me and for their patience, motivation, enthusiasm and colossal knowledge. Actually, their guidance helped me in all time of research and dissertation writing. I could not have imagined having better supervisors and mentors like these ones during my PhD study.

Besides, I would like to thank my co-supervisor and mentor Prof. Hee Taik Kim from Hanyang University (South Korea) for his gentle mentorship in the lab and for providing me with all the necessary facilities needed for lab work along with hosting my research stay at the Chemical Engineering Dept-Hanyang University. I also place my record and sincere thanks to Dr. Godlisten Shao and Dr. Yusufu Jande for their encouragement, insightful comments and hard questions during my lab work at Hanyang; in fact, Dr. Godlisten's benevolence and his unique mentoring attributes were of high help in taking me step by step during the experimentation and analysis phase of my research. Heartfelt thanks should as well go to Prof. Robert Szilagy from the University of Pannonia, Hungary and Engineer Roth Gergo from the Muleengine (Hungary) for their kind assistance in the simulation of the intercalation process employed in this study.

Similarly, I would like to thank Sister Su Yeon Kim (Hanyang University) for her dedicated assistance in the lab as well as Mr. Ilomo, Pius, and Norbert (Chemistry Dept. UDSM) for their dedicated support in Thermogravimetry, Molecular vibrational and release studies. Also, I would like to thank Mr. Bomani (Chief Chemist-SEAMIC), Mzee Mmole (Chemical processing manager-SEAMIC) and his technician Mr. Dachi Mohamed who were good friends and provided me with technical expertise. They were always willing to help and give their best advice during technical difficulties whilst doing my preliminary lab work and data analysis. Likewise, I hereby air out my thanks to Mr. Kishila Siyatoi (guide at Oldonyo Lengai), Lashipa Sadila (Ward executive officer, Engaresero, Punyiny ward), Mr. Ngoseki Maimura (Engaresero Lodge) and Lanjo Wakenyi (CBO officer-Engaresero) for their hospitality and care during sampling at Oldonyo Lengai Volcanic Mountain. I also highly value the support given me by Mr. Sungwira

together with the councillor of Kisarawe ward during sampling of kaolin in the Kazimzumbwi forest.

Furthermore, I wish to thank my spiritual leaders, Rev. Dr. Huruma Nkone, Apostle Trice Shumbusho, Pastor P. Sule and Rev. Bishop John Shumbusho along with my lovely brother in Christ Dr. Eugene Megni Agbicodo and my parents Mzee Ibahati Sempeho Siafu and Rose Elias Shenkhome for their prayers, encouragement and their best wishes. Similar appreciations should go to Prof. Esther Lugwisha (Chem. Dept. UDSM) and Dr. Leornard Akwilapo (Deputy permanent secretary in the ministry of education, science and technology, Tanzania) whose mentoring and creative far sight thinking during my M.Sc. research paved a way for the inception of the idea through which this study was established.

Chauvinistically, I would like to thanks my NM-AIST classmates: Barnes Mphande, Stanley Ferdinand, Rene Costa, Hashimu Hamisi, Heavy Njau, Moyo Moses, Asson Malisa, Isack Onoka and Erick Mutegoa in conjunction with my Hanyang Research fellows: Hye-In Kim, Sung Jeong Jeon, Sung-So Park, Hyo Ryoung Lim, Mohammad Akram, Hyungsub Kim, Keeryung Park, Akiyama Hiroyuki, Muhammad Salman, and Nadir Abbas as well as my friends, Bahiru Bewket, Gelson Jorge, Dami Tamica and Ah Reum Ko for their visionary critiques, for the stimulating discussions, for the sleepless nights we were working together as a team and for all the fun we have had in our being together as colleagues. I really remember the love we shared.

On top of that, I again place my record and my sincere gratitude to Prof. K. Njau (Dean, School of MEWES-NMAIST) for supporting my project and his leadership attributes, Prof. Tatiana Pogrebnaya for her careful endeavours in shaping my research and Prof. Eugene Park (HoD, MESE-NMAIST) whom I'm indebted for his insightful comments and guidance from the early stages of my studentship until the point when he allocated the best advisors who mentored my research. I also owe the entire NM-AIST community, Hanyang University and UDSM faculty for facilitating my research work, finances, expertise and sincere-valuable guidance through this venture. Indeed, I will not forget to kindly express my heartfelt thanks to my financial supporters, NM-AIST under Prof. Burton Mwamila, COSTECH, Korean government, and Prof. Hee Taik Kim from the dept. of Chemical Engineering-Hanyang University for providing me with an excellent atmosphere for conducting my research.

Finally but prime in significance, I would like to thank my dear wife, Miss Niconia Amos Bura who was always there cheering me up and stood by me through the good times and bad especially when my job was terminated owing to my decision to go for studies; despite all the frustrations and difficulties I went through she exhibited the attributes of a good wife and the best friend in my life. High appreciations to my son Joshua and my daughters Grace and Tricerosé for their understanding when I was busy with my research work.

May the Lord God richly bless you beloved. Glory is to God in Christ Jesus.

Shalom shalom.

DEDICATION

To My lovely family

Niconia Amos Bura, Joshua, Grace and Tricerosé

And

To my beloved parents

Mzee Ibahati Sempeho and Bi Rose Shenkhome

TABLE OF CONTENTS

LIST OF TABLES

Table **Page**

LIST OF FIGURES

Figure **Page**

LIST OF PLATES

Plate **Page**

ILLUSTRATIONS and CHARTS

LIST OF APPENDICES

LIST OF ABBREVIATIONS AND SYMBOLS

AA….acrylic acid

AIBN… azobisisobutryronitrile

Am.…acrylamide

APS.…ammonium persulphate

ATR…. Attenuated total reflection

CCFs.…Conventional Chemical Fertilizers

CDU….Crotonylidene Diurea

CEN….European Standardization Committee

CFs…… conventional fertilizers

CH.....Chitosan solution (10%)

CRFs….Controlled release fertilizers

CRSs……..Controlled release systems

D.I…Deionised water

DAP…… Di ammonium phosphate

DENOM….Denominator

DMSO....Dimethyl sulfoxide intercalant

DSs….delivery systems

DTG…. Derivative Thermogravimetric

EA_{rel} ….energy of activation of the release,

EEFs…..Enhanced Efficiency Fertilizers

FCC…. Face Centred Cubic Unit Cell

FKPC....KPC fired at 850 °C

FKPPDMSO.... KPDMSO fired at 850 °C

FTIR.…Fourier transform infrared spectroscopy

FUE….Fertilizer use efficiency

FWHM…Full width at half maximum

Fy....KPF synthesized using HK_3 as precursor

GA...Glutaldehyde solution (10%)

GHG….Greenhouse gases

HK_3.... KHP treated kaolinite

hkl….integers denoting the Miller indices form a notation system in crystallography for planes in crystal (Bravais) lattices

HPMC…..Hydroxypropylmethylcellulose

IBDU…. isobutylidene-diurea

KHP....$KHC_8H_4O_4$ acid

KPC.... Hydroxyaluminum intercalated kaolinite

KPC-400....KPC calcined at 400 °C

KPCU... Urea intercalated kaolinite via KPC intermediate intercalation step

KPDM....Methanol intercalated kaolinite via KPDMSO intermediate intercalation step

KPDMSO....DMSO intercalated kaolinite

KPDMSO-400.... KPDMSO calcined at 400 °C

KPDMU....Urea intercalated kaolinite via KPDMSO-KPDM intermediate intercalation step

KPDMUG....Gum *arabic* encapsulated KPDMU

KPF....Kaolinite intercalated with cationic ferrous oligomers

KPFU.... Urea intercalated kaolinite via KPF intermediate intercalation step

KU.... Urea intercalated kaolinite without passing through intermediate intercalation steps

LOI….Loss on ignition

MAP….Mono ammonium phosphate

MBA….N,N-methylene bisacrylamide

MDU……Methylene diurea

MPF…..Minjingu phosphatic fertilizer

NaKP....NaCl treated kaolinite

NM-AIST….Nelson Mandela African Institution of Science and Technology

NUE….Nutrients use efficiency

NUMER…Numerator

PAPR…..partially acidulated phosphate rocks

PSCU….polymer or sulphur-coated urea granules

Q_1....GA-CH Coarcervated KPFU

QRFs……quick-release fertilizers

RBF…Round bottomed flask

RLCF…….Reacted Layer Coated Fertilizer

RT….Room temperature

SCU…. sulphur-coated urea

SEAMIC…. Southern and East African Mineral Centre

SEM.… scanning electron microscope

SHMP….Sodium hexametaphosphate

SRFs….Slow release fertilizers

TG…. Thermogravimetry

TVA…..Tennessee valley authority

UDSM….University of Dar es Salaam

UF….Urea-Formaldehyde

U-K…Urea-kaolinite

UT.…Urea-Triazone

XRD….X-ray powder diffraction

XRF….X-ray fluorescence

YYY....Ferrous contaminated kaolinite

ZP….zeta potential

CHAPTER ONE

Introduction

This chapter describes the general introduction of the study. It mainly focuses on the background information of the study, the statement of research problem, justification of the study, hypothesis, and scope of the study along with the organization of the study and the significance of the proposed study.

1.1 Background Information

Controlled release fertilizers (CRFs) or Slow release fertilizers (SRFs) are fertilizer granules intercalated within excipients to control nutrients release and improve nutrient supply to crops thereby minimizing environmental, ecological and health hazards (ukessays.com, 2013b). Generally, CRFs exhibit superior features over traditional forms, such as decreased rate of nutrient losses from the soil by rain or irrigation water, sustained supply of nutrition for a prolonged time, increased fertilizer use efficiency (FUE), reduced frequency of application, minimized potential negative effects associated with over dosage and reduced toxicity (M. Liu, Liang, Zhan, Liu, & Niu, 2007).

Urea is the most widely used nitrogen fertilizers because of its high nitrogen (N) content (46%) and comparatively low cost of production. Nonetheless, due to surface runoff, leaching and vaporization, the utilization efficiency or plant uptake of urea is generally below 50% (M. Liu, et al., 2007). Actually, urea is associated with up to 60 to 70% loss of the nitrogen being applied and contributes to greenhouse gases (GHG) emissions and water pollution (Alexandre Meybeck & Vincent Gitz, 2012). In fact, adverse effects during seed germination, seedling growth, and early plant growth in soil have been attributed to urea itself, to biuret and other impurities in urea fertilizers, and to products formed by hydrolysis or other transformations of urea in the soil (Bremner & Krogmeier, 1988; STEPHEN & WAID, 1964). These adverse effects could be reduced by amending urea fertilizers with small amounts of a urease inhibitor (Bremner & Krogmeier, 1988), or by encapsulation with polymers and nanoclays (Shaviv, 2001).

In effect, CRFs usage is an advanced way to supply crop's nutrients (cf. conventional ways) due to gradual pattern of nutrient release, hence improves fertilizer use efficiency (FUE) (Subbarao, Kartheek, & Sirisha, 2013). Essentially, CRFs contain a plant nutrient in a form, which after application delays its accessibility for plant uptake considerably longer period than a common fertilizer. This is gotten by coating fertilizer with sulphur, nanoclays or semipermeable polymeric material (Association, 2000). Control over the release pattern depends on the thickness of the coatings within the formulation (England, Camberato, & Lopez). The fact that crops need for nutrients in acidic soil is different from that in alkaline conditions; researchers have recently attempted to design stimuli-responsive release coatings for encapsulating fertilizer according to different acid and basic environments (Ma et al., 2013).The proposed study aims at designing agronomically apposite urea based CRFs utilising synthetic polymers, natural gum exudates and nanoclays.

1.2 Research problem and justification of study

Despite being the most widely used nitrogenous fertilizer by virtue of its high nitrogen content (46%) and comparatively low cost of production, urea is associated with up to 60 to 70% loss of the nitrogen being applied owing to ammonia produced through hydrolysis of urea by soil urease ($NH_2CONH_2 + H_2O \rightarrow 2NH_3 + CO_2$). Fundamentally, due to surface runoff, leaching and vaporization, the utilization efficiency or plant uptake of urea is generally below 50% thereby escalating fertilization expenditure per season and reduce crop productivity. Thus, there is a need to amend conventional urea fertilizer with nanocomposite excipients to synthesize urea based CRFs so as to improve its utilization efficiency (FUE) by plants to more than 50% and minimize the losses thereby reducing repeated fertilization expenditure per season and maximize crop yields.

1.3 Objectives

1.3.1 General objective

The general objective of this work was to design CRF formulations using polymeric, nanoclays and nanocomposite excipients.

1.3.2 Specific objectives

i. To prepare nanocomposite excipients using polymers and nanoclays
ii. To intercalate urea into the nanocomposite excipient materials
iii. To characterize the CRF formulations basing on the release profiles, and physicochemical properties
iv. To evaluate the release profiles from CRFs' release

1.4 Hypotheses/Research questions

Agronomically suitable CRFs can be prepared using synthetic polymers, natural polymers and polymer-clay nanocomposite excipients.

1.5 Scope of the Study

This study was delimited on the preparation of nanocomposite excipients through intercalation, encapsulation and co-polymerization/co-encapsulation, release studies and the characterization of urea based CRF formulations basing on the release profiles, and physicochemical properties.

1.6 Organization of the Study

This dissertation is organized into nine chapters. Chapter one presents the introductory information about the study; a summary is given concerning the background of the study, problem identified needing solution, the rationale of the study, objectives, hypothesis and the reasons as to why this study was worth doing.

Chapter two focuses on the detailed review of literature on the subject of CRF formulations. The ABC's of CRFs classifications, their preparation methods, the concept of release and its mechanism, models useful for predicting nutrient release, description of the release failure concept, the properties of CRFs release and biodegrability of the excipient molecules as well as the compositions of CRFs formulations along with the history behind CRF formulations and polymer-clay superabsorbent composites were given. The last two sections in this chapter were added after the publication process for the purpose of enriching this dissertation after writing new papers related to volcanic ashes as well as the need for narrating the historical background

of CRFs which this study seeks to advance; so these sections do not appear in the published paper appearing as footnotes in the first page of this chapter.

Chapter three focuses on the preliminary lab work carried out to establish the suitability of Pugu kaolin for advanced applications with the aim of exploring the inherent mechanical and physico-chemical characteristics of the raw materials to be used for CRFs designing. The properties such as grain size distribution, drying-firing patterns, shrinkage behaviours upon wetting and thawing, porosity, water absorption, bulk density and compressive strength were investigated.

Chapter four focuses on the urea-kaolinite nanocomposite excipients designed to test the release properties of urea fertilizer from the gum arabic encapsulated kaolinite-urea intercalation compounds. The properties including the effect of beneficiation on the particle distributions, kaolinite mineralogy and chemical composition, intercalation order and Scherrer' particle analysis along with the vibrational analysis, thermo cracking and release profiles were investigated.

Chapter five focuses on the effect of coupling two intercalants through calcination as a bridging intermediate phase on the dynamics of urea-kaolinite nanocomposites excipients. Along with the properties such as raw analysis, X-ray indexing and particle analysis, Thermogravimetry and infrared absorption measurements which were executed, more efforts were also put to scrutinize the SEM-EDX behaviours and morphological diversity of the due to unique structural patterns observed in the synthesized nanocomposite excipients.

Chapter six focuses on the comparative study on the laboratory synthesized cationic ferrous oligomers vis-à-vis naturally oligomerized ferrous cations basing on the observations made during the preliminary study (Chapter 3) pertaining to the X-ray diffraction patterns that, there was a natural induced intercalation reactions in ferrous contaminated kaolins. The properties including contrasting characteristic of the beneficiated in relation to intercalated ones, whole rock analysis, oriented clay analysis, intercalation studies and the thermo-kinetic behaviours were investigated.

Chapter seven focuses on the investigation of SEM and EDX related properties of the reinforced nanocomposite materials prepared using urea and carbonatite volcanic ashes from Oldoinyo

Lengai active volcanic mountain. The elements of the occurrence of natural urea based Biocementation process were also studied.

Chapter eight focuses on the evaluation of outcomes of using silicone oil as dopant on the properties of urea based CRFs excipients designed via co-encapsulation of *in situ* polymerized chitosan biopolymer and synthetic acrylamide polymer. In that way, the properties investigated were limited to molecular vibration, particle analysis, X-ray diffractions as well as the atomic and weight percentages of elemental compositions.

Chapter nine focuses on the personal reflection on the empirical findings. This section contains immense knowledge, new concept and some unique observations made besides the existing literature stand points. Preferentially, this chapter contains thematic core/yolk of the presented study since the synergy between findings and theories along with policies have been detailed totter with a well drawn conclusion and thoughts for the future studies proposed to be done in order to deepen our understanding and knowledge of the urea based CRFs.

Finally, preamble pages containing the cover page, title page, abstract, author's declaration and copyright information, certification, acknowledgement, dedication, table of contents, list of figures, plates, illustrations, appendices, list of abbreviations and symbols. Also, there are postscript pages/ addendum containing list of references and appendices.

1.7 Significance of the research

CRFs reduces the demand for short-season manual labour obligatory during critical periods (Shaviv, 2001). The anticipated agronomic returns related to the use of Nano-CRFs include reduction of stress and specific toxicity (as a result of synchronizing nutrient release with plant demand), increased availability of nutrients, supply of nutrient forms preferred by plants, and enhancement of synergistic effects between nutrients(Shaviv, 2001).

Essentially, this study is worth doing for the reason that CRFs exhibit grander features over conventional fertilizers. These features include, decreased rate of nutrient losses from the soil by rain or irrigation water; sustained supply of nutrients for a prolonged time; increased FUE; reduced frequency of fertilizer application thereby saving farmers' time and resources; and also,

reduced agronomic toxicity and abate potential negative effects associated with over dosage. Techno-economic studies shows that fertilizer application becomes simple, time saving, cost effective and improve FUE if fertilizing inputs are encapsulated using Nano-excipients. However, most of these studies concentrate on the synthetic polymers formulations which are expensive making it difficult to commercialize product to diverse market. In that view point, we proposed to design Nano CRF by using natural nanocomposite excipients to come up with an efficient, effective, reliable and cost effective CRFs formulations basing on the prevailing resource limitations to boost African SME's competitiveness.

CHAPTER TWO

Meticulous Overview on the Controlled Release Fertilizers[1]

Abstract

Owing to the high demand for fertilizer formulations that will exhaust the possibilities of nutrient use efficiency (NUE), regulate fertilizer consumption, and lessen agrophysicochemical properties and environmental adverse effects instigated by conventional nutrient supply to crops, this review recapitulates controlled release fertilizers (CRFs) as a cutting-edge and safe way to supply crops' nutrients over the conventional ways. Essentially, CRFs entail fertilizer particles intercalated within excipients aiming at reducing the frequency of fertilizer application thereby abating potential adverse effects linked with conventional fertilizer use. Application of nanotechnology and materials engineering in agriculture particularly in the design of CRFs, the distinctions and classification of CRFs, and the economical, agronomical, and environmental aspects of CRFs has been revised putting into account the development and synthesis of CRFs, laboratory CRFs syntheses and testing, and both linear and sigmoid release features of CRF formulations. Methodical account on the mechanism of nutrient release centring on the empirical and mechanistic approaches of predicting nutrient release is given in view of selected mathematical models. Compositions and laboratory preparations of CRFs basing on *in situ* and graft polymerization are provided alongside the physical methods used in CRFs encapsulation, with an emphasis on the natural polymers, modified clays, and superabsorbent nanocomposite excipients

Keywords: CRFs, Excipients, Encapsulation, Graft-polymerization, Intercalation, *insitu*-Polymerization, Nanocomposites, NUE, Release.

[1] Sempeho, S. I., H. T. Kim, E. Mubofu and A. Hilonga (2014). "Meticulous Overview on the Controlled Release Fertilizers." Advances in Chemistry **2014**.

2.1 Introduction

Controlled release fertilizers (CRFs) are fertilizer granules intercalated within carrier molecules commonly known as excipients to control nutrients release thereby improving nutrient supply to crops and minimize environmental, ecological and health hazards (Ukessays.com, 2013c). In that sense, CRFs usage is an advanced way to supply crop's nutrients (cf. conventional ways) due to gradual pattern of nutrient release, which improves fertilizer use efficiency (FUE) (Subbarao, et al., 2013). In other words depending on the thickness of the coatings within the formulation, CRFs enables nutrients to be released over an extended period leading to an increased control over the rate and pattern of release (England, et al.),consequently the excipients plays a role of regulating nutrients release time and eliminate the need for constant fertilization and higher efficiency rate than conventional soluble fertilizers (Ukessays.com, 2013c).

Occasionally the term controlled release fertilizers (CRFs) and slow release fertilizers (SRFs) have been used interchangeably, yet they are different. Typically, the endorsed differences between slow-release and controlled-release fertilizers are not clear (AAPFCO, 1997; Trenkel, 2010). However, the term CRF is generally applied to fertilizers in which the factors dominating the rate, pattern and duration of release are well known and controllable during CRF preparation (Shaviv, 2005; Trenkel, 2010). SRFs on the other hand are characterized by the release of the nutrients at a slower rate than is usual but the rate, pattern and duration of release are not well controlled (Shaviv, 2005; Trenkel, 2010); they may be strongly affected by handling conditions such as storage, transportation and distribution in the field, or by soil conditions such as moisture content, wetting and drying, thawing and freezing, and biological activity (S Raban, Zeidel, & Shaviv, 1997; Shaviv, 1996; Shaviv, 2001). Thus, while in SRFs the nutrient release pattern is fully dependent on soil and climatic conditions and it cannot be predicted (or *only v*ery roughly) (Trenkel & Association, 1997); with CRFs, the release pattern, quantity and time can be predicted within certain limits. For example, the classification of sulphur-coated urea (SCU) is subject to debate (Trenkel, 2010) due to a significant variation in the release patterns between different batches of fertilizer (Goertz, 1993; Shaviv, 2005; Trenkel, 2010). As a result, SCU is considered to be SRF despite being debated.

CRFs use is associated with several economic, agronomical and environmental returns. Economically, CRFs supply nutrients to the crops for the entire season through a single application thereby saving spreading costs and reduce the demand for short-season manual labour required for topdressing operations (Shaviv, 2001). Agronomically, CRFs usage is associated with the improvement of plant growth conditions, such as reduction of stress and specific toxicity resulting from excessive nutrient supply in the root zones. Similarly, CRFs increase the availability of nutrients due to the controlled release of nutrients into a "fixing" medium during the fixation processes in the soil as well as supplying nutrients in the forms preferred by plants; in that way the synergistic effect between nutrients in the CRFs is enhanced (Shaviv, 2001). In the environmental perspective, CRFs improves NUE and in so doing reduces losses of surplus nutrients [over plant needs] to the environment (Shaviv, 2001). Consequently, high levels of fertilizer accumulation in the environment is minimized, thereby lessening several environmental problems associated with conventional fertilizer use such as eutrophication which causes O_2 depletion, death of fish, unpleasant odour to the environment and aesthetic problems (Clark, 1989; Sharpley & Menzel, 1987; Shaviv, 2001).

2.2 Literature review

2.2.1 Classification of CRFs

Several classifications of CRFs have been proposed. In this review, we will attempt to discuss a few of them. Based on Shaviv's grouping (Shaviv, 2005), CRFs may be classified as follows:

Organic-N-Low-Solubility Compounds

These can be subdivided into biologically decomposing compounds usually based on urea-aldehyde condensation products, such as Urea-Formaldehyde (UF), Urea-Triazone (UT), Crotonylidene Diurea (CDU), and chemically decomposing compounds, such as isobutylidene-diurea (IBDU). Succinctly, UF is prepared by reacting excess urea under controlled conditions of pH, temperature, U- F ratio, and reaction time. UT solution is based on the reaction of urea-ammonia-formaldehyde. CDU is prepared by reacting urea with acetaldehyde under the catalysis of an acid. IBDU is prepared by reacting liquid isobutyraldehyde with solid urea (Du, Zhou, & Shaviv, 2006; Shaviv, 2001; Trenkel, 2010; Trenkel & Association, 1997).

Fertilizers in which a Physical Barrier Controls the Release

These can be subdivided into granules coated by hydrophobic polymers or as matrices in which the soluble active materials dispersed in a continuum that restricts the dissolution of the fertilizer. The coated fertilizers can further be divided into fertilizers with organic polymer coatings that are either thermoplastic or resins; and fertilizers coated with inorganic materials such as sulphur or mineral based coatings. The materials used for preparation of matrices can also be subdivided into hydrophobic materials such as polyolefins, rubber, *etc*.; and gel-forming polymers (hydrogels) which are hydrophilic in nature. Broadly, the use of coated fertilizers in agricultural practices is quite common as compared to the use of matrices. For instance, sulphur-coated urea (SCU) was developed at the Tennessee Valley Authority laboratories and manufactured commercially for almost 30 years (SP Landels, 1994; Shaviv, 2001). Its preparation is based on coating preheated urea granules with molten sulphur. The CRF alkyd-typeresin-coated fertilizer (Osmocote) was first produced commercially in California in 1967. It is a copolymer of dicyclopentadiene with a glycerol ester (Shaviv, 2001). In fact, these formulations control the rate of nutrient release offering multiple environmental, economic, and yield benefits (IPNI, 2013). Gel-based matrices are still being developed (Shaviv, Zlotnikov, & Zaidel, 1995).

Inorganic Low-Solubility Compounds

This type of CRFs includes fertilizers such as metal ammonium phosphates (e.g. $MgNH_4PO_4$) and partially acidulated phosphate rocks (PAPR). Besides, the biologically and microbially decomposed N-products, such as UF, are commonly referred to in the trade as slow-release fertilizers and coated or encapsulated/occluded products as controlled-release fertilizers (Shaviv, 2001; Trenkel, 2010). Essentially, Zhang's writings provide a deep detailed account on the subject in a much more broad sense (Min, Yuechao, Fupeng, & Yanxi, 2005).

2.2.2 Preparation of CRFs Formulations

Slowing the release of plant nutrients from fertilizers can be achieved by different methods and the resulting products are known as slow- or controlled-release fertilizers. With controlled-

release fertilizers, the principal method is to cover a conventional soluble fertilizer with a protective coating (encapsulation) of a water-insoluble, semipermeable or impermeable-with-pores material. This controls water penetration and thus the rate of dissolution, and ideally synchronizes nutrient release with the plants' needs. The most important manufactured materials include, (i) materials releasing nutrients through either microbial decomposition of low solubility compounds e.g. organic-*N* low-solubility compounds, such as urea-aldehyde condensation products, or chemically decomposable compounds e.g. IBDU (Shaviv, 2005; Trenkel, 2010); (ii) Materials releasing nutrients through a physical barrier, e.g. sulphur-coated urea (SCU) (Trenkel, 2010); (iii) Materials releasing nutrients incorporated into a matrix, which itself may be coated, including gel-based matrices, which are still under development (Shaviv, 2005; Shaviv, et al., 1995; Trenkel, 2010); Materials releasing nutrients in delayed form due to a small surface-to-volume ratio e.g. super-granules, briquettes, tablets, spikes, and plant food sticks (Trenkel, 2010); and others (Shaviv, Raban, & Zaidel, 2003a, 2003b; Yuechao, Yuqing, Min, Jianqiu, & Haining, 2007).

According to Liu *et al*., (M. Liu, et al., 2007), intercalation of nutrients into the excipients is normally achieved by two methods. In the first method, the compound to be loaded is added to the reaction mixture and polymerized *in situ* whereby the compound is entrapped within the gel matrix whereas in the second method, the dry gel is allowed to swell in the compound solution and after equilibrium swelling, the gel is dried and the device is obtained. This involves graft-polymerization (Ekebafe, Ogbeifun, & Okieimen, 2011; Hosseinzadeh, 2010; W. Li, Zhang, Liu, & Liang, 2012; D. Lu, Xiao, & Xu, 2009). The benefits and drawbacks are that for the former method, the entrapped compound may influence the polymerization process and the polymer network structure; while for the latter, the loaded compound always accumulates on the surface during the drying of the loaded hydrogel, which consequently leads to a „burst effect"; moreover, the loading amount may be low if the compound affects the water absorbency strongly.

Typical physical methods for encapsulating fertilizers include spray coating, spray drying, pan coating, and rotary disk atomization. Special equipment for these methods are rotary drum, pan or ribbon or paddle mixer and fluidized bed (Ukessays.com, 2013c). The details of these methods are beyond the scope of this paper.

2.2.3 Nutrient Release in the CRFs Context

In this perspective, with regard to the European Standardization Committee (CEN) nutrient release [of course from the excipients] can be manifest by the transformation of a chemical substance or rather fertilizer nutrients into a plant-available form (e.g. dissolution, hydrolysis, degradation, *etc.*), whereas slow-release is the release wherein the rate of a nutrient release from the fertilizer is slower than that from a fertilizer in which the nutrient is readily available for plant uptake (Kloth, 1996). CEN's declaration alleged that: "fertilizer should be described as CRFs if at room temperature the nutrients released exceeds 15% in 24 hours, or no more than 75% released in 28 days, or at least about 75% released at the stated release time" (Shaviv, 2001; Trenkel, 2010) giving different release patterns. That is to say, CRFs that do not meet these three CEN's criteria are non-pertinent for the subject of controlled release formulations since the patterns will not comply with the standard ones namely linear and sigmoidal release patterns (Figure 2.1).

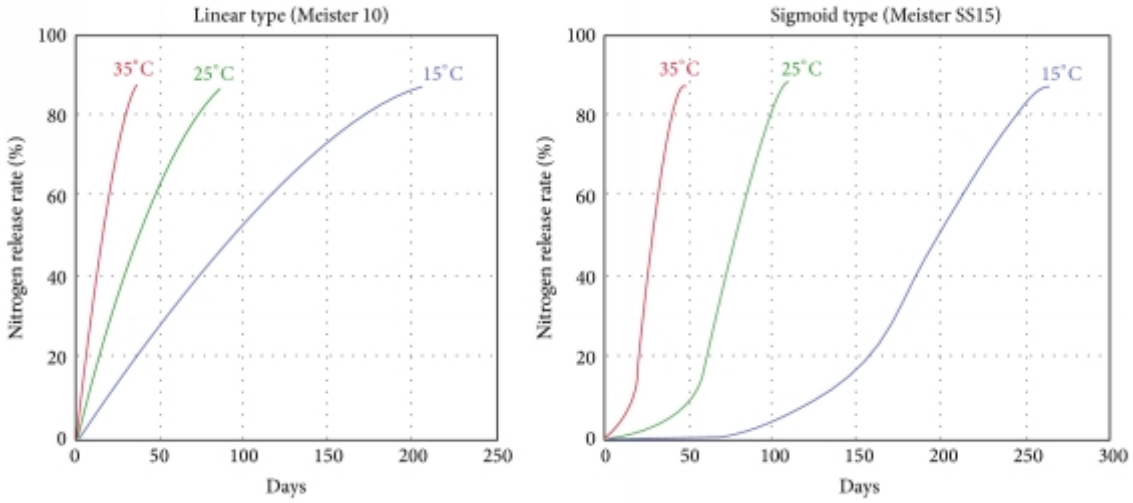

Figure 2.1.The effect of temperature on the release rate of Meister® [8, 30]

As mentioned above, release patterns can be classified into linear and sigmoidal release types (Shoji & Gandeza, 1992; Trenkel, 2010). Examples of linear-release formulations presenting nutrient release between 30 to 270 days at 25 °C for Meister® formulation is given in the Figure 2.2, whereas for sigmoidal-release formulations presenting nutrient release between 40 to 200 days at 25 °C for Meister® is shown in Figure 2.3 (Trenkel, 2010).

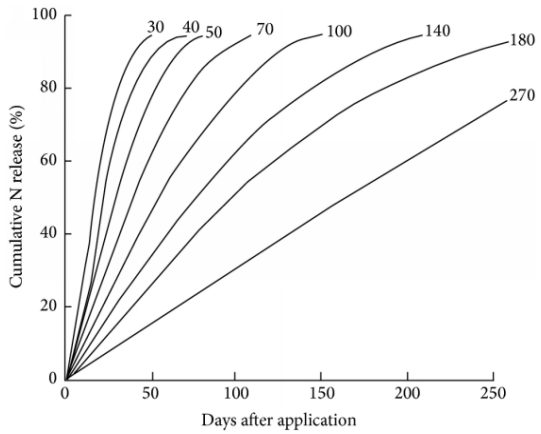

Figure 2.2. Linear release pattern

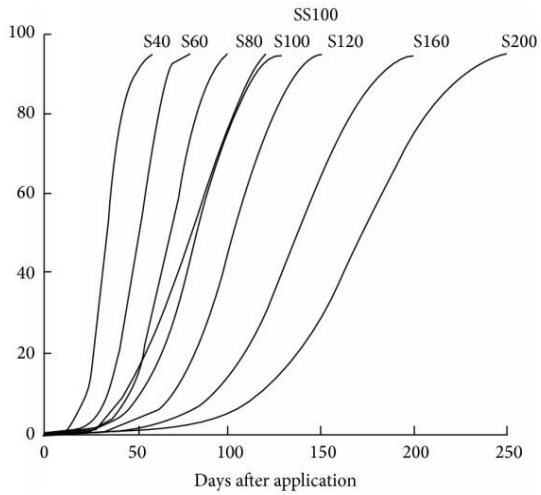

Figure 2.3. Sigmoidal release pattern

Actually, the characteristic features of CRFs encompass the release pattern (*i.e.* shape, lag, lock off); release duration; differential release between N, P and K; effect of temperature on release; and effect of the medium/environmental conditions on release (Shaviv, 2005; Trenkel, 2010). In most cases, the energy of activation of the release, EA_{rel}, is calculated on the basis of estimates of the rate of the release (percentage released per day) during the linear period obtained from the release curves (Du, et al., 2006).

As far as CEN's definition of release is concerned, the example from Meister® formulation described above should comply with the criterion that at least about 75% of nitrogen should be released at the stated release time for this CRF to be approved. As a matter of fact, Kanno (Kanno, 2013)indicated that at the end of 160 days the nitrogen intake reached 79% of the applied N [Figure 2.4] and so conforming to CEN's conditions.

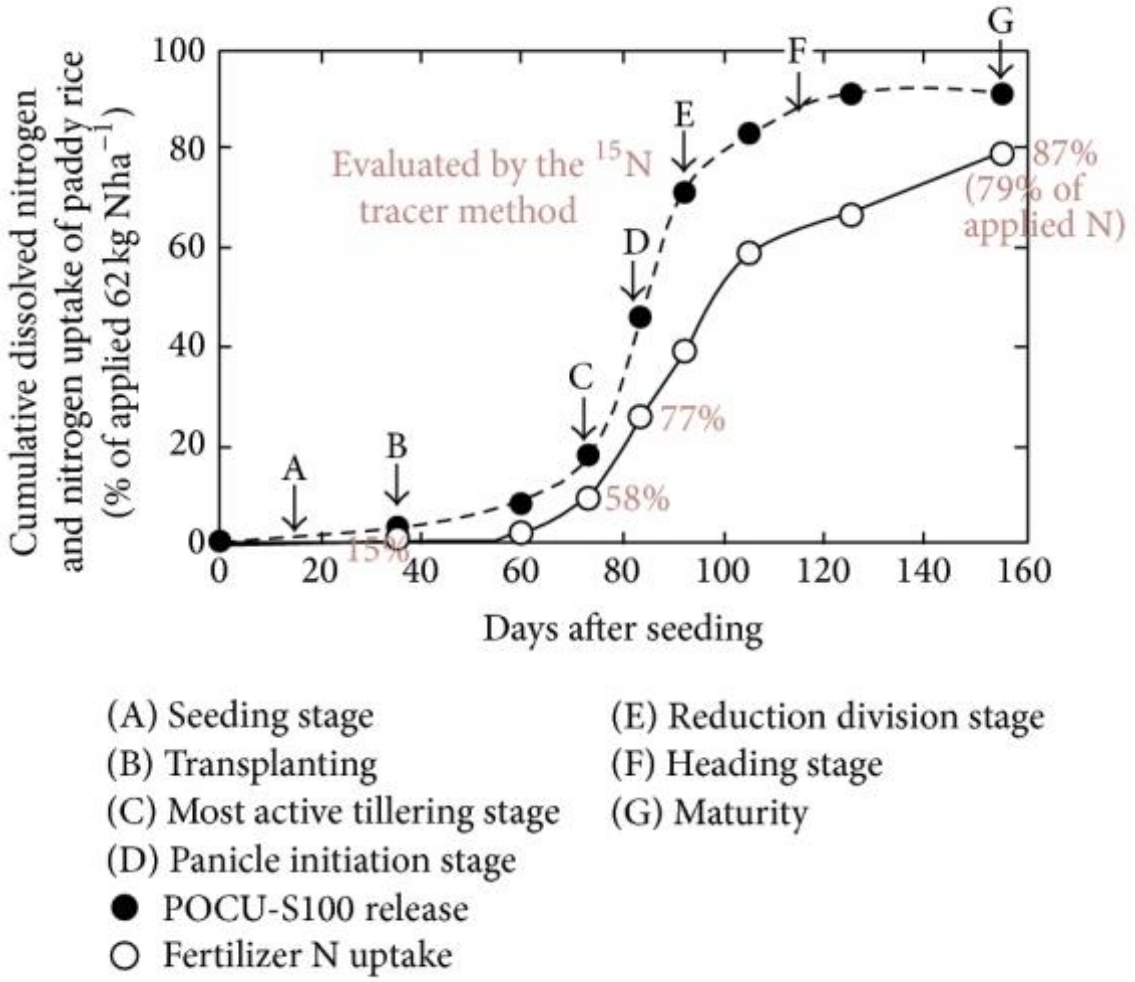

Figure 2.4. Relationship between dissolved N and fertilizer derived N uptake of paddy rice

In point of fact, establishing nutrient release profiles requires data from both field and laboratory testing. In the laboratory, release of nutrients from the excipients is done using water and soil matrices (Fujita, 1996; Trenkel, 2010). Field testing involves net bags placed in the ploughed layer of soil in the actual field (Fujita, 1996; Trenkel, 2010). Industrial Methods involve extract at 25 °C, 40 °C and at 100 °C (Trenkel, 2010). However, Du *etal*., (Du, et al., 2006) provide a new procedure where release characteristics are tested in three different systems namely, (i) free water (which he termed common procedure); (ii) water saturated sand packed in columns; and (iii) sand at field capacity moisture.

2.2.4 Mechanism of Nutrients Release from CRFs Formulations

Consistent experimental data with reference to release phenomena of nutrients from polymer coated CRFs are indispensably beneficial for better agronomic and environmental results (Du, et al., 2006). Jcam Agri.Co., Ltd (Agric., 2014), after a period of laboratory testing of Meister CRFs, the obtained the results described in Table 2.1 and 2.2 for both Linear and sigmoid pattern. The designed formulation which is marketed as Meister® has it mechanism proposed by the company and the summary is give in the Figure 2.5 below. The mechanism is based on three significant steps namely, water adsorption, dissolution of urea and leaching.

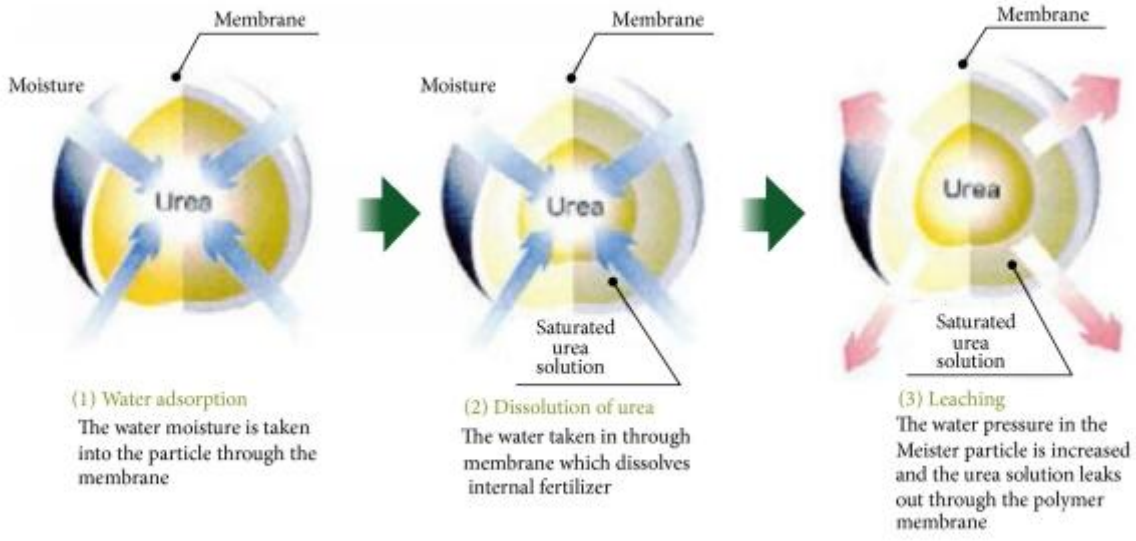

Figure 2.5. Release of nitrogen from polyolefin coated urea in water at 25 ^{o}C

Table 2.1. Linear release pattern

Brand Name	80% Release (days at 20 ℃)	80% Release (days at 25 ℃)	Japanese Brand Name	N content (%)
MEISTER-5	50	30	LP-30	42
MEISTER-7	70	40	LP-40	42
MEISTER-8	80	50	LP-40	50
MEISTER-10	100	70	LP-70	42
MEISTER-15	150	100	LP-100	42
MEISTER-20	200	140	LP-140	42
MEISTER-27	270	180	LP-180	42
MEISTER-40	400	270	LP-270	42

Table 2.2. Sigmoid release pattern

Brand Name	Time Lag Days / Release Days at 20 ℃ in soil	at 25 ℃ in soil	Japanese Brand Name	N content (%)
MEISTER-5	35/35	20/20	LP-S40	41
MEISTER-7	45/45	30/30	LP-S60	41
MEISTER-8	60/60	40/40	LP-S80	41
MEISTER-10	45/105	30/70	LP-S100	41
MEISTER-15	70/80	45/55	LP-SS100	41
MEISTER-20	90/90	60/60	LP-S120	41
MEISTER-27	120/120	80/80	LP-S160	41
MEISTER-40	150/150	100/100	LP-S200	41

In addition to that, Guo *et al.*, (Guo, Liu, Liang, & Niu, 2006) proposed the mechanism of nitrogen release from urea-formaldehyde (UF) slow-release fertilizer granules based on three steps. **Step one:** the coating materials become swollen by absorbing water from the soil and so get transformed into hydrogels which contribute to increase the orifice size of the 3D network of the coating materials so that it benefits the diffusion of the fertilizer in the core of the gel network. As a result, a layer of water between the swollen coatings and the UF granule core is

formed. **Step two:** water slowly diffuses into the crosslinked polymer network and dissolves the soluble part of UF; consequently the soluble part of the fertilizer gets slowly released into the soil through the swollen network with the dynamic exchange of the water in the hydrogel and the water in the soil. **Step three:** the soil microorganisms penetrate through the swollen coatings and assemble around the UF granule thereby degrading the insoluble part of nitrogen in UF granule into urea and ammonia which in turn is slowly released into the soil via dynamic exchange. Such steps have also been described as lag period, linear stage and decay period by other researchers (Du, et al., 2006).

This mechanism can be adapted to effectively explain the release behaviour in other CRF formulations. Different mathematical mechanistic models based on empirical and mechanistic approaches plus empirical and semi-empirical models have been proposed for prediction of the nutrient release using chemo-physical parameters as will be discussed in the coming sections. Nevertheless, most mechanisms reveal that nutrients release from CRFs is mainly controlled by diffusion mechanism with respect to temperature, thickness of the coating material, type of nutrient and the presence or absence of the relevant soil microorganisms.

2.2.5 Predicting Nutrient Release from CRFs

Profoundly, a number of empirical and semi-empirical mechanistic mathematical models have been put forward in order to provide realistic theoretical assumptions connected to the patterns of nutrients release mechanisms basing on the nature and the properties of the delivery systems (DSs) (Shaviv, 2001); and in that case, release models have been used as tools for improving the CRFs' design methodology leaving behind conceivable breakthroughs in assessing prospective hazards such as leaching or volatilization losses and effects such as "bursting" or "tailing effect" (S Raban, et al., 1997; Shaviv, 1996; Shaviv, 2001). Such conceptual approaches include the diffusion model, zero order kinetics model, first order kinetics model, Higuchi model, Korsmeyer-Peppas model, Hixson–Crowell model, Weibull model, Baker-Lonsdale model, Hoffenberg model, sequential layer model, Couarraze model and Peppas-Sahlin model. In particular, most of the proposed release models assumes that the release of nutrients from coated CRFs is either controlled by the rate of solute diffusion from the fertilizers or by the rate of water/vapour penetration into the CRF through the coating (Shaviv, 2001).

a) Diffusion Model

Considering a mathematical model developed for urea release from sulphur-coated granules under soil conditions (Jarrell & Boersma, 1980; Shaviv, 2001), the assumption was that: urea diffuses from the granule through pores or holes caused by erosion of the coating and that, the transport is influenced by temperature and soil water content; thus, diffusion occur through the coating. This model was verified using Fick's first law as:

$$\frac{dm}{dt} = -DS_k \frac{dC_k}{dx_k} \qquad (1)$$

Where, m is the mass of urea diffusing out of the granule, D is the effective diffusion coefficient of urea in water, S_k is the cross-sectional area through which diffusion occurs, and C_k is the urea concentration. The subscript k is the value for the internal pore coating, or outside segments (Shaviv, 2001). The predictive power of this model is certainly restricted to the fact that particle flux is directly proportional to the spatial concentration gradient. Nonetheless it is not the spatial concentration gradient that causes particle movement, *i.e.* particles do not push each other (Crank, 1975). That is to say, particles do exhibit random motion on the molecular level and this random motion ensures that a tracer will diffuse thereby decreasing the concentration gradient (Crank, 1975).

Moreover, a study by Jarel and Boersma (Jarrell & Boersma, 1979) revealed that the diffusion of urea through the sulphur coating occurred in two steps represented in the following models:

$$\frac{dm_r}{dt} = \frac{DS_p}{M_o l} C_{sat} \; for \; t < t_1 \qquad (2)$$

$$\frac{dm_r}{dt} = \frac{DS_p}{M_o l} (1 - m_r)\rho, for \; t > t_1 \qquad (3)$$

where, m_r = m/M_O; while M_O is the initial mass of urea in the granule, C_{sat} is the concentration of saturated urea solution, l is the coating thickness; ρ is the density of solid urea, and t_1 is the onset of the period of the decaying rate of release as the solution inside the granule becomes unsaturated.

Similarly, this study is also boundless for the reason that, it ignores some important factors and features that are relevant to diffusion of active bioactive substances from an excipient or rather a membrane-coated granule (sphere). It is for that reason that the following Arrhenius type of

model pertaining to the diffusion coefficient D was suggested (Jarrell & Boersma, 1980; Moore, 1972; Shaviv, 2001):

$$D = AT\, e^{\left(-\frac{EA_{release}}{T}\right)} \qquad (4)$$

Where T is the Kelvin absolute temperature and $EA_{release}$ stands for the apparent energy of activation for urea diffusion from the excipients. This expression as proposed provides a conceivable explanation for the temperature dependence on the CRFs release rates. On the same side, a similar model for simulating nutrients release from the CRFs in a 1D coordinate system is known (Glaser, Stajer, & Videnský, 1987); however, an additional assumption in favour of this model is that: the diffusion coefficient is time dependent, thus giving the following expression:

$$D = D_0 t^n \qquad (5)$$

Where t is time, D_0 is an initial value at t=0 and n is an empirical constant. The time dependence of D presents a lag in the curve describing cumulative release with time (*i.e.*, sigmoidal release pattern) which could otherwise not have been obtained by simply applying Fick's law described before (Shaviv, 2001).

b) Sequential Layer Model

This model assumes that during the release of an active ingredient from the hydrophilic excipients, significant water concentration gradients are formed in the first place at the matrix/water interface and by so doing there is a creation of water imbibition into the system and as a result, there occur dramatic physicochemical changes namely, the exact geometry of the active substance within the excipients, axial and radial direction of the mass transport, and water diffusion coefficient on the matrix. Due to swelling of the excipients following water imbibition phenomenon, the concentration of participating species (*i.e.* polymer and a chemical substance) significantly changes thereby causing increased dimensions of the system. Consequently, the dissolution of the active ingredient occurs and so, it diffuses out of such hydrophilic system following concentration gradients. Essentially, the amount of water available for dissolution is directly proportional to the diffusion coefficient of the active substance within the excipients. In

that view, dissolution rate constant, k_{diss}, of the active ingredient-excipient system can be computed and is given as:

$$M_{pt} = M_{po} - k_{diss} A_t t \qquad (6)$$

Where M_{pt} and M_{po} are the dry polymer matrix mass at time t, and t = 0, respectively; A_t is the surface area of the device at time *t* (Barzegar-Jalali, 2008; Chime Salome, Onunkwo Godswill, & Onyishi Ikechukwu, 2013; P. Costa & Sousa Lobo, 2001; Dixit, 2014; Mahat, 2010; Nanjwade, 2013; Narender, 2014; Shaviv, et al., 2003b; Siepmann & Peppas, 2001).

c) Hopfenberg Model

The primary assumption in this model is that: nutrients are released from the surface-eroding excipients possessing some geometries ranging from slabs, spheres and infinite cylinders displaying heterogeneous erosion. This approach can be mathematically expressed as:

$$\frac{M_t}{M_\infty} = 1 - \left(1 - \frac{k_0 t}{C_0 a}\right)^n \qquad (7)$$

Where M_t is the concentration of the chemical substance dissolved in time t, M_∞ is the total matrix (chemical-excipient) concentration dissolved when the system is exhausted, k_o is the erosion rate constant, C_o is the initial concentration of chemical substance/fertilizer in the matrix and a_o is the initial radius for a sphere of cylinder or the half-thickness for a slab. The value of *n* is 1, 2 and 3 for a slab, cylinder and sphere, respectively (Barzegar-Jalali, 2008; Chime Salome, et al., 2013; P. Costa & Sousa Lobo, 2001; Dixit, 2014; Mahat, 2010; Nanjwade, 2013; Narender, 2014; Shaviv, et al., 2003b; Siepmann & Peppas, 2001).

d) Weibull Model

As far as CRFs formulation is concerned, this model accounts for the release of nutrient molecules from the erodible matrix formulations with an assumption that, factors influencing the overall release rate are exclusively mass dependent; while other factors stand to be time dependent (Barzegar-Jalali, 2008)(Barzegar-Jalali, 2008)(Barzegar-Jalali 2008)(Barzegar-Jalali 2008)(Barzegar-Jalali 2008)(Barzegar-Jalali 2008)(Barzegar-Jalali 2008). The model depicts that, a plot of logarithm of the amount of nutrient molecules dissolved in an excipient' solution versus the logarithm of time will be linear and it is mathematically given as:

$$Log[-ln(1-m)] = b\ log(t - T_t) - loga \qquad (8)$$

Where, *a*, relate to the time scale of the process corresponding to the ordinate [– In (1 – m)] = 1. T_t refer to the lag time before the onset of the release process and *t* is time after release phenomena, *b* is the shape parameter corresponding to the ordinate value (1/a) when time t = 1 and *m* relate to the fraction of the active ingredient in the excipient' solution at time t (Barzegar-Jalali, 2008; Chime Salome, et al., 2013; P. Costa & Sousa Lobo, 2001; Dixit, 2014; Mahat, 2010; Nanjwade, 2013; Narender, 2014; Shaviv, et al., 2003b; Siepmann & Peppas, 2001).

Despite limitations associated with this model including, the in-ability to sufficiently characterize the release kinetics of the nutrient molecules, and the limited use for establishing *in vivo/in vitro* correlation; the model is known to be grander in the fact that, the release half-life can easily be calculated and also, the errors associated with it are only single figures *i.e.* minimum. In fact, the number of single figure errors is known to be higher than other models (Barzegar-Jalali, 2008).

e) Korsmeyer- Peppas Model

Basing on the CRFs context, this semi-empirical model is effective in the determination of the concentration of nutrient molecules released from the excipients' membranes. Theoretically, the simple expression allied to this model is given as:

$$f_t = at^n \qquad (9)$$

Where, *a* refer to a constant incorporating structural and geometric characteristics of the given active substance, *n* is the release exponent indicative of the release mechanism, and *t* is fractional release of active substance [M_t/M_∞] described in equation 7 above (P. Costa & Sousa Lobo, 2001).

f) Higuchi Model

Predominantly, this model explicates the release of water soluble and low soluble nutrient substances merged into the semisolid or solid excipients molecules; it has been lengthily applied in the diffusion matrix formulations. The assumption core to this model stipulate that:initial concentration of the nutrient molecules incorporated into the matrix is much higher than the solubility of the former (Dixit, 2014). Another assumption state that: the diffusion of the nutrient

molecules with excipients takes place only in one dimension such that the edge effect is negligible. The third one depicts that: nutrient particles are much smaller than the system' thickness. Also, matrix swelling and dissolution are negligible and so, diffusivity of an active nutrient substance is constant; and the last assumption is that, perfect sink conditions are always attained in the release environment (Dixit, 2014).

Considerably, the assumptions underlying this model reveal that there are two systems which may considered when formulating mathematical expression for the release systems. Such systems are (i) when the nutrient molecules are dispersed in a homogeneous uniform matrix, which of course acts as diffusional mechanism and (ii) when they are incorporated into the planar heterogeneous matrix where their concentration in the matrix is lower than their solubility such that release process occurs through pores in the excipients by penetrative leaching out (Narender, 2014). Conceptually, Figure 6 can be used to formulate a language to express this model.

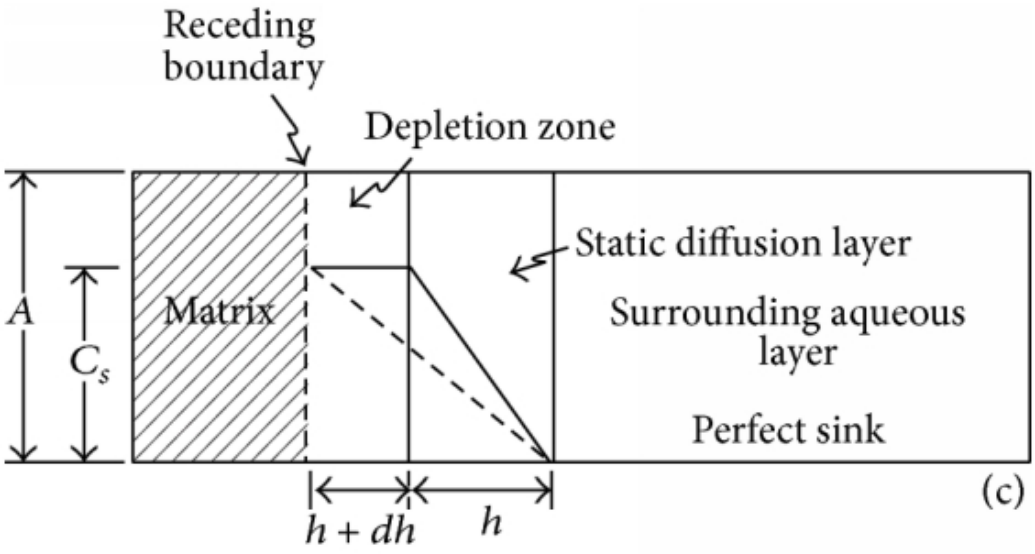

Figure 2.6 Conceptual Higuchi model

According to Fick's first law:

$$\frac{dM}{Sd_t} = \frac{dQ}{dt} = \frac{DC_s}{h} \qquad (10)$$

At this instant, when the nutrients molecules are dispersed within the homogeneous excipient matrix, the borderline indicated by the dashed vertical line [Figure 2.6] moves to the left by an

infinitesimal distance (*dh)* and that the infinitesimal amount (*dQ)* of the nutrients released because of this shift is given as:

$$dQ = Adh - \frac{1}{2} C_s dh \qquad (11)$$

When equation (11) is substituted in (10), equation (12) is obtained and is given as:

$$\frac{DC_s}{h} = \left(A - \frac{1}{2} C_s\right) \frac{dh}{dt} \qquad (12)$$

Basing on Narender's derivation steps (Narender, 2014), it is possible to follow Higuchi's steps for derivation as follows:

$$2A - \frac{C_s}{2DC_s} \int hdh = \int dt \qquad (13)$$

$$t = (2A - C_s) \frac{h^2}{4DC_s} + C \qquad (14)$$

Integrating "C" when h=0, equation (15) is obtained as:

$$h = \left(\frac{4DC_s t}{2A - C_s}\right)^{\frac{1}{2}} \qquad (15)$$

Recall equation (11):

$$dQ = Adh - \frac{1}{2} C_s dh \qquad (16)$$

This equation can be integrated to take the following simple form:

$$Q = hA - \frac{1}{2} hC_s \qquad (17)$$

Substituting equation (17) into (16) we obtain the Higuchi equation for the homogeneous nutrient-excipients matrices below:

$$Q = [D(2A - C_s)C_s t]^{\frac{1}{2}} \qquad (18)$$

This can be further simplified to take a form of:

$$f_t = Q = A\sqrt{D(2C - C_s)C_s t} \qquad (19)$$

Where, *Q* is the concentration of the given nutrient released in time *t* per unit area *A*, *C* is the initial concentration of the nutrient, C_s is the nutrient solubility in the matrix media and *D* is the diffusivity of the nutrients molecules (diffusion coefficient) in the matrix substance (Dixit, 2014; Narender, 2014).

On the other hand, the heterogeneous nutrient-excipient matrix system take a different form and in that way equation (18) is modified in order to take into account the porosity and tortuosity of the matrix. Conceptually, the mathematical expression will be:

$$\frac{dQ}{dt} = \left(\frac{ADC_s}{2t}\right)^{\frac{1}{2}} \qquad (20)$$

Where, *dQ/dt* is the concentration of nutrients released at time t, *A* is the total amount of nutrients in unit volume of matrix, *D* is the diffusion coefficient of the nutrients in matrix, *Cs* is the solubility of the nutrients in polymeric matrix and *t* is the time (Dixit, 2014; Narender, 2014).

g) Hixson Crowell Model

This model assumes that the release rate of a nutrient molecules contained in a polymeric excipient is limited to the dissolution rate of its particles and not by the diffusion that could take place through polymeric matrix. The assumptions underlying this model include: (i) dissolution occurs normal to the surface of the solute particles, (ii) agitation is uniform all over the exposed surfaces and there is no stagnation and also (iii) the particle of solute retains its geometric shape (Barzegar-Jalali, 2008; Chime Salome, et al., 2013; P. Costa & Sousa Lobo, 2001; Dixit, 2014; Mahat, 2010; Nanjwade, 2013; Narender, 2014; Shaviv, et al., 2003b; Siepmann & Peppas, 2001).

According to Narender (Narender, 2014), the radius of a given bioactive particle is given as *r* and surface area is thus $4\Pi r^2$. For that reason, during release process the radius is reduced by *dr* and so, the infinitesimal volume of one particle fragment lost can be differentiated to be:

$$dV = 4\pi r^2 dr \qquad (21)$$

However, infinitesimal volume of *n* particle fragment lost can be differentiated as:

$$dV = 4N\pi r^2 dr \qquad (22)$$

Recalling equation (22), the surface of *n* particles can be found as:

$$S = 4N\pi r^2 \qquad (23)$$

Since from the Noyes –Whitney law, the infinitesimal change in weight is given by the equation:

$$dW = kSC_s dt \qquad (24)$$

Then, the density of the nutrient molecules in the matrix could be multiplied by the infinitesimal volume change as $\rho dV = dW$ to give the following equation:

$$\rho dV = kSC_s dt \qquad (25)$$

Substituting (22) and (23) (25) equation (26) is obtained:

$$-4\rho N\pi r^2 dr = 4N\pi r^2 KC_s dt \qquad (26)$$

Equation (26) can be simplified further by integrating it with respect to r = ro, at t = 0 to give the following expression:

$$r = ro - \frac{kC_s t}{\rho} \qquad (27)$$

Equally, it is possible to substitute the radius in equation (27) with the weight of *n* particles to give the following expression:

$$W^{1/3} = \left(\sqrt[s]{N\rho\frac{\pi}{6}}\right) d \qquad (28)$$

Since the diameter *d* can be substituted for *2r*, then it is possible to substitute *d* from (27) with 2*r* from (28) to yield the Hixson-Crowell cube root equation below:

$$W_o^{\frac{1}{3}} - W_t^{\frac{1}{s}} = kt \qquad (29)$$

Where, W_o is the initial concentration of nutrient molecules in the matrix, W_t is the remaining concentration of nutrient molecules in the matrix at time *t*, κ (kappa) is a constant incorporating the surface-volume relation (Narender, 2014).

h) Zero Order Kinetics Model

This model describes the delivery system at which the concentration of nutrients released per unit time is constant. This model assumes that: in the course of dissolution process the area does not change and no equilibrium conditions are obtained. In that case, this model has been useful in the release of bioactive species/nutrients from the matrix that do not disaggregate and release the nutrients slowly from the excipients. Mathematically, the model can be expressed as:

$$Q_o - Q_t = K_o t \qquad (30)$$

Where, Q_t is the amount of nutrients dissolved in time *t*, Q_0 is the initial amount of nutrients in the solution (most times**,** $Q_o = 0$) and K_o is the zero order release constant expressed in units of concentration/time. According to Mahat (Mahat, 2010), the zero-order release kinetics account for various different mass transport phenomena such as diffusion of water and bioactive species and the swelling and degradation of the excipients.

i) First Order Kinetic Model

This model is applied in the release kinetics to describe the absorption and elimination of the bioactive ingredients/nutrients from the excipients. This model assumes that: a graph of release data versus time will be linear. Conferring to this model, the rate of bioactive species released from the excipients matrix is directly proportional to the concentration; that is to say, the release rate of nutrient molecules is concentration dependent (Chime Salome, et al., 2013). Mathematical expression for this model is given as:

$$lnQ_t = lnQ_0 + k_t \qquad (31)$$

Where, Q_t is the concentration of nutrients yet to be released at time *t*, Q_0 is the concentration of nutrients yet to be released at time zero, and K_t is the first order release constant.

j) Baker-Lonsdale Model

This model was established from the Higuchi model in attempts to describe the dissolution of bioactive species from spherical matrix based excipients and hence, it has been quite suitable model for microcapsules or microspheres systems. In a very simplified form it is possible to express this model as:

$$F_t = \frac{3}{2}\left[1 - \left(1 - \frac{M_t}{M_\infty}\right)^{\frac{2}{3}}\right] - \frac{M_t}{M_\infty} = k_t \qquad (32)$$

Where, Ft is the fraction of bioactive species released at time t, M_t is the amount released at time t, and M_∞ is the amount released at infinite time (Barzegar-Jalali, 2008; Chime Salome, et al., 2013; P. Costa & Sousa Lobo, 2001; Dixit, 2014; Mahat, 2010; Nanjwade, 2013; Narender, 2014; Shaviv, et al., 2003b; Siepmann & Peppas, 2001).

2.2.6 Failure Release

Experiments on the modified polymer or sulphur-coated urea granules (PSCU) conducted by Raban (Srnadar Raban, 1994) revealed the main processes occurring during the failure release mechanism. The release process starts as water vapours penetrate through the coating. The rate of water penetration is defined by the driving force (vapour pressure gradient), the coating

thickness, and features of the coating material. The water vapours condense and dissolve the fertilizer, thus causing a build-up of internal pressure inside the coated granule. The increase of internal pressure above a threshold value is likely to cause rupture of the coating (in contrast to the case of diffusion when the coating resists the pressure).The destruction of the coating leads to instantaneous release of the fertilizer.

Zaidel (Zaidel, 1996) analysed the forces involved during water penetration into a single granule and the rate of pressure build up in it, from which it was possible to develop an expression for the time of "burst" or rupture (t_b) of a single coating (membrane)

$$t_b \cong \frac{r_o l_o Y}{P_h \Delta\pi M} \qquad (33)$$

Where, r_0 is the granule radius, l_0 is the coating thickness, Y is the yield stress of the coating (Pa), Ph is the water permeability of the membrane ($cm^2 day^{-1}$ Pa^{-1}), $\Delta\pi$ is the gradient of osmotic pressure across the membrane (Pa), and M is Young's module of elasticity of the coating (Pa).

2.2.7 CRFs Release Properties

Characterization of release from a given SRF/CRF is one of the most important steps in assessing the efficacy of a given fertilizer. Trenkel (Trenkel & Association, 1997) provides a partial list of methods used by several manufacturers of coated fertilizers to assess the release of different SRFs/CRFs. Tests performed at temperatures ranging from 2 °C to 60 °C at varying sampling frequencies are reported.

Release characteristics may be attributed to both physical effects (such as reduced diffusion rates in soils, moisture and temperature fluctuations (Southern Agricultural Insecticides, 1998)) and chemical effects (pH changes, root excretion) as well as to the action of microbes on bio-degradable materials (UF, sulphur coating, waxes, *etc*.). This implies that a correlation between laboratory tests and release rates obtained under field conditions is required in order to achieve the highest NUE with the CRFs (Shaviv, 2001). Release curves are the best common methods used in the characterization of nutrient release from the CRF formulation as seen in Figures (2.1-2.4) above.

Despite the release curves, several other parameters are known to be used in evaluating the properties of a particular CRF formulation such as water permeability (X. Han, Chen, & Hu, 2009) swelling ratio and dissolution rate (Jamnongkan & Kaewpirom, 2010a) which account for release behaviour. Others include, zeta potential (ZP) and particle size (Ltd, 2013; NanoComposix, 2012), together with morphology and thermal degradation properties (Gill, Moghadam, & Ranjbar, 2010).

2.2.8 CRFs and Biodegradability

Biodegradability means that a material has the proven capability to decompose in the most common environment where the material is disposed of within three (3) years through natural biological processes into nontoxic carbonaceous soil, water, carbon dioxide or methane.

Partial Biodegradation: This relates to the minimal transformation that alters the physical characteristics of a compound while leaving the molecule largely intact. In other words, it refers to the alteration in the chemical structure of a substance, brought about by biological action, resulting in the loss of a specific property of that substance. Partial biodegradation is not necessarily a desirable property, since the intermediary metabolites formed can be more toxic than the original substrate. Therefore, mineralization is the preferred aim is such cases.

Complete Biodegradation: This occurs when the molecular cleavage is sufficiently extensive to remove biological, toxicological, chemical and physical properties associated with the use of the original product, eventually forming carbon dioxide and water.

Readily biodegradable: This is an arbitrary classification of chemicals which have passed certain specified screening tests for ultimate biodegradability; these tests are so stringent that it is assumed that such compounds will rapidly and completely biodegrade in aquatic environments under aerobic conditions.

Inherently biodegradable: This is a classification of chemicals for which there is unequivocal evidence of biodegradation (partial or complete) in any test of biodegradability.

Despite the fact that an understanding of biodegradability is vital, the questions remains to be how biodegradable is the material? According to Han *et al*.,(X. Han, et al., 2009), the test of biodegrability in CRF formulation is achieved by cutting CRF films into small squares such as 3x3cm. Each specimen is then weighed and placed in agricultural soil (in a pot); subsequently, the pots are exposed to ambient conditions for 50 days. Variations in film morphology and disintegration time are then recorded as a test for biodegrability (X. Han, et al., 2009).

Similarly, terms like "environmentally friendly", "environmentally preferable", and "environmentally responsible" have been used to describe a material produced by biodegradable starting materials. In that case, one can freely use these terms interchangeably without distorting the meaning of the biodegrability concept.

2.2.9 Composition of CRF' Formulations

Basically most CRFs may contain among others, the following components:

a. Polymer Solution

A number of polymers have been used in fertilizer coating; such polymers could be thermosetting, thermoplastic or biodegradable ones. Some of common thermoset polymers include urethane resin, epoxy resin, alkyd resin, unsaturated polyester resin, phenol resin, urea resin, melamine resin, phenol resin, silicon resin. Among them, urethane resin is very commonly used (Ukessays.com, 2013c). In addition, polyacrylamide is known to reduce soil erosion and so in this review we recommend that more studies should be conducted for its advanced use in CRFs (K. N. Nwankwo, 2001; Subbarao, et al., 2013). Thermoplastic resins are not very commonly used in practice because they are either not soluble in a solvent or make a very viscous solution which is not suitable for spraying, however, polyolefin is used in the art for coating the fertilizer granules. Biodegradable polymers are naturally available and so, they are known to be environment friendly because they decompose in bioactive environments; degrade by the enzymatic action of microorganisms such as bacteria, fungi, and algae and their polymer chains may also be broken down by non-enzymatic processes such as chemical hydrolysis. However, both synthetic and natural polymers containing hydrolytically or enzymatically labile bonds or groups are degradable (D. Lu, et al., 2009). In field agriculture,

the use of polymers is only limited by their relatively high cost, which has restricted their use mainly in light and medium soils with high sand content (Chatzoudis & Rigas, 1998). Therefore, in this review we have decided to concentrate on some natural biopolymers that are useful in CRF practices, for instance, natural rubber which was used by Hanafi to develop CRFs formulations (Hanafi, Eltaib, & Ahmad, 2000).

- *Natural Polymers in CRFs Practices*

Hitherto, natural polymers have been used to replace synthetic ones for the reason that they are inexpensive, can control soil erosion (K. N. Nwankwo, 2001), and they have low toxicity and excellent biodegradability (Singh, Sharma, & Malviya, 2011). Basically, natural polymers are more superior to the synthetic polymers owing to their highly organized macroscopic and molecular structure which in turn adds to their strength and biocompatibility (Singh, et al., 2011). There are three basic types of natural polymers widely used in the controlled release delivery systems. These are neutral e.g. Hydroxypropylmethylcellulose (HPMC), cationic e.g. Chitosan, and anionic polymers e.g. κ- carrageenan and sodium alginate. Several natural polymers including a few lists below have been used in the design of controlled release formulations of drugs and fertilizers as described hereunder.

Chitosan: This is a cationic polysaccharide composed of linear copolymers of glucosamine and *N*-acetyl glucosamine resulting from partial deacetylation of chitin obtained from crustacean shells. The natural rich sources of chitosan include chitin of invertebrates, insects and yeasts (Shobhit Kumar & Gupta, 2012). Researches indicate that complexes formed between chitosan with bioactive compounds and other polymers are useful in modifying the release profile characteristics in different preparations (Singh, et al., 2011). In fact it is found to provide first order release kinetics especially when particle size of less than 75 micron were used (Shobhit Kumar & Gupta, 2012). Several studies have been conducted using chitosan nanoparticles; the findings reveal that it is possible to intercalate NPK fertilizers into chitosan nanoparticles prepared by polymerizing methacrylic acid (Corradini, De Moura, & Mattoso, 2010b). Interestingly, chitosan nanoparticles obtained showed spherical shapes and uniform sizes of approximately 78 nm (Corradini, et al., 2010b).

The mechanism to optimize the incorporation of the N, P and K elements into the designed chitosan nanoparticles is yet to be described (Corradini, et al., 2010b); this creates a gap for further research. Jamnongkan (Jamnongkan & Kaewpirom, 2010a), reported CRF hydrogels prepared from chitosan, polyvinyl alcohol and polyvinyl alcohol/chitosan, using glutaldehyde as a crosslinker. The synthesized CRF hydrogels exhibited high swelling ratio (Jamnongkan & Kaewpirom, 2010a). Wu *et al*. (Wu & Liu, 2008), managed to prepare chitosan-coated nitrogen, phosphorus and potassium compound fertilizer with controlled-release and water-retention (CFCW) capacity using inversion suspension polymerization (Wu & Liu, 2008). Besides, the CFCW synthesized possessed excellent water retention capacity and thus, a good formula for agricultural use and in the renewal of arid and desert environments.

Xanthan gum: This is a high molecular weight, water soluble, anionic-bacterial heteropolysaccharide; it is a hydrophilic polymer, biocompatible and inert thus, it provides time dependent release kinetics (Singh, et al., 2011). Xanthan gum (XG) is used as a rheology modifier and is derived as a result of microbial fermentation of glucose from the bacterial coat of *Xanthomonas campestris* (Singh, et al., 2011). As a matter of fact, the applications of XG in the CRFs industry is less common, however, findings prove that XG matrices exhibit quite consistent higher ability to retard drug release for controlled-release formulation (Talukdar, Vinckier, Moldenaers, & Kinget, 1996). This calls for further investigations on its use in CRFs.

Carrageenan: This is a naturally occurring high molecular weight anionic gel-forming polysaccharide extracted from certain species of red seaweeds (Rhodophyceae) such as *Chondruscrispus*, *Euchema*, *Gigartina stellata* and *Iridaea* (Singh, et al., 2011). It is made up of the repeating units of galactose and 3,6 anhydrogalactose. Depending on the different degree of sulfation, they are classified into various types: ι-(mono-sulfate), κ-(di-sulfate), and λ-carrageenan (tri-sulfate). ι- and κ-carrageenan forms gel while highly sulphated λ- carrageenan is a thickening agent and does not form gel, which influences their release kinetics (Singh, et al., 2011). The integrated method for production of carrageenan and liquid fertilizer from fresh seaweeds is known (Eswaran et al., 2005). In their work, the fresh biomasses of seaweeds *Kappaphycus alvarezii* were crushed to release sap which was then used for extraction of *K-carrageenan.* The extract was found to be a superior raw material for production of liquid fertilizer after suitable treatment with additives. A novel biopolymer-based super absorbent

hydrogel synthesized past graft copolymerization of acrylic acid onto kappa-carrageenan backbones is reported to have been successfully researched (Hosseinzadeh, 2010). Release studies revealed that Kappa- carrageenan is effective in minimizing burst release (bust effects vs. tailing effects); in fact the burst release is found to depend highly on the degree of cross-linking and the mesh space available for drug diffusion (Hezaveh & Muhamad, 2013).

Pectin: is a methoxy ester of pectic acid found in the higher plants cell walls (Shobhit Kumar & Gupta, 2012; Singh, et al., 2011). Certain fruits such as apple, quince, plum, gooseberry, grapes, cherries and oranges also are known to contain pectin (Singh, et al., 2011). Little is known about pectin based CRFs, however, a pectin-based hydrogel used for removing Cu^{2+} and Pb^{2+} ions from water and waste water and in the release of phosphate, potassium, and urea has been reported. The finding revealed that the pectin based hydrogels effective in conserving water necessary or absorption by horticultural plants (Guilherme et al., 2010). Non-Fickian mechanism was seen to control the release process of fertilizer nutrients from the hydrogels.

Tamarind Seed Polysaccharide (TSP): Tamarind Seed Polysaccharide (TSP) is a galactoxyloglucan (a monomer of mainly three sugars-galactose, xylose and glucose in a molar ratio of 1:2:3) isolated from seed kernel of *Tamarindus indica* (Singh, et al., 2011). Being a natural biopolymer TSP is non-toxic, biocompatible and cheap agro-based material for use in CRFs practices giving zero order release kinetics (Shobhit Kumar & Gupta, 2012).

Mimosa pudica seed mucilage: Mimosa mucilage is known to act as a matrix forming agent for sustained delivery of formulations (Singh, et al., 2011). According to Kumar, Mimosa mucilage biopolymer exhibited bio adhesion time of 10 hours and more than 85% release of drug in10 hours (Shobhit Kumar & Gupta, 2012), however its use in CRFs industry is yet to be exploited.

Leucaena leucocephala seed polysaccharide (LLSP): LLSP is a galactoxyloglucan hydrophilic gum isolated from seed kernel of *L. leucocephala*. In the controlled release art, LLSP has been used for controlled release of water-soluble plus water-insoluble drugs (Singh, et al., 2011). Intercalation of nitrogen fertilizer into the *L. leucocephala* residues under different moisture situation indicated that N content in soil released from residues increased with the time. Relatively higher amount of N release was observed in *L. leucocephala* ,although the rate of N-

release was more with low N concentration residues (Das et al., 1993). In fact, this biopolymer is known to be a suitable natural disintegrant thereby being potentially useful in solid dispersion formulations for modifying rheological flow properties. It is also useful as suspending and emulsifying agent owing to its pseudo plastic and thixotropic flow patterns (Pendyala, Baburao, & Chandrasekhar, 2010).

Guargum: This is a non-ionic naturally occurring, hydrophilic polysaccharide extracted from the seeds of *Cyamopsis tetragonolobus*, and is used as binder and disintegrant (Singh, et al., 2011). It acts as the release-retarding polymer which follows a first-order release kinetic. *C. tetragonolobus* has been confirmed to be a suitable excipient for controlled release practices, although its use in CRFs is not clear and so opening door for further researches (Shobhit Kumar & Gupta, 2012). Findings revealed that increased gum concentration raises the swelling index value which is ideal for slow release kinetics (Deshmukh, Singh, & Sakarkar, 2009; Singh, et al., 2011). In addition, *Alginate* which is a natural polysaccharide obtained from marine brown algae, seaweeds as well as produced by some bacteria such as *Pseudomonas aeruginosa* or *Azobacter vinelandi* could be used in the same way. In a point of fact, Alginate is a hydrophilic salt of alginic acid consisting of two uronic acids, β-D- mannuronic acid (M) and α-L-glucouronic acid (G).

Terminalia catappa gum (TC): It is a gum exudates obtained from *Terminalia catappa* Linn. It is a natural release retarding polymer. The drug release retarding behaviour of TC gum is well studied (S. V. Kumar, Sasmal, & Pal, 2008; Patel, Joshi, Pawar, Bajaj, & Jasra, 2010). Kumar (S. V. Kumar, et al., 2008), demonstrated the excellent swelling properties of TC gum in water and its ability to sustain the release of dextromethorphan hydrobromide from matrix tablet. Therefore tablet formulations containing TC gum as an excipient may ensure the utility of the TC gum in controlled drug delivery systems of sparingly water-soluble, low molecular weight drug substance. Nevertheless, how suitable TC gum is in CRFs is not clear.

Gellan gum: This is a hydrophilic, high molecular weight, anionic deacetylated exocellular polysaccharide gum isolated as a fermentation product from a pure culture of *Pseudomonas elodea*. It consists of a tetrasaccharide repeating unit of one β-D-glucuronic acid, one α-L-rhamnose, and two β-D-glucose residues. On top of that, *Grewia gum* which is a natural,

hydrophilic polysaccharide obtained from the inner bark of the tree, *Grewia mollis* is known to hydrate on contact with water and swells to form a highly viscous dispersion making very suitable for CRFs (Jamnongkan & Kaewpirom, 2010a).

Mucunagum: Mucuna gum is a biodegradable, amorphous polymer composed of mainly D-galactose along with D-mannose and D-glucose and isolated from the cotyledons of plant *Mucuna flagillepes*. Interestingly, studies shows that formulations without crosslinking showed the fastest drug release (Gill, et al., 2010). This signifies that Mucuna based CRFs would exhibit similar features.

Gum copal (GC): It is a naturally occurring hydrophobic resin isolated from the plant *Bursera bipinnata* and shows follow zero order release kinetics. To add more, Gum dammar (GD) which is a GC sister is also anticipated to exhibit similar release kinetics as in GC. Primarily, GD is a naturally occurring hydrophobic gum obtained from plant *Shorea wiesneri*.

Karaya gum: It is a hydrophilic naturally occurring gum obtained from *Sterculia urens* and composed of galactose, rhamnose and glucuronic acid. It swells in water and thus used as release rate controlling polymers in different formulations.

Furthermore, Kumar (Shobhit Kumar & Gupta, 2012) provides an additional list of natural polymers used in controlled release systems including the following:

Rosin: a clear, pale yellow to dark amber thermoplastic resin present in oleo resins of the tree *Pinus roxburghi* and *Pinus taeda belonging* to the family Pinaceae. Rosin acts as a hydrophobic matrix forming agent for development of controlled drug delivery systems. It could be used as a binding agent, coating and matrix forming agent and so can be utilized as microencapsulating agent (Shobhit Kumar & Gupta, 2013).

Gum acacia: it is from stems of the *Acacia arabica* tree; can be used as encapsulating agent (E.-X. Lu, Jiang, Zhang, & Jiang, 2003). Locust bean gum provides excipient which give sufficient mucoadhesive applications (Dionísio & Grenha, 2012; Malik, Arora, & Singh, 2011; Vijayaraghavan, Vasanthakumar, & Ramakrishnan, 2008). Other gums in a list include, Khayagum from Khaya *grandifiola* used as binding and coating agent (O. Odeku & Itiola, 2002;

O. A. Odeku & Fell, 2004, 2005), Tragacanth gum used for sustained release (Shobhit Kumar & Gupta, 2012), Okra gum from *Hibiscus esculentus* used in the formulation of sustained-release (Kalu, Odeniyi, & Jaiyeoba, 2007), and *Hibiscus rosasinesis* mucilage used to improve binding efficacy and hence acting as release-retarding agent (Ameena et al., 2010; Jani & Shah, 2008). Moreover, olibanum and its resin (Chowdary, Mohapatra, & Krishna, 2006), Gum copal and gum dammar (Morkhade, Fulzele, Satturwar, & Joshi, 2006), Fenu greek Mucilage (Nokhodchi et al., 2008), Dika Nut Mucilage (*Irvingia gabonensis*) both used as binding agents (O. A. Odeku & Patani, 2005).

b. Modified Clays

Nano-Clay is the most common nano-particle which has been used to produce CRFs. The layered clays like montmorillonite and kaolinite are made of high aspect ratio nanolayers. Large surface areas and reactivity of nanolayers is much greater than that of micrometre size materials. Also, their surfaces and interfaces provide an active substrate for physical, chemical, and biological reactions. Because of these features nanolayers could be a suitable carrier or reservoir of fertilizers. Mechanisms which are involved in interaction between clay and organic materials depend on some factors like clay type, functional groups of organic material and physical or chemical properties of organic material. For example basic molecules bond strongly to montmorillonite unlike anionic molecules which exhibit much weaker interactions. Similarly, benzoic acid or anionic species are adsorbed on the edge face of clay (cationic or crystal violet particles) after being adsorbed on the basal plane (Ukessays.com, 2013c). Basically, modification of clay can be achieved in many ways and different types of modified clay are named according to the methods followed such as pillared layered clays, organo clays, nanocomposites clays, acid and salt-induced modified clays, and thermally and mechanically induced modified clays. The use of each modified clay types given above, preparation and their application in nano-CRFs is given by Basak (Basak, Pal, & Datta, 2012).

- Organo-Clay Chemistry

Characteristically, clay minerals are natural materials with particle size < 2 µm. Smectites, classified as 2:1 phyllosilicate clays, have a crystal lattice unit formed by one alumina

octahedral sheet sandwiched between two silica tetrahedral sheets (Figure 2.7). The ion substitution or the site vacancies at the tetrahedral and/or octahedral sheets gives rise to a negatively charged surface. The exchangeable cations between the layers compensate the negative charge and may be easily exchanged by other metal cations, explaining the high ion exchange capacities of these minerals (70–120 meq/100g). Due to this crystalline arrangement, smectites are able to expand and contract the interlayer while maintaining the two dimensional crystallographic integrity. The interlayer between units contains positive cations and water molecules (Parolo, Fernández, Zajonkovsky, Sánchez, & Bastion, 2011b).

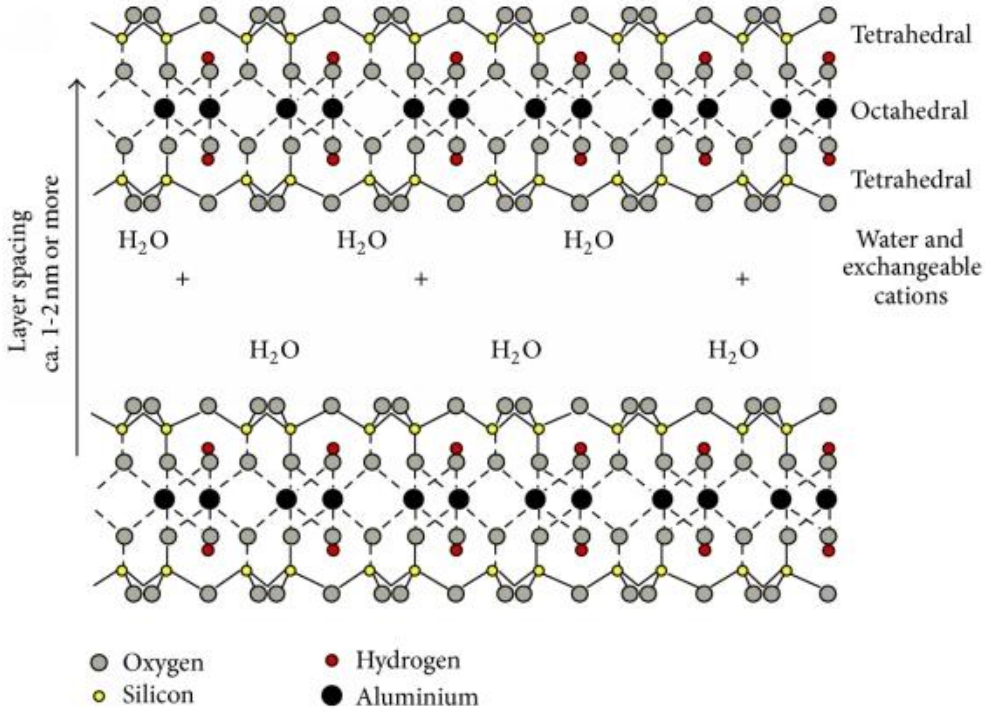

Figure 2.7. Structure of clay minerals

On the other hand, kaolinite, the main constituent of kaolin, is made up of tiny, thin, pseudo hexagonal, flexible sheets of triclinic crystals with a diameter of 0.2-12 µm. The cation exchange capacity of kaolinite is considerably less than that of smectite in the order of 2–10 meq/100g, depending on the particle size, but the rate of the exchange reaction is rapid, almost instantaneous (Grim, 1968). Kaolinite adsorbs small molecular substances such as lecithin, quinolone, paraquat, diaquat, *etc*. The adsorbed material can be easily removed from the particles because adsorption is limited to the surface of the particles (planes, edges), unlike the

smectite where the adsorbed molecules are also bound between layers. This adsorption behaviour influences researchers to investigate kaolin as a vehicle for bioactive compounds and hence creating widespread pharmaceutical application of kaolin group of minerals as it is with smectites (Aguzzi, Cerezo, Viseras, & Caramella, 2007).

Properties such as colloidal particle size, crystalline structure, high specific surface area, charge and swelling capacity confer on smectites and kaolin optimum rheological behaviour and excellent adsorption capacities for inorganic and organic substances such as drugs. In particular, the electrically charged surface of clay controls the interaction with other environmental ions, molecules, polymers, microorganisms and particles. These processes have various technological applications such as drug delivery systems, controlled release fertilizers *etc*.

c. Other Components

Several other ingredients are known to compose CRFs formulations namely, crosslinker such as glutaldehyde (Jamnongkan & Kaewpirom, 2010a) and methylene-bisacrylamide (MBA) (Liang, Yuan, Xi, & Zhou, 2009); fertilizer nutrients such as urea, ammonium nitrate *etc*.; initiators such as azobisisobutryronitrile (AIBN) (Hanafi, et al., 2000), ZnO (Hanafi, et al., 2000), and Ammonium persulphate (APS) (Liang, et al., 2009) have been used to create polymer before crosslinking; surfactants such as sodium octadecylphosphate and sometimes a dispersion medium such as cyclohexane to disperse surfactant molecules (M. Liu, et al., 2007). Infact, Different surfactants have been used in CRFs designs and the commonly used ones include non-ionic surfactant molecules (Talaat et al., 2008).

2.2.10 Polymer/Clay Superabsorbent Composites

According to Ekebafe (Ekebafe, et al., 2011), the polymer-clay superabsorbent composites have been of great interest to researchers due to their comparative low production costs and high water absorbency. Apt superabsorbent composites by graft copolymerization reaction of acrylic acid (AA) and acrylamide (Am) on attapulgite micro powder using N,N-methylene bisacrylamide (MBA) as a crosslinker and ammonium persulphate (APS) as an initiator in an aqueous solution is reported by the author. In fact, Ekebafe describes acrylamide as a kind of non-ionic monomer possessing good salt resistant performance and so a suitable raw material

for superabsorbent synthesis (Ekebafe, et al., 2011). In addition, attapulgite is described as a good substrate for superabsorbent composite materials due to its aluminosilicate layers with reactive surface hydroxyl groups.

2.2.11 The History of CRFs Formulations

a) Trends in the Nitrogenous Fertilizers

i) The first nitrogenous fertilizers: Chilean nitrate (16% N)

On the whole, the dawn of CCFs can be traced past 1800s' scientific regime allied to the history of fertilizers and their development known to gyrate around the discovery and invention of various primary materials and/or industrial processes such as nitrogen fixation into ammonia, suitable catalysts, urea synthesis, sulphur, phosphate rock, potash minerals, sulphuric acid and phosphoric acid crucial for fertilizer manufacturing industries (Tandon, 2010). As noted elsewhere, the major contributions were those of Liebig, Lawes, Haber, Bosch, Wohler, Johansen and Frasch which primarily originated in Germany, Norway, UK and North America (Tandon, 2010). As per the context of this study, the first known mineral fertilizer was sodium nitrate (16% N), also known as nitrate of soda or Chilean nitrate. It is considered as the first natural mineral containing fixed N and, the only natural source of nitrate N. In other words, it was the first known nitrogenous form of fertilizer. Candidly, the deposit of real commercial significance was initially found in north Chile sited in South America and hence the name Chilean nitrate albeit the fruitful discovery of this mineral in many other countries of the World. First commercial mining of this material was done in the early 19th century by the Spaniards and later imported to Europe and America in 1830s. Synthetic sodium nitrate was first produced in 1928 in USA, although several other manufacturing schemes are currently known to be in use widely. Despite being a fertilizer of small, localized and special applications Chilean nitrate is still used as a standard against which the salt index of various fertilizers is measured. Its salt index is taken as 100 (Tandon, 2010).

ii) The first organic compound synthesized: Urea (46% N)

Apparently, urea was the first organic compound to be synthesized from inorganic materials via separation process from urine by Rouelle in 1773, and hence the name urea. Literature shows that, in 1782, Prout separated pure crystalline urea; also, it was first synthesized by Friedrich Wohler (1800-1882) of Germany in 1828 by heating ammonium cyanate (Church, 1964; Tandon, 2010). According to another source (Organization & Center, 1998; Tandon, 2010; UNIDO-IFDC, 1979), urea was first synthesized by reacting ammonia with cyanuric acid. In any case, the synthesis of urea by Wohler revolutionized the chemical technology scene in general and the fertilizer scene in particular to such an extent that he himself may not have expected. Commercial production of urea had to wait until 1922 after the large scale synthesis of ammonia was made possible by Fritz Haber (1868-1934) and Carl Bosch in 1910. The I.G. Farben industry in Germany was the first company to synthesize urea commercially from ammonium carbamate in 1920. In 1922, large scale production of urea by the BASF process started. Urea now dominates the N fertilizer scene.

iii) Ammonium Sulphate (21% N)

Ammonia was first recorded in 1754 by J. Priestly who upon distilling ammonium chloride with quick lime was able to produce ammonia gas (Tandon, 2010). Ammonium Sulphate was first produced as a byproduct of the coke oven industry towards the mid-half of 19^{th} century. In other words, it was the first nitrogenous fertilizer to be produced, first as a byproduct of the manufacture of coal gas in 1815 in England and later from coke-oven battery gas (Beaton, 2005). By 1905, the idea of passing air through an electric arc was successfully developed in Norway to produce nitric acid. The path-breaking synthesis of ammonia in a reactor was achieved by two Germans Fritz Haber and Carl Bosch in 1910 (Tandon, 2010). The key link in ammonia synthesis was the search for a suitable and easily available catalyst. One of Bosch's colleagues was fortunate to find that red iron oxide was as good as the scarcely available osmium. In recognition of their contribution, Haber was awarded the Nobel Prize in 1918 and Bosch in 1931. In a point of fact, Carl Bosch (the Nobel Prize Laureate) unveiled that more than 20,000 experiments were carried out in the course of engineering catalyst apt for industrial synthesis of ammonia (Tandon, 2010; Timm & Danz, 1964).

According to (Tandon, 2010), the first commercial plant for ammonia synthesis began operation in 1913 by BASF AG at Ludwigshafen-Oppau in Germany. Soon it yielded 30 tones of fixed N/day. This period and development can be considered as the starting point for large scale production of a variety of concentrated fertilizers containing nitrogen alone as in urea or an array of NP/NPK materials.

iv) Anhydrous Ammonia and Nitrogen Fertilizers

Similarly, it was said by (Tandon, 2010) that, solid and liquid fertilizers also emerged as an important N fertilizer on its own. Anhydrous ammonia was first applied directly in the field on a commercial scale in the United States during 1943-44; it's diluted form, *i.e.*, aqua ammonia or rather ammonium hydroxide was found to be useful in fluid fertilizers.

v) Calcium Cyanamide (35% N)

Fundamentally, calcium Cyanamide or cyan amide is one of few CCFs known in the category of N-fertilizers which does not take the ammonia synthetic route. The first synthesis of this fertilizer was carried out by Frank and Caro in Germany in 1898 by reacting calcium carbide with N at high temperature (Tandon, 2010; Timm & Danz, 1964). In 1905 the first facility for its industrial production was set up in Italy; thereafter in 1910 commercial production was initiated in USA where literature depicts that production reached 14,000 tons per year by the end of 1930s and owing to that it became a popular fertilizer for many years in the west (Tandon, 2010).

vi) Ammonium Nitrate (33%) and Calcium Ammonium Nitrate (20-26%)

The initial production of ammonium nitrate (AN) which is known to be used as an explosive during the WWI started in Europe following the success in the commercial production of ammonia gas as described before (Tandon, 2010). Thereafter, it was used for the first time as CCF after World War I when the war surplus material was released for other uses. In attempt to eliminate environmental hazards associated with its explosion when in contact with organic materials or other unfavorable conditions, AN was modified by using limestone and in turn calcium ammonium nitrate (CAN) came to being as a result thereby lessening the N content in from 33% in AN to 20-26% in CAN (Tandon, 2010).

vii) Fertilizers Containing NP and NPK

Literally, in 1926 the superphosphate group of fertilizers which include the Mono Ammonium Phosphate or MAP ($NH_4H_2PO_4$) (21% N) and Diammonium Phosphate or DAP $(NH_4)_2HPO_4$ (21%) was first ammoniated with aqua ammonia to synthesize ammonium phosphate in the US (Tandon, 2010). Equally, the first large-scale continuous production of DAP was instigated between 1920 and 1954 where two grades of DAP were commercially produced in the US using wet process phosphoric acid began. Afterwards, the modern-day processes for the MAP and DAP production were developed at the TVA (Tandon, 2010).

viii) Nitro-Phosphates

According to (Tandon, 2010), the nitro phosphates (aka, nitric phosphates or ammonium nitrate phosphates [ANPs]) are CCFs forms wherein phosphate rock is acidulated with nitric acid unlike in super phosphates (described above) where sulphuric acid, phosphoric acid or ammonium phosphates is used to acidulate the rock. At some point in 1927-1928, Erling Johansen was recorded to have invented the nitro phosphate process and named it as the ODDA process after the town of ODDA in Norway where it was developed. On the same line, PEC process was another synthetic route invented for the production of nitro phosphates referring to the French firm Potasse et Engrais Chimiques (Tandon, 2010). Since 1938 when the nitrophosphates were first commercially produced in Norway till now, R&D created variety of nitro phosphate grades and that, all the nitro phosphates produced contain 50% of their N as nitrate and 50% as ammonium. The water soluble proportion of their total P_2O_5 varies from 30% to 90% depending on the process used (Tandon, 2010).

ix) Ammonium Phosphate Sulphate (APS)-20% N and Urea Ammonium Phosphate (UAP)

The times gone by since the first production of APS can be taken as back as 1933. Hitherto, the most marketed APS grade produced does contain 20% N, 20% P_2O_5 and 13% S. Conversely, UAP are complexes of Mono ammonium phosphate and urea and that, probably its production goings-on started in Japan past more than 50 years ago. Later, technology for the production of urea ammonium phosphate was also developed at the TVA (Tandon, 2010).

x) NPK complex fertilizers (12% N)

Conspicuously, literature survey shows that, the inquisitiveness in the development and then production of NPK complex fertilizers smoothly progressed as a result of the following scenarios: (i) the development of ammonium phosphates, (ii) the easy availability of MOP and the associated potash sources, and (iii) the invention of nitro phosphate synthetic scheme in 1965 which likely was a step forward towards the commercial production of NPK complex fertilizers (Tandon, 2010).

b) Trends in the Controlled Release Fertilizers

Accordingly, the subject of CRFs (also termed as Enhanced Efficiency Fertilizers" [EEF]) was born out curiosity in controlling the rate of release of soluble fertilizer N, improving FUE as well as the need for minimization of toxic agronomic effects. According to (Shaviv, 2001; Trenkel, 2010; Zhang, Zhang, & Ma, 2009) "the production technology for the new fertilizer industry came mainly from research institutions and the R & D platforms of fertilizer industries. As early as the 1930s, from the N fertilizer production using synthetic ammonia, European countries and the US, made use of the newly introduced technology of organic synthesis and developed organic N fertilizer grades with slow-release functions. These include urea formaldehyde and isobutylidenediurea (Shaviv, 2001). In the 1960s, high biopolymer technology was rapidly applied in the research on coated fertilizer and they developed CRF products coated with alkyds and phenolics. In the 1970s, research on controlled release N fertilizers such as polyolefin coated urea was undertaken" (Zhang, et al., 2009).

As we have described before (Sempeho, Kim, Mubofu, & Hilonga, 2014), the commonly known examples in the CRFs group is urea formaldehydes or ureaforms whose production scheme was patented by BASF in Germany in 1924 which on 1947 the produced ureaforms materials were patented as fertilizer formulations in the USA and then commercially produced in 1955 (S Landels, 2010; Tandon, 2010). Classically, ureaforms were prepared by reacting urea with formaldehyde under controlled conditions keeping U:F mole ratio >1 (Tandon, 2010); in that way, a typical ureaform contains 38% N. According to (Tandon, 2010; Trenkel, 2010) the family of ureaforms contains a range of product depending on polymerization including, methylene

ureas (MU) containing intermediate chain length polymers (this was developed during the 1960s), methylene diurea (MDU) containing short chain polymers (this was developed in the 1980s), and later more other CRFs were formulated including isobutylidene diurea (IBDU) containing 31% N (produced in Belgium, Germany and Japan), crotonyledene diurea or CDU containing about 32% N (produced in Japan), Sulphur coated urea (SCU) developed by the TVA (US Patent 3,295,950), NPK fertilizers coated with sulphur developed in Japan (Miyata, 1989; Tandon, 2010).

Into the bargain, an additional group of CRFs developed during that same era include the polymer coated fertilizers initially produced in the USA starting in 1967 under the brand name "Osmocote" (Tandon, 2010). According to (Mayer, 2010), "the Osmocote market has mainly been limited to high value plants such as commercial ornamental nurseries, greenhouses, citrus and strawberry production"; as a result, the need for more research came up where another type of coating based on a polyurethane-like coating was developed; it was obtained by reacting poly-isocyanates with polyols on the surface of the fertilizer and forming an attrition-resistant CRF. This technology was called Reacted Layer Coated Fertilizer (RLCF) (Mayer, 2010). Principally, RLCF may be useful in a number of prilled materials to accomplish good control over the nutrient release pattern and rate. Some commonly marked products with this technology can be found elsewhere (Mayer, 2010). The development of CRFs and their respective characteristics may be found in a detailed account elsewhere (S Landels, 2010; Trenkel, 2010). According to (Tandon, 2010), "various innovative, challenging and dedicated developments by intelligent and hard working chemists, technologists and entrepreneurs gave birth to and shaped the fertilizer sector" and that, major places of action were Germany, Norway, UK and the USA whereas major contributions in the CRFs history include those of Liebig, Murray, Lawes, Haber, Bosch, Frasch, the TVA Group along with all those who discovered major mineral deposits. "Leaders are always few in number whether one talks of men or materials (Tandon, 2010)".

Essentially, since the onset of the actual CRFs technology in 1950s and the subsequent max out urbane improvements of CRFs products between the 1980s and 1990s, the earliest marketable CRFs formulations offered for sell were strictly N-based; however, the CRF technology has currently expanded to include potassium (K), phosphorus (P), and other nutrients including micronutrients (Mayer, 2010). A point to remember about the why's of CRFs as opposed to

quick-release fertilizers (QRFs) (G. Liu et al., 2014) is as we have said and as said elsewhere that: the aim of CRFs engineering particularly in the N-related fertilizers owing to certain attributes already mentioned earlier is to control the volatilization of ammonia in ABC along with the control the release of water-soluble N fertilizer, which is chiefly the processes of ammonization and nitrification of urea to reduce loss, with the objective of increasing the utilization of N fertilizer (Sempeho, et al., 2014; Trenkel, 2010; Zhang, et al., 2009). Correspondingly, the main factors determining the effectiveness of CRFs are the coating agent's magnitude and the ratio of coating materials. Equally, the easiest way to critically contemplate the literature a propos the trends on the CRFs' progression entails categorizing the history into three stages namely, the exploration era; the popularization era; and the integration era with industrial production of CRFs as noticed elsewhere (Fan, 2009); that said, what we have described in this section is just a diminutive abridgment of CRFs holistically described, but for a better understanding one should follow the three categories mentioned to better grasp the perspectives of CRFs formulations and their emergence.

2.2.12 The ABCs of the Oldoinyo Lengai Volcanic Ashes

Fundamentally, Oldoinyo Lengai is one of the few currently known active volcanic mountains that emit carbonatite volcano lavas. It is found in Tanzania ($2^{o}45'S$, $35^{o}54'E$); nevertheless, details of its geographical location can be found in chapter nine (9) of this document. According to (Dawson, 1998), the volcanic ashes sampled from Oldoinyo Lengai are younger peralkaline nephelinites (< 2000 a) and that, mineralogically they're constituted of wollastonite nephelinite with alkalinity indices ([Na + K] / Al) of 1.43 through wollastonite-combeite nephelinite to combeite nephelinite with alkalinity indices ([Na + K] / Al) of 2.15. Actually, both of these minerals are known to have a common set of phenocrysts namely, nepheline, clinopyroxene, Ti-andradite, combeite and apatite; however, it was reported that some of the phenocrysts and groundmass phases are different such as wollastonite phenocrysts and groundmass melilite found in wollastonite nephelinite; and phenocrystal sodalite and groundmass lamprophyllite i.e, delhayelite and aegirine rich pyroxene found in combeite nephelinite. Besides, combeite nephrite is known to be richer in alkalis, Ba, Sr and halogens than in wollastonite nephelinite; this phenomenon was ascribed to several reasons discussed elsewhere (Dawson, 1998). Although my aim is not to go into the details of mineralogy of Oldoinyo Lengai volcanic ashes, it is equally

significantly necessary to summarize the mineralogy of Oldoinyo Lengai volcanic ashes as outlined below:

a. Phenocrysts

This includes (i) Nepheline which consist of phenocryst cores containing about 20-22 mol percent kalsilite (Ks) and excess Si together with zones and patches containing various amounts of K and Fe; (ii) Combeite which consist of excess Na over the simplified $Na_2Ca_2Si_3O_9$ end member composition together with significant concentration of Fe and Mn.

b. Clinopyroxene

This consist of molecular compositional variations of aegirine, diopside and hedenbergite (takes > 95%) and low alumina pyroxenes (takes < 1.50%) and TiO_2 (< 1.0%).

c. Ti-andradite

Here the garnet fall within the compositional range of ijolites which range from melanite to schorlomite with varying concentration of Ti and Fe and minors of Na_2O (0.52 weight percent), Mn (0.45 weight percent), and ZrO_2 (0.64 weight percent).

d. Titanite

This contain three main elements namely, Ca, Ti and Si together with minor amounts of FeO (1.86 weight percent), and Na_2O (0.52 weight percent), Nb_2O_5 (0.83 weight percent), ZrO_2 (0.62 weight percent), SrO (0.61 weight percent), and Ce_2O_3 (0.17 weight percent).

e. Apatite

The compositional variation ranging from SrO, La_2O_3, Ce_2O_3 *etc*., has been broadly reviewed in Dawson (1998).

f. Sodalite

This is characterised with unusual high concentration of Fe_2O_3 and low but substantial amount of K_2O.

g. Wollastonite

The unique feature of Oldoinyo Lengai Volcanic ashes is that despite diverse compositional differences in the mineralogy, the difference between the wollastonite in wollastonite nephelinite and wollastonite-combeite nephelinite is not significant.

h. Groundmasses

Similalr, these are known to contain (i) potassic nepheline which are rich in Fe_2O_3; (ii) combeite and sodalite; (iii) pyroxene; (iv) melilite which are iron and soda rich; (v) delhayelite which is halogen rich aluminosilcate (KCaNa); (vi) perovskite; (vii) lamprophyllite; (viii) magnetite; (ix) glass which consist of silica undersaturated and high in Fe, alkalis, F, Cl, S and low Mg.

Conclusion

Regardless of being widely used, fertilizers particularly nitrogenous ones by virtue of their high nitrogen content (≈ 46%) and somewhat low cost of production, most of them are associated with up to 60 to 70% loss of the nitrogen being applied owing to ammonia produced through hydrolysis of say urea by soil urease ($NH_2CONH_2 + H_2O \rightarrow 2NH_3 + CO_2$). Fundamentally, due to surface runoff, leaching and vaporization, the utilization efficiency or plant uptake of urea for example, is generally below 50% thereby escalating fertilization expenditure per season and reduce crop productivity. Such drawbacks related to the use of nitrogenous fertilizers could be corrected by amending conventional nitrogenous fertilizers with suitable excipients in order to manufacture CRFs so as to improve FUE by plants and minimize the losses thereby reducing repeated fertilization expenditure per season and maximize crop yields. CRFs reduces the demand for short-season manual labour obligatory during critical periods, reduces stress and specific toxicity (as a result of synchronizing nutrient release with plants' demands), increase availability of nutrients, supply of nutrient forms preferred by plants, and augment synergistic effects between nutrients and plant roots. In that viewpoint, it is worth noting that researchers

ought to design Nano-CRFs by using natural excipients materials to come up with efficient, effective, reliable and cost effective CRFs formulations basing on the prevailing resource limitations thereby minimizing food crisis and other challenges facing crop production. Essentially, scientists should anticipate to mend agronomic returns through scientific novelties; the motive behind must be geared towards researching, innovations and commercialization of the CRF products.

CHAPTER THREE

The Properties of Feldspathic Dental Porcelain from Tanzanian Aluminosilicate Materials: A Preliminary Study[2]

Abstract

Kaolin and quartz from Pugu and feldspar from Morogoro were used to produce feldspathic dental porcelain bodies. Mineralogical results from XRD revealed the presence of kaolinite, illite, microcline and clinochlore in the kaolin samples; albite, microcline, sanidine in the feldspar samples and only silica in the quartz samples. The chemical results studies by XRF revealed the presence of BaO, SiO_2, Al_2O_3, TiO_2, Cr_2O_3, MnO, K_2O, CaO, Cl, SO_3, MgO, Na_2O, and Fe_2O_3 in varying proportions. Particle size distribution of all the raw materials were determined and particles < 63 μm were used for preparation of batches. The batches of different compositions with ranges: quartz (12-22%), feldspar (75-88%) and kaolin (3-5%) were fired at 1100, 1200 and 1250 °C, and the developed properties were tested. The physico-mechanical properties studied exhibited volumetric shrinkage between 2 and 55.17%, open porosity between 6.67 and 40.00%, water of absorption between 7.1 and 40%, bulk densty of 1.43 – 5.68 g/cm3, and compressive strength at 0.13 - 32.25 MPa. The optimal firing temperature for the best results was found to be 1250 °C. The results obtained indicate that kaolin and quartz from Pugu and feldspar from Morogoro are potential raw materials for the production of dental porcelain

3.1 Introduction and Literature Review

Dental ceramics are the preferred materials for oral restorations capitalising on its favourable characteristics, such as; adequate aesthetics, high fracture strength and chemical stability (Rosenblum & Schulman, 1997). Dental ceramics may also be used to create crowns, veneers,

[2] Siafu, S. I. and E. H. J. Lugwisha (2014). "The Properties of Feldspathic Dental Porcelain from Tanzanian Aluminosilicate Materials." International Journal of Development Research **4**(11): 2260-2265

inlays, onlays and denture teeth. A desirable feature of ceramics is that their appearance can be customised to simulate the colour, translucency and fluorescence of natural teeth. They are biologically and chemically inert, inherently brittle with a good resistance to abrasion. When ceramic powder is comprised of quartz, kaolin, pigments, opacifiers, and a suitable flux with distilled water, the product is traditionally known as dental porcelain. A more acceptable terminology is dental ceramics, however, these two terms are always used interchangeably (Jablonski, 2008). The classification of dental porcelain based on composition include, feldspathic porcelains, leucite reinforced feldspathic porcelain, aluminous ceramics, glass infiltrated composites, alumina polycrystals, glass ceramics, leucite reinforced glass ceramics, lithium disilicate reinforced glass ceramics and zirconium oxide ceramics (Martínez Rus, Pradíes Ramiro, Suárez García, & Rivera Gómez, 2007). The classification can also be based on the residence temperature during the firing circle, resulting into three categories namely high (1300 – 1400 °C), medium (1100 – 1300 °C), and low (850 – 1100 °C) fusing dental porcelains (Carradó, 2001; Moffa, 1988) High fusing dental porcelains are used for denture teeth, medium for pontics, whereas the low fusing porcelain are used for metal-ceramic restorations. The composition of typical feldspathic dental porcelain by weight is; feldspar (75-85%), quartz (12-22%), kaolin (3-5%) and metallic pigments which increase opacity of dental porcelain (< 1%) (Craig, Peyton, & Asgar, 1975). Scientific investigations have been carried out on the applications of Tanzanian kaolin, quartz and feldspar in refractories and other industrial uses (L.D Akwilapo, 1999; Leonard D Akwilapo & Wiik, 2003, 2004; Lobitzer, Giacomini, Muller, Notstaller, & Schwaighofer, 1982; E. Lugwisha, 2009a, 2009b; Lynne, Strand, & Lyng, 1980; Mwakarukwa, 1988) but up to this moment there are no literature explaining their applications in dental industry. This research therefore explored the suitability of some selected Tanzanian non-metallic silicate minerals in the dental application. The study in particular dealt with feldspathic porcelains in low and medium firing temperatures utilizing kaolin, quartz and feldspar. The properties of dental ceramics which were determined in this study included chemical composition, mineralogy, density, porosity, volumetric shrinkage and compressive strength. Testing results from each property were used to assess the suitability of the fired samples.

3.2 Materials and Methods

3.2.1 Raw materials

The raw materials were kaolin clays and quartz from Pugu deposits and feldspar from Morogoro Tanzania. The chemical composition of the raw materials was determined by XRF using the Semi Quantitative XRF Analysis technique (Siemens SRS 3000 X-ray Fluorescence (Rhodium anode, 8 analyzer crystals with beryllium windows 125 μm). The semi quant program was used throughout. The mineral characterization of the raw materials were performed on Siemens D-5005 X-ray Diffractometer using Cu Kα1 radiation (λ = 1.54056 Å). The samples underwent diffraction in the measuring range 2θ ranging between 2°– 65°.

3.2.2 Particle size distribution of the raw materials and Batch composition

The grain size distribution was determined from weight distribution in screen residues combined with sub-sieve analysis carried out using Andreasen pipette sedimentation method. In kaolin, the non-clay fraction was 37.57% while the clay fraction in the range 0 – 63 μm was 62.43%. In feldspar and quartz, grain particle size in the range > 63 μm were 24.82, 22.16 and in the range between 0 – 63 μm were 75.18, 77.84, respectively. The 0-63 μm particles sizes were selected for all raw materials for batch preparation in order to improve the physico-mechanical properties of the test specimens (Il'ina, 2007). The use of raw materials of heterogeneous composition such as 0-63 μm ensures reduced void spaces as a result of an increase in the inter-particle contacts of small particles (Von Fraunhofer, 2013).

3.2.3 Sample preparation

Kaolin purification was done by means of wet beneficiation followed by homogenization to minimize errors attributable to sample heterogeneity. Then clay fraction separation (by means of deflocculating agent and peristaltic pumps) was done to obtain fractions needed for XRF and XRD analysis. Batch compositions typical of the ranges used in dental porcelain were chosen. Thirteen different body compositions were prepared; these are indicated in Table 3.1. The body formulations were mixed with a given volume of water so that the resulting slip contained 35% water. Sodium silicate (3%) and sodium hexametaphosphate were added in order to act as deflocculant. The mixtures were ball milled and left to equilibrate for 36 hours to allow particles

in the slips to undergo sorption reactions with electrolytes and surfactants in the liquid while altering their viscosity and casting characteristics. The slips were then casted into truncated cones in plaster of Paris moulds.

Table 3.1. Batch compositions (mass percent) of the raw mixes used in dental porcelain

Batch → Components ↓ (mass percent)	S_1	S_2	S_3	S_4	S_5	S_6	S_7	S_8	S_9	S_{10}	S_{11}	S_{12}	S_{13}
Feldspar	75	76	77	78	79	87	81	82	83	84	85	80	77
Quartz	20	19	19	19	19	12	18	15	14	14	13	19	22
Kaolin	5	5	4	3	2	1	1	3	3	2	2	1	1

3.2.4 Drying and Firing

The cones were dried in an open air for seven days and then in an oven at 110 °C for 48 hours. The prolonged drying was considered suitable for the purpose of avoiding surface cracking which would have occurred during firing due to excessive surface drying. Advanced firing was done at 1100, 1200 and 1250 °C, at a holding time of 8 hours at a heating rate of 300 °C per hour. The fired samples were then allowed to cool slowly at room temperature by natural convention for 24 hours.

3.2.5 Volumetric shrinkage

The volume of specimens with truncated cone shapes were determined by the formula $V= (\pi/3)h(Rr + R^2 + r^2)$ before and after firing. Where R and r are the radii of (base circle and top circle, respectively) the ends of the cone; h is the height of the cone. R, r and h were measured by using veneer caliper. The difference in volume before and after firing was used to calculate percentage shrinkage by using the formula $(\Delta V/V1) \times 100$; where ΔV is the volume difference and V1 is the volume before firing.

3.2.6 Open Porosity

Weights of dry specimens were determined by using Sartorius analytical balance. True and bulk volume was determined by using measuring cylinder and the formula $\rho = W/V$ was used to

determine the true density and the bulk density; where ρ = density, w = weight and v = volume. Porosity (Q) was then determined by using the formula: 1-ρbulk /ρ particle.

3.2.7 Water of absorption

The specimens were soaked in water at room temperature for 48 hours. The mass before and after saturation was determined and thereafter used to calculate percentage water absorption by using the formula:

Percentage water absorption = Ma – Mb/Mb x 100%. Where, Ma = mass after saturation (saturated specimen), Mb= mass before saturation (dry specimen).

3.2.8 Bulk Density

The bulk density, B (g/cm^3), of the specimen is the quotient of its dry mass divided by the exterior volume, including pores, is given by B = D/V. Where D is the mass of dry specimen and V is the exterior volume. The exterior volume, V is given by, where M is the saturated mass and S is the suspended mass.

3.2.9 Compressive strengths

For load determination, each specimen was compressed by compression tester UTM of type UPD 40 with energy 400 V, 50 Hz, 6A and maximum load 400 KN. Compressive strength was then determined from the formula: Cs = L/A. Where, Cs = compressive strength, L = load in Newton, and A = area in mm^2.

3.3 Results and Discussion

3.3.1 The chemical composition

The chemical composition and the loss on ignition (LOI) are presented in Table 3.2. The dominant oxides for kaolin (63.64%, 31.43%) and feldspar (62.3%, 14%) were SiO_2 and Al_2O_3, respectively, the typical proportion percentage constituents needed for dental feldspathic glass.

As can be seen, there is a significant amount of alumina in both kaolin and feldspar. Alumina in dental porcelains is known to increase the strength of the dental ceramic materials (Chu et al.,

2003) and is useful in maintaining opacity properties (McLean & Hughes, 1965; Southan, 1968). Alkali oxides whose role is to improve the coefficient of the thermal expansion of the ceramic articles were found in significant amount (13%) in feldspar in which only BaO was also detected; in fact, the levels of coloured oxides TiO_2 which imparts yellow brown colour, Cr_2O_3 green colour, MnO for lavender pigment and Fe_2O_3, were in acceptable amounts. Fe_2O_3 is useful for colouring dental porcelain (Southan, 1968) but when colouring is not needed this oxide becomes undesirable. The quartz used was seen to contain considerable amount of silica needed in the batches.

Table 3.2. Chemical compositions (mass percent) of the raw materials

Sample Parameter	Raw Kaolin (%)	Feldspar (%)	Quartz (%)	Beneficiated Kaolin (%)
SiO_2	63.64	62.30	94.93	54.99
Al_2O_3	31.43	14.00	0.38	40.20
Na_2O	0.43	0.81	-	0.09
MgO	0.16	0.04	0.04	0.13
SO_3	0.25	0.98	1.00	0.08
Cl	0.76	0.19	0.19	0.04
K_2O	1.39	12.20	0.09	0.96
CaO	0.06	7.65	0.98	0.04
TiO_2	0.80	0.04	0.11	1.02
Cr_2O_3	0.03	0.14	0.21	0.04
MnO	0.01	0.04	0.03	0.01
Fe_2O_3	1.01	0.85	1.95	2.00
BaO	-	0.46	-	-
LOI	0.03	0.30	0.09	0.40
Total	100	100	100	100

Source: Researcher

3.3.2 The Mineralogical Composition

Clay minerals and non clay minerals identified in kaolin and feldspar are given in Figure 3.1. XRD results revealed that the major content in kaolin samples was kaolinite [$Al_2Si_2O_5(OH)_4$] at d = 7.16, 4.41, and 3.56 Å around 14° and 29° 2θ, respectively, surbordinated with illite [$KAl_2(Si_3AlO_{10})(OH)_2$] at d = 3.33 Å around 31° 2θ; while the minor minerals observed in kaolin were quartz (SiO_2) at d = 4.25 (24° 2θ) and 3.34 Å (31° 2θ) and microcline [$KAlSi_3O_8$] at d = 4.22 (25° 2θ). In the feldspar sample, the prominent minerals were Albite [$NaAlSi_3O_8$] at d =

4.02 (26° 2θ) and 3.19 Å (33° 2θ) and Microcline [$KAlSi_3O_8$] at d = 4.22 (24° 2θ) and 3.24 Å (32° 2θ). The minor peaks were observed in the mineral sanidine [$K(Si_3Al)O_8$] identified by the presence of peaks around 27°, 35°, and 54° 2θ and oligoclase [$(Na,Ca)Al(Al,Si)Si_2O_8$] identified by the presence of peaks around 38°, 42°, 45° and 49° 2θ. In quartz, the mineral silica (SiO_2) was the only peak at d = 4.25 and 3.34 Å.

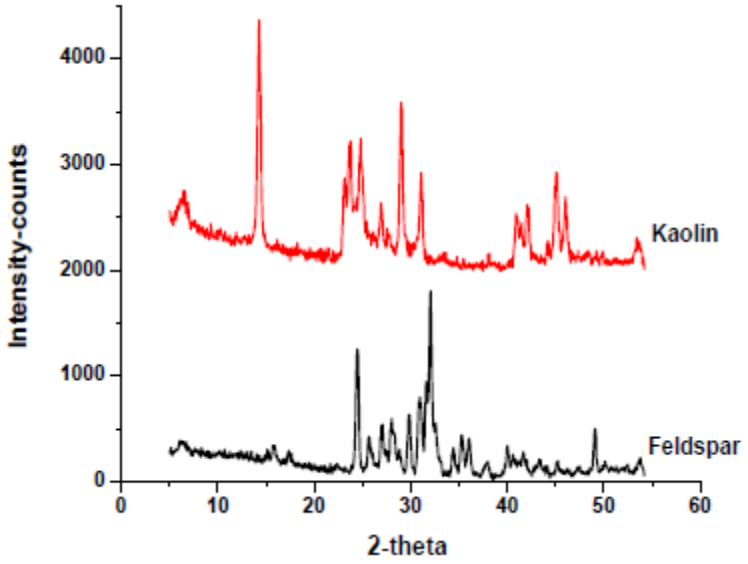

Figure 3.1 XRD patterns of (a) Kaolin from Pugu and (b) feldspar from Morogoro

3.3.3 Volumetric Shrinkage

The variation of percentage shrinkage with firing temperatures 1100, 1200 and 1250 °C and composition (Figure 3.2) shows that shrinkage is a function of batch composition and temperature. The non-uniform shrinkage pattern has been obtained in different composition fired at the same temperature. However, the onset of shrinkage above 1000 °C, which is known to depend on the formation of liquid phase, depends on the composition of the batches (L.D Akwilapo, 1999). Bodies with high silica content normally experience a low shrinkage during firing while bodies with high feldspar start to densify at as low as 1000 °C thus cause higher contraction (Kobayashi, Ohira, Ohashi, & Katoh, 1991). For example the highest shrinkage at 1250 °C is recorded for S6(K1-F87-Q12) batch. It is reasoned that the low quartz content in the raw porcelain mixes, which decreased even further after firing, caused the higher shrinkage of this sample. Associated with this was the higher content of feldspar which also participates in the

melt formation. From Figure 2, it is revealed that firing temperature and holding time affect shrinkage more than does composition of the fired specimen. The effect of composition was seen to be substantial upon dealing with specimen of different composition fired at the same temperature but upon raising firing temperature to about 50 °C, the effect of composition was outweighed by the changes brought in through rise in temperature. It was noticed that shrinkage increased to about twice when firing temperature rose from 1100 to 1250 °C. The reason behind this is that, the distribution and size of particles involved in solid state reactions significantly affected the firing shrinkage of porcelain materials because at high temperature, fusion of particles and their ability to penetrate inter-particle spaces is maximized (Fraunhofer, 2009). There is a decrease in void spaces and an increase in densification and compaction with raise in firing temperature. Results obtained from this study are in line with the results described by (Southan, 1968).

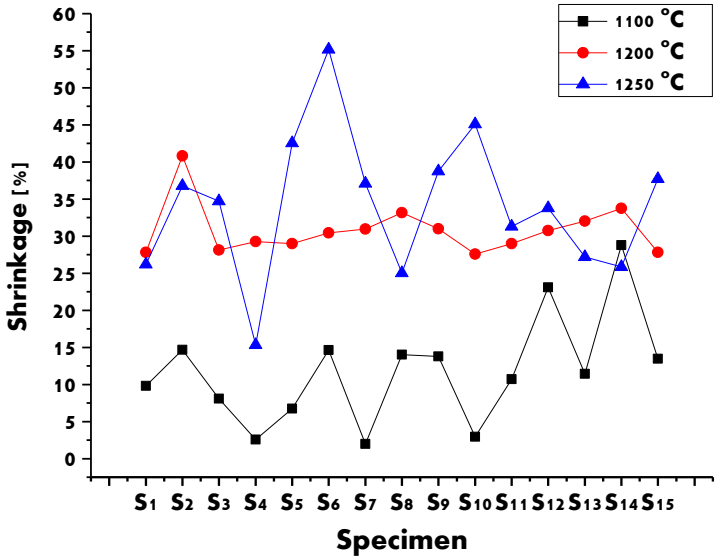

Figure 3.2. Variation of volumetric shrinkage with firing temperature

3.3.4 Porosity

The general trend observed (Figure 3.3) revealed that there was a decrease in porosity with an increase in firing temperature from 1100 to 1250 °C, hence porosity was seen to be dependent on firing temperature. All compositions prepared in this work exhibited very low porosity at 1250 °C. The decrease of open porosity at higher temperature is associated with the further formation

of melt/liquid phase which blocks the open porosity of the body and reduces them on cooling (Leonard D Akwilapo & Wiik, 2003). This observation is reported by (Gobi, Rajamannan, & Viruthagiri, 2009) who also noted that the amount of liquid phase increases with firing temperature. However, in some cases porosity may increase at higher firing temperature (> 1200) than expected as observed in batches S, S3, S10-S13. Such increase in porosity at higher firing temperature is thought to be caused by bloating which takes place as gases are expelled from the matrixes and cause an increase in porosity (L.D Akwilapo, 1999; Cheung & Darvell, 2002).

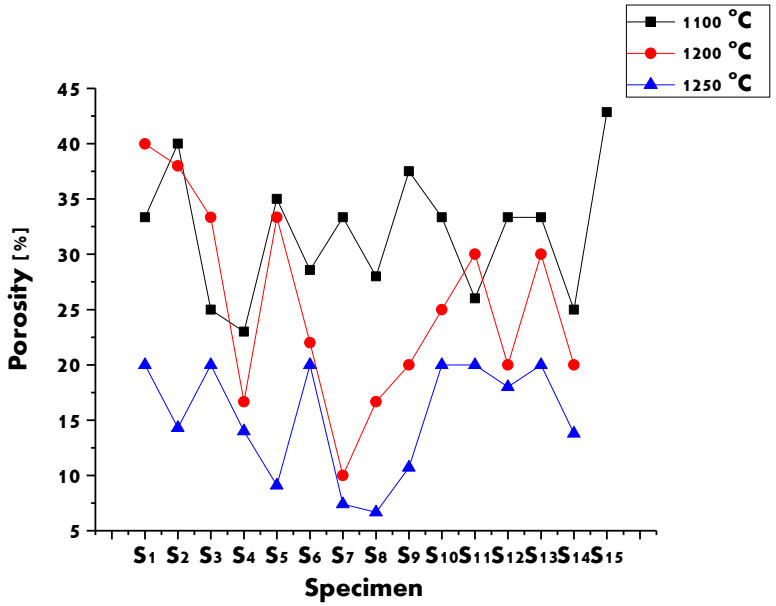

Figure 3.3. Variation of porosity with firing temperature of the 13 batches

3.3.5 Water of Absorption

It is clearly seen (Figure 3.4) that percentage water of absorption was found to decrease substantially when firing temperature was raised from 1100 to 1250 °C. Water absorption decreases with increase in temperature due to the formation of the liquid phase at high firing temperatures. The liquid phase formed is the one which fills the pores and decreases the porosity. Similar trend was obtained by (Khabas, Kulinich, Vereshchagin, & Babushkin, 2003), where he found that upon firing dental porcelain specimen at 900 °C, 1000 °C and 1100 °C the percentage water of absorption kept on decreasing. The difference with (Khabas, et al., 2003) results and our results is that he obtained very low percentage water of absorption of 1.10% 0.97% and 0.78% at 900, 1000, and 1100 °C respectively. His results might have been influenced by the undercoat

layer on the samples which acted as a mask. Water absorption is directly related to open porosity. According to (Khabas, et al., 2003) high water of absorption signifies an increased open porosity.

3.3.6 Bulk Density

The variation in bulk density of the tested samples (Figure 3.5) shows that bulk density increased with increase in firing temperature. This is because at higher temperature samples will form higher amount of melt phase, the more melt is formed the higher will the density of the material be, this is due to the filling of the pores by melt (Leonard D Akwilapo & Wiik, 2003). The bulk density also shows dependence on the amount of kaolin mixed in the batches. Batches with relatively higher kaolin content e.g. S_1 and S_2 showed a higher value of bulk density. However, the bulk densities obtained from all compositions and temperatures in this study were found to be low for the production of dental materials with compressive strength comparable to natural teeth strength (Williams, 1979).

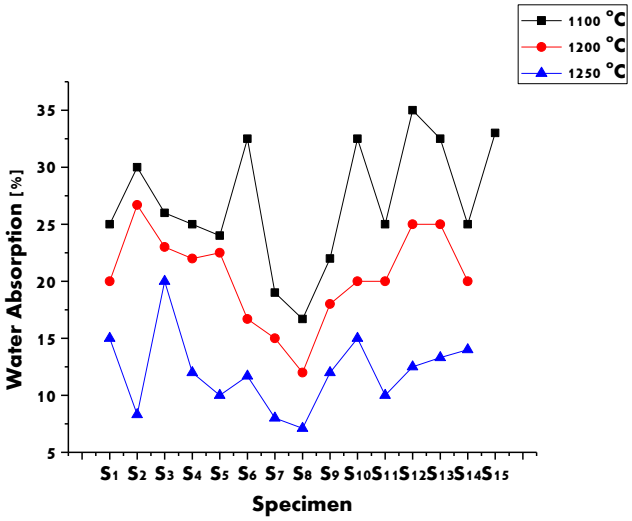

Figure 3.4. Variation of water of absorption with firing temperature

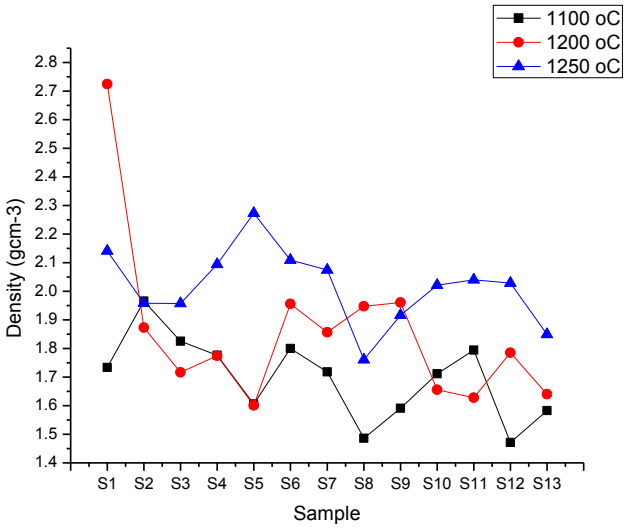

Figure 3.5. Variations in bulk density with firing temperature of the of the 13 batches

3.3.7 Compressive Strength

Compressive strength was observed to increase with increasing firing temperature from 1100 to 1250 °C. Indeed, it was clearly seen that all specimen used showed a decreasing porosity when firing temperature was raised from 1100 to 1250 °C (Figure 3.3) which is also related to the increase of bulk density. This might be one of the factors leading to the patterns observed in Figure 3.6. Similar observation was made by (W. Yan et al., 2011) whose results revealed that the decrease in porosity, increase in bulk density and well distribution of pore sizes are factors which can be ascribed for increased compressive strength. At 1250 °C, the highest compressive strength observed was 32.25 MPa for S_1 composition. However, the compressive strength results obtained in this study are compared below with standard samples reported in the literature. Khabas (Khabas, et al., 2003) report the compressive strength of four samples as: 31.97 MPa, 39.30 MPa, 39.48 MPa and 48.00 MPa for GFSn (abrupt cooled), GFSn (slow cooled), GF + 10% SnO_2 and natural tooth dentine, respectively. On the other hand, (Williams, 1979) in his work reported the compressive strength of ten samples on dental stone materials in the range 51.71 – 78.6 MPa.

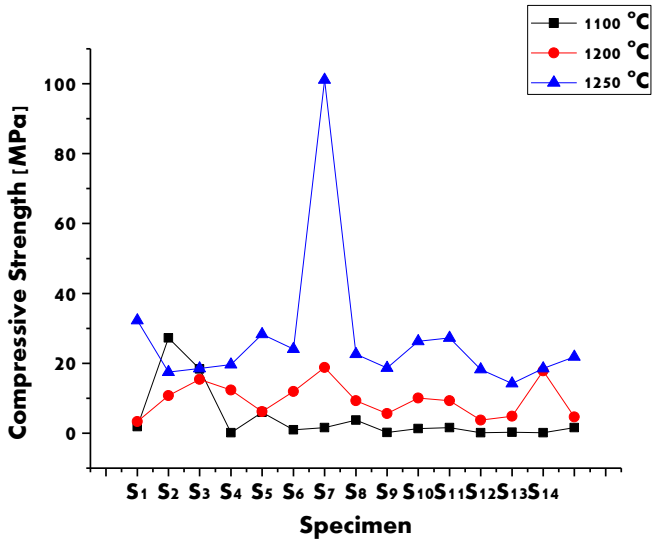

Figure 3.6. Variation in compressive strength with firing temperature

Conclusion

The present study has revealed the potentiality of Tanzania aluminosilicate minerals: kaolin, feldspar and quartz for use in medical applications. However, there is a need to improve compressive strength and to decrease porosity of the test specimen prepared in this work due to the fact that the prepared dental porcelain were found to have an average low compressive strength and high porosity as compared to that in natural teeth. This might have probably been attributed by the preparation methods and the size of the particles used. More work must be done to investigate other mechanical properties which were not tested in this work due to shortage of funds. The foundation made from this pioneered study will open up the doors for more researches in order to improve the findings obtained by applying the techniques used in this study or more advanced techniques. Thus, further endeavours into these Tanzania aluminosilicate minerals in dental applications will increase their value both for industrial and medicinal applications.

CHAPTER FOUR

Encapsulated Urea-Kaolinite Nanocomposite for Controlled Release Fertilizer Formulations[3]

Abstract

A controlled release fertilizer (CRF) was prepared by first intercalating urea fertilizer into the kaolinite interlayer spaces in two consecutive intermediate stages involving dimethyl sulfoxide and methanol kaolinite complexes followed by a one pot encapsulation process with gum arabic biopolymer to obtain a crosslinked nanocomposite CRF formulation. The nanomaterials engineered were characterized with XRD, ATR-FTIR, TGDTG, SEM and XRF techniques. Andreasen pipette sedimentation technique was functional in analyzing distribution of particles in the raw samples whereas particles sizes of the nanocomposites were determined using X-ray diffraction patterns and Scherrer equation. Randomly oriented wholerock X-ray diffraction analysis as well as oriented clay analysis by X-ray diffraction method as untreated air-dried, glycolated and heated shown the presence of kaolinite as major phase in both raw and beneficiated samples and that, indexing procedures revealed the existence of FCC Bravais crystal lattice structure. Wet beneficiation technique used was found to be very effective in eliminating impurities from 39.58% to 0.36% for the raw and beneficiated kaolinite respectively. Intercalation reactions were successful with the strength order of methanol intercalated kaolinite (KPDM) > dimethyl sulfoxide intercalated kaolinite (KPDMSO) > urea (synthetic fertilizer) intercalated kaolinite (KPDMU). Thermal decomposition of the nanomaterials was achieved at a maximum of 600 °C with variations depending on the intercalant whereas the particle sizes of the synthesized nanomaterials were in the range of 14.6 nm to 92.5 nm. SEM analysis revealed a change of order from thick compact overlapping euhedral pseudohexagonal platelets to irregular booklets which later transformed to vermiform morphology and dispersed euhedral pseudohexagonal platelets upon intercalation. Similarly, dispersed euhedral pseudohexagonal platelets was seen to coexist with blocky-vermicular booklets; also, a unique brain-from agglomeration which transformed into poor roundish particles organized in mart morphology was observed following CRF preparation and encapsulation with gum arabic. Release profiles were determined spectrophotometrically with hypochlorite and phenol method where 100% of urea was released in 97 hours from urea-kaolinite nanocomposite while 87% was released in 150 hours from the encapsulated nanocomposite. The findings established the fact that it is possible to use Pugu kaolinite to prepare urea controlled release systems with in-expensive natural resources using simple procedures.

Keywords: CRF(s), Nanocomposite, Encapsulation, Beneficiation, Intercalation, Vermiform, Euhedral-Pseudohexagonal, FCC

[3] Sempeho, S. I., H. T. Kim, E. Mubofu, A. Pogrebnoi, G. Shao and A. Hilonga (2015). "Encapsulated Urea-Kaolinite Nanocomposite for Controlled Release Fertilizer Formulations." Journal of Chemistry **2015**: 17

4.1 Introduction and Literature Review

In point of fact, urea is the most widely used nitrogen fertilizer in most parts of east Africa because of its high nitrogen (N) content (46%) and comparatively low cost of production; however, due to surface runoff, leaching and vaporization, the utilization efficiency or plant uptake of urea is generally below 50% (M. Liu, et al., 2007). In fact, it is associated with up to 60 to 70% loss of the nitrogen being applied and contributes to greenhouse gases (GHG) emissions and water pollution (A Meybeck & V Gitz, 2012) which in turn causes adverse effects during seed germination, seedling growth, and early plant growth in soil due to urea itself, to biuret and other impurities in urea fertilizers, and to products formed by hydrolysis or other transformations of urea in the soil (Bremner & Krogmeier, 1988; STEPHEN & WAID, 1964). Such limitations can be reduced by amending urea fertilizers with small amounts of either urease inhibitor (Bremner & Krogmeier, 1988), by encapsulation with synthetic or biopolymers or by intercalation with nano-clays to formulate CRFs (Sempeho, et al., 2014; Shaviv, 2001).

Essentially, CRFs are prepared through encapsulation with low permeability excipients (Shavit, Shaviv, Shalit, & Zaslavsky, 1997) using resin, wax, sulfur, polymer, silicates *etc*., that prevents the nutrients it contains from being immediately available to the plant; as a result nutrients are released over an extended period leading to an increased control over the rate and pattern of nutrient release. Control over the release pattern depends on the thickness of the coatings within the formulation (England, et al.). Precisely, CRFs exhibit superior features over traditional forms, such as decreased rate of nutrient losses from the soil by rain or irrigation water, sustained supply of nutrition for a prolonged time, increased fertilizer use efficiency (FUE), reduced frequency of application, minimized potential negative effects associated with over dosage and reduced toxicity, thus making CRFs' manufacturing and usage inevitable in the agricultural revolution era (M. Liu, et al., 2007). This paper describes the application of both intercalation reactions and encapsulation mechanisms to prepare urea based CRF by using Pugu kaolinite and gum arabic biopolymer.

Archetypally, kaolinite belongs to a class of layered materials with its "crystals built by the stacking of two dimensional units known as layers that are bound to each other through weak forces" (Satyanarayana & Wypych, 2004). The existence of such weak forces bounding the two

dimensional layers in place to form sheets makes layered materials including kaolinite and others described elsewhere (Auerbach, Carrado, & Dutta, 2004; Cnenr-ns; Hillier; Kloprogge, 2004; Weaver, 1956) capable of undergoing intercalation reactions. According to (Satyanarayana & Wypych, 2004) as quoted herein, "intercalation reactions occur by topotactic insertion of mobile guest species (neutral molecules, anhydrous or solvated ions) into the accessible crystallographic defined vacant sites located between the layers (interlayer spacings) in the layered host structure. In this intercalation compounds, strong covalent bond occur in the layers and weak interactions, between host lattice and guest species or co-intercalated solvents. Ionic and solvent exchange reactions are related to the replacement of solvated guest species (cations and anions) located into the interlayer spacings. In this case, only the solvents, the cations or the solvated cations can be replaced, depending on the reaction conditions".

Fundamentally, the term intercalation involves insertion of a guest molecule into a host lattice whereby the guest–host structure or intercalation compound is only slightly perturbed from the host structure and that, the reaction used to form the compound is reversible (Jacobson & Nazar, 2006). Typically, these reactions are just topochemical processes which involve conserving the natural host lattice structure in the course of the forward and reverse reactions unlike normal solid state reactions which involve extensive bond breaking and structural reorganization and require temperatures in excess of 600 °C. For all intents and purposes as other reaction do, intercalation reactions also consist of bond breaking in the host as well as bond formation between the guest and host, a process which result to an increase in the basal spacing of the unit cell of the layer host lattice upon intercalation. In our context we refer intercalation reactions in the layered silicates; particularly the kaolinite in the kaolins group of minerals which comprise among others nacrite, dickite and halloysite (Sempeho, Lugwisha, & Akwilapo, 2012) with kaolinite being the most abundant and differs from the other three members of the group by including molecular water in the interlayer, (T Al-Ani & Sarapaa, 2008) an inherent property which makes kaolinite suitable for undergoing intercalation reactions. Principally, kaolinite is 1:1 clay mineral consisting of two dimensional sheets of corner sharing SiO_4tetrahedral and or AlO_4 octahedral thereby categorized as a layered phyllosilicate capable of undergoing intercalation interactions, and so, "commonly employed in polymer/clay nanocomposites due to their swelling properties which results from their ability to hold water and other organic

molecules between the silicate layers, high aspect ratio, high cation exchange capacities and large surface area" Chen *et al*, (2008).

Generally, layered phyllosilicate based controlled release fertilizers (CRFs) are fertilizer granules intercalated within carrier molecules commonly known as excipients to control nutrients release thereby improving nutrient supply to crops and minimize environmental, ecological and health hazards; consequently the excipients plays a role of regulating nutrients release time and eliminate the need for constant fertilization and higher efficiency rate than conventional soluble fertilizers (Sempeho, et al., 2014). Precisely, CRFs usage is an advanced way to supply crop's nutrients (cf. conventional ways) due to gradual pattern of nutrient release, which improves fertilizer use efficiency (FUE) (Sempeho, et al., 2014). In this paper, a comprehensive investigation was done to intercalate urea fertilizer into the Pugu kaolinite interlayer spaces through a series of two intermediate consecutive stages involving dimethyl sulfoxide and methanol. Afterwards, urea fertilizer was intercalated by a way of replacing methanol intermediate complex through substitution mechanism and finally, the urea intercalated Pugu kaolinite was encapsulated with gum arabic natural degradable biopolymer to form a crosslinked nanocomposite controlled release urea fertilizer.

4.2 Materials and Methods

4.2.1 Materials

Kaolinite was collected at Pugu hills in the Coast region Kisarawe Tanzania by using quartering sampling technique described by (Sempeho, Esther, & Leonard, 2012). Urea (ACS reagent, 99.0-100.5%) was supplied by Sigma Aldrich, Acacia powder (extra pure reagent) was supplied by Junsei Chemical Co., Ltd, Japan, DMSO (Extra pure, ≥ 99.5%) was supplied by Daejung chemicals & metals, Co. Ltd, Gyonggi-do, Korea, Sodium chloride (Extra pure, ≥ 99.0%) was supplied by Samchun pure chemicals Co. Ltd, Gyonggi-do, Korea, Silver chloride (ACS reagent, 99.0%) was supplied by Sigma Aldrich, methanol (extra pure, ≥ 99.5%) was supplied by Daejung chemicals & metals, Co. Ltd, Gyonggi-do, Korea, acacia powder (Extra pure reagent) was supplied by Junsei Chemical Co., Ltd, Japan, deionized distilled water (D.I was supplied by Prof. Kim's lab, and isopropanol was supplied by Daejung chemicals & metals, Co. Ltd, Gyonggi-do, Korea.

4.2.2 Methodology

Since most raw kaolins are associated with some iron-bearing and black-colored materials which limit their usability (Saikia et al., 2003), beneficiation thence remain to be an inevitable process necessary for their characterization, materials synthesis and other advanced applications related to kaolin group of minerals where kaolinite is amongst. Purification of raw Pugu kaolinite was carried out with wet beneficiation technique by simple size separation using "Classifier". The method involved the separation of fine platy kaolinite from coarse quartz, feldspar, mica and other impurities using different setting velocities associated with particle size as governed by Stockes's law. The entire procedure which involves crushing to pulverization and soaking as well as running the classifier unit to drying has been comprehensively described in (Sempeho, Lugwisha, et al., 2012). Beneficiated kaolinite was modified by dispersed few grams in a 0.1 M NaCl solution and treated ultrasonically at 50 °C for 30 hours and then magnetically stirred for more 30 hours under constant stirring. The product was filtered under vacuum filter and washed several times to remove excess chloride whereas; washing was stopped after negative reaction with $AgNO_3$. The washed product was dried in a vacuum oven at 60 °C and stored as NaKP.

Intercalating dimethyl sulfoxide (DMSO) into the kaolinite interlayer spaces was done as follows. A measured amount of modified Pugu Kaolinite in a given volume of distilled water (D.I) was mixed with DMSO solution in a ratio of 1:6:1 respectively and then agitated in a magnetic stirrer for 21 days at 80 °C with a very small addition of water droplets to hinder desiccation of the stirring mixture. After 21 days of continuous stirring the suspension was aged for one week by way of stirring at room temperature. The resultant suspension was then washed with excess isopropanol and dried at 60 °C in a vacuum oven. The powdered product obtained was labeled KPDMSO. By using KPDMSO powder as a starting material, 2 g were taken and dispersed in a 60 ml of methanol solution followed by a 5 days stirring at RT. After 5 days of continuous stirring the suspension was left to mature over the weekend and afterward, washing with isopropanol was done. The washed preparation was then dried at 60 °C in a vacuum oven; the product in powder form obtained was named KPDM.

Preparation of urea-kaolinite intercalated fertilizer formulation was carried via urea-methanol replacement mechanism. Methanol intercalated kaolinite (KPDM) was used as a starting material

where, a 1:1 ratio of this intermediate intercalation compound and urea were dispersed in a 60 ml of methanol solvent and then stirred for 5 days at 40 °C. After 5 days of continuous stirring, excess isopropanol was used to wash the intercalation compound obtained in order to get off unreacted matter and impurities. The new urea fertilizer produced was labeled KPDMU and dried at 40 °C in a vacuum oven to remove excess solvent. For the purpose of preparing urea based nanocomposite CRF formulation, acacia powder was employed as an encapsulating material to crosslink the urea-kaolinite intercalation compound. To the starting material (KPDMU), few grams were shaken with acacia powder in a ratio of 1:2 in a vessel containing 60 mL methanol as a solvent and then stirred for 150 hours at room temperature. Subsequently, the nanocomposite material obtained was filtered in a vacuum oven and dried at 40 °C to dryness and kept for analysis as KPDMUG. As pointed out elsewhere (Weiss, Thielepape, Going, Ritter, & Schaer, 1963; C. Yan, Chen, Zhang, & Han, 2005), the apparent intercalation ratio (AIR) was determined as shown in equation 4.1.

$$AIR = \frac{Intensity\ \ (first\ \ peak\ )\ intercalate\ _{f(001)}}{Intensity\ \ (first\ \ peak\ )\ intercalate\ _{f(001)} + Intensity\ \ (first\ \ peak\ )\ initial\ \ sample\ _{f(001)}} \qquad (4.1)$$

Generally, a diffraction pattern must first be indexed before being analyzed. Indexing was done by first determining the unit cell parameter from the peak position and then Miller indices due to the fact that diffraction pattern is a direct result of two things: (i) the size and shape of the unit cell which determine the relative position of the diffraction peak, and (ii) the atomic position within the unit cell which determine the relative intensities of the diffraction peaks. The details of the procedures used for indexing (Sher, 2010) consists of six steps: (i) peak identification, (ii) determining $Sin^2\theta$, (iii) calculating the ratio of $Sin^2\theta/Sin^2\theta_{min}$, multiplied by the appropriate integers, (iv) determining the integer values of $h^2+ k^2+ l^2$, (v) identifying the Bravais lattice from the Miller indices, and (vi) calculating the lattice parameters. Determination of the estimate crystallite size was performed with X-ray diffraction pattern by using Scherrer equation (equation 4.2).

$$\beta(2\theta) = \frac{K\lambda}{L\cos\theta} \qquad (4.2)$$

where, K is Scherrer constant for shape factor values, λ is wavelength of X-radiation, θ is half the diffraction angle, β is peak width and L is the crystallite size (Speakman, 2014). According to (Speakman, 2014), the most common K values include, 0.94 for Full Width at Half Maximum (FWHM) of spherical crystals with cubic symmetry, 0.89 for integral breath of spherical crystals

with cubic symmetry and 1 because 0.94 and 0.89 both round up to 1 as well as the values of 0.62 to 2.08 because of variation in *K*.

Characterization of the samples involved was done as follows. FTIR-ATR measurements were performed in the near infrared region at wavelength between 7500-360 cm^{-1} using a Bruker Optic GmbH (alpha model, Laser class 1) Spectrometer with attenuated total reflectance (ATR). XRD patterns of raw and beneficiated Pugu kaolinite for mineralogical characterization were executed on SIEMENS D-5005 X-ray Diffractometer using Cu Kα1 radiation. The 2θ scan range was between 2° – 65°. On the other hand, the XRD patterns for the intercalation compounds as well as the nanocomposites were performed using RIGAKU COORPERATION, D/MAX-2500/PC X-ray Diffractometer equipped with a back monochromator operating at 40 kV and 100 mA at the scanning range of 5° – 80° with a step size of 0.1° and a time/step of 1 s using copper cathode as the X-ray source (λ) 1.54056 Å).Thermogravimetry measurements of samples were taken using TG/STA Linseis STA PT 1000 simultaneous TG/DTG thermal analyzer at a scanning rate of 5 °C per min from room temperature to 800 °C under nitrogen atmosphere. The samples surfaces morphology was investigated by using Field Emission Scanning Electron Microscopy (SEM-Hitachi-s-4800, Japan). The accelerated voltage was 15 kV. The chemical composition of the raw materials was determined by X-ray Fluorescence (XRF) using the semi quantitative XRF analysis technique (SIEMENS SRS 3000 X-ray Fluorescence (Rhodium anode, 8 analyzer crystals with beryllium windows 125 μm). The technique used is as we have described in our other recently published paper (E. H. J. Lugwisha & Siafu, 2014). For the raw kaolinite sample the analysis of particle size distribution was carried out by using sub-sieve analysis technique which involves the application of Andreasen pipette sedimentation method. The details of the procedures are found in our recent article (E. H. J. Lugwisha & Siafu, 2014).

4.3 Results and Discussion

4.3.1 Effect of beneficiation on the distribution of kaolinite particles

The distribution of particles in the original and beneficiated Pugu (Table 4.1) revealed that the 39.58% was a reject portion since it was constituted with a non-kaolinite portion of particles greater than 63 μm which wasn't our interest since it was constituted of the non-kaolinite particles; 60.42% was the kaolinite fraction contained particles below 63 μm which

was the anticipated working range because it was constituted of mostly kaolinite particles.

Table 4.1. Effect of beneficiation on the distribution of raw kaolinite

Sample	Percentage weight of particles (%)	
	≥ 63 µm	≤ 63 µm
Raw Pugu kaolin	39.58	60.42
Beneficiated Pugu kaolin	0.36	99.64

Source: (Sempeho et al., 2015b)

Upon beneficiation trials, there was a significant improvement in the distribution of particles; the non-kaolinite fraction was reduced to 0.36% from the 39.58% of the non-beneficiated portion, whereas the particles below 63 µm constituted 99.64% as compared to 60.42% of the non-beneficiated portion Essentially, it is necessary to note that, the results from beneficiation trials reveal the fact that the method used was efficient and effective since there was a significant substantial a reduction of non-kaolinite fraction from 39.58% of the raw Pugu kaolinite to 0.36% of the beneficiated Pugu kaolinite.

4.3.2 Kaolin mineralogy

The randomly oriented wholerock X-ray diffraction analysis for both the original Pugu kaolin, and the beneficiated Pugu kaolin revealed the mineral contents present as seen in Table 4.2. Basing on the wholerock powder mount diffractograms of raw Pugu kaolin the clay portion was only kaolinite while the non-clay portion or rather mineral impurities present in the kaolin were quartz (SiO_2), clinochlore [$Mg_5Al(Si,Al)_4O_{10}(OH)_8$] and microcline [$KAlSi_3O_8$]. An observation made in the diffractograms of beneficiated kaolin is that the clay portion contained kaolinite [$Al_2Si_2O_5(OH)_4$], illite [$KAl_2(Si_3AlO_{10})(OH)_2$] and clinochlore [$Mg_5Al(Si,Al)_4O_{10}(OH)_8$] accompanied with the disappearance of quartz and microcline. According to (Sempeho, Esther, et al., 2012) the formation of illite is generally favoured by alkaline conditions and by high concentrations of Aland K. That said the appearance of illite in the beneficiated kaolin may be a result of reaction between Al and K from microcline and water thereby causing weathering of silicates. (T Al-Ani & Sarapaa, 2008); The case for the appearance of clinochlore may be attributed to the introduction of Mg-based impurities. Although the pH of water used during beneficiation was not checked, it is suspected that the pH also contributed to this clay minerals

transformation because the solubility of alumina is pH dependent and silica solubility increases parallel with the increase in pH (T Al-Ani & Sarapaa, 2008).

Table 4.2. Mineralogical composition of the raw materials

Sample	Major Phase	Minor Phase
Original Kaolin	Kaolinite [$Al_2Si_2O_5(OH)_4$]	Quartz [SiO_2] Microcline [$KAlSi_3O_8$]
Beneficiated Kaolin	Kaolinite [$Al_2Si_2O_5(OH)_4$]	Clinochlore [$Mg_5Al(Si,Al)_4O_{10}(OH)_8$] Illite [$KAl_2(Si_3AlO_{10})(OH)_2$]

Source: (Sempeho, Kim, et al., 2015b)

Since the results from oriented air dried samples above were not enough to confirm the clay mineral groups obtained, it was therefore necessary to perform oriented clay analysis by X-ray diffraction method as untreated air-dried, glycolated and heated at 550 °C for two hours on the original and beneficiated kaolin samples with the aim of distinguishing layer types and clay mineral groups. When the air dried samples were diffracted, peaks were developed on the diffractograms which revealed three main clay minerals namely kaolinite, illite and clinochlore. Identification and hence confirmation of these clay minerals was achieved from the differences on the diffractograms obtained by glycolating the samples, drying them, then diffraction process carried out; and by heating the samples at 550 °C for two hours prior to the diffraction process (Sempeho, Esther, et al., 2012). This behaviour of stability in chemical treatment (glycolated) and heat transformation (at 550 °C) confirmed the presence of illite (E. H. J. Lugwisha, 2011). However, when the samples were glycolated, dried and diffracted some peaks were shifted in some samples. But on heating the samples at 550 °C followed by diffraction, these shifted peaks collapsed. This characteristic of altering the diffraction patterns is a distinguishing characteristic of kaolinite group (E. H. J. Lugwisha, 2011). Shortly, the mineralogical analysis test on the clay fraction revealed that the major content on both the original and beneficiated kaolin samples was kaolinite subordinated with illite.

4.3.3 Chemical composition

The chemical composition of both raw and beneficiated Pugu kaolinite used in this study is given in Table 4.3. As can be seen that beneficiation process was very successful; there was a reduction of silica content from 63.64 to 54.99% upon beneficiation whereas alumina content got increased

from 31.43 to 40.2%. Variations in the composition of other oxides were also noticed as depicted in Table 4.3; however, a peculiar observation was that the amounts of TiO_2 and Fe_2O_3 instead of getting decreased upon beneficiation were seen to increase from 0.8% and 1.01% to 1.02% and 2% respectively whereas the amount of MnO was seen to be unaffected with beneficiation process employed.

Table 4.3. Chemical composition of the raw materials

	Oxide Composition												
Sample	SiO_2	Al_2O_3	Na_2O	MgO	SO_3	Cl	K_2O	CaO	TiO_2	Cr_2O_3	MnO	Fe_2O_3	LOI
Pugu Kaolin	63.64	31.43	0.43	0.16	0.25	0.76	1.39	0.06	0.80	0.03	0.01	1.01	0.03
Beneficiated Kaolin	54.99	40.20	0.09	0.13	0.08	0.04	0.96	0.04	1.02	0.04	0.01	2.00	0.40

Source: (Sempeho, Kim, et al., 2015b)

4.3.4 XRD analysis

The calculated lattice parameters from the indexing procedures are given in Table 4.4. Basing on the sequence of $h^2 + k^2 + l^2$ values, most *hkl* reflections allowed are either all even or all odd; thus, the Bravais lattice was FCC. The average lattice parameter was 19.35 Å. By using Bragg's equation under assumption that "*n*" is unit to confirm the results obtained with the six step method, Table 4.5 was created whose sequence also suggested an FCC Bravais lattice. As can be seen in Table 5, the *hkl* and $(1/d^2)$Ƶ columns that the quotients are integers that indicate an FCC Bravais lattice.

Similarly, the X-ray diffraction results reveals that the intercalation reactions were successful and so, Pugu kaolinite can be used as CRF excipients for urea based fertilizers. This is evidenced with the fact presented in Figure 4.1 where, intercalation of DMSO into the kaolinite interlayer spaces to form a pale yellow KPDMSO composite was achieved at the intercalation ratio of about 89.2% and that the basal lattice space for the first peak of the prepared kaolinite-DMSO nanocomposite was 1.12 nm which represents a lattice expansion of 0.41 nm as compared to the originally beneficiated Pugu kaolinite which had a basal spacing of 0.71 nm. Similarly, methoxy intercalated kaolinite (KPDM) presented in Figure 4.2 had the intercalation ratio of about 87.4% and basal lattice parameter for the first peak of the prepared kaolinite-methanol nanocomposite

was 1.10 nm which represents a lattice expansion of 0.39 nm in relation to the beneficiated Pugu kaolinite.

Table 4.4. Indexed XRD patterns

Peak#	2θ	$Sin^2\theta$	$1*Sin^2\theta/Sin^2\theta min$	$2*Sin^2\theta/Sin^2\theta min$	$3*Sin^2\theta/Sin^2\theta min$	$h^2 + k^2 + l^2$	hkl	a (Å)	d (nm)
1	12.540	0.012	2.519	5.038	7.557	8	220	19.950	0.715
2	24.850	0.046	9.775	19.549	29.324	29	520	19.280	0.358
3	12.550	0.012	2.523	5.045	7.568	8	220	19.930	0.705
4	24.900	0.047	9.813	19.625	29.438	29	520	19.240	0.357
5	7.890	0.005	1.000	2.000	3.000	3	111	19.390	1.119
6	23.590	0.042	8.817	17.635	26.452	27	333 or 511	19.220	0.377
7	8.040	0.005	1.037	2.074	3.112	3	111	19.040	1.099
8	23.600	0.042	8.825	17.650	26.476	27	333 or 511	19.210	0.377
9	8.140	0.005	1.063	2.125	3.188	3	111	18.810	1.086
10	22.340	0.038	7.925	15.850	23.775	24	422	19.480	0.398

FCC sequence

Source:(Sempeho, Kim, et al., 2015b)

Table 4.5. Indexing XRD pattern: Bragg's equation

Peak #	Sin θ	d (nm)	$\frac{1}{d^2}$	$\frac{1}{d^2}\mathbb{Z}$	*Hkl*
1	0.109	0.727	1.895	2	110
2	0.215	0.358	7.803	10	310
3	0.109	0.705	2.014	3	111
4	0.216	0.357	7.833	10	310
5	0.069	1.119	0.798	1	100
6	0.204	0.377	7.040	9	300
7	0.070	1.099	0.828	1	100
8	0.205	0.377	7.047	9	300
9	0.072	1.086	0.848	1	100
10	0.194	0.398	6.326	8	220

FCC Bravais Sequence

Source:(Sempeho, Kim, et al., 2015b)

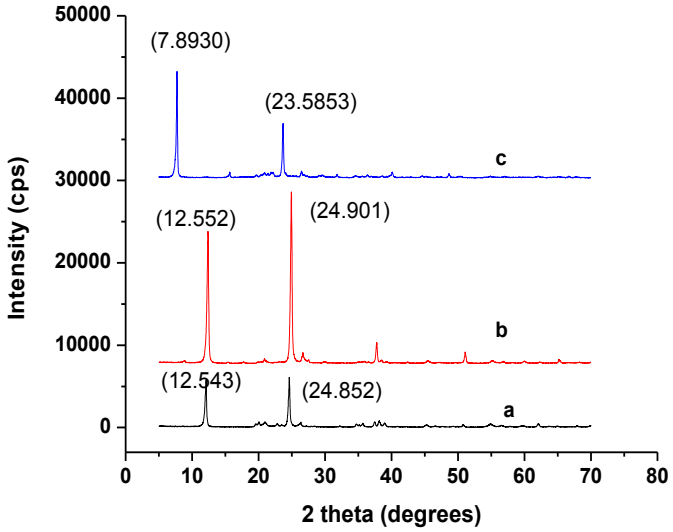

Figure 4.1. X-ray diffractograms of (a) beneficiated Pugu kaolinite, (b) NaKP, and (c) KPDMSO

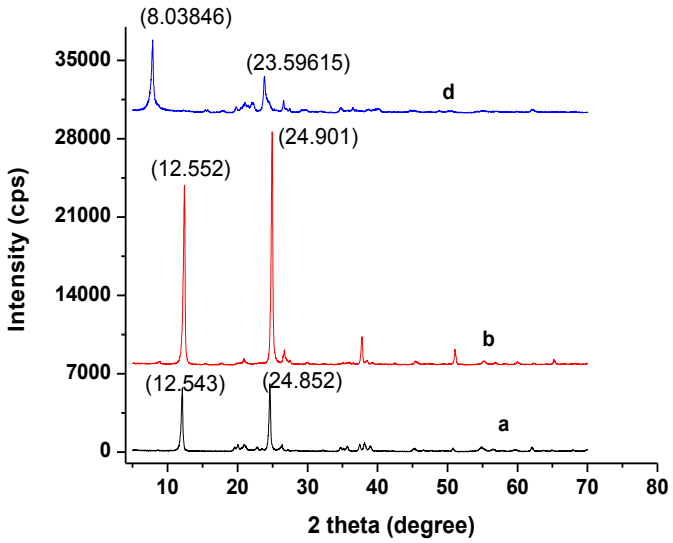

Figure 4.2. X-ray diffractograms of (a) beneficiated Pugu kaolinite, (b) NaKP, and (c) KPDM

Furthermore, when kaolinite was treated with urea fertilizer, the resulting urea intercalated kaolinite (KPDMU) presented in Figure 4.3 had the intercalation ratio of about 91.10% and basal spacing of 1.09 nm which signify that the lattice parameter had been stretched out to distance of 0.38 nm as related to the beneficiated kaolinite. A closer look at the salt modified kaolinite (NaKP), a unique phenomenon was observed; basal spacing of the beneficiated kaolinite did shrink (instead of being expanded) to a distance of about 0.0005 nm which represents a

difference of the basal lattice parameter of 0.7047 nm and 0.7052 nm for the modified kaolinite and the beneficiated kaolinite respectively.

Fundamentally, intercalation reactions were successful in the order of KPDM > KPDMSO > KPDMU. DMSO being a strong intercalant as compared to methanol and urea, the trend was expected to be KPDMU > KPDM > KPDMSO; the reason for an increased intercalation ratio for the KPDMU can be attributed to the fact that, "in the dynamic intercalation process, kaolinite and urea in the mixer suffer from the action of high-speed stirring and high temperature. The shear force produced by the intense stirring accelerates delamination of crystal layers of kaolinite and increases the intercalation reaction speed of urea into kaolinite" thereby stimulating the movement of urea molecules which in turn intensify the contact probability between urea molecules and kaolinite; as a result, the intercalation ratio is increased and so the trend was altered (C. Yan, et al., 2005). Thus, via DMSO-kaolinite intercalate as an intermediated prepared by using salt treated kaolinite urea fertilizer was intercalated into the kaolinite interlayer spaces by displacing methanol. The intercalated urea-kaolinite was then encapsulated with gum arabic to make the urea based CRF formulation.

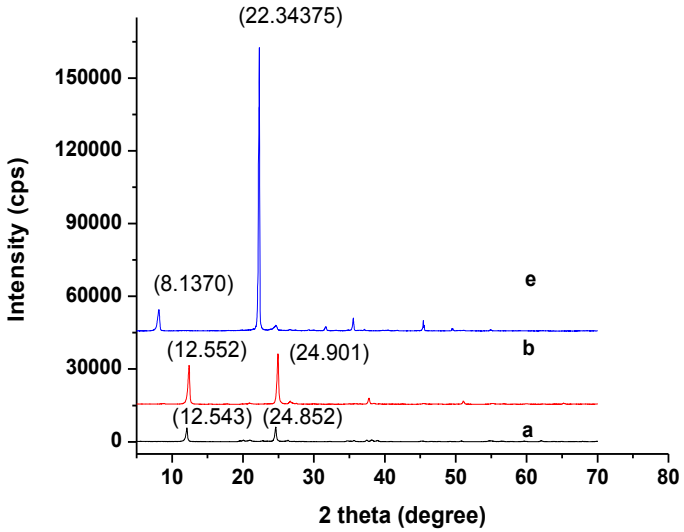

Figure 4.3. X-ray diffractograms of (a) beneficiated Pugu kaolinite, (b) NaKP, and (c) KPDMU

4.3.5 Particle size analysis

The particle sizes determined for the intermediate intercalation compounds (KPDMSO and KPDM), urea intercalated kaolinite CRF (KPDMU) as well as the nanocomposite CRF formulation (KPDMUG) are given in Table 4.6.

Table 4.6. Analysis of particle sizes from Scherrer equation

Sample	crystallite size (nm)				
	K = 2.08	K = 1	K = 0.94	K = 0.89	K = 0.62
KPDMSO	92.46	44.45	41.79	39.56	27.56
KPDM	48.81	23.47	22.06	20.88	14.55
KPDMU	50.84	24.44	22.98	21.75	15.16

Source: (Sempeho, Kim, et al., 2015b)

Since our work was based on cubic systems, the best particles selected are those whose shape factor values include 0.94 and 0.89 together with their extreme cases thereby coming to our conclusion of deciding to report a range of sizes. The size for DMSO intercalated kaolinite nanoparticles were in a range of 27.56-92.46 nm, whereas those of methanol intercalated kaolinite nanoparticles were in a range of 14.55-48.81 nm and those from urea-kaolinite CRF formulation were found to be between 15.16-50.84 nm. Precisely, nanoparticles from KPDMSO were twice as bigger than the rest for the reason not yet clear to us but an assumption we have is that this might be contributed by the size and structural pattern of DMSO.

4.2.1 SEM analysis

A detailed analysis on the SEM images was carried out on the KKK, NaKP, KPDMSO, KPDM and KPDMU samples. Typically, the SEM images in Figure 4.4 reveals the presence of a layered morphology common to kaolinite minerals, however, the appearance of these morphologies were seen to vary with kaolinite modifications. The beneficiated kaolinite is characterized with predominantly wider and thick compact overlapping euhedral pseudohexagonal platelets (Figure 4.4a); this concurs with (Uwins, Mackinnon, Thompson, & Yago, 1993). A change in the

stacking sequence of kaolinite layers was observed upon chemical treatment with NaCl, where there occurs a mixture of irregular crystallites and thin very compacted layers appearing like booklets (Figure 4.4b).

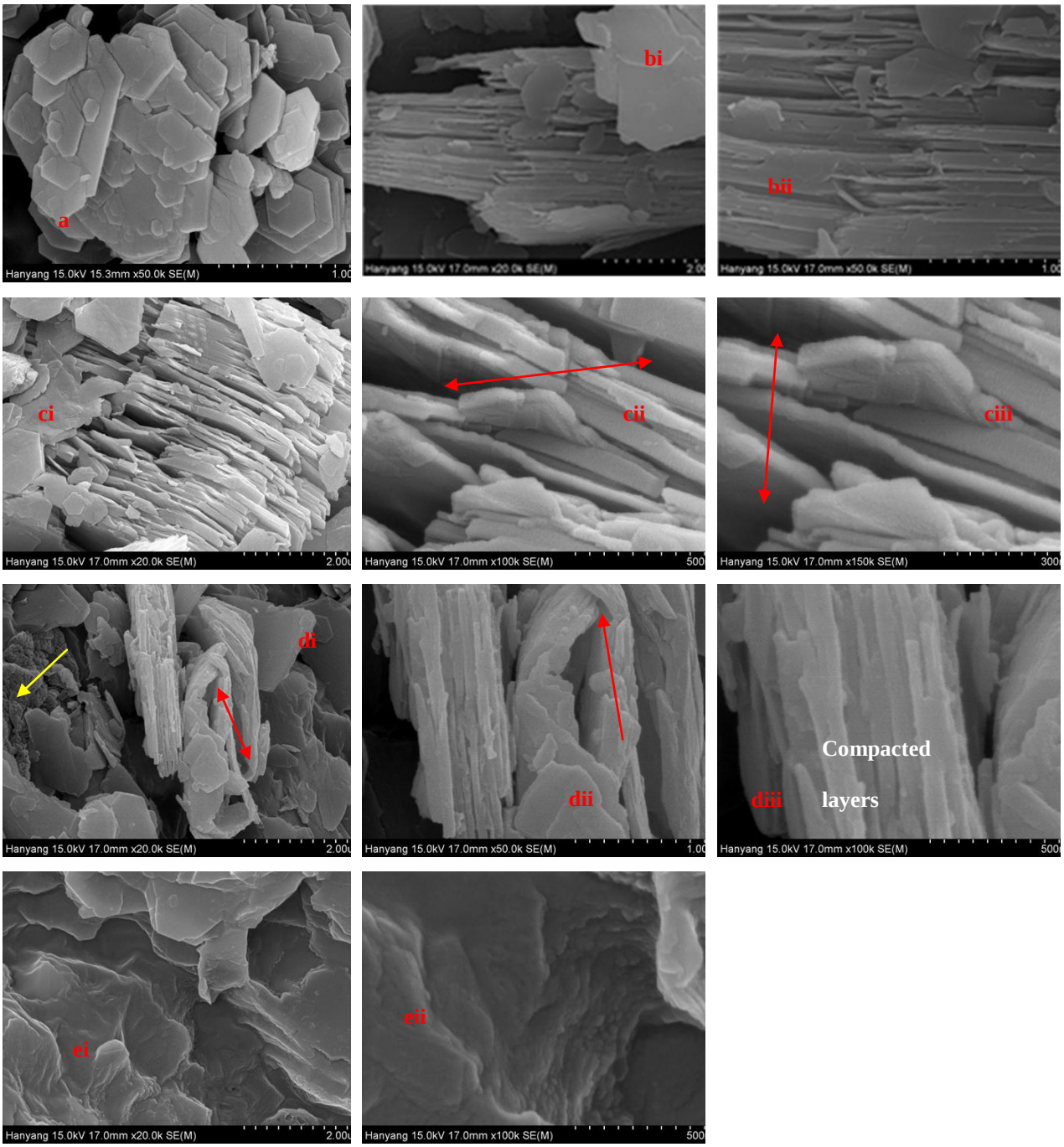

Figure 4.4. SEM images for (a) beneficiated Pugu kaolinite (KKK), (b) NaKP, (c) KPDMSO, (d) KPDM, and (e) KPDMU

That is to say, NaKP exhibited many stacked thin euhedral pseudohexagonal platelets and part vermiform shaped particles. However, both beneficiated kaolinite and the salt treated kaolinite exhibited a high degree of crystallinity and stacking of the kaolinite particles which corresponds to kaolinite mineral (Letaief & Detellier, 2009). As a matter of fact, the hexagonal faces of these particles corresponds to the crystallographic (*001*) basal planes (Gardolinsky, 2005). As expected, most particles were highly anisometric with thickness along the z-axis much smaller than its other dimensions (Gardolinsky, 2005; Santos, 1989). Our observation is, when kaolinite is harshly treated with salts particularly, NaCl a change in the order of arrangement of kaolinite occurs such that the surface area for intercalation is increased due to well arrangements of functional layers. Similarly, it was observed that particles with pseudo hexagonal morphology in NaKP predominates over those with vermiform morphology, a similar observation found by (Beaufort et al., 1998).

Moreover, the DMSO intercalated kaolinite exhibited a decreased compactness between layers where the distance was widened (Figure 4.4c, red arrow). For the most part, vermicular booklet morphology characterized the DMSO intercalated kaolinite with a very small appearance of the dispersed euhedral pseudohexagonal platelets. A similar observation though in a different setting made Baeufort to conclude that "aggregates of kaolin with blocky habits coexist with vermicular booklets" an observation which we have considered to be valid in this work (Beaufort, et al., 1998). Such observation made us to sense that under certain conditions the appearance of vermiforms mixed with either stacked or dispersed euhedral pseudohexagonal platelets should be expected. When methanol replaced DMSO to form KPDM in the kaolinite interlayer spaces the following features were observed (Figure 4.4d): (i) there distance between layers had shrink as compared to distances observed in DMSO intercalated kaolinite (Figure 4.4diii), (ii) a further decrease of the appearance of the blocky aggregates with euhedral pseudohexagonal platy morphology indicating an increased number of clean layers available for intercalation reactions, (iii) the vermicular booklets were seen to show bending forms in some parts (red arrows), and (iv) an appearance of well-coordinated roundish agglomerated particles resembling brain morphology was seen and we named this phenomena "brain-form agglomeration" which we believe could further facilitate intercalations (orange arrow).

Furthermore, a complete disappearance of both dispersed euhedral pseudohexagonal platelets, vermicular booklets as well as brain-form agglomeration was observed in the nanocomposite KPDMUG (Figure 4.4e) when the urea intercalated kaolinite was encapsulated with acacia powder and instead, the surface' morphology was observed to exhibit smooth mat at lower magnification which in the higher magnification the appearance was that of numerous small round particles assembled in a mat (Figure 4.4eii).

4.2.1 FT-IR analysis

Treated kaolinite and beneficiated Pugu kaolinite are represented in the Figure 4.5 and 4.6 respectively. A close view at these figures reveals that, the vibrations occurring at 3683 cm^{-1} of the treated kaolinite and 3684 cm^{-1} of beneficiated kaolinite corresponds to the in phase OH stretching of the inner surface hydroxyl of the kaolinite (Aroke & El-Nafaty; Dawley, Scott, Hill, Leszczynski, & Orlando, 2012; C. O. Mgbemena, N. O. Ibekwe, R. Sukumar, & A. Menon, 2013a; Olejnik, Aylmore, Posner, & Quirk, 1968), whereas the vibrations seen at 3650 cm^{-1} are ascribed to the out phase OH stretching vibrations of the inner surface hydroxyl groups.

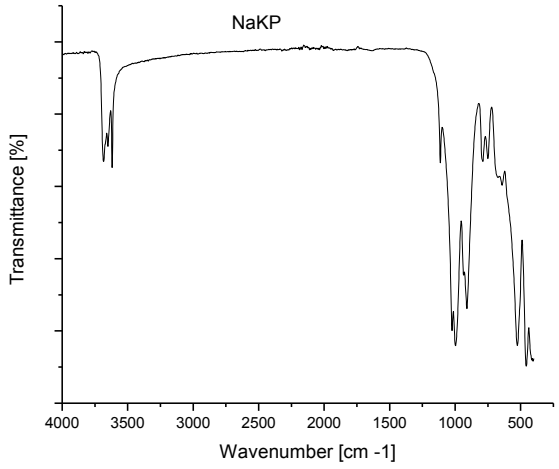

Figure 4.5. ATR-FTIR Spectrum of NaKP

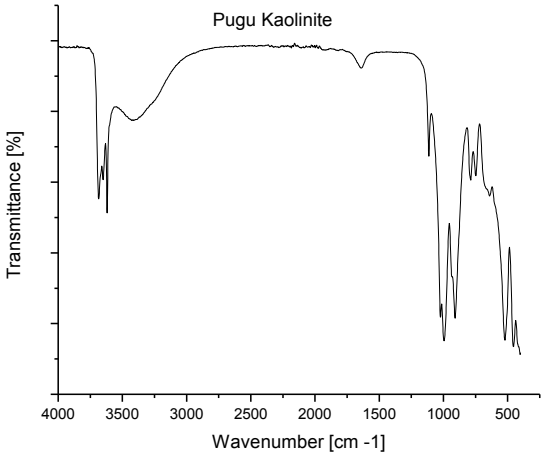

Figure 4.6. ATR-FTIR spectrum of beneficiated Pugu kaolinite

The bands exhibited at 3618 cm^{-1} are characteristic of inner layer OH stretching due to Al-O-H stretching vibrations of alumina of the kaolinite in the octahedral configuration while the

characteristic OH stretching vibrations of the kaolinite in a tetrahedral configuration is exhibited at frequencies 749 cm $^{-1}$ of the treated kaolinite (Olejnik, et al., 1968), and is due to Si-O-Si symmetrical stretching (Heah, Kamarudin, Mustafa Al Bakri, et al., 2012). The band seen at 1113 cm $^{-1}$ is ascribed to the apical Si-O stretching mode and this is consistent with the band frequencies of 1112 cm $^{-1}$ reported by (Balan, Saitta, Mauri, & Calas, 2001). While this was ascribed to Si-O normal to the planar stretching; the absorption band observed at 1023 to 997 cm $^{-1}$ for the treated kaolinite and 995 cm $^{-1}$ for the beneficiated kaolinite corresponds to the Si-O planar stretching which in fact concur with 1025 to 995 cm $^{-1}$ reported by (Aroke & El-Nafaty). To be more precise, the bands at 1023 cm $^{-1}$ represent the in plane Si-O planar stretching and 997 cm $^{-1}$ or 995 cm $^{-1}$ represents the out phase Si-O planar (Aroke & El-Nafaty; Dawley, et al., 2012; Mgbemena, et al., 2013a) and the alternating Si-O and Al-O bonds (Heah, Kamarudin, Mustafa Al Bakri, et al., 2012); this is in close agreement to the 995 cm $^{-1}$ obtained by (Heah, Kamarudin, Mustafa Al Bakri, et al., 2012), 997 cm $^{-1}$ obtained by (Dang, Chen, & Lee, 2013). Another band seen at 910 cm $^{-1}$ for the treated kaolinite and 909 cm $^{-1}$ for the beneficiated kaolinite which closely relates to others of similar range reported in literature such as 913 cm^{-1} (Dawley, et al., 2012), 907 cm $^{-1}$ (Heah, Kamarudin, Mustafa Al Bakri, et al., 2012), 912 cm $^{-1}$(Mgbemena, et al., 2013a) and 907 (Liew, Kamarudin, Mustafa Al Bakri, et al., 2012) is attributed to the OH deformation of inner hydroxyl groups due to the Al-OH bending (Dawley, et al., 2012). Elsewhere, this band is ascribed to the Al-OH bending mode of kaolinite (Heah, Kamarudin, Mustafa Al Bakri, et al., 2012), Al $^{(VI)}$-OH vibrations (Mgbemena, et al., 2013a) and Al $^{(VI)}$-OH vibrations (Liew, Kamarudin, Mustafa Al Bakri, et al., 2012). The band at 788 cm $^{-1}$ is ascribed to the Al-O-Si asymmetric bending of the bonds whereas the bands at 525 cm $^{-1}$ and 520 cm $^{-1}$ for the modified and beneficiated kaolinite respectively is given to the Si-O-Al (VI) where Al $^{3+}$ is in octahedral coordination (Heah, Kamarudin, Mustafa Al Bakri, et al., 2012; Liew, Kamarudin, Mustafa Al Bakri, et al., 2012; Tironi, Trezza, Irassar, & Scian, 2012). When you compare the diagrams for both beneficiated and treated kaolinite, one can easily notice a roughly total identity between them. However, for the beneficiated kaolinite, we noticed the presence of a new broader absorption band at 3412 cm $^{-1}$ which was absent in the treated kaolinite. This band corresponds to the peak maxima for water due to O-H stretching vibration and it is observed to be broader owing to the hydrogen bonding after wet beneficiation process (Banwell & McCash, 1994; Kazuo Nakamoto, 1997; Pope & Fry, 1997). Substantially, this band can be assigned to a

combination of both stretching (asymmetrical + symmetrical) and overtone of bending vibrations (Venyaminov & Prendergast, 1997).

Most probably the direct intercalation of DMSO into the interlayer sheets of kaolinite was first achieved by (Olejnik, et al., 1968); the rule is that, when DMSO molecules are intercalated into the kaolinite layers [which elsewhere has been described as ion substitution or site vacancies at the tetrahedral/octahedral sheets (Sempeho, et al., 2014)] there would be a noticeable significant changes in the OH stretching region upon absorption of IR bands. This is clearly seen in Figure 4.5, 4.6 and 4.7 respectively where the IR absorption bands of original, treated and DMSO intercalated kaolinite are presented. Fundamentally, the infrared spectrum of the kaolinite-DMSO complex was expected to reveal the presence of alumina in both octahedral and tetrahedral configuration for the intercalated kaolinite. As can be seen the absorptions lies in the near IR region whereby the vibrational frequencies at 3698 to 3619 cm^{-1} represent the characteristic hydroxyl stretching vibrations of alumina of the kaolinite in the octahedral configuration whereas the bands at 736 cm^{-1} correspond to the characteristic hydroxyl stretching vibrations of alumina of the kaolinite in the tetrahedral configuration for the AlO_4 antisymmetric stretching and that at 633 cm^{-1} it is attributed to the characteristic hydroxyl stretching vibrations of alumina of the kaolinite in the tetrahedral configuration for the AlO_4 symmetric stretching. These predictions agree with (Czarnecka, 2013; Olejnik, et al., 1968). The vibrations at 3657 cm^{-1} are attributed to the OH stretching of the inner surface hydroxyl of the original kaolinite. Furthermore, we had observed that upon DMSO intercalation a new band at 3698 was formed in the kaolinite-DMSO complex; this is related to the disappearance of the 3683 cm^{-1} band frequency of the treated kaolinite. In addition, an increased in wavelength from low to high although a small shift has been observed signify that the intercalation was successful. This was confirmed by the appearance of a series of new bands upon intercalation as seen in Figure 4.7. The occurrence of infrared bands at 3012 and 2936 cm^{-1} which is close to results obtained by (Mgbemena, et al., 2013a) reveals the formation of organo-clay compound and in this context we refer to the formation of kaolinite-DMSO intermediate nanocomposite. We have in turn ruled out that these bands would respectfully be representing the $–CH_2$ stretching for both symmetric and asymmetric vibrations.

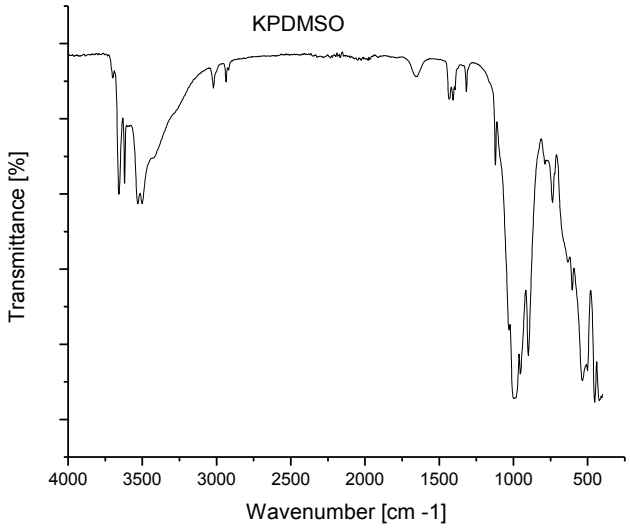

Figure 4.7. ATR-FTIR spectrum of KPDMSO

Moreover, the new sharp two split peak at 3530 and 3501 cm $^{-1}$ correspond to the formation of the moderately hydrogen bonds between some of the inner-surface hydroxyls of the kaolinite layers and the sulfonyl oxygen of the intercalated DMSO molecules; this agrees with Thompson's predictions (Thompson & Cuff, 1985). Similarly, our conclusion also agrees with (Frost, Kristof, Paroz, & Kloprogge, 1998; Horvath, Kristof, & Frost, 2010; Clifford T Johnston, Sposito, Bocian, & Birge, 1984) whose works reported IR bands at 3538 and 3502 cm $^{-1}$. Moreover, the peak at 3657 cm $^{-1}$ correspond to the inner surface hydroxyl hydrogen bonded to the S=O group as referred elsewhere (Horvath, et al., 2010). There is also a unique CH band split into two bands at 1434 cm $^{-1}$ and 1407 cm $^{-1}$ and is attributed to the in plane methyl deformation vibration of DMSO; in point of fact, this is in agreement with (Horvath, et al., 2010) who obtained a two split IR bands at 1411 and 1430 cm $^{-1}$ due to intercalated DMSO methyl deformation.

Basing on the literature surveyed, we have concluded that, the distinct intense IR band seen at 1317 cm $^{-1}$ represents the deformation of the inner surface OH groups hydrogen bonded to the S=O group of the DMSO molecules intercalated into the kaolinite layers and this reveals that only one type of hydrogen bonded inner surface OH group was formed during DMSO-kaolinite interaction as put forward by (Horvath, et al., 2010). The analysis results also shows that there's

only one type of water molecules vibrations present; this is evidenced by the appearance of single broad band at 1655 cm $^{-1}$ which is ascribed to water bending vibrations and that, this single water molecules is hydrogen bonded to only one type of DMSO molecule associated with the kaolinite inner surface OH groups observed at 1029 cm $^{-1}$. According to (Olejnik, et al., 1968), the vibrational assignments at 1121 cm $^{-1}$ corresponds to the in plane Si-O vibrations; at 998 cm $^{-1}$ and 951 cm $^{-1}$ represents Al-OH vibrations; at 736, 633 and 603 cm $^{-1}$ vibrations stands for the gibbsite like layers of the kaolinite; and also, bands at 536, 501 and 452 cm $^{-1}$ correspond to the Si-O-Al skeletal vibrations.

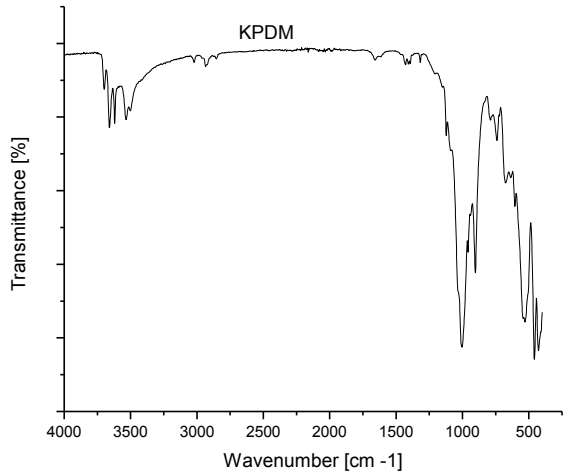

Figure 4.8. ATR-FTIR spectrum of KPDM

Furthermore, upon introducing methoxy group into the kaolinite layers several changes were observed in the IR spectrum as compared to the beneficiated and treated kaolinite and KPDMSO-kaolinite. As seen for KPDM in Figure 4.8, new bands were observed at 3698, 3659 and 3619 cm $^{-1}$ with similar reasons to ones given for KPDMSO above. However, the band at 3619 cm $^{-1}$ is shown to be un-shifted from the original kaolinite, modified kaolinite, DMSO intercalated kaolinite and now in the methanol intercalated kaolinite; this is in fact, in agreement with 3620 cm $^{-1}$ wavelength obtained by (Czarnecka, 2013). The doubly split weak broad band at 3533 cm $^{-1}$ is ascribed to the externally adsorbed water as suggested by (Czarnecka, 2013) and (Tunney & Detellier, 1996); this band has also been considered as the OH stretching of methanol molecules and/or to water molecules formed during the esterification reaction of kaolinite inner-surface OH groups and methanol molecules (Matusik, Scholtzová, & Tunega, 2012).

The region around 3021 to 2800 cm $^{-1}$ is marked by the three split band and is ascribed to the methanol-kaolinite interaction. To be clearer, the OH stretching bands from alcohol molecules is visualized by band at 3012 cm $^{-1}$ while at 2800 cm $^{-1}$ attributed to the C-H stretching mode of methanol intercalated into the interlayer spaces of kaolinite sheets. The band at 2935 cm $^{-1}$ refers to the C-H stretching region which confirms the presence of -OCH_3 groups in the kaolinite interlayer spaces (Tunney & Detellier, 1996) and (Matusik, et al., 2012). A similar observation was made by (Larkin, 2011) in that, bands at 3021 cm $^{-1}$ and 2935 cm $^{-1}$ represents the C-H stretching mode of methanol; according to him, these vibrations are attributed to the CH_3 out phase and in phase stretches of the methanol respectively which in turn act as an evidence for the grafting reaction of methoxy group in the kaolinite interlayer space as noted by (Czarnecka, 2013).

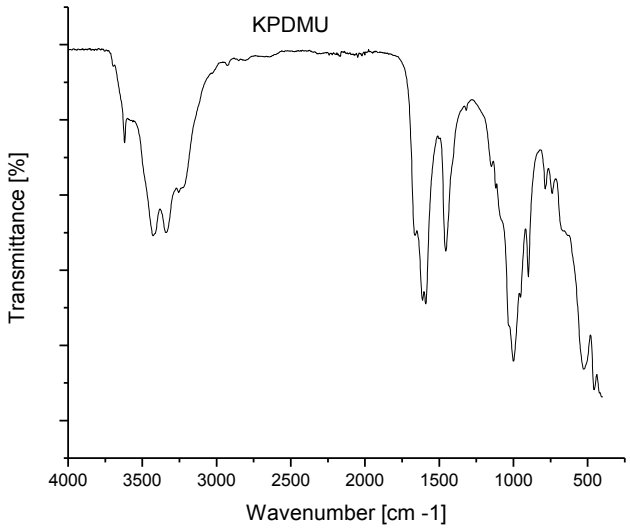

Figure 4.9. ATR-FTIR spectrum of KPDMU

Correspondingly, the bands at 1122 cm^{-1} is ascribed to the C-O stretching deformation in methanol molecules; this agrees with the C-O stretching deformation of 1123 cm $^{-1}$ in methanol-kaolinite obtained by (Czarnecka, 2013) while the new band recorded at 1003 cm $^{-1}$ which also agrees with 1004 cm $^{-1}$ obtained by (Czarnecka, 2013) represents the lattice Si-O vibration bands due to methanol-kaolinite intercalation and it correspond to a shift from 1113 cm $^{-1}$ of the modified kaolinite. The observed low intensity bands at 957 cm $^{-1}$ corresponds to the Al-OH deformation whereas the band seen at 902 cm $^{-1}$ is ascribed to the Al-OH in-plane bending

vibration of the inner hydroxyl of kaolinite and this corresponds to a shift from 899 cm $^{-1}$ of KDMSO and 910 cm $^{-1}$ of the modified kaolinite and 909 cm^{-1} of the beneficiated and treated (NaKP) kaolinite mineral. We have attributed the new kaolinite band at 789, 740, 675, 635 and 427 cm $^{-1}$ in contrast to the beneficiated and treated (NaKP) kaolinite to the modifications of the bands related to the Si-O and Al-OH vibrations resulting from the perturbation of the kaolinite structure due to grafting of the methanol molecule; this again is in agreement with some of the results obtained elsewhere (Czarnecka, 2013).

Noticeably, the IR spectra of both KPDMSO and KPDM revealed that DMSO molecules were successfully replaced by methanol molecules. This was evidenced by either a shift of characteristic bands or disappearance/appearance of new bands between the two. Similarly, there's a clear substantial changes in the intensity of IR spectra in the OH region due to intercalation of DMSO and methoxy and the grafting of methoxy into the interlayer spaces of kaolinite sheets. This implies that there was a significant alteration in the local environment of inner surface hydroxyl groups when DMSO molecules were replaced with methanol molecules during intercalation and grafting process. In fact, the presence of methoxy groups into the kaolinite layers is revealed by the significant decrease in the intensity of band representing interlamellar Al-OH of the silicate sheets at 957 cm $^{-1}$ in the KPDM as compared to that of 953 cm $^{-1}$ in the KPDMSO; this phenomena is ascribed to the formation of Al-O-C bonds resulted from the grafting of methoxy groups into the kaolinite interlayer spaces, a fact has been put forward and hence agrees with the findings obtained by (Matusik, et al., 2012).

According to (Horvath, et al., 2010), urea and kaolinite sheets interact via hydrogen bonds both through the NH_2 groups connected to the tetrahedral oxygens and through hydroxyl groups of the ions (located in the coordination sphere) connected to the carbonyl groups of urea. As seen, for the KPDMSO and KPDM (Figure 4.7 and 4.8), the position of the OH- bands were similar at 3698, 3657 and 953/957 cm $^{-1}$, however, for the KPDMU (Figure 4.9) there's a complete disappearance of the outer hydroxyl stretching vibrations while the inner hydroxyl stretching vibrations occurring at 3619 cm^{-1} remained. Basing on the predictions established by (Larkin, 2011), the vibrations occurring at 3427 cm $^{-1}$ could be attributed to the out of phase vibrations of the N-H stretch in the tetragonal urea while at 3340 cm^{-1} could be assigned to the in phase vibrations of the N-H stretch (Horvath, et al., 2010) and this agrees with the bands at 3420, 3436

and 3333 cm $^{-1}$ obtained by (Fischer & McDowell, 1960), while on the other hand, the free C = O stretch and some free bending NH_2 motions (Piasek & Urbanski, 1962b) due to urea is ascribed to the 1612 cm $^{-1}$ vibrations; this is in agreement with (HJ Becher, 1956; Piasek & Urbanski, 1962b). In addition, the vibrations observed at 1590 cm $^{-1}$ represents the H-N-C + C-N stretch and the in phase CH_3 bend of urea occur at 1455 cm^{-1} vibration. In reference to known computer simulations the possible orientation of urea in the kaolinite-urea complex described that urea molecules points towards the silica sheet such that, the hydrogen bonding is formed between the N-H group and the siloxane surface while conjugation between the C = O and N-H groups no longer exists; in so speaking the free C = O vibration bands in the IR spectra was expected to be seen (Horvath, et al., 2010; Rutkai, Makó, & Kristóf, 2009). In many cases, the C = O stretching vibrations in saturated aliphatic aldehydes, ketones and acids have frequencies in the range 1740—1700 cm $^{-1}$ (Piasek & Urbanski, 1962b); which is higher than the observed vibrations for the KPDMU and the reason as pointed out by (Piasek & Urbanski, 1962b) is attributed to the existence of resonance structures caused by the presence of the free C=O molecules which interact with NH_2; a mechanism which has been described elsewhere (Piasek & Urbanski, 1962b).

Precisely, the IR bands seen at 1455 cm $^{-1}$ represents the asymmetric or scissoring C-N vibrations while those occurring at 1000 cm $^{-1}$was ascribed to C-N symmetric modes and this is in agreement with 1465 and 1000 cm $^{-1}$ by (Piasek & Urbanski, 1962b) and 1468 and 1010 cm $^{-1}$ by (HJ Becher, 1956). The bands occurring at 1149 cm $^{-1}$ represents the wagging or rocking N-H vibrations due to urea intercalated into the kaolinite layers; again this agree with N-H vibrations at 1155 cm $^{-1}$ obtained by (Piasek & Urbanski, 1962b). According to predictions made by (Barlow & Corish, 1959a) and (HJ Becher, 1956), the vibrations occurring at 786 cm $^{-1}$ was ascribed to mutual N-H and CO out-of-plane wagging vibrations or in other words it is called the skeletal out-of-phase bending frequency equally attributable to larger deformational force constant, resulting from the decrease in the N-N distance of tetragonal urea (Fischer & McDowell, 1960). Finally for the KPDMU, the infrared bands occurring at 739 cm $^{-1}$ represent the characteristic hydroxyl stretching vibrations of alumina of the kaolinite in a tetrahedral configuration for the AlO_4 antisymmetric stretching while the SiOAl skeletal vibrations are observed at 527 cm^{-1}.

Above that, unique changes were observed when gum arabic was used to encapsulate the urea-kaolinite intercalation compound to form the targeted nanocomposite KPDMUG. As can be seen in Figure 10, there's a complete disappearance of kaolinite peaks at 3683, 3650 and 3618 cm $^{-1}$. As a matter of fact, the vibration occurring at 3618 cm $^{-1}$ which once was noted to remain in the KPDMSO, KPDM and KPDMU despite the associated treatments, the peak disappeared upon crosslinking with gum Arabic and this is a unique observation that we have recorded. Noticeably, the out phase vibration of the KPDMU at 3427 cm $^{-1}$ has disappeared altogether. The band at 3340 cm $^{-1}$ for KPDMU was raised to 3346 cm $^{-1}$ in the KPDMUG. Two completely new bands appeared at 3212 and 2924 cm $^{-1}$ with unique positioning and that is to say, there's a shift of the position 3427 cm $^{-1}$ of KPDMU to 3346 cm $^{-1}$ of KPDMUG and 3340 cm $^{-1}$ of KPDMU to 3213 cm $^{-1}$ of the KPDMUG although the peak shape was seen to change from narrow-sharp to broad for the KPDMUG. Such a phenomena as pointed out by (Fischer & McDowell, 1960) that, upon crosslinking KPDMU with gum Arabic, the out phase vibration shifted from 3427 cm $^{-1}$ of KPDMU to 3346 cm $^{-1}$ of KPDMUG while the in phase vibration shifted from 3340 cm $^{-1}$ of KPDMU to 3213 cm $^{-1}$ of the KPDMUG. This phenomena indicated that, upon crosslinking with gum arabic, urea' unit cell was going from tetragonal to hexagonal shape as revealed from the spectra changes in the N-H stretching region of both KPDMU and KPDMUG.

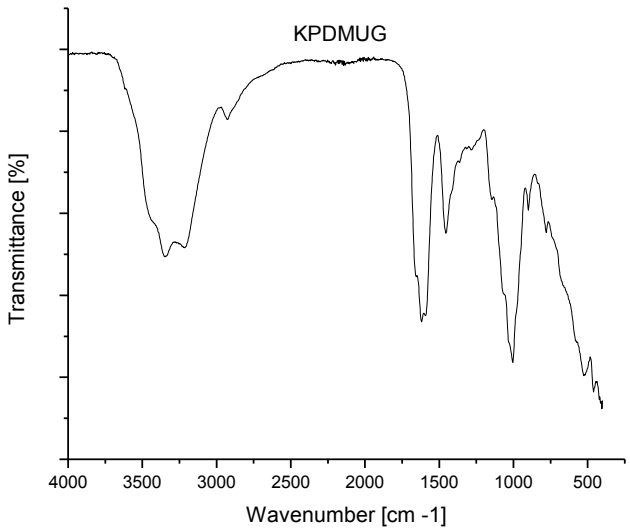

Figure 4.10. ATR-FTIR spectrum of KPDMUG

According to the assumptions made by (Fischer & McDowell, 1960), the tetragonal urea has its structure characterized by shorter hydrogen bonds which in fact made us to assume that there will be lengthening of H-bonds in the hexagonal type. That is to say, during the formation of complex crosslinked urea-kaolinite structure, hydrogen bonding caused a change in orientation from more favorable tetragonal structure to a less favorable hexagonal structure which in turn reduced the stability of the later as contrary given by (Fischer & McDowell, 1960).

Our prediction on the peak positioning after critical review in (Padil, Nguyen, Ševců, & Černík; Vahur, 2014) and (Almuslet, Elfatih, Al Sayed, & Mohamed, 2012) is that, the band seen at 3346 cm^{-1}represents the N-H stretch of urea while that in 3213 cm^{-1} correspond to the O-H stretching vibrations which signifies that there's a hydrogen bonded hydroxyl group between the polymer and the intercalated nanocomposite. Precisely, this absorption band shows that the O-H bond was formed in the bonding of the intercalated nanocomposite and the crosslinking polymeric membrane (Padil, et al.). A general observation in our view is that, the strong broad at 2924 and 1619 cm^{-1} is typical for carbohydrates which in our case refers to gum arabic grafted onto the substrate (Vahur, 2014). In a narrower view, the vibrations at 2924 cm^{-1} was ascribed to the C-H stretching; this deviates a little bit from 2933 cm^{-1} obtained by (Almuslet, et al., 2012). Basing on the fact that this band emerged as a new shoulder upon crosslinking with gum arabic on the KPDMU, our conclusion has therefore been that it represents the symmetric stretching of both CH_2 and CH groups which in turn proves the existence of grafting of gum arabic on the nanocomposite KPDMU (Almuslet, et al., 2012). The strong-high intensity peak at 1619 cm^{-1} correspond to the COO asymmetric stretching (*i.e.* *v*C=O; *v*C-O) resulting from the interaction between gum Arabic and the urea-kaolinite nanocomposite. This can be equally compared with 1610 cm^{-1} obtained by (Almuslet, et al., 2012). Basing on the observations made before, we have concluded that the vibrations observed at 1455 cm^{-1} were ascribed to the in phase bending of urea. A close analysis of the frequencies seen at 1004 cm^{-1} made us to ascribe us to the C-N vibrations. In addition, the infrared band occurring at 779 cm^{-1} represents the characteristic hydroxyl stretching vibrations of alumina of the kaolinite in a tetrahedral configuration for the AlO_4 antisymmetric stretching while the SiOAl skeletal vibrations are observed at 525 cm^{-1}.

4.2.1 Thermogravimetric analysis

TG-DTG analysis was employed in investigating thermal degradation and stability of the samples under N_2 atmosphere. Relative to the TG thermograms for pure urea fertilizer (Figure 4.11), DMSO intercalated kaolinite (Figure 4.12) exhibited three degradation phases: the first was observed around 48-98 °C attributed to the evaporation of externally adsorbed water on the kaolinite platelets, and this is related to 43 °C obtained by (Czarnecka, 2013). The second degradation was observed around 120-170 °C corresponding to the removal and decomposition of DMSO, whereas the third phase was observed at around 520-575 °C which corresponds to the dehydroxylation of kaolinite sheets. Considerably, in average these results are respectively comparable to 154 and 485 °C obtained by (Chakraborty, Sukul, Dana, & Malik, 2013) and also, 181 °C and 514 °C obtained by (Czarnecka, 2013). On the other hand, methanol intercalated kaolinite is associated with two decomposition stages (Figure 4.13): the first which is comparably narrow was observed around 75-250 °C corresponding to the removal of water moisture adsorbed on the sample as well as externally adsorbed methanol molecules, and this was relatively lower than 350 °C obtained by (Czarnecka, 2013). The second degradation stage which is comparatively wider was observed at around 450-600 °C corresponding to the decomposition of methanol-kaolinite intercalated compound and this observation reveals that methanol intercalated compound is highly hygroscopic such that the high amount of adsorbed water was completely removed at 250 °C.

According to (Vaughan, 1955), kaolins undergo dehydroxylation transformation within 400-700 °C temperature range; however, the maximum dehydroxylation of kaolinite in the modified kaolinite (NaKP) was observed (Figure 4.14) at 575 °C, therefore, a close look at the dehydroxylation transformation of 450-600 °C for methanol intercalated kaolinite prepared would reveal an increased thermal stability. Furthermore, slight but significant changes in the thermal decomposition behavior with three degradation stages were observed when urea replaced methanol in the kaolinite interlayer spaces to form KPDMU (Figure 4.15). The first weight loss was observed at approximately 100-125 °C corresponding to the following: (i) the loss of non-constitutional water, (ii) removal of interlayer water, (iii) elimination of water coordinated to exchangeable cations or structural water as mentioned in (Pereira, Minussi, da Cruz, Bernardi, &

Ribeiro, 2012), and (iv) degradation of urea; this disclose the fact that the release properties of our engineered urea CRF formulation would work best at that temperature range.

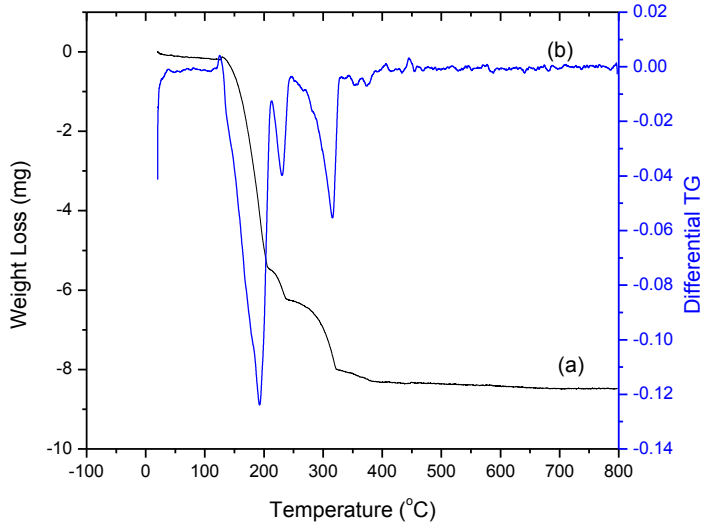

Figure 4.11.(a) TGA thermograms of Urea (b) Differential plot of urea fertilizer

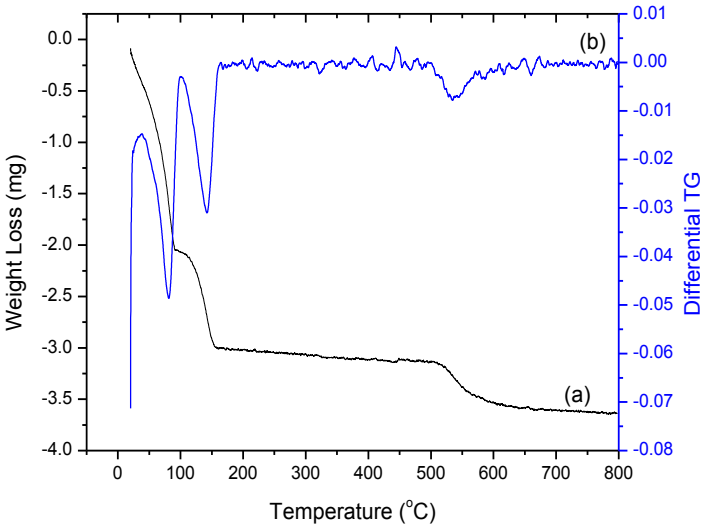

Figure 4.12. (a) TGA thermograms of KPDMSO (b) Differential plot of KPDMSO

Basing on the findings obtained by (M. M. Costa, Cabral-Albuquerque, Alves, Pinto, & Fialho, 2013), urea loss at about 140-250 °C is caused by both, (i) its own vaporization, and (ii) degradation to its complementary form known as biuret [$NH(CO)_2(NH_2)_2$].

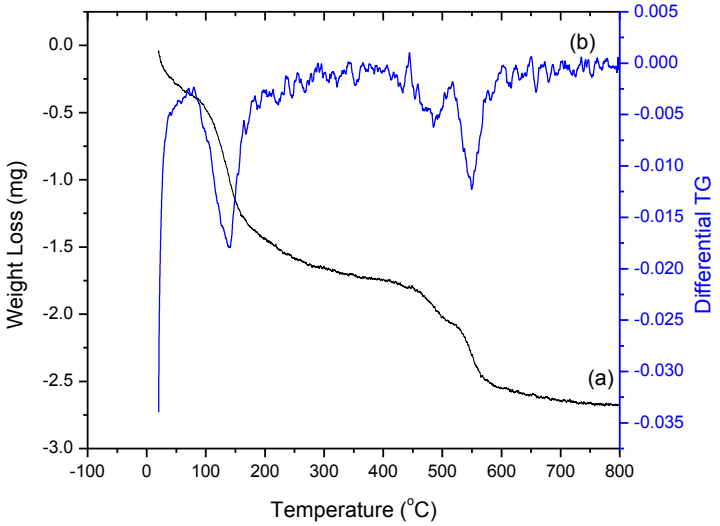

Figure 4.13. (a) TGA thermograms of KPDM (b) Differential plot of KPDM

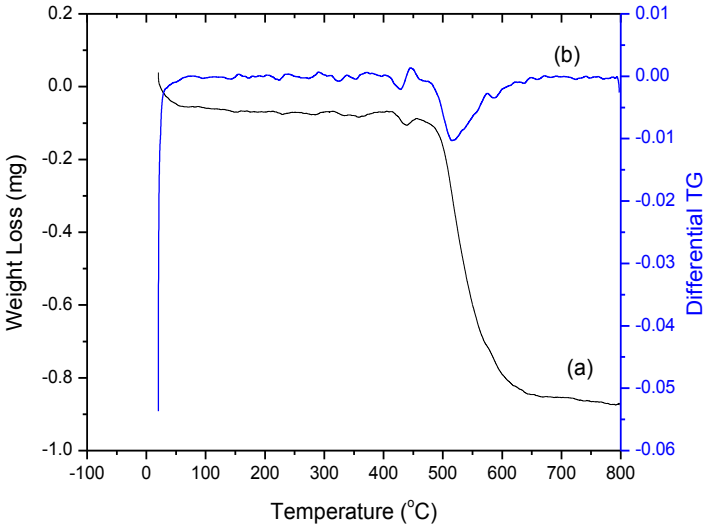

Figure 4.14. (a) TGA thermograms of NaKP (b) Differential plot of NaKP

The second weight loss was observed at about 225-350 °C attributed to (i) the continuous sublimation of urea, and (ii) decomposition or self-condensation of biuret [$NH(CO)_2(NH_2)_2$] to more complex decomposition product to the completion of vaporization and degradation reaction (M. M. Costa, et al., 2013). The third weight loss was observed at around 500-575 °C and was ascribed to the dehydroxylation of kaolinite a phenomena constituted by the decomposition of urea-kaolinite intercalated compound as well as elimination of structural hydroxyl and organic matter (Czarnecka, 2013; Pereira, et al., 2012; Vaughan, 1955). Comparatively, the thermal

stability of methanol intercalated kaolinite and urea intercalated kaolinite increase in the inverse order.

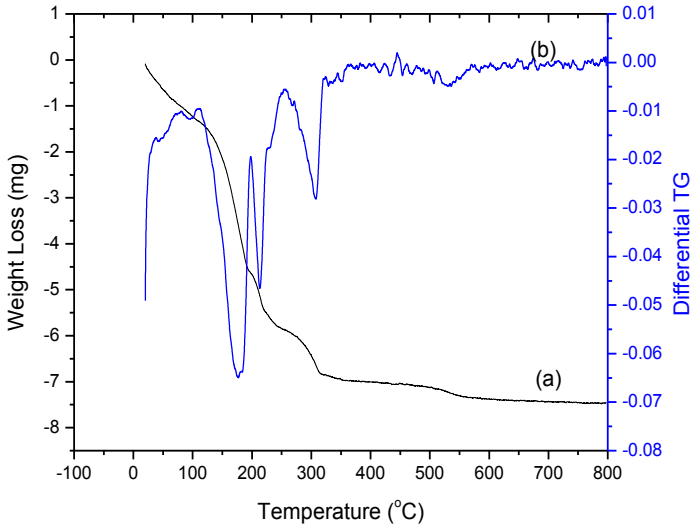

Figure 4.15. (a) TGA thermograms of KPDMU (b) Differential plot of KPDMU

Finally, the TG thermogram for the KPDMUG nanocomposite is associated with two degradation stages: the first was observed at approximately 48-425 °C ascribed to the moisture evaporation, decomposition of the gum arabic biopolymer as well as the elimination of interlayer

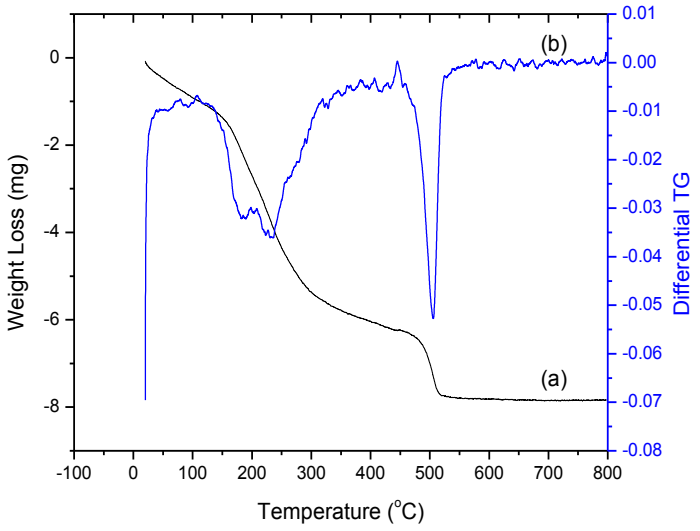

Figure 4.16. TGA thermograms of KPDMUG (b) Differential plot of KPDMUG

moisture and water coordinated in the exchangeable cations as named by (Pereira, et al., 2012). In fact, decomposition of gum arabic has been found to be in a range between 72 – 318 °C (Gary et al., 2010) which signify that temperature below that and above that range are due to moisture evaporation as well as elimination of interlayer moisture and coordinated water respectively. The second stage occurred at about 475-550 °C corresponds to the dehydroxylation of kaolinite. In this work, the first thermal degradation phase of the nanocomposite is the most titillating and significant since it reflect the objective of our study aiming at designing urea based CRF formulation via kaolinite intercalation reactions followed by encapsulation. As seen in (Figure 4.16), the first degradation temperature with maxima at 425 °C ascribed to urea reveal an increased thermal stability of the nanocomposite (KPDMUG) relative to the urea intercalated kaolinite (KPGMU) whose first thermal degradation temperature was noted to be at 205 °C maxima.

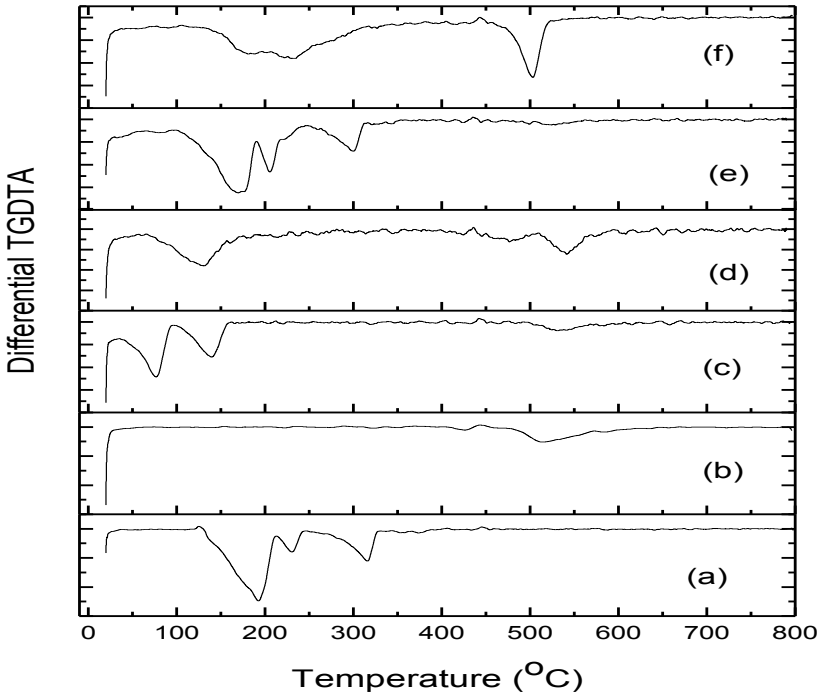

Figure 4.17. Differential thermograms

In addition to that, the derivative thermogravimetric analysis (DTG) as seen in (Figure 4.17) provides the information regarding the thermal stability behavior of the prepared materials. KPDMSO and KPDM are dominated by decomposition of non-constitutional water and kaolinite

degradation; when compared to the DTG curve of NaKP, KPDMSO has an increased thermal stability by 10 °C (520 for NaKP vis-à-vis 530 for KPDMSO), whereas KPDM has an increased thermal stability by 30 °C (520 for NaKP vis-à-vis 550 for KPDM) and this portrays a substantial increase in melting temperature of the intercalated compounds as related to the modified kaolinite NaKP. Contrary, the DTG curve of urea intercalated kaolinite and the nanocomposite are characterized by the urea degradation, a phenomena which was also noted (although in a different setting) by (Pereira, et al., 2012) which in our case is marked by temperature regimes of: 199 °C, 226 °C, and 320 °C for pure urea; 175 °C, 215 °C, and 302 °C for urea intercalated kaolinite (KPDMUG) as well as, 180 °C, 240 °C and 510 °C for nanocomposite (KPDMUG). The presence of some free kaolinite residues not crosslinked were also noted and are revealed by the high 510 °C decomposition temperature observed only to the KPDMUG but absent in the pure urea and KPDMU.

4.2.1 Urea release profiles

The release of urea from pure urea, KPDMU, and KPDMUG as a function of time (in 5 hours intervals) was done by first weighing the amount of sample and then introducing the sample into the known volume of water contained in the dialysis bags. The system was shaken continually throughout the release trials. Measurements were taken after every 5 hours intervals by simply drawing the solution from the dialysis membranes for analysis. Spectrophotometric determination of the amount of urea in water with hypochlorite and phenol technique was done thereafter. The method was adopted from (Emmet, 1969) involving 8 steps which involves transferring a 20.0 ml aliquot of sample, which should be colourless, free from solid matter and at room temperature to a 25 ml volumetric flask containing a microstirring magnet. Sample cavitation was barred through rapid addition because the microbubbles contribute to the blank signal; then 3.0 ml of distilled water were added and stirred vigorously followed by the addition of 0.30 ml of NaOCl reagent. After 5 seconds, 0.50 ml NaOBr was added with one hand whereas, (0.30 + X) ml of HC1 reagent was added with the other hand after 2 more seconds ("X") is the volume in ml of HC1 reagent required to titrate 0.50 ml of NaOBr reagent to pH 7.0). Furthermore, after 20 seconds 0.50 ml of H_3BO_3 buffer reagent was added with one hand followed with addition of 0.30 ml ethanolic phenol reagent after 2 more seconds with the other hand and stirred for 20 more seconds. After these 20 seconds, the absorbency of the sample

solution at 454 nm was compared against distilled water. The blank sample procedures may be found elsewhere (Emmet, 1969). Calculations were then done to determine the concentration of urea by multiplying the difference between the blank and the general sample absorbencies by the difference between the general and standard sample absorbencies and divide by three twentieths the urea-N concentration of the added standard solution. The reader is recommended to view the detailed procedure and the mechanisms associated from the original author of this method (Emmet, 1969). Besides, the rate of urea release as a function of time for a period of 150 hours was then investigated and summarized in Figure 4.18.

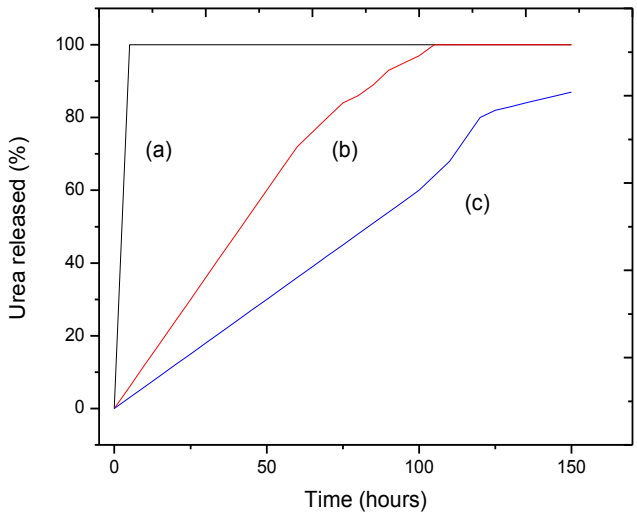

Figure 4.18. Release rate of (a) pure urea (b) KPMDU and (c) KPDMUG as a function of time at pH 7 and room temperature.

As can be seen, upon arduous dissolution test performed 100% of the pure urea was released in just the first five hours of the first attempt to draw the aliquot a result which was expected due to volatility of urea fertilizer associated with up to 60 to 70% loss in few minutes of the nitrogen being applied to the field (A Meybeck & V Gitz, 2012) such that its utilization efficiency or plant uptake of urea is generally below 50% (M. Liu, et al., 2007). For the urea intercalated kaolinite nanocomposite (KPDMU) the observation made was that 100% of the intercalated urea was released within 97 hours thereby unveiling the fact that Pugu kaolinite can retain urea and so can be used as a natural excipient for the preparation of CRF formulations. This observation indicate that urea adsorption and its subsequent intercalation into the kaolinite interlayer spaces was

successful such that for its dissolution to take place an extended period of time was needed to induce its release mechanism.

Furthermore, the ability of gum arabic biopolymer to retard urea dissolution was also noticed by its ability to retard urea release for a period of more than 150 hours. As can be seen, only 87% of the encapsulated urea contained into the kaolinite sheets was released after 150 hours. Such appealing results confirm our hypothesis that Pugu kaolinite layers can be expanded to accommodate molecular moieties; that said it can be used to design CRF formulations basing on urea fertilizer. As it was pointed out elsewhere (Pereira, et al., 2012) [a fact which we also agree] that "in conventional application, the materials would be exposed to low water contents, and one can expect a better retention effect by the nanocomposites". That is to say, the period of urea release from both urea intercalated kaolinite nanocomposite and encapsulated urea nanocomposite is expected to be more than these reported values done in the harsh laboratory settings.

Conclusion

In Tanzania, nitrogenous fertilizers have been used for years by virtue of their high nitrogen content to supplement nitrogen to crop plants. However for urea despite having high nitrogen content of about 46%, it has been associated with approximately 60 to 70% loss of the nitrogen being applied because of ammonia produced through hydrolysis of urea by soil urease a problem which could be minimized by inhibiting soil urease through encapsulation with synthetic or biopolymers as well as intercalation with nano-clays. In this paper we have described the amendments of urea fertilizer through intercalation into the kaolinite interlayer spaces and then encapsulating the intercalation compound with gum arabic biopolymer for the purpose of preparing urea control release fertilizer which in turn will minimize its volatility as well as improve its utilization efficiency (FUE) by plants and also minimize the losses thereby reducing repeated fertilization expenditure per season and maximize crop yields. The entire experimental setup involved take in sampling of raw kaolinite from Pugu hills Tanzania, beneficiation of the raw kaolinite, activation of kaolinite layers, preparation of intermediate intercalation compounds and intercalation of urea fertilizer into the kaolinite layers by replacement reaction. Similarly, the intercalated urea fertilizer was subsequently encapsulated by using gum arabic biopolymer. The

nanomaterials synthesized were characterized by using several techniques including ATR-FTIR, XRD, SEM, XRF, TGDTG and particle size analysis via Scherrer equation along with distribution of particles through the application of Andreasen pipette sedimentation method. Our effective beneficiation process was able to minimize non-clay portion from 39.58% of the raw Pugu kaolinite to 0.36% of the beneficiated Pugu kaolinite as well as increasing the clay portion from 60.42% to 99.64% of raw and beneficiated kaolinite respectively. The morphology of the samples were observed to change from thick compact overlapping euhedral pseudohexagonal platelets to irregular booklets which then changed to vermiform morphology and dispersed euhedral pseudohexagonal platelets coexisting with blocky-vermicular booklets. The unique brain-from agglomeration and later poor roundish particles organized in mat morphology was observed. The particle sizes of the prepared nanocomposites ranges from 14.55 nm to 92.46 nm whereas the indexing procedures revealed the existence of FCC Bravais lattice for the kaolinite under study; also, X-ray mineralogy tests indicated the major phase in the Pugu kaolin under study after beneficiation to be kaolinite subordinated with illite. The Intercalation ratios were found to be in the order of KPDM > KPDMSO > KPDMU while the TGDTG thermograms showed that the nanocomposites prepared were capable of decomposing starting from evaporations at 48 °C to 600 °C for the dehydroxylation of kaolinite layers. Release profiles were established in period of 150 hours where the release rates were 100% in the first 5 hours of trials, 100% in the period of 97 hours and 87% in the period of 150 hours for pure urea, urea intercalated kaolinite nanocomposite and the encapsulated nanocomposite respectively.

CHAPTER FIVE

Dynamics of Kaolinite-Urea Nanocomposites via Coupled DMSO-Hydroxyaluminum Oligomeric Intermediates[4]

Abstract

Kaolinite-urea nanocomposites were prepared via intercalation reactions in an attempt to investigate the dynamic nature of kaolinite morphology for advanced applications in controlled release systems (CRSs). Characterization was carried out by using SEM-EDX, XRF, ATR-FTIR, XRD and DT/DTG along with the Andreasen pipette sedimentation technique which was used to determine the grain size distribution of the raw kaolinite. The X-ray diffraction pattern revealed the existence of an FCC Bravais lattice where the intercalation ratios attained were 51.2%, 32.4%, 7.0% and 38.4% for hydroxyaluminum oligomeric intercalated kaolinite, substituted urea intercalated kaolinite, calcined DMSO intercalated kaolinite and hydroxyaluminum re-intercalated kaolinite respectively along with their respective crystallite sizes of 33.51-31.73 nm, 41.92-39.69 nm, 22.31-21.13 nm and 41.86-39.63 nm. The outcomes demonstrated that the employed intercalation routes require improvements as the intercalation reactions were in average only ≈ 32.3%. The observations unveiled that, it is possible to manipulate kaolinite structure into various morphologies including dense-tightly packed overlapping euhedral pseudo hexagonal platelets, stacked vermiform morphologies, pustulated forms and unique patterns exhibiting a self-assembled curled glomeruli-like morphologies. Such a diversity of kaolinite morphologies expedites its advanced applications in the controlled release systems (CRSs) such as drug delivery systems and controlled release fertilizers (CRFs).

Keywords: Nanocomposite, Intercalation, Oligomer, Vermiform, Nanostructures, Curled-glomeruli-like-morphologies

[4] Sempeho, S. I., Kim, H. T., Mubofu, E., Pogrebnoi, A., Shao, G., & Hilonga, A. (2015). Dynamics of Kaolinite-Urea Nanocomposites via Coupled DMSO-Hydroxyaluminum Oligomeric Intermediates. Indian Journal of Materials Science, **2015**(ID 920835), 1-10.

5.1 Introduction and Literature Review

Kaolinite intercalation reactions has been a topic of interest to researchers owing to the scientific and technological advancements in the areas of composites, nanotechnology, controlled released formulations (Sempeho, et al., 2014) such as drug delivery systems and controlled release fertilizers among others (Joshi, Kevadiya, Patel, Bajaj, & Jasra, 2009; B. Kevadiya, Patel, Joshi, Abdi, & Bajaj, 2010; B. D. Kevadiya et al., 2012; Khazaeli, Pardakhty, & Hassanzadeh, 2010; Kielmann, Jeschke, & García-Rubio, 2014; B. Li, He, Evans, & Duan, 2004; Nandi, Goswami, & Purkait, 2009; Pinto et al., 2011). Progressive applications arising from kaolinite engineering designs have been feasible processes because this inexpensive chemical mineral can be modified through ion exchange mechanisms by just intercalation of ionic species into the kaolinite interlayer spaces; in fact, the hydrated form of the mineral consists of kaolinite sheets interspersed with monomolecular sheets of water molecules which is essential feature for intercalation reactions or in other word is termed as *clay' advantageous properties* (Macewan, 1947; Sunardi, Irawati, Arryanto, & Sutarno, 2011).

According to (Suresh, Borkar, Sawant, Shende, & Dimble, 2010), the fate of the mentioned ion-exchange mechanism include both (i) the widening of gap between the single sheets thereby facilitating the insertion of organic species into the interlayer spaces, and (ii) the alteration of the surface charges of each single sheets from being hydrophilic to organophilic (Giannelis, 1996). The likelihood that an intercalation reaction will be feasible depends on the interactions between polar functional group-containing compounds and layered phyllosilicates such as kaolinite, a mechanism which involves the interaction between clays with exchangeable cations as well interactions with siloxane surfaces via surface adsorption (H. Li, Sheng, Teppen, Johnston, & Boyd, 2003). According to (H. Li, et al., 2003), the ion-dipole mechanism may involve either the direct interactions of organic compounds with exchangeable cations or in-direct interaction through the intermediation of water molecules surrounding the cations where also, an increase in the charge valence of exchangeable cation is known to enhance the ion-dipole interactions (Bowman, 1973; H. Li, et al., 2003; Loux, Liebl, & Slife, 1989; Sawhney & Singh, 1997).

However, it has been evidenced that, nonpolar surface interactions between organic compounds and the siloxane surfaces of the clays may also occur; and also, the weakening of ion-dipole

interactions is possible at times when water molecules surrounding strongly hydrated cations such as Ca^{2+} and Mg^{2+} inhibit the direct interaction between polar functional groups and the exchangeable cations (Jaynes & Boyd, 1991; Cliff T Johnston, de Oliveira, Teppen, Sheng, & Boyd, 2001; Laird & Fleming, 1999; H. Li, et al., 2003). Fundamentally, the presence of charges on the clay minerals is an inherent property which facilitate most intercalation reaction; where, the main source of these charges on the clay minerals is isomorphous substitution reactions (R_1) permanent charge due to isomorphous substitution) for the reason that it confers permanent charge on their surface of the layers (Lajos, 2008).

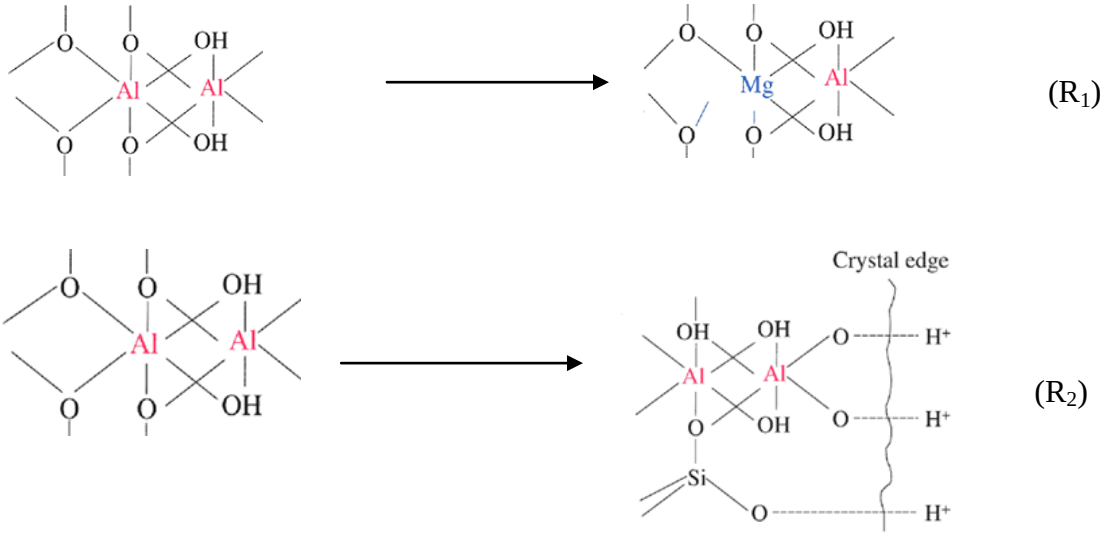

(R_1)

(R_2)

Essentially, the development of charges on the clay surfaces can also be attributed to (i) ionization of hydroxyl groups as well as (ii) the presence of surface and broken-edge OH^- groups apart from the major isomorphous substitution reactions (Lajos, 2008). That is to say, pH dependent charge (which is not permanent as for the isomorphous substitution) develop when there is ionization of hydroxyl groups on the surfaces of other particles (R_2) pH dependent charges on the edges describing the fact that, at lower pH, H^+ are tightly bound and so less tendency to intercalations); whereas, the presence of surface and broken-edge OH^- groups (which exposes the functional groups for maximum interactions) gives rise to the needed electronegativity along with the kaolinite particles' ability to adsorb and so intercalate ionic species. Thus, as pointed out by (Lajos, 2008), clay particles are stacked in layers like sheets of papers where each sheet is slightly separated from those on either side and has negative charges

on it which could be balanced by positive ionic species, a phenomena which is critical for the kaolinite interactions including intercalations reactions (Figure 5.1).

In this paper, we have described the dynamic morphological changes in the kaolinite nanocomposite structures basing on the urea intercalated kaolinite as a function of DMSO-hydroxylaluminum oligomeric intermediate intercalation compounds and calcination reactions. The aim was to study the changes associated with coupling DMSO intercalated with kaolinite with hydroxylaluminum oligomeric cations to prepare well-ordered self-assembled particles into beautiful and unique curled patterns.

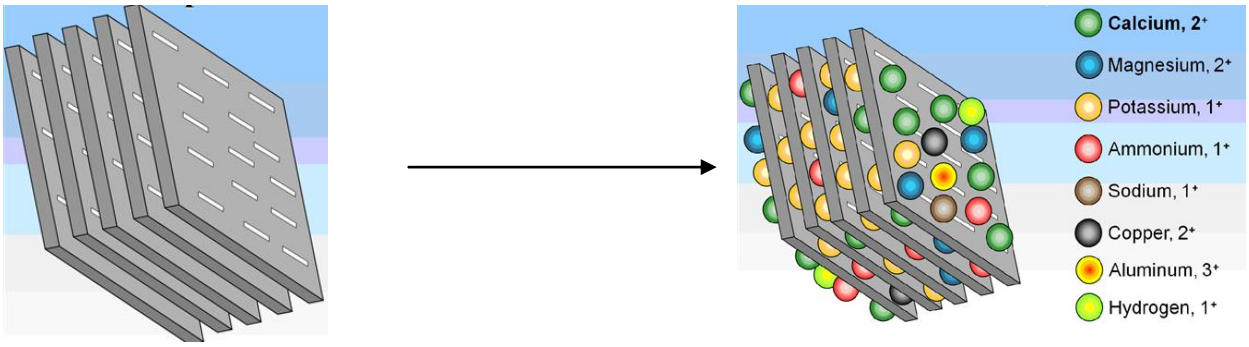

Figure 5.1. Ability of negatively charged clay particle to intercalated ionic species

NB: This figure has been adopted from (Lajos, 2008)

5.2 Materials and Methods

Kaolinite was collected at Pugu hills in the Coast region Kisarawe Tanzania by using quartering sampling technique described by (Sempeho, Esther *et al*. 2012). Urea (ACS reagent, 99-100%) was supplied by Sigma Aldrich, DMSO (Extra pure, ≥ 99.5%) was supplied by Daejung chemicals & metals, Co. Ltd, Gyonggi-do, Korea, Sodium chloride (Extra pure, ≥ 99.0%) was supplied by Samchun pure chemicals Co. Ltd, Gyonggi-do, Korea, Silver chloride (ACS reagent, 99.0%) was supplied by Sigma Aldrich, Deionized distilled water (D.I) was supplied by Prof. Kim's lab, Sodium hydroxide (extra pure grade, min. 93.0%) was was supplied by Duksan pure chemical, Ansan city, Kyungkido-South Korea and Aluminium chloride (99.99%) was supplied by Junsei chemical Co. Ltd, Japan.

5.2.1 Materials Preparation

a) Beneficiation and treatment of raw samples

Wet beneficiation technique was achieved by simple size separation using "Classifier". The method involved the separation of fine platy kaolinite from coarser quartz, feldspar mica and other impurities using different setting velocities associated with particle size as governed by Stockes's law (Bajaj & Jasra, 2007; Brown & Brindley, 1980; Ciros Co., 2013; Jovanović & Mujkanović, 2013; Jovanović & Volkov-Husović, 2012; Martin, 1984; Oder, 1976; Stein & Cheremisinoff, 1986). The entire procedure which involved crushing to pulverization and soaking as well as running the classifier unit to drying has been comprehensively described in (Sempeho, Lugwisha *et al*. 2012). A known amount of Pugu kaolinite was dispersed in a 0.1 M NaCl solution and treated ultrasonically at 50 °C for 30 hours and then magnetically stirred for 30 hours. The product was filtered under vacuum filter and washed several times to remove excessive chlorides; washing was stopped after negative reaction with $AgNO_3$. The washed product was dried in a vacuum oven at 60 °C and stored as B_1.

b) Preparation of kaolinite-intercalation nanomaterials

$AlCl_3$ solution (0.1 M) was mixed with 0.1 M NaOH solution at a 1:2 molar mixing ratio respectively. The mixture was stirred at 85 °C for 6 hours and then aged for 12 hours. A 5% beneficiated kaolinite suspension was prepared and was ultrasonically mixed with an excess of hydroxyaluminum oligomeric solution at 70 °C for 3 hours. The product was named B_2 which was then washed in a vacuum pump to remove unreacted materials and chloride ions as tested by $AgNO_3$ solution. By using B_2 powder as a starting material, a small portion was taken and then mixed with 5 g of urea and stirred for 72 hours at 60 °C. The urea-kaolinite nanocomposite obtained was washed in a vacuum pump with excess water and dried at 60 °C in a vacuum oven and stored as B_3. A small portion of beneficiated and modified Pugu Kaolinite was magnetically stirred with DMSO solution in a ratio of 1:6 for 21 days at 80 °C with a very small addition of water droplets. The suspension was then aged for 7 days and then washed with excess isopropanol and dried at 60 °C in a vacuum oven to obtain powder. The DMSO intercalated kaolinite obtained in powder form was calcined at 850 °C (10 °C /min) for 8 hours with 6 hours holding time and cooling rate of 7 °C /min. The calcined sample was named B_4. To the calcined

powdered sample, 0.38 g was measured in a Sartorius analytical balance and mixed with 0.98 g of urea in excess of hydroxylaluminum oligomeric solution prepared as described above. The mixture was stirred at 105 °C to dryness and the powder obtained was named B_5.

5.2.2 **Characterization**

a) Infrared Spectroscopy. By using a Bruker Optic GmbH (alpha model, Laser class 1) Spectrometer with attenuated total reflectance (ATR) the FTIR-ATR measurements were performed in the near infrared region at wavelength between 7500-360 cm^{-1}.

b) X-ray Diffraction. SIEMENS D-5005 X-ray Diffractometer (Cu Kα1 radiation and 2θ scan range was between 2° – 65°) was used to determine raw kaolinite mineralogy whereas the XRD patterns for the intercalation compounds were executed on RIGAKU COORPERATION, D/MAX-2500/PC X-ray Diffractometer (Cu Kα1) equipped with a back monochromator operating at 40 kV and 100 mA at the scanning range of 5° – 80° with a step of 0.1° and a time/step of 1 s.

c) Thermogravimetry (TG/DTG).Thermograms were taken using TG/STA Linseis STA PT 1000 simultaneous TG/DTG thermal analyzer at a scanning rate of 5 °C per min from room temperature to 800 °Cunder nitrogen atmosphere.

d) Scanning Electron Microscopy-Energy-dispersive X-ray spectroscopy *(SEM-EDAX).*The samples surfaces morphology was investigated by using Field Emission Scanning Electron Microscopy (SEM-Hitachi-s-4800, Japan) coupled with EDX device. The accelerated voltage was 15 kV.

e) XRF Analysis. The raw kaolinite was analyzed for chemical composition using X-ray Fluorescence (XRF) employing the Semi Quantitative XRF Analysis technique (SIEMENS SRS 3000 X-ray Fluorescence (Rhodium anode, 8 analyzer crystals with beryllium windows 125 μm) (E. H. J. Lugwisha & Siafu, 2014).

f) Indexing the Diffraction Patterns and Particle size determination

The X-ray diffraction patterns were indexed by using mathematical method by first determining the unit cell parameter from the peak position and then Miller indices. The indexing procedures are as described in our other article (Sempeho et al., 2015a). For the nanocomposites, the crystallite sizes were estimated using X-ray diffraction patterns and the Scherrer equation whereas the analysis of particle size distribution of the raw kaolinite was done with sub-sieve

analysis technique by applying Andreasen pipette sedimentation method (E. H. J. Lugwisha & Siafu, 2014).

5.3 Results and Discussion

5.3.1 Raw kaolinite analysis

The investigation of kaolinite mineralogy was carried out by using randomly oriented whole rock X-ray analysis as well as the oriented whole rock X-ray diffraction as a function of untreated air-drying, glycolation and heating at 550 °C; the result revealed the presence of quartz (SiO_2), clinochlore [$Mg_5Al(Si,Al)_4O_{10}(OH)_8$] and microcline [$KAlSi_3O_8$] as non-kaolinite portions in the raw kaolinite which after beneficiation quartz and microcline disappeared.; this signify that the beneficiation procedure was effective. After beneficiation, kaolinite [$Al_2Si_2O_5(OH)_4$] was observed as a major dominant phase accompanied with a very small amount of illite [$KAl_2(Si_3AlO_{10})(OH)_2$] and clinochlore [$Mg_5Al(Si,Al)_4O_{10}(OH)_8$] which are also clay portion.

The chemical composition of raw as well as beneficiated kaolinite used revealed a reduction of silica content from 63.64 (present in the raw kaolinite) to 54.99% (in the beneficiation kaolinite). Similarly, there was an increase in alumina content from 31.43 to 40.2% before and after beneficiation respectively (Table 5.1). Besides, the compositions of other oxides varied from oxide to oxide although the amounts of TiO_2 and Fe_2O_3 in particular showed a reverse order of increasing instead of decreasing upon beneficiation whereas the amount of MnO was seen to be unaffected with beneficiation process employed as we stated elsewhere (Sempeho, Kim, et al., 2015a).

Table 5.1 . Chemical composition of the raw materials

	Oxide Composition												
Sample	SiO_2	Al_2O_3	Na_2O	MgO	SO_3	Cl	K_2O	CaO	TiO_2	Cr_2O_3	MnO	Fe_2O_3	LOI
Pugu Kaolin	63.64	31.43	0.43	0.16	0.25	0.76	1.39	0.06	0.80	0.03	0.01	1.01	0.03
Beneficiated Kaolin	54.99	40.20	0.09	0.13	0.08	0.04	0.96	0.04	1.02	0.04	0.01	2.00	0.40

5.3.2 X-ray indexing and particle size analysis

As seen in Table 5.2, the Miller indices sequence obtained from indexing procedures and the lattice parameter determination reveal the existence of an FCC Bravais lattice for the reason that the *hkl* reflections allowed correspond to that lattice structure with the average lattice parameter being 12.597 Å. Analysis of the intercalation reactions was based upon the replacement reaction where the oligomeric cations were first vigorously inserted into the kaolinite interlayer spaces followed by its substitution with urea fertilizer to formulate B_3. The X-ray diffraction revealed that the intercalation of oligomeric cations into the kaolinite interlayer spaces (B_2) proceeded at an apparent intercalation ratio of 51.2% (Table 5.3) corresponding to the expansion of basal lattice space of about 0.098 Å. For the B_3 nanocomposite the intercalation compound was formed at an intercalation ratio of 32.4% related to the basal expansion of lattice parameter of about 0.186 Å.

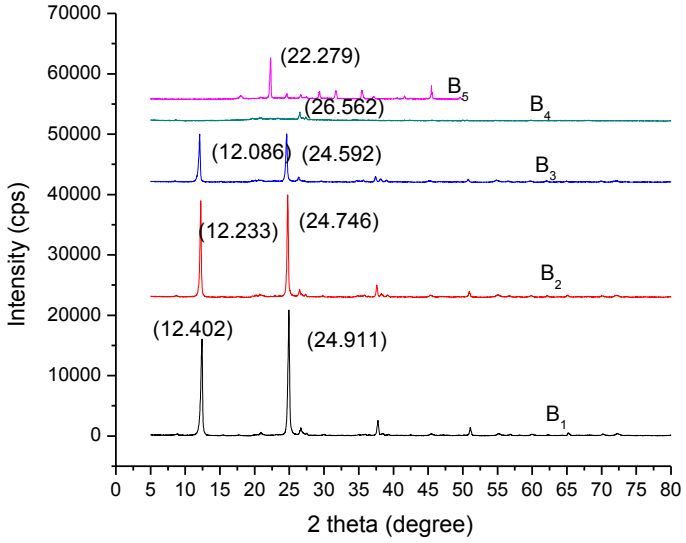

Figure 5.2. X-ray diffractograms for B_1, B_2, B_3, B_4 and B_5

Calcination reaction was then carried out on the DMSO intercalated kaolinite prepared as per our other article (Sempeho, Kim, et al., 2015a) which had an intercalation ratio of 89.2% but as seen in Figure 5.2 after calcination step described above this intercalation ratio of 89.2% dropped to 7.0% for the calcined B_4 and this was attributed to the disintegration of intercalant DMSO present in the kaolinite interlayer spaces to form corresponding DMSO decomposition material.

This drastic drop from 89.2% to 7.0% of intercalation ratio is associated to contraction (instead of the usual expansion of interlayer distances) of about 3.778 Å in the kaolinite layers upon calcination to 850 °C as stated in the procedures above. The impact of hydroxylaluminum oligomer in re-expanding the interlayer distance of the contracted calcined B_4 was then determined which revealed the fact that, the reaction for the re-intercalation of B_4 with hydroxylaluminum oligomeric cations preceded with an intercalation ratio of 38.4% (for B_5) from the 7.0% of the starting material (*i.e.*, B_4) and this correspond to the expansion of 0.634 Å in the basal lattice spaces from the compact calcined B_4.

On the other hand, the sizes of the nano-particulate materials obtained are presented in the Table 2as per Scherrer's equation. The order of particle sizes was observed to be in the following trend $B_3 \approx B_5 > B_2 > B_4$ which account for the fact that the size of hydroxylaluminum intercalated kaolinite (B_2) is lower than its re-intercalated counterpart (B_5). Similarly, we have established that, the size of urea intercalated kaolinite utilizing hydroxylaluminum intercalated kaolinite as an intermediated stage is greater than the size of urea intercalated kaolinite utilizing hydroxylaluminum intercalated kaolinite as an intermediated stage manipulated from the calcined DMSO intercalated kaolinite as the first generation intermediated complex cations.

Table 5.2. X-ray indexing and particle size analysis

Peak	2θ	$\sin^2\theta$	$3\sin^2\theta/\sin^2\theta_{min}$	$h^2+k^2+l^2$	*Hkl*	a (Å)	d (nm)
1	12.402	0.012	3.158	3	111	12.352	0.713
2	24.911	0.047	12.592	13	320	12.877	0.357
3	12.233	0.011	3.073	3	111	12.522	0.723
4	24.746	0.046	12.428	12	222	12.453	0.360
5	12.086	0.011	3.000	3	111	12.673	0.732
6	24.592	0.045	12.276	12	222	12.529	0.362
7	26.562	0.053	14.285	14	321	12.546	0.335
8	19.581	0.029	7.820	8	220	12.813	0.453
9	22.279	0.037	10.104	10	310	12.608	0.399

FCC crystal Bravais sequence

Table 5.3. Particle size and intercalation ratio

Material	A.I.R (%)	Average *l* (nm)
B_2	51.20	33.51-31.73
B_3	32.40	41.92-39.69
B_4	7.00	22.31-21.13
B_5	38.40	41.86-39.63

A.I.R = apparent intercalation ratio

l = particle size

5.3.3 FT-IR analysis

Kaolinite as other clay minerals can be identified by using the absorption bands due to structural O-H, Al-O-H and Si-O groups. That is to say, discussion regarding the IR absorption bands on the kaolinite minerals is mainly limited to the OH, Al-O-H and Si-O near infrared absorptions. Considering Figure 5.3, the inner hydroxyl groups in the OH stretching bands between the tetrahedral and octahedral sheets corresponds to the absorption near 3618 cm $^{-1}$ which as seen refers to 3618 cm $^{-1}$ for B_2 and B_3. This observation relates to 3620 cm $^{-1}$ obtained by (Madejova, 2003). There are two more absorption bands in the OH stretching region which are known to reside at the octahedral surface of the kaolinite layers forming weak hydrogen bonds with the oxygen of the Si-O-Si bonds on the lower surface of the next layers (Madejova, 2003) and they correspond to absorption bands near 3693 cm $^{-1}$ for B_3 and 3684 cm $^{-1}$ for B_2 representing the in-phase symmetric stretching vibration whereas the other corresponds to the absorption bands near 3650 cm $^{-1}$ for B_2.

The transformation from B_2 to B_3 which involved the replacement of the oligomeric cations with urea in the kaolinite interlayer spaces is marked by the three observations namely, a band shift from 3684 cm $^{-1}$ in B_2 to 3693 cm $^{-1}$ in B_3 while maintaining the 3618 cm $^{-1}$ peak position, the disappearance of 3650 cm $^{-1}$ band in B_3, and the appearance of six new peaks at 3426, 3334, 3256, 1669, 1587, and 1461 cm $^{-1}$. According to (Larkin, 2011), the bands observed at 3426 cm $^{-1}$ corresponds to the N-H out-phase stretching vibrations whereas the 3340 cm $^{-1}$ vibrations represents the in-phase N-H stretching vibrations in the tetragonal urea (Horvath, et al., 2010) which is in accord with the vibrations observed at 3420, 3436 and 3333 cm $^{-1}$ by (Fischer & McDowell, 1960). The absorption bands observed at 1669 cm $^{-1}$ represents both the free C = O

stretching vibrations along with free NH_2 bending vibrations due to urea which agrees with (HJ Becher, 1956; Piasek & Urbanski, 1962b). Moreover, the C-N stretching vibrations as well as the in-phase CH_3 bending vibrations due to urea correspond to the vibrations observed at 1587 cm^{-1} and 1461 cm^{-1} respectively. Similarly, the vibrations seen at 1461 cm^{-1} could also be attributed to the asymmetric or scissoring C-N vibrations (HJ Becher, 1956; Piasek & Urbanski, 1962b). In addition, the 3256 cm^{-1} vibrations are attributed to the O-H stretching vibrations associated with the formation of hydrogen bonding when urea replaced the oligomeric cations in the kaolinite inter layer spaces in (Almuslet, et al., 2012; Padil, et al.).

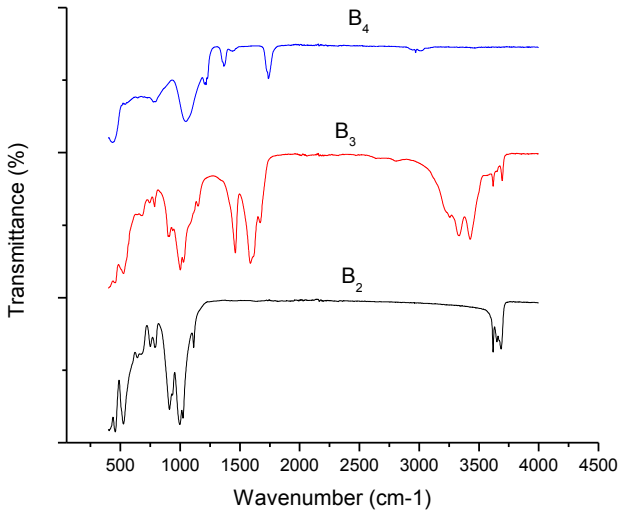

Figure 5.3. ATR-FTIR diffractograms for B_2, B_3, and B_4

Besides, the vibrations observed at 1113 cm^{-1} for B_2 and 1149 for B_3 correspond to the apical Si-O normal stretching mode which agrees with 1112 cm^{-1} obtained by (Balan, et al., 2001) whereas those observed at 1023 for B_2 and 1027 cm^{-1} for B_3 were attributed to the in-plane Si-O planar stretching vibrations and also vibrations seen at 997 for B_2 and 1001 cm^{-1} for B_3 correspond to both the out-phase Si-O planar as well as the alternating Si-O and Al-O bonds (Aroke & El-Nafaty; Dawley, et al., 2012; Heah, Kamarudin, Mustafa Al Bakri, et al., 2012; Mgbemena, et al., 2013a); which agrees with the 997 and 995 cm^{-1} obtained by (Dang, et al., 2013) and (Heah, Kamarudin, Mustafa Al Bakri, et al., 2012) respectively. The OH deformation of inner hydroxyl groups owing to the Al $^{(VI)}$-OH bending vibrations of kaolinite were related to

the IR bands observed at 910 cm $^{-1}$ for B_2 and 900 for B_3 which agrees to 907-912 cm $^{-1}$ from (Dawley, et al., 2012; Heah, Kamarudin, Mustafa Al Bakri, et al., 2012; Liew, Kamarudin, Mustafa Al Bakri, et al., 2012; Mgbemena, et al., 2013a). Furthermore, the vibrations observed at 788 to 749 cm $^{-1}$ for B_2 and 786 to 744 cm $^{-1}$ for B_3 correspond to the Al-O-Si asymmetric bending vibrations while the vibrations observed at 525 cm $^{-1}$ for B_2 and B_3 is related to the Si-O-Al $^{(VI)}$ bending vibrations given that the Al $^{3+}$ occupy the octahedral coordination as described elsewhere (Heah, Kamarudin, Mustafa Al Bakri, et al., 2012; Liew, Kamarudin, Mustafa Al Bakri, et al., 2012; Tironi, et al., 2012).

The bands observed at 1204 and 1216 cm $^{-1}$ correspond to the amorphous SiO_2 where the change from octahedral coordination of Al $^{3+}$ in kaolinite to tetrahedral coordination in metakaolinite is related to the appearance of coordination vibration of Al $^{(IV)}$-O at 777 and 434 cm $^{-1}$ and the disappearance of characteristic bands at 910 and 525 cm $^{-1}$ in B_2 and 900 and 525 cm $^{-1}$ for B_3 (Ilić, Mitrović, & Miličić, 2010; Soleimani, Naghizadeh, Mirhabibi, & Golestanifard, 2012), however, the appearance of the bands at 1047 cm $^{-1}$ in B_4 reveal the fact that the Si-O bonds and Si-O-Al of the original DMSO intercalated kaolinite remained unaffected but with just a slight alteration in the bands from 1023 and 1027 cm $^{-1}$ for the respective B_2 and B_3 to 1047 cm $^{-1}$at B_4. Similarly, a close look of the 1047 cm $^{-1}$ peak of the B_4 containing metakaolinite and 1023 cm $^{-1}$ of the beneficiated kaolinite bewrayed a considerable alteration in the Si-O-Si or Si-O-Al bond which appeared as narrow band for the beneficiated kaolinite transformed into the broad band of metakaolinite containing B_4 which might be attributed to the decreasing crystallinity in the kaolinite structure following calcination of the DMSO intercalated kaolinite to form its metakaolinite counterpart (B_4) (Soleimani, et al., 2012).

In practice, the intercalant agent DMSO (used in this work) is known to be highly stable at temperatures below 150 °C above which gradual decomposition start to form relatively volatile materials in the form of paraformaldehyde; these include among others dimethyl sulphide, dimethyl disulfide, bis-(methylthio)methane, water vapour and traces of methylmercaptan, dimethyl sulfone (R_3-R_6). In that way the reactions R_3 to R_6 describes the reactions which took place during calcination process to synthesize metakaolinite (B_4) which was in turn attributed to the absorption bands observed at 1365, 1438, 1738 and 2970 cm $^{-1}$, 1 for S=O sulfonyl stretching, S=O sulphate ester stretching, C=O stretch and either CH stretch or dimeric OH

carboxylic acid stretch respectively as seen in the reactionsR_3 to R_6 (Corporation, 2005; Gaylord, 2005a).

$$H_3CSOCH_3 \rightarrow H_3CSH + HCHO \Rightarrow (HCHO)_X \quad (R_3)$$

$$2H_3CSH + HCHO \rightarrow (H_3CS)_2CH_2 + H_2O \quad (R_4)$$

$$2H_3CSH + CH_3SOCH_3 \rightarrow H_3CSSCH_3 + H_3CSCH_3 + H_2O \quad (R_5)$$

$$2H_3CSOCH_3 \rightarrow H_3CSO_2CH_3 + H_2CSCH_3 \quad (R_6)$$

5.3.4 SEM-EDAX Analysis

The SEM micrographs were taken to determine the morphology of the nanomaterials prepared. The existence of an overlapping euhedral pseudo hexagonal platelets exhibiting a dense-tight-thick layers was observed in the beneficiated kaolinite (Figure 5.4 a, b), a feature which is typical to most kaolinite minerals (Uwins, et al., 1993).

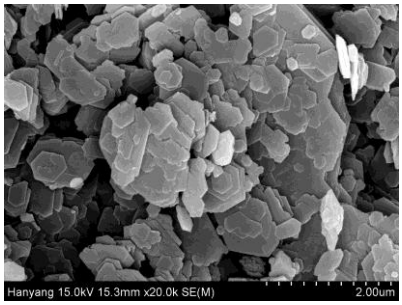

Figure 5.4a. SEM micrograph of beneficiated kaolinite

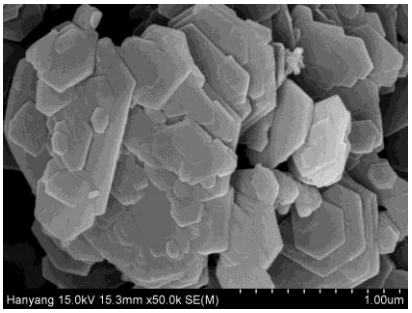

Figure 5.4b. SEM micrograph of beneficiated kaolinite

Besides, when beneficiated kaolinite was chemically treated with salt solution a change in the stacking sequence was observed in that, there was a formation of mixed vermiform shaped particles along with some skinny stacked euhedral pseudo hexagonal platelets (Figure 5.5a, b). As we have described in our other article (Sempeho, Kim, et al., 2015a), the hexagonal faces observed in these particles relate to the crystallographic (*001*) basal planes whereas the stacking sequence of layers correspond to the typical pattern of kaolinite minerals (Gardolinsky, 2005; Letaief & Detellier, 2009).

Thus, it is clear that the changes observed from complete compact overlapping euhedral pseudo hexagonal platelets in the beneficiated kaolinite to the mixed vermiform with skinny stacked

euhedral pseudo hexagonal platelets in the treated kaolinite ruled out the fact that salt treatment exposed and so activated the functional groups in the layers thereby increasing the active surface area necessary for intercalation process.

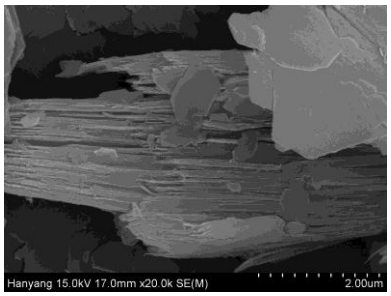

Figure 5.5a. SEM micrograph of B_1

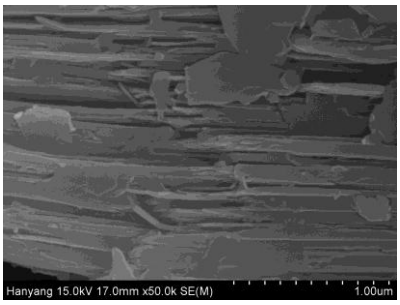

Figure 5.5b. SEM micrograph of B_1

Relatively, the stacking sequence of the intermediate intercalation compound consisiting of kaolinite-hydroxyl-alumun oligomeric cations (B_2) with both beneficiated kaolinite and the treated kaolinite (B_1) revealed substantial changes in the morphology of kaolinite layers (Figure 5.4a, b; 5.5a, b; and 5.6a ,b). As seen (Figure 5.6a, b) for B_2 the distance between layers has broaden as compared to beneficiated kaolinite and B_1 which in turn explicates the expansion of interlayer distance as a result of intercalation of oligomeric cation. However, the morphology as seen was still vermicular.

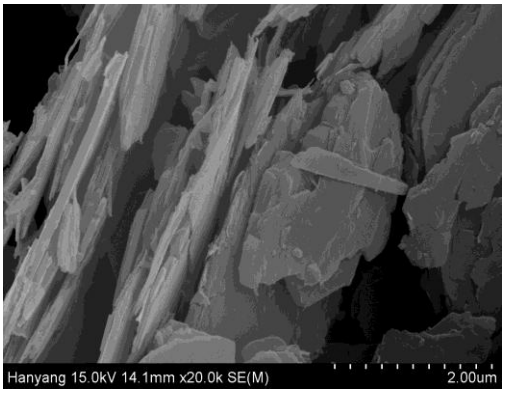

Figure 5.6a. SEM micrograph of B_2

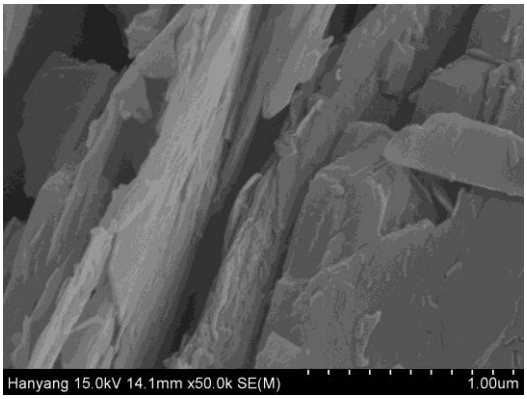

Figure 5.6b. SEM micrograph of B_2

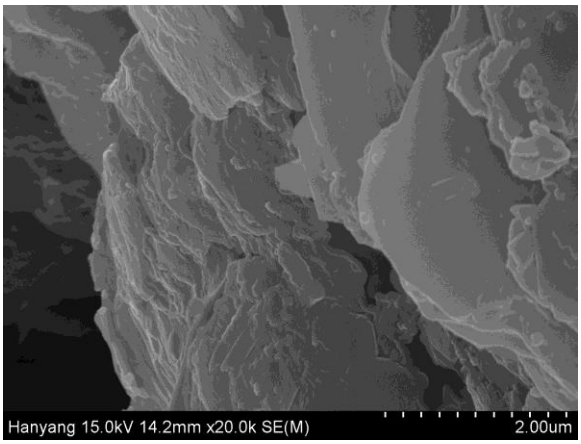

Figure 5.7a. SEM micrograph of B_3

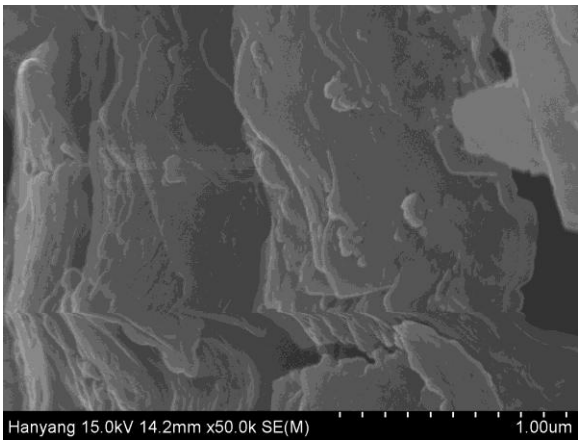

Figure 5.7b. SEM micrograph of B_3

Eventually, there was a complete disappearance of stacked layer sequences when urea replaced hydroxyl-alumina oligomers in the kaolinite interlayer spaces due to the formation of a well packed urea-kaolinite intercalation compound after intercalation trials (Figure 5.7a, b); as can be seen, the layers have been almost completely covered with organic molecules.

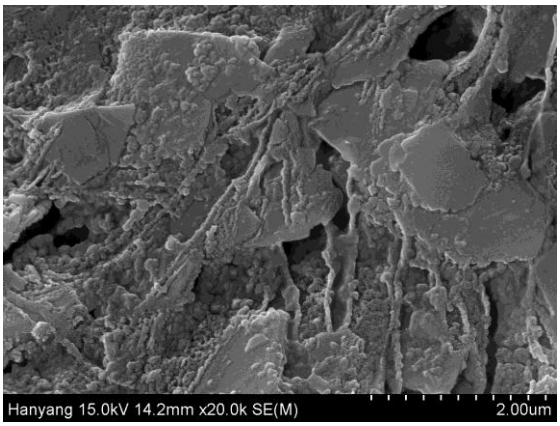

Figure 5.8a. SEM micrograph of transitional B_5

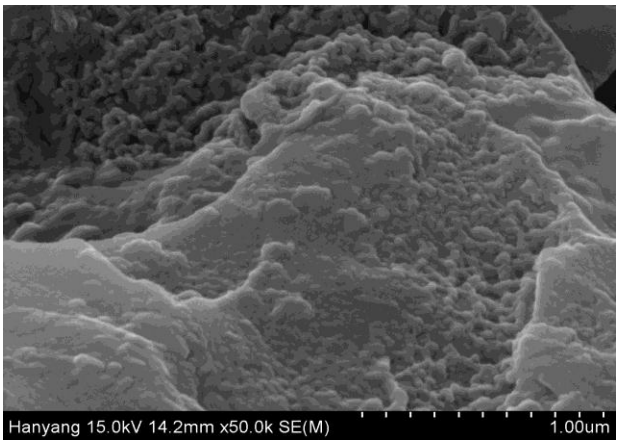

Figure 5.8b. SEM micrograph of transitional B_5

Furthermore, the re-intercalation trials as described in the experimental procedures brought up unique and impressive results. In the first attempt of coupling DMSO => calcination => hydroxyl aluminum-urea intercalation => and re-intercalation set-up there was a transitional transformation of the vermicular kaolinite layers observed before (Sempeho, Kim, et al., 2015a) into morphologies resembling like a “pimpled surface” or rather a “pustulated skin” wherein, the

particles were organized in a woven network (Figure 5.8a, b). In our viewpoint, this was just an intermediate stage since upon several other trial repetitions a complete transformation was observed forming unique structural morphologies portrayed in sample B_5 (Figure 5.9a, b) which resembled like a systematically perforated glomeruli embedded on each other to form something like desert cactus shaped morphologies.

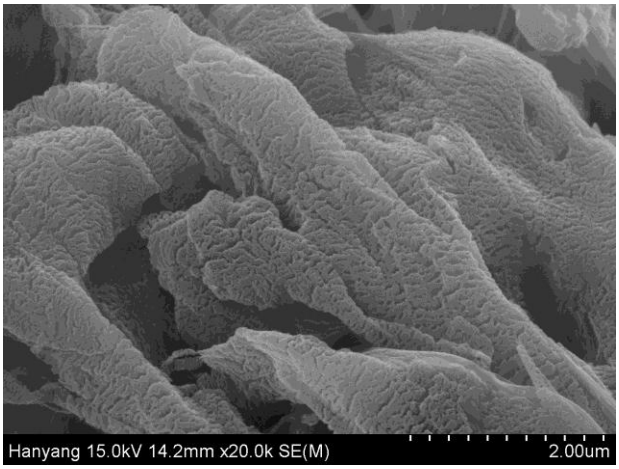

Figure 5.9a. SEM micrograph of B_5

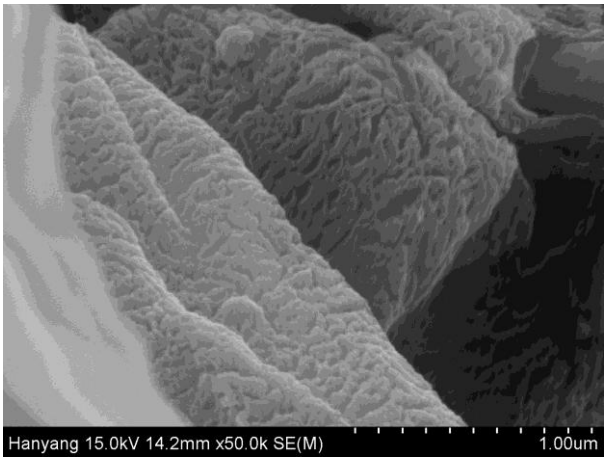

Figure 5.9b. SEM micrograph of B_5

This phenomena might be associated with tendency of hydroxyaluminate oligomer to curl; in most cases "this phenomena occurs when air drying takes place an action that creates an alternating aluminum-chlorohydrate water arrangement and then, diffusion of water between the aluminum chlorohydrate layers during air drying result in a curled film" (Teagarden, Hem, & White, 1982). In that way we have ruled out that, the natural stacking sequence of kaolinite layers can be manipulated to (i) expand the layers in order to accommodate organic species as well as (ii) be transformed into what we have called "pustulated skin" pattern and (iii) subsequently into curled glomeruli-like pattern organized into desert cactus (like) self-assembled Nano-structures which were further analyzed with EDAX to give results shown in Figure 5.10. Therefore, our engineering design increased the confidence to advance more investigations on Pugu kaolinite for advanced uses. The composition of B_5 from EDAX involved both atomic as well as weight percent composition (Figure 5.10).

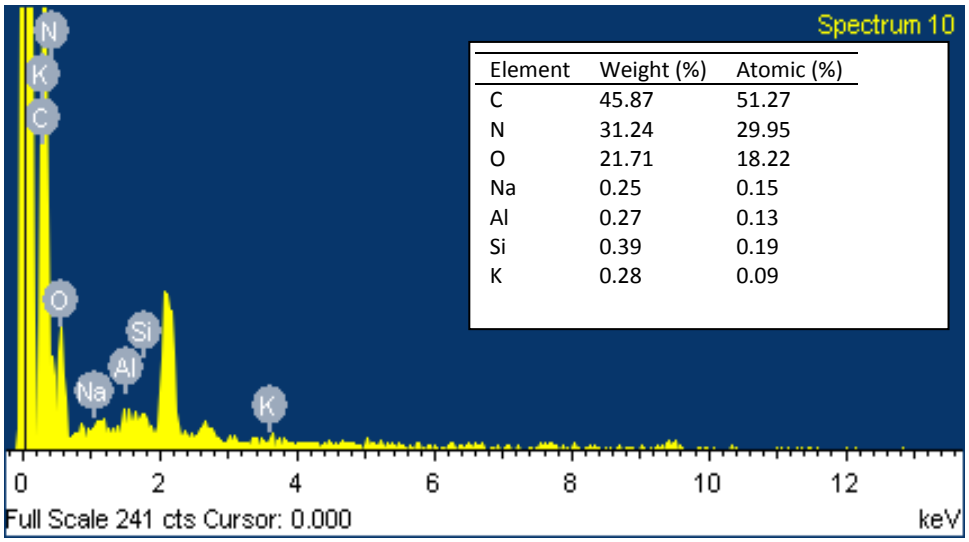

Figure 5.10. Composition of B_5 from EDAX

5.3.5 TG-DTG analysis

Thermogravimetric analysis was done under N_2 atmosphere to investigate the thermal degradation and stability of aluminum oligomer intercalated kaolinite compounds to a maximum of about 800 °C. While the thermograms for both urea and B_1 are presented in Figure 5.11 and 5.12, their role is only played for comparison; our discussion was set on the analysis of B_2, B_3 and B_4.

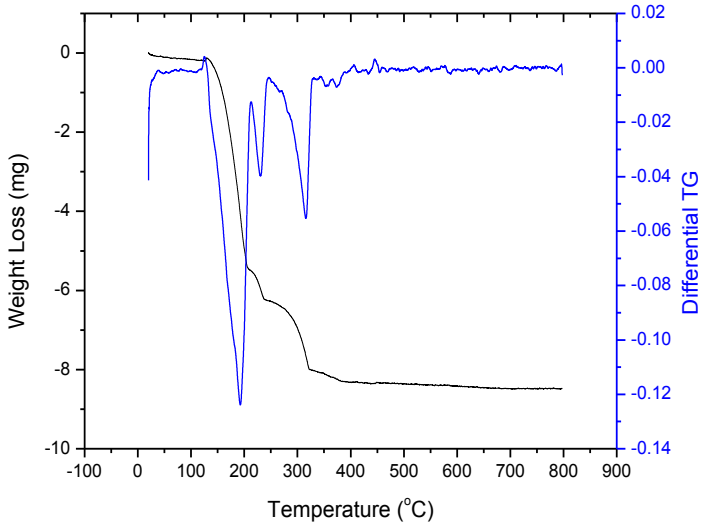

Figure 5.11. Urea TGA thermograms (black) and its differential plot (blue)

As can be seen in Figure 13, B_2 was characterized by 4 degradation phases which include 25-250 °C, 250-450 °C, 500-650 °C and 670-800 °C. The first phase corresponds to the removal of moisture that is externally adsorbed on the surfaces of the sample as well the decomposition of Keggin ions or Keggin cluster associated with the calcination of B_2. It has been generally accepted that, hydroxylaluminum oligomers tend to polymerize into large discrete anions in the form of $[H_2W_{12}O_{40}]^{6-}$ commonly called Keggin ion or Keggin cluster (McColm & O'Bannon, 1994) and that upon heating, these cluster-ions undergo condensation reactions in the interlayer spaces thereby forming higher polymers such as the Al_{24}-polycations (Fu, Nazar, & Bain, 1991; Thomas & Occelli, 2000).

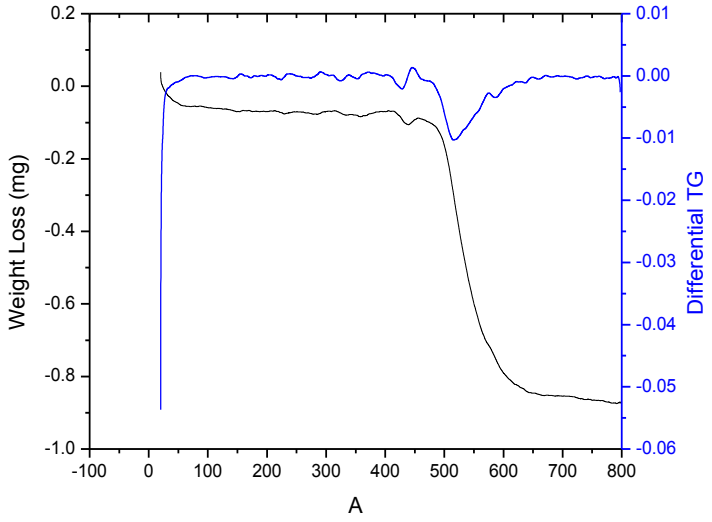

Figure 5.12. B_1 TGA thermograms (black) and its differential plot (blue)

Moreover, this degradation phase was also ascribed to the removal of water molecules bonded to the aluminium atoms on the Keggin cluster which as said before, tend to form due to the polymerization of the oligomers (Abeysinghe, 2012). This observation agrees with what was stated elsewhere (Abeysinghe, 2012) that "the water molecules that are bonded to the aluminium atoms on the cluster are more likely to be removed around 150-300 °C", a temperature which is within range of our observation. In fact, the TG thermograms pattern (Figure 5.13) closely resembles with the thermograms for Keggin cluster obtained by (Abeysinghe, 2012).

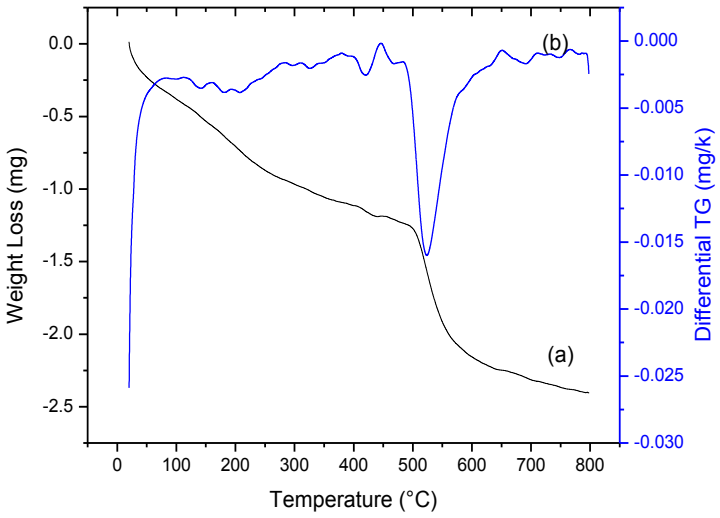

Figure 5.13. B_2 TGA thermograms (a) and its differential plot (b)

According to (Occelli & Tindwa, 1983), at 150 °C water associated with oligomeric intercalated kaolinite micropore structure began to be removed and that, the water loss associated with both kaolinite structure and the intercalated compound B_2 continues as far as the third decomposition phase at 500-650 °C which is attributed to the middle stage kaolinite dehydroxylation.

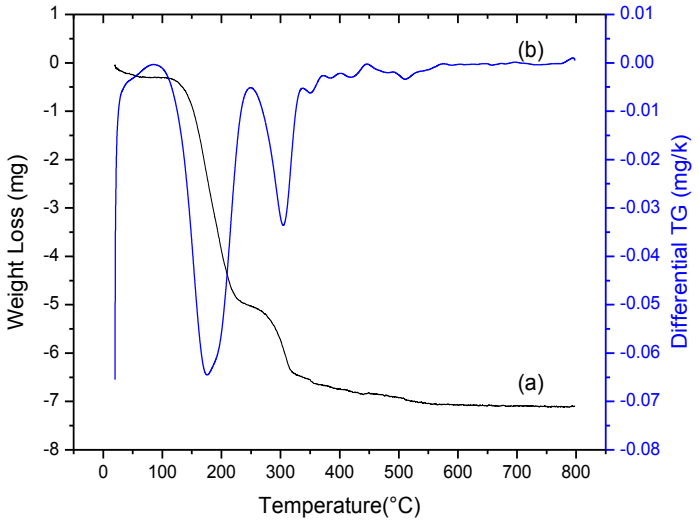

Figure 5.14. B_3 TGA thermograms (a) and its differential plot (b)

The decomposition phase at 250-450 °C as well as that of 500-650 °C were ascribed to the liberation of CO_2, and interlayer water as these gaseous species thought to be present in the

oligomeric intercalated kaolinite (B_2) are known to be liberated around these decomposition phases as a result of the decomposition of the intercalated compounds of B_2 along 250-450 °C, and later further decomposition at 500-650 °C (Abeysinghe, 2012). This phase was also ascribed to the kaolinite hydroxylation reactions. On top of that, the decomposition phase at around 670-800 °C correspond to both kaolinite dehydroxylation as well as the kaolinite dehydroxylation transformation phases (Vaughan 1955, Pereira, Minussi *et al*. 2012, Czarnecka 2013).

Upon replacement of hydroxylaluminum oligomer with urea in the kaolinite interlayer spaces there were several changes which were observed in the thermograms (Figure 5.14); externally adsorbed water and the elimination of structural water were ascribed to the first and second degradation phases that is 25-70 and 75-230 °C respectively.

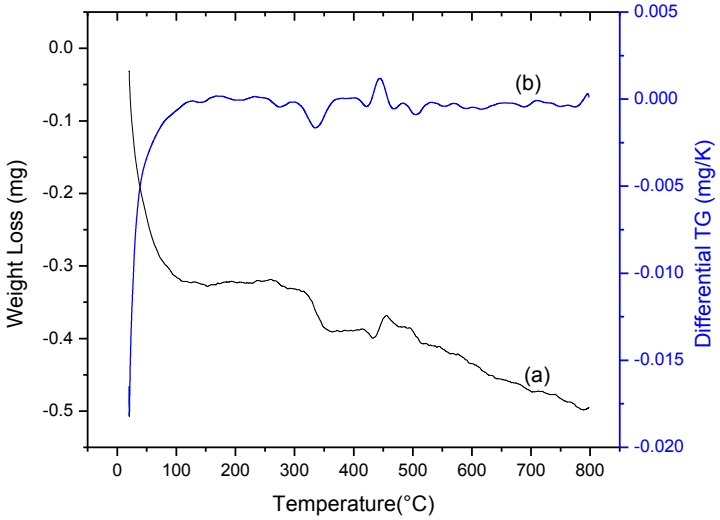

Figure 5.15. B_4 TGA thermograms (a) and its differential plot (b)

Similarly, the second and third degradation phases at around 75-230 °C and 250-320 °C associated with a loss in urea correspond to both urea vaporization along with its degradation to biuret [$NH(CO)_2(NH_2)_2$] which is a complementary form of urea decomposition reaction. Besides, the preliminary stages of kaolinite dehydroxylation as well as continuous sublimation of urea to its complex decomposition product corresponds to fourth and fifth degradation phases seen at 350-550 °C and 550-800 °C (Costa, Cabral-Albuquerque *et al*. 2013). The existence of DMSO decomposition products was observed in Figure 5.15, where the pattern of kaolinite

dehydroxylation has disappeared signifying that dehydration below 850 °C was successful during calcination trials.

The peak observed in Figure 5.15 could likely correspond to the DMSO decomposition products. In our view, we have made an assumption that the DMSO decomposition products observed in Figure 15 might have reacted with the hydroxylaluminate oligomeric cations upon the re-intercalation trials to give the features observed in Figure 5.8 and 5.9; however, further investigation to explore the mechanism and the chemistry behind in necessary.

Conclusion

In this paper we have described the fate of coupling double intercalant agents namely DMSO and hydroxylaluminum oligomeric cations on the kaolinite properties utilizing calcination reactions as intermediate stages. The raw kaolinite was first beneficiated using wet beneficiation technique and then chemically modified with sodium chloride solution. Matured and aged hydroxylaluminum oligomeric solution was prepared and used for intercalation reaction and later for urea-replacement reaction in the kaolinite interlayer spaces. Calcined DMSO intercalated kaolinite was re-intercalated by using hydroxylaluminum oligomeric cations to prepare nano materials which exhibited a curling behaviour from the normal stacked frequency of euhedral pseudo hexagonal platelets of the raw kaolinite to vermiform morphologies with SEM-EDX analysis. The nanomaterials were characterized further with XRF, ATR-FTIR, XRD and DT/DTG, The crystallite sizes were determined using Scherrer equation from the indexed XRD diffraction patterns. Andreasen pipette sedimentation technique was used to determine the grain size distribution of the raw kaolinite. Basing on the analysis result, we have ruled out that it is possible to manipulate kaolinite structure from the known dense overlapping euhedral pseudo hexagonal platelets, to stacked vermiform morphologies, to pustulated form and also into a unique pattern which exhibited what we have called a curled glomeruli-like shape organized into self-assembled structure resembling a desert cactus.

CHAPTER SIX

Controlled Release Urea Fertilizer Based on Pugu Kaolinite and Ferrous Oligomer Intermediate Intercalation[5]

Abstract

Urea is the most widely used nitrogen fertilizer because of its high nitrogen content and comparatively low cost of production. However, due to surface runoff, leaching and vaporization, the utilization efficiency or plant uptake of urea is rather low. The urea-kaolinite intercalation for controlled release of urea was investigated in order to arrest these shortcomings and hence improve crop yield. Wet beneficiation technique based on Stokes's law followed by treatment of samples with salts was employed. Oligomeric ferrous cations were used to prepare intermediate kaolinite intercalation compounds which were then used to prepare urea-kaolinite intercalation nanocomposites by using substitution reaction. Gum *arabic*-chitosan coarcervation reaction was used to encapsulate the urea intercalated kaolinite. The nanocomposites were characterized by XRF, ATR-FTIR, XRD, SEM, EDAX and TG-DTG techniques. The X-ray diffraction patterns revealed the existence of an FCC Bravais lattice before and after intercalation trials. Crystallite sizes were determined using Scherrer equation and found to be 64.58-19.25, 80.01-23.85, 81.51-24.30 and 75.43-22.37 nm for the iron-rich kaolinite, iron oligomeric intercalated kaolinite, urea intercalated kaolinite and the coarcervation encapsulated nanocomposite respectively. The apparent intercalation ratios of these nanocomposites were 37.53%, 70.41%, 76.83% and 15.30% respectively.

Keywords

Intercalation, beneficiation, oligomer, nanocomposites, coarcervation, encapsulation

[5]Submitted: Progress in Materials Science-Elsevier

6.1 Introduction and Literature Review

Urea conventional fertilizer has been widely used for decades in attempts to supplement crop nitrogen however, its accessibility to plants is below 50% owing to surface run offs, leaching, vaporization and its hydrolysis by soil urease (M. Liu, et al., 2007) as described in equation 6.1.

$$NH_2CONH_2 + H_2O \rightarrow 2NH_3 + CO_2 \qquad (6.1)$$

In order to improve its availability to crops, urea can be amended by using urease inhibitor (Bremner & Krogmeier, 1988), encapsulation with natural or synthetic polymers (Shaviv, 2001), intercalation into the interlayer spaces of nano-clays or layered silicates (Sempeho, et al., 2014) or by combining both intercalation as well as encapsulation process. Generally, urea amended as described above has enhanced fertilizer use efficiency (FUE) (Subbarao, et al., 2013) and also it exhibit grander features over the conventional urea formulations (Agric, 2014).

Kaolinite being a layered phyllosilicate mineral is known to be a 1:1 layered aluminosilicate mineral with its crystal lattice unit formed by one alumina octahedral sheet sandwiched between one silica tetrahedral sheets (Sempeho, et al., 2014). The occurrence of ion substitution or the site vacancies at the tetrahedral and/or octahedral sheets gives rise to a negatively charged surface; the exchangeable cations between the layers compensate the negative charge and may be easily exchanged by other metal cations giving rise to sorption reactions which in turn facilitate intercalation reaction (Parolo, Fernández, Zajonkovsky, Sánchez, & Bastion, 2011a). Owing to that, surface modifications occur (Basak, et al., 2012) and as a result, large surface areas and reactivity of nano layers form on the surfaces and interfaces of nano-layers which act as substrate for chemical reactions thereby making kaolinite nano-layers suitable excipients for CRFs formulations including controlled release urea fertilizers (Ukessays.com, 2013a). These properties influences researchers to investigate their suitability as excipients (Aguzzi, et al., 2007). Essentially, the resulting intercalation materials can be analyzed by several techniques including X-ray diffraction analysis, vibrational spectroscopy, NMR, EDX, SEM, TEM, XRF *etc.*

In this paper we report the preparation of urea intercalated kaolinite nanocomposite as an excipient for use in the designing of urea controlled release fertilizer formulations by applying several steps including activation of functional layers, preparation of intermediated intercalated

oligomers, intercalation of urea as well as chitosan-gum arabic coarcervation for the purpose of achieving a well crosslinked CRF formulation.

6.2 Materials and Methods

6.2.1 Materials

Kaolinite was collected at Pugu hills in the Coast region Kisarawe Tanzania by using quartering sampling technique described by (Sempeho, Esther *et al*. 2012). Urea (ACS reagent, 99.0-100.5%) was supplied by Sigma Aldrich, DMSO (Extra pure, ≥ 99.5%) was supplied by Daejung chemicals & metals, Co. Ltd, Gyonggi-do, Korea, Sodium chloride (Extra pure, ≥ 99.0%) was supplied by Samchun pure chemicals Co. Ltd, Gyonggi-do, Korea, Silver chloride (ACS reagent, 99.0%) was supplied by Sigma Aldrich, deionized distilled water (D.I was supplied by Prof. Kim's lab, sodium hydroxide (extra pure grade, min. 93.0%) was was supplied by Duksan pure chemical, Ansan city, Kyungkido-South Korea and aluminium chloride (99.99%) was supplied by Junsei chemical Co. Ltd, Japan.

6.2.2 Methods

i) Beneficiation of raw samples

Wet beneficiation technique was achieved by simple size separation using "Classifier". The method involved the separation of fine platy kaolinite from coarser quartz, feldspar mica and other impurities using different setting velocities associated with particle size as governed by Stockes's law. The entire procedure which involves crushing to pulverization and soaking as well as running the classifier unit to drying has been comprehensively described in (Sempeho, Lugwisha *et al*. 2012).

ii) Modification of Pugu Kaolinite

A known amount of Pugu kaolinite was dispersed in a 0.1 M NaCl solution and treated ultrasonically at 50 °C for 30 hours and then magnetically stirred for more 30 hours under constant stirring. The product was filtered under vacuum filter and washed several times to remove excess chlorides whereas; washing was stopped after negative reaction with $AgNO_3$. The

washed product was dried in a vacuum oven at 60 °C and stored as NaKP. Similarly, 6 g of kaolinite were agitated with 60 ml of 0.1 M $KHC_8H_4O_4$ (KHP) and stirred at moderate temperature 27 hours and then washed and kept as HK_3.

iii) Preparation of the nanocomposites

A 1:1 molar solutions of $Fe(NO_3)_3$ and NH_4OH were thoroughly stirred for 6 hours at 85 °C and aged for 15 days where the OH/Fe ratio was 2. 25 ml of this aged solution was agitated with 5% kaolinite suspension at 70 °C and matured for one week where after washing it was dried in a vacuum oven and kept as KPF. Little of KPF suspension was measured and mixed with 5 g of urea fertilizer; stirring was done for 6 hours and the dried product was labeled KPFU. Also, 6% kaolinite suspension was prepared using HK_3 and dispersed under continuous stirring for 8 days at 80 °C in the 150 ml of the prepared OH/Fe intercalant solution to give materials which were labeled as Fy.

A 2% chitosan solution was prepared by dissolving 10 g chitosan powder into 500 ml of 10% glacial acetic acid to get the pH of the solution in a range of 4-5. The solution was stirred for 40 hours at RT and was labelled CH. On the hand, gum arabic solution was prepared by dispersing 10 g of acacia powder into the 500 ml of 10% glacial acetic acid; the mixture was stirred for 40 hours and kept as GA. Thereafter, a small portion of KPFU was measured and dispersed in 40 ml of GA and stirred for 20 hours at RT. After 20 hours of continuous stirring, 35 ml of CH was added drop wise into the stirring mixture and stirred for more 24 hours where after, 10 ml of 25% glutaldehyde solution was introduced to crosslink the mixture which was again stirred further for 90 minutes followed by 30 minutes sonication. The product obtained was named Q_1; it was washed using n-hexane in a vacuum pump under hood and was dried in a vacuum oven at 60 °C to get off the excess solvent.

iv) Characterization

The FTIR-ATR analyses were carried out using a Bruker Optic GmbH (alpha model, Laser class 1) Spectrometer with attenuated total reflectance (ATR) at the University of Dar es Salaam. XRD measurement were performed on RIGAKU COORPERATION, D/MAX-2500/PC X-ray Diffractometer equipped with a back monochromator operating at 40 kV and 100 mA at the

scanning range of 5° – 80° with a step size of 0.1° and a time/step of 1 s using copper cathode (Cu Kα1) as the X-ray source (λ) 1.54056 Å) at Hanyang University. The X-ray diffraction patterns were indexed by using mathematical method by first determining the unit cell parameter from the peak position and then miller indices; the estimations of the crystallite size was performed by using X-ray diffraction pattern basing on Scherrer equation. Thermogravimetric analyses were conducted on TG/STA Linseis STA PT 1000 simultaneous TG/DTG thermal analyzer at a scanning rate of 5 °C per min from room temperature to 800 °C under nitrogen atmosphereat the University of Dar es Salaam.SEM-EDX images of the samples were taken with Field Emission Scanning Electron Microscopy (SEM-Hitachi-s-4800, Japan) coupled with EDX facility at Hanyang university. The accelerated voltage was 15 kV. The chemical composition of the raw materials was determined by X-ray Fluorescence (XRF) using the Semi Quantitative XRF Analysis technique (SIEMENS SRS 3000 X-ray Fluorescence (Rhodium anode, 8 analyzer crystals with beryllium windows 125 μm) at SEAMIC center. The particle size distribution was carried out by using sub-sieve analysis technique which involves the application of Andreasen pipette sedimentation method. The details of the procedures can be found elsewhere (E. H. J. Lugwisha & Siafu, 2014).

6.3 Results and Discussion

6.3.1 Preliminary characterization of beneficiated and intercalated kaolinite

Sampled raw kaolinite was analyzed for chemical composition (Table 6.1) and grain distribution (Table 6.2). As noticed, the findings revealed an improved purity of the kaolinite after beneficiation due to a significant reduction in the percentage of impure oxides and the disappearance of non-clay fractions (appendices 1-4). Besides, the grain size distribution with Andreasen pipette sedimentation showed that the clay portion constituted 60.42% whereas the rest was constituted by non-clay portion. The impact of the wet beneficiation trials was significant basing on the fact that the clay portion was observed to rise from 60.42 to 99.64% after beneficiation trials.

Table 6.1. Elemental chemical composition of the raw and beneficiated kaolin

	Weight Percent	
Element	Raw Pugu kaolin	Beneficiated Pugu kaolin
Si	63.64	54.99
Al	31.43	40.20
Na	0.43	0.09
Mg	0.16	0.13
S	0.25	0.08
Cl	0.76	0.04
K	1.39	0.96
Ca	0.06	0.04
Ti	0.80	1.02
Cr	0.03	0.04
Mn	0.01	0.01
Fe	1.01	2.00
LOI	0.03	0.40
Total	100	100

Table 6.2. The grain size distribution

Grain size (μm)	Kaolin (%weight)	Beneficiated Kaolin (%weight)
(> 63 μm)	37.57	0.35
(2 – 63 μm)	54.95	78.53
(< 2 μm)	2.39	21.03
(< 63 μm)	57.34	99.56

6.3.2 Whole Rock Analysis

A portion of both the original and the beneficiated kaolins taken for the randomly oriented whole rock X-ray diffraction analysis revealed the presence of dominant and minor peaks as seen in the appendices 1-4. The clay Whole Rock Powder mount XRD of Pugu kaolin indicated that the clay mineral impurities observed were quartz (SiO_2), clinochlore [$Mg_5Al(Si,Al)_4O_{10}(OH)_8$] and microcline [$KAlSi_3O_8$] while the clay minerals observed were kaolinite [$Al_2Si_2O_5(OH)_4$] and illite [$KAl_2(Si_3AlO_{10})(OH)_2$]. The disappearance of quartz and microcline in the beneficiated kaolin and the appearance of clinochlore and illite were noticed.

6.3.3 Oriented Clay Analysis

For the purpose of distinguish layer types and clay mineral groups; oriented clay preparation was carried out on the original and beneficiated kaolin samples. As I have described elsewhere that; "To identify the clay minerals present, the oriented samples were analyzed by X-ray diffraction method as untreated air-dried, glycolated and heated at 550 °C for two hours. When the air-dried samples were diffracted, peaks were developed on the diffractogram which revealed three main clay minerals namely kaolinite, illite and clinochlore. The results from oriented air dried samples above were not enough to confirm the clay mineral groups obtained.

Identification and hence confirmation of these clay minerals was achieved from the differences on the diffractograms obtained by glycolating the samples, drying them, then diffraction process carried out; and by heating the samples at 550 °C for two hours prior to the diffraction process. Diffraction results (Appendices 1-4) shows that some of the diffractogram peaks in both original and beneficiated kaolin samples were not affected by the two prescribed treatments. This behaviour of stability in chemical treatment (glycolated) and heat transformation (at 550 °C) confirmed the presence of illite. However, when the samples were glycolated, dried and diffracted some peaks were shifted in some samples. But on heating the samples at 550 °C followed by diffraction, these shifted peaks collapsed. This characteristic of altering the diffraction patterns is a distinguishing characteristic of kaolinite group". That said, the major kaolin mineral observed on both the original and beneficiated kaolin samples was kaolinite subordinated with illite.

6.3.4 Characterization of nanocomposites

The X-ray diffraction patterns obtained were indexed and results summarized as follows:
First. Despite being an induced process, intercalation process could occur naturally in areas rich in iron oxides; however the intercalation ratio found in this study was low. As can be seen in Figure 6.1, when beneficiated kaolinite was agitated with iron rich clay soil there was an expansion in lattice parameters of about 3.61 Å associated with intercalation of about 37.53%. The size of the kaolinite crystals intercalated with natural iron rich clay soil was found to be around 64.58-19.25 nm.

Second. Upon inducing intercalation process with the laboratory aged and matured Fe $^{3+}$ oligomers to synthesize KPF, the intercalation ratio for the nanomaterial got increased to 70.41% due to lattice expansion (d_{001}) along the c-plane of about 3.62 Å; the crystallite size was found to be in the average of 80.01-23.85 nm. Our observation was that, although there were a low intercalation ratio, the size of kaolinite crystals intercalated with natural iron rich clay soil was (YYY) smaller than that one originating from the use of ferrous oligomers (KPF). Besides, with intercalation induced via natural iron-rich clays, there was a loss in XRD peak intensity (Figure 6.1) a phenomena also observed by (Bhattacharyya & Gupta, 2006) although under different settings. A significant increase in the XRD peak intensity was observed after intercalation with ferrous oligomeric cations.

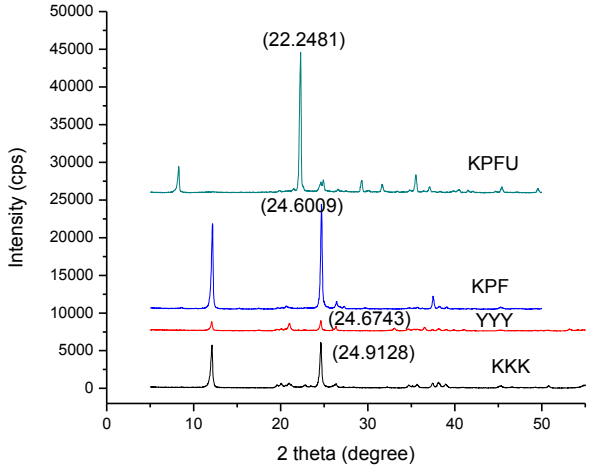

Figure 6.1.X-ray diffractograms for KKK, YYY, KPF and KPFU

Third. When urea fertilizer was used to replace the hydroxyferrous oligomeric cations within the kaolinite interlayer spaces to form KPFU, there was a sharp increase in the expansion of *d*-spacing (≈ 3.99 Å) corresponding to an intercalation ratio of about 76.83% (Figure 6.1) while the crystallite size was increased to 81.51-24.30 nm. We have established that the crystallite sizes as well as the intercalation ratio were seen to increase in the order of YYY > KPF > KPFU and that urea expanded the interlayer spaces of kaolinite more than the rest.

Fourth. Both, the crystallite sizes along with the intercalation ratio were seen to decrease exponentially when gum Arabic-chitosan coarcervation reaction was used to crosslink the urea intercalated kaolinite (KPFU). The encapsulated nanocomposite named Q_1 which relate to the

KPFU was analyzed with XRD and found that the intercalation ratio dropped from 76.83% of KPFU to 15.3% after coarcervation and that the crystallite size was reduced to 75.43-22.37 nm. The dropping of intercalation ratio after coarcervation might be associated with the alteration of kaolinite layers as seen in Figure 6.2a,b where well-ordered urea intercalated kaolinite has completely changed to mat of scattered particles; no layers could be seen. As a matter of fact, a comparison between Figure 6.2a and 6.2c revealed that urea substituted ferrous oligomers successfully within the kaolinite interlayer spaces and was intercalated to give an ordered layer arrangement, a pattern which was not that clear for KPF and Q_1.

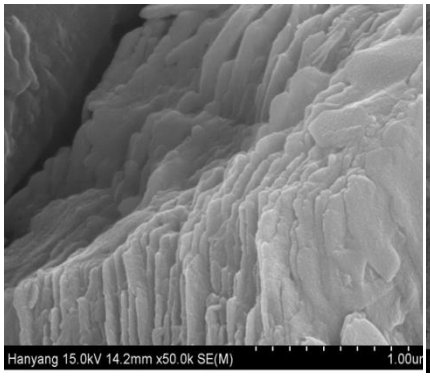

Figure 6.2a. SEM micrograph for KPFU

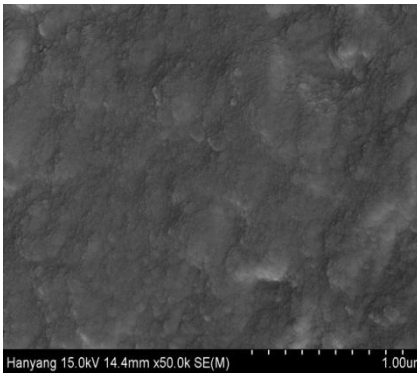

Figure 6.2b. SEM micrograph for Q_1

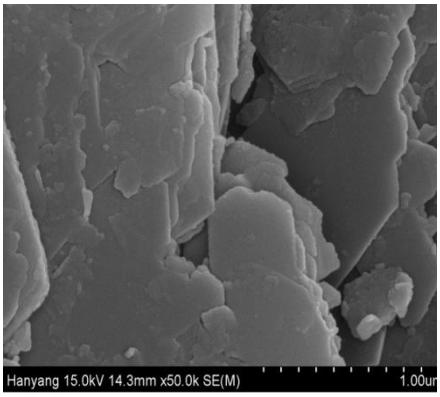

Figure 6.2c. SEM micrograph for KPF

EDX analysis (Figure 6.3) showed the absence of nitrogen after crosslinking via gum-arabic-chitosan coarcervation process; this indicated that the coarcervate instead of acting as a crosslinking agent for encapsulation either (a) it substituted urea in the kaolinite interlayer spaces

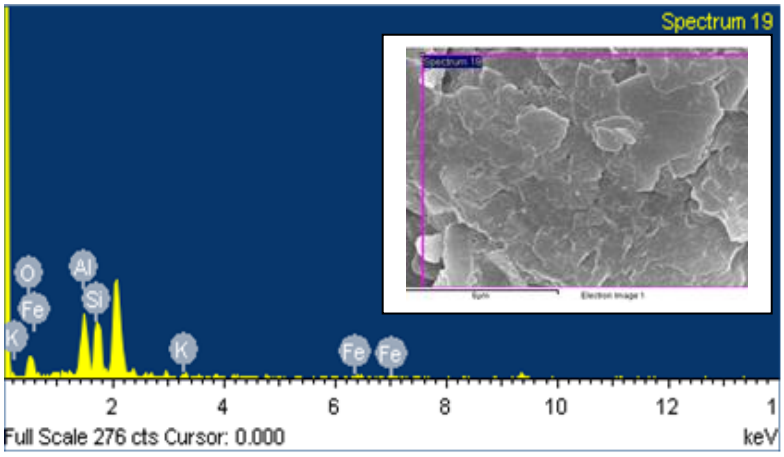

Figure 6.3. Energy Dispersive X-ray Spectra (EDX) for the composition of KPCU

completely, or (b) it crosslinked the formed nanocomposite *in situ* such that (i) urea was completely absent with EDX analysis (ii) intercalation ratio dropped substantially but with unique observation of an increased expansion (iii) crystallite size got decreased due to elimination of urea relatively to the urea intercalated kaolinite (KPFY).

The difference between salt and acid activation of kaolinite sheets as a function of intercalation ratio was carried out by preparing both, KPFU and MFYU as described in the procedures. The results as seen in Figure 6.4 revealed that, urea intercalated kaolinite synthesized via acid activation corresponded to the intercalation ratio of about 25.2% with a lattice expansion of 3.55 Å as compared to the lattice expansion of about 3.99 Å corresponding to an intercalation ratio of about 76.83% for the salt activated one (KPFU); and also, the crystallite sizes were respectively in the range of 75.43-22.49 nm and 81.51-24.30 nm.

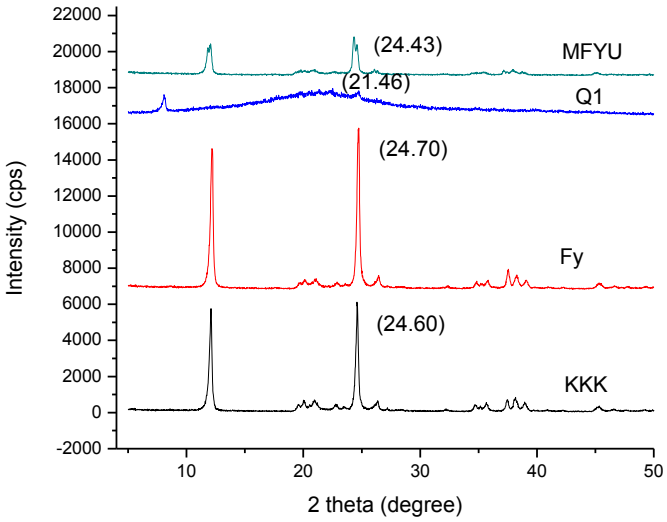

Figure 6.4.X-ray diffractograms for KKK, Fy, Q1 and MFYU

Such an observation portrayed that, urea intercalated more into the kaolinite interlayer spaces following salt treatment than with acids. Therefore, when preparing controlled formulations such as controlled release fertilizers, drug delivery systems *etc.* involving the application intercalation with kaolinite the type of activating material used to activate the functional kaolinite layers matters. A close view on Figure 6.5a and 6.5b would confirm that fact there was a loss in the order of arrangement of kaolinite nano-layers following acid treatment resulting to disintegration

of particles and a distorted vermiform morphology. On the other hand, following salt activation the functional kaolinite nano-layers were observed to be compact and orderly arranged, a feature which is critical for an effective intercalation process.

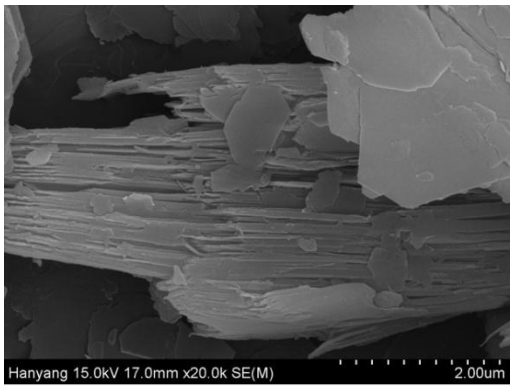

Figure 6.5a. SEM micrograph for salt activated kaolinite

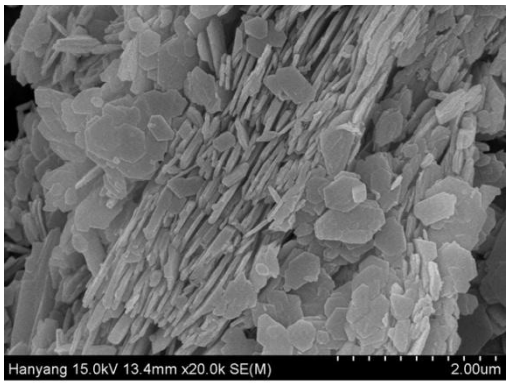

Figure 6.5b. SEM micrograph for acid activated kaolinite

6.3.5 Molecular vibration study

As has been generally known, the Attenuated Total Reflectance Infrared Spectroscopy (ATR-FTIR) allows the scrutiny of dipolar functional groups in close proximity (Ca. $\leq$ 1 µm) to the interface between a sample and an internal reflection element IRE; in that case, this technique was used to study the molecular vibrations of the intercalated nanocomposite materials. As a matter of fact, attempts to intercalate iron-related molecules into the interlayer spaces of kaolinite minerals are known (Nakagaki et al., 2006; Yvon & Jean-Maurice, 1994). In this study the following observations were made basing on the IR absorption bands observed in Figure 6.6:

One. The structure of kaolinite after intercalation with ferrohydrate oligomeric cations was maintained due to the presence of characteristics absorption bands for kaolinite between 3696-3618 cm $^{-1}$ in the kaolinite intercalated with natural iron rich clay (YYY), kaolinite intercalated with aged and matured tailor made iron-oligomeric cations (KPF) as well as its subsequent urea intercalated kaolinite nanocomposite (KPFU). The occurrence of OH-stretching vibrations along these wavelengths is typical.

Two. Owing to their weak intensity and their band positions, the Al-Fe $^{3+}$ OH vibrations are known to be difficult to analyze (Mauro et al., 2014; Yvon & Jean-Maurice, 1994). That is to

say, the formation of Fe $^{3+}$ oligomeric intercalated kaolinite is associated with the formation of Al-Fe $^{3+}$ OH bands whose peak position and intensity is a bit puzzling to assess. However, in most cases the vibrational frequencies for the Al-Fe $^{3+}$ OH bands do occur around 1200-800 cm $^{-1}$(Katya A. Bazilevskaya, Douglas Archibald, & Martínez, 2006); that may also go up to about 1250-1400 cm^{-1} in the complex trigonal and tetragonal forms (K Nakamoto, 1986; Peak, Ford, & Sparks, 1999; Peak, Luther III, & Sparks, 2003). As seen in the Figure 6.6, weak-less intense bands can be observed between 2400-2000 and between 1500-1800 cm^{-1}suggesting that the interaction between the ferrohydrate oligomers and the kaolinite' Si-OH matrix during the intercalation process was weak. This observation closely agrees with the Fe-F interaction found between 1530-500 cm^{-1} elsewhere (Mauro, et al., 2014). A simple generalization from this observation is that, though it is possible to prepare the kaolinite intercalated with ferrohydrate oligomers as stipulated in this paper, the interaction involved between the intercalant and the kaolinite functional layers is less intense or weak whether the intercalant is synthetic or natural as noted in YYY and KPF; however despite the weak interaction, intercalation is possible and there is a possibility to optimize the interaction since the intercalation ratio was seen to increase from YYY to KPF and KPFU.

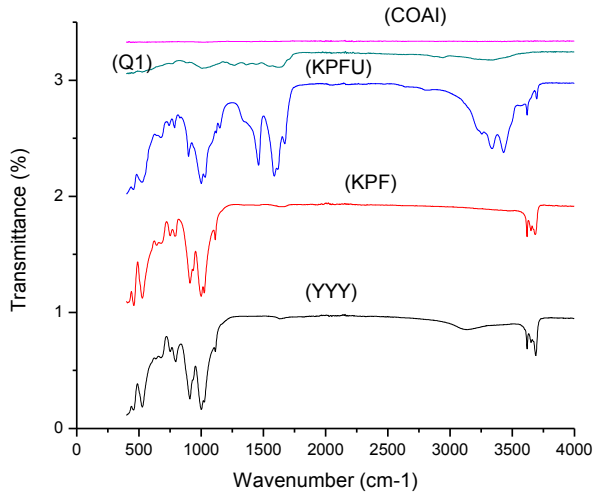

Figure 6.6. ATRFTIR diffractograms for YYY, KPF, KPFU, Q1 and COAI

Three. The appearance of unique broad band at around 3141 cm^{-1} in the YYY was noticed; it was ascribed to the presence of impurities due to the natural iron rich clay used. Similar

observation related to same reason was made at around 1001 cm $^{-1}$ absorption band and this correspond to the C-N or Si-O bands (Czarnecka, 2013) thereby giving out a clue that there were (i) some organic forms of impurities present (ii) and the natural intercalant materials. This was proven to be true due to the absence of these two bands in the KPF since it was prepared from pure intercalant solution of Fe $^{3+}$ Oligomer (Figure 6.6).

Four. The presence of ferrohydrate oligomers in the kaolinite interlayer spaces did not affect the nature of X-ray pattern obtained; as can be seen, the distinctive kaolinite absorption bands at 3689-3618 cm^{-1} were retained after intercalation interaction (Figure 6.6). A similar observation was recorded for the absorption bands at: 1113 cm $^{-1}$ related to the apical Si-O stretching modes of kaolinite (Balan, et al., 2001); 1024 to 999 cm $^{-1}$ related to the Si-O planar vibrational modes (Aroke & El-Nafaty); 910 to 909 cm $^{-1}$ related to the OH deformation of inner hydroxyl groups due to Al-OH bending of kaolinite (Dawley, et al., 2012; Liew, Kamarudin, Al Bakri, et al., 2012; C. O. Mgbemena, N. O. Ibekwe, R. Sukumar, & A. R. Menon, 2013b); 788 to 796 cm $^{-1}$reletad to the Al-O-Si asymmetric bending; 526 to 459 finger print related to the Si-O-Al $^{(VI)}$ vibrations for the octahedral Al $^{3+}$ as can be seen in the Figure 4 (Heah, Kamarudin, Al Bakri, et al., 2012; Liew, Kamarudin, Al Bakri, et al., 2012; Tironi, et al., 2012).

Five. There was an observable disappearance of the characteristic outer-hydroxyl vibration at 3650 cm $^{-1}$ (Figure 6.6) when urea substituted ferrohydrate oligomers in the kaolinite interlayer spaces; nevertheless, the results indicated that the inner-hydroxyl vibrations at 3618 cm $^{-1}$ remained unaffected along with some outer-hydroxyl vibration at 3696 cm $^{-1}$ (although in an altered state due to a band shift from 3684 cm $^{-1}$ of KPF to 3696 cm $^{-1}$ of KPFU due to the presence of urea in the interlayer spaces). The appearance of absorption bands typical for urea molecules at 3430 cm $^{-1}$; 3337 cm $^{-1}$; 3255 cm $^{-1}$; 1671 cm $^{-1}$; 1587 cm $^{-1}$; 1460 cm $^{-1}$; 1149-1120 cm $^{-1;}$ and 1000 cm $^{-1}$ confirmed the successful intercalation process. Respectively, these vibrations correspond to the: out-phase N-H stretching; in-phase N-H stretching due to intercalated urea; the O-H stretching vibrations due to H…bonding associated with urea-kaolinite interaction during the urea- oligomer substitution process in the kaolinite nano-layers; free C=O stretching due to urea; H-C-N stretching due to intercalated urea; CH3-in-phase stretching due to urea; rocking N-H vibrations due to intercalated urea and the C-N symmetric modes resulting from the presence of urea molecules in the kaolinite functional layers (Almuslet,

et al., 2012; Barlow & Corish, 1959b; H Becher, 1956; Fischer & McDowell, 1960; Horvath, et al., 2010; Larkin, 2011; Piasek & Urbanski, 1962a; Rutkai, et al., 2009; Vellora Thekkae Padil, Nguyen, Ševců, & Černík, 2014).

Six. The effect of coarcervation process on both, kaolinite structure as well as intercalated urea was significant. On view of Figure 6.6, both the inner and the outer hydroxyl bands previously recorded at 3696 and 3618 cm $^{-1}$ for KPFU and 3684, 3650 and 3618 cm $^{-1}$ for KPF. The general view on these results revealed that, the coarcervation process created a strong encapsulating membrane which led to the disappearance of nitrogen of urea upon EDX analysis as stated before. Our prediction were that, the disappearance of nitrogen (from urea) in the EDX elemental analysis of the KPFU nanocomposite may be a result of two things: (a) there could be a complete substitution of urea with the formed coarcervate matrix in the kaolinite interlayer spaces, or (b) urea might have reacted with the coarcervate to form a more complex composite product leading to a fading of characteristic urea absorption bands in the KPFU as seen in Figure 6.6. A crystal clear conclusion between the two extremities is still a conundrum. A comparison between the infrared spectrum for the coarcervate alone (COAI) and the urea-intercalated kaolinite encapsulated via coarcervation (Q_1) depicted some useful information from Figure 6.6.

The band observed at 3326 cm^{-1} in the Q_1correspoding to a split band at 3428 and 3334 cm $^{-1}$ band in COAI was attributed to the –OH groups overlapping with the stretching band of N-H whereas the split band at 2943 and 2873 cm $^{-1}$ of Q_1 corresponding to the singlet 2935 cm $^{-1}$ of COAI was ascribed to the aliphatic C-H stretching vibrations (Agnihotri & Aminabhavi, 2004; Chloé & Fabien, 2013). Another split band observed at 1619 and 1552 cm $^{-1}$ of Q_1 corresponding to the singlet 1594 cm $^{-1}$ of the coarcervate (COAI) was assigned to the C=N stretching vibrations and N-H angular deformation, also to the vibrations resulting from the distinctive C=O vibrations of acetylated amino group from some chitosan (Agnihotri & Aminabhavi, 2004; Chloé & Fabien, 2013). Furthermore, a split absorption band was observed at 1441 and 1361 cm $^{-1}$ of Q_1 corresponding to the 1459 cm $^{-1}$ of the coarcervate (COAI) was considered to represent the C-H bending vibrations of the of the aliphatic CH_2 groups (Agnihotri & Aminabhavi, 2004; Chloé & Fabien, 2013). Correspondingly, the need for the optimization of the procedures used in the preparation of coarcervate was noticed due to the existence of absorption band at 1267 cm^{-1} of Q_1 comparable to 1230 cm^{-1} of COAI related to the carboxylic acid (-COOH) moieties (Chloé

& Fabien, 2013)which indicated that there were some free NH_3^+ ions of the chitosan which did not participate in the coarcervation process as a result of reaction conditions.

6.3.6 Thermo-kinetic study

The intercalation compounds and the encapsulated nanocomposite were analyzed for thermal behavior under N_2 atmosphere in order to determine their thermal stability between 0 to 800 °C. Basing on the pattern seen in Figure (6.7), ferrohydrate intercalated kaolinite (KPF) exhibited three degradation phases including; 25-375 °C, 425-450 °C and the 475-800 °C phases. On the other hand, the urea-intercalated kaolinite counterpart also exhibited three decomposition stages from 25-130 °C, 150-270 °C and 500-800 °C whereas the encapsulated coarcevated nanocomposite Q1 exhibited four degradation phases ranging from 25-150 °C, 150-370 °C, 375-455 °C and 455-800 °C.

In all the cases, the first degradation phase correspond to the elimination of water as well as the first stages of decomposition of the intercalated species which include ferrohydrate oligomer, urea for KPFU and coarcervate for Q1; same phase was ascribed to the removal of externally adsorbed water molecules. The phases ranging from 400-800 °C in all the cases relate to the decomposition of the oligomer, elimination of constitution water as well as the dehydroxylation of kaolinite (Chakraborty, et al., 2013; Czarnecka, 2013; Pereira, et al., 2012; Vaughan, 1955). For urea intercalated kaolinite (KPFU) urea loss due to its degradation into its biuret form $[NH(CO)_2(NH_2)_2]$ correspond to the second degradation phases between 150-270 °C (M. M. Costa, et al., 2013). The pattern of urea degradation was not observed after crosslinking the urea intercalated kaolinite (KPFU) via coarcervation process. As can be seen in Figure 6.7, the second degradation phase at around 170 °C to 380 °C revealed the fact that there was a decomposition of the coarcervate and not urea as we had observed before in the X-ray and EDX analysis. As observed elsewhere, pure chitosan decompose at around 100 C to 310 °C (Agnihotri & Aminabhavi, 2004) whereas gum Arabic decompose at around 25-375 °C (Chen et al., 2010). The formation of coarcervate and its subsequent probable reactions including (i) substitution of urea with coarcervate, or (ii) coarcervate-urea reaction within the interlayer spaces of kaolinite correspond to the 170-380 °C degradation phase which is an average of intercalated urea (150-270 °C), chitosan (100-310 °C) and gum Arabic 25-375 °C. That is to say, as far as the melting

point of intercalated urea is concerned, the thermogravimetric patterns revealed the likelihood of the presence of chemical interaction between the coarcervate and the intercalated urea; this phenomena indicate that crosslinking of urea intercalated kaolinite by using coarcervation process as described in this paper is in average call for further investigation in order to control the interactions between the intercalated fertilizer and the coarcervate.

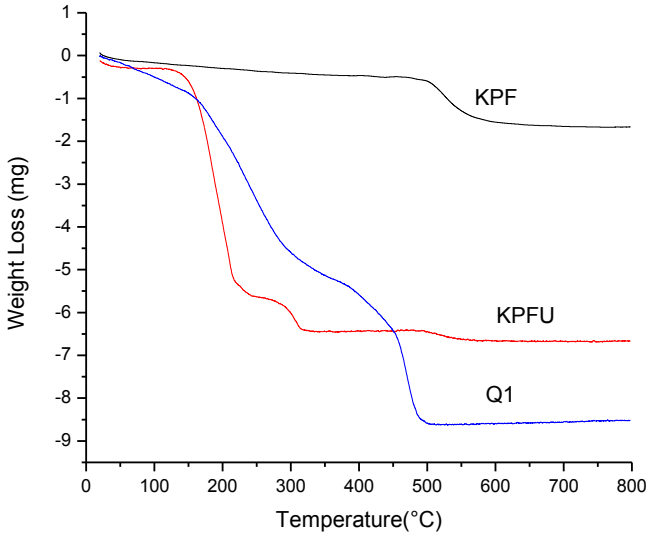

Figure 6.7. TGA thermograms for KPF, KPFU and Q_1

Conclusion

As we have argued at the inception point to say that, the urea CRF formulations for use in the advanced agronomic practices can be prepared through kaolinite intercalation reactions utilizing an important stage called intermediate intercalation step. Since it is difficult to intercalate the kaolinite interlayer spaces by virtual of being a 1: 1 layered phyllosilicate, the application of an intermediate intercalation stage was seen to be necessary step in that, strong intercalant was first used to expand the kaolinite interlayer spaces which in turn allowed for urea intercalation by substitution reactions. In that way, the choice of an intermediate intercalating species is of paramount consideration in the engineering of urea-kaolinite intercalation compounds. The findings that we have presented suggest that iron oligomers are strong intercalants and so, can be used in the intermediate intercalation stage to attain an intercalation ratio of about 70.4%. Correspondingly, this intermediate intercalation compound can be successfully substituted with

urea to produce urea-kaolinite intercalation compound with an intercalation ratio of about 76.8%. To date the literature is silent regarding the ability of iron oligomers to intercalate kaolinite and be used in the urea CRF industry. Furthermore, the findings presented have revealed the iron-rich kaolinite (red clay contaminated kaolinite) has a natural tendency for Fe^{3+} oligomerization thereby naturally intercalating the kaolinite interlayer spaces. This observation is by its own unique and the presented findings have attempted to explore that phenomenon. The study of iron oligomerization and its usefulness for urea CRF formulations is important because (i) it will challenge literature on the likelihood to intercalate the 1:1 kaolinite structure with easy, (ii) it will result to novel synthetic pathway for the industrial production of urea CRFs, and (iii) it will revolutionize the modern agronomic practices involving fertilizer industry. As a result of reflecting on the findings obtained, we propose that it will be more fruitful to pursue further research about the synthesis of urea CRF formulations via kaolinite intercalation reactions utilizing both laboratory synthesized ferrous oligomers as well as the naturally oligomerized Fe^{3+} species from red clays.

CHAPTER SEVEN

SEM/EDX Study on the Urea Reinforced Volcanic ash Nanocomposites

Summary

There is a growing demand for the designing of strong and durable biomaterials with properties that suits bio-inorganic applications. Urea's Biocementation process was documented in the preparation of high strength calcite nanoparticles, foundry binders, Biomason, and stone spray robotics; however there is no attempt made to design the urea reinforced a volcanic ash nanocomposite which is the subject of this study. Urea reinforced volcanic ash nanocomposites were prepared and characterized with SEM for their surface morphology and particle sizes as well as chemical composition with EDX. Structures appearing like the middle ear anvil and hammer as well as the nanoropes reinforced ash nanocomposites were observed. SHMP was seen to interfere with the formation and the stability of the reinforced nanocomposites whose particle sizes were 0.27 and 0.89 μm for the reinforced urea-ash nanocomposites and 0.89 μm for the nano anvil-hammer structures. Atomic and weight percentages of nitrogen as compared to the other elements were observed to exhibit an antagonistic pattern. Variance test showed that there is a difference in the mean particle sizes exhibited by the compared two nanocomposites at the 5% level of significance. Thus, the preparation of reinforced urea-volcanic ash nanocomposites was demonstrated and indicated that the preparation of high strength biomaterials by using urea and Oldoinyo volcanic ashes is possible.

Keywords: Biocementation, Nanocomposites, Nanoropes, anvil-hammer nanostructures, reinforcement, encapsulation

7.1 Introduction and Literature Review

Urea despite being a widely used nitrogenous fertilizer owing to its high nitrogen content of about 46%, it has also been investigated for its ability to associate with a biological cementation process. Biocementation or BioGrout is a technology in which microorganisms control the precipitation of calcium carbonate between sand particles producing high strength (Al-Thawadi, 2013). The mechanism of urea Biocementation was explained by Trimble to say: urea acts as a fertilizer and so encourages soil bacteria to flourish; the bacteria reacts with the calcium to form calcite which is a sticky substance that glues the grains of sand together (Peter, 2014). The reaction mechanism proposed by (Al-Thawadi, 2013) is given in the equation 7.1.

$$CO(NH_2)_2 + 2H_2O + Ca^{2+} \xrightarrow{\text{urease}} 2NH_4^+ + CaCO_3 \qquad (7.1)$$

Several studies demonstrated this phenomena including the preparation of sandstone-like biomaterial from sand and urea (Janet, 2014), consolidation of sand particles by aggregates of calcite nanoparticles synthesized by ureolytic bacteria under non-sterile conditions (Al-Thawadi, 2013), preparation of biostone from sand and urea from urine (Peter, 2014), Urea is also known to enhance the binding and the curing process of urea-modified furans foundry binders (Fink, 2013), as well as enhancing the formation of Biomason, a material prepared by professor Ginger Krieg Dosier with Nasa anticipated to be used as a shelter in the Mars (Colin, 2011). According to (Colin, 2011) "The material which they plan to market under the name Biomason - is made by combining aggregate with bacteria, yeast, calcium chloride, water and urea, a component of urine. Many types of aggregate can be used including, in places like the UAE, sand. The mixture is placed in a mould, where a process known as Biocementation takes place. The bacteria feed on the urea and, in a series of biological and chemical processes, the microbes transform the calcium into crystals that fuse the loose grains of sand- or Mars dust- together like glue. This produces a strong and durable solid material with a composition and physical properties similar to those of natural sandstone".

Furthermore, Anna Kulik (Kulik et al., 2012) also investigated the sand particles aggregation for the preparation of the stone spray robotics. In a recently published patent, an invention related to a method of manufacturing soil reinforced by microbe-based bio-binders and soil produced by the method was investigated (Bang et al., 2014). According to the method, the soil was prepared

by binding sand whose major components were silica and alumina, ureolytic microbes, urea, calcium ion, and polymer fibres, where the content of polymer fibres in sand ranged from 0.05 weight percent (%) to 5 weight percent (%) and the microbes provided $CaCO_3$ at a rate at $1\sim7 \times 10^{-9}$ g $CaCO_3$ ppt $cell^{-1}\ hr^{-1}$ under optimum conditions. It was said that the current move on the urea investigation as a biobinder is of paramount importance life since the biobinders are not harmful, do not cause environmental pollution and sufficiently secure the soil strength and resistance (Bang, et al., 2014). To the best of our knowledge, no attempts have ever been made to architecture a urea reinforced volcanic ash nanocomposites. This paper therefore describes the preparation of urea reinforced carbonatite volcanic ashes from Oldoinyo Lengai Arusha Tanzania for use as excipients for controlled release formulations.

7.2 Materials and Methods

7.2.1 Materials

Volcanic ashes were collected at Oldoinyo Lengai active volcanic mountain at Ngorongoro Arusha Tanzania, Urea (ACS reagent, 99.0-100.5%) was supplied by Sigma Aldrich, Sodium hexametaphosphate [$(NaPO_3P)_6$] (chemical pure reagent) was supplied by Daejung chemicals & metals, Co. Ltd, Gyonggi-do, Korea, deionized distilled water (D.I was supplied by Prof. Kim's lab), and liquid paraffin (extra pure grade) was supplied by Duksan pure chemicals, Ansan city Kyungkido-Korea.

7.2.2 Methods

a) **S**ampling

As seen from appendix 5, the raw samples were sampled at 2980 m altitude from Oldoinyo Lengai Volcanic Mountain Arusha Tanzania. The sampling procedures involved random collection at the high altitude (plate 7.1), middle altitude (plate 7.2) and the basement (plate 7.3). The ashes were then soaked and gently agitated with Denver propeller equipped with soft scrubber apparatus and propelled at 12 times 100 rpm for 60 minutes and then at 14 times 100 rpm for more 60 minutes. The slurry was left to settle for 17 hours. Submicron sieve analysis was carried out from the suspended particles; drying was done at 105 °C and particles kept for sample preparation.

Plate 1. Scattered volcanic ashes at high altitude of Oldoinyo Lengai

Plate 2. Scattered volcanic ashes at steeper mid altitude of Oldoinyo Lengai

Plate 3. Scattered volcanic ashes at the basement of Oldoinyo Lengai

b) Sample preparation

About 1.04 g of ashes was dispersed into agitating distilled water at 140 °C for 20 minutes. Urea fertilizer was then introduced and stirred for 30 minutes after lowering the temperature to RT. 5 ml of liquid paraffin was added drop wise into the solid dispersions and stirred for 5 minutes until homogenous mixtures was obtained. After 5 minutes 1.40 g of sodium hexametaphosphate was agitated with the mixture for more 8 hours. The sample was dried in a vacuum oven and labeled AU_4. The procedures were repeated but reversed by dissolving urea into distilled water at 40 °C followed by addition of ashes. The mixture was agitated without addition of paraffin and sodium hexametaphosphate. After drying and the sample was labeled AU_0.

c) Characterization

The samples surfaces morphology was investigated by using Field Emission Scanning Electron Microscopy (SEM-Hitachi-s-4800, Japan). The accelerated voltage was 15 kV. Elemental analysis was carried out by using EDX facility whereas Image Tool software was used for particle size analysis. The two sample test for variance for the particles sizes of both AU_0 and AU_4 was performed using Origin Pro 8 software.

7.3 Results

The morphology of the raw but washed volcanic ashes, the urea reinforced volcanic ashes without polymeric paraffin and deflocculating sodium hexametaphosphate AU_0 and the urea reinforced volcanic ashes with polymeric paraffin and deflocculating sodium hexametaphosphate (SHMP) AU_4 are presented in Figure 7.1-7.3 respectively.

Accordingly, the respective elemental analysis for each sample which depicted the chemical composition of both AU_0 and AU_4 are presented in Figure 7.4 and 7.5. Likewise, the variations in the peak intensities as well as the presence and/or the disappearance of certain elements together with their respective weight and atomic contribution (or, composition) are given in details in the Table 7.1 hereunder. The sizes of the particles which have been taken as an average of the count are summarized in Table 7.2. The two sample test for variance for the particles sizes of both AU_0 and AU_4 are presented in Table 7.3.

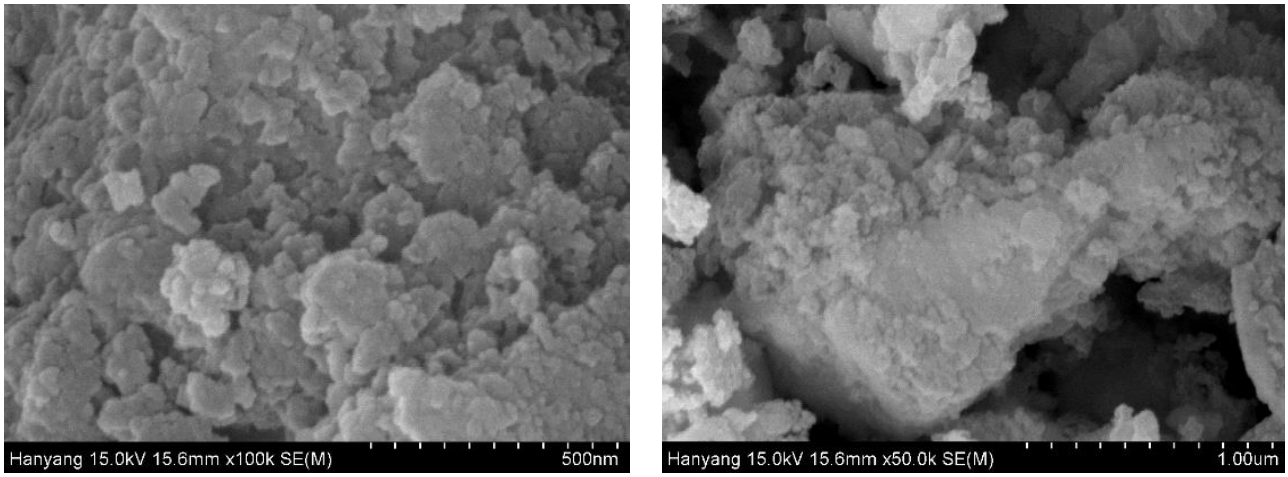

Figure 7.1. SEM micrographs for the washed Oldoinyo Lengai volcanic ashes

Table 7.1. Chemical composition of AU_0 and AU_4

Element	Weight (%)		Atomic (%)	
	AU_0	AU_4	AU_0	AU_4
C	16.66	51.17	20.82	62.13
N	37.44	9.94	40.13	10.35
O	37.41	19.18	35.11	17.48
Na	-0.36	6.68	-0.24	4.24
Mg	-0.38	0.55	-0.23	0.33
Si	5.99	6.38	3.20	3.31
Ca	3.18	5.43	1.19	1.98
Fe	0.07	0.67	0.02	0.17

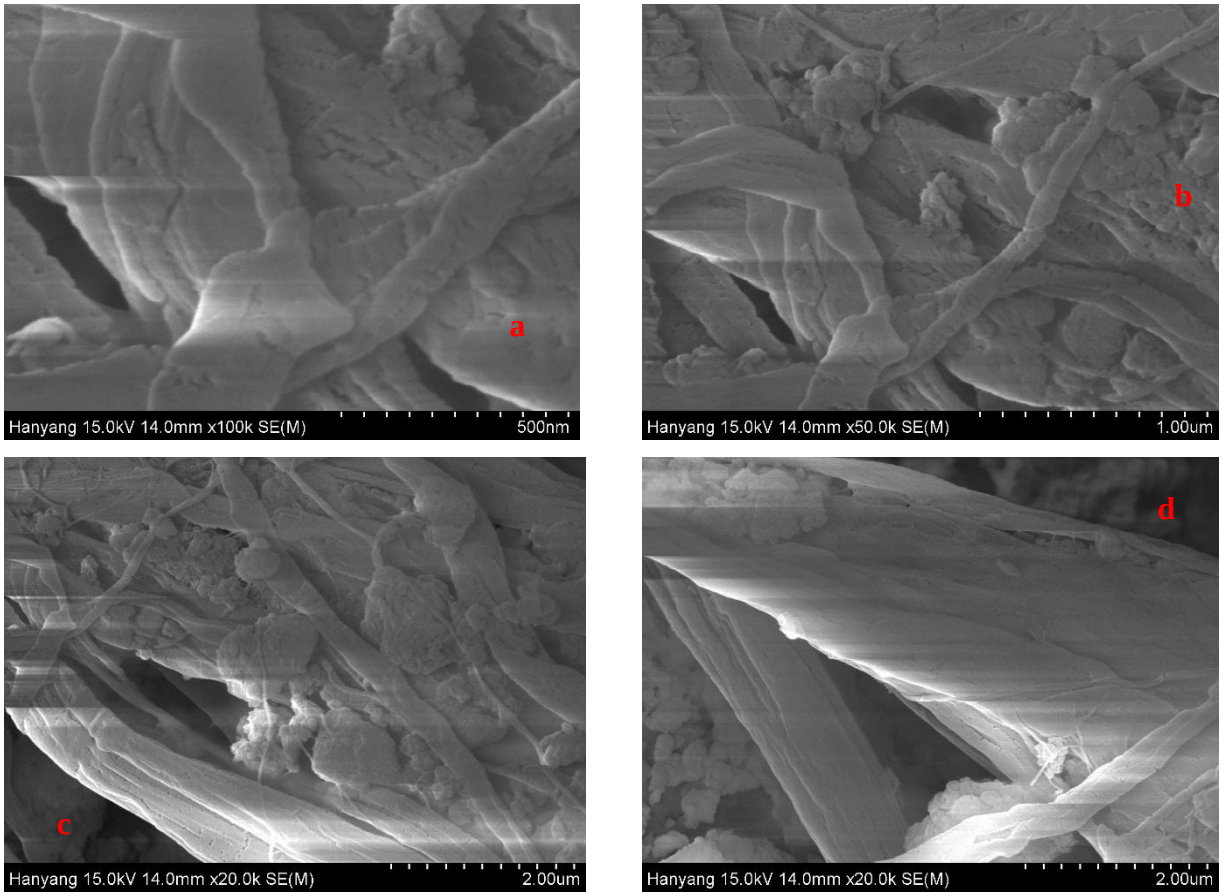

Figure 7.2. SEM micrographs for AU_0

Table 7.2. Particle sizes analysis

Length (μm)	
AU_0	AU_4
0.15	1.04
0.19	0.74
0.20	0.62
0.21	0.93
0.31	0.91
0.33	0.51
0.27	1.18
0.26	0.77
0.37	0.69
0.20	1.06
0.64	1.15
0.18	0.91
0.18	1.08

Table 7.3. Two-sample test for variance

Descriptive Statistics

	N	Mean	SD	Variance
AU_0	13	0.27	0.13	0.02
AU_4	13	0.89	0.21	0.05

F Statistics

F	Numer. DF	Denom. DF	Prob > F
0.38	12	12	0.11

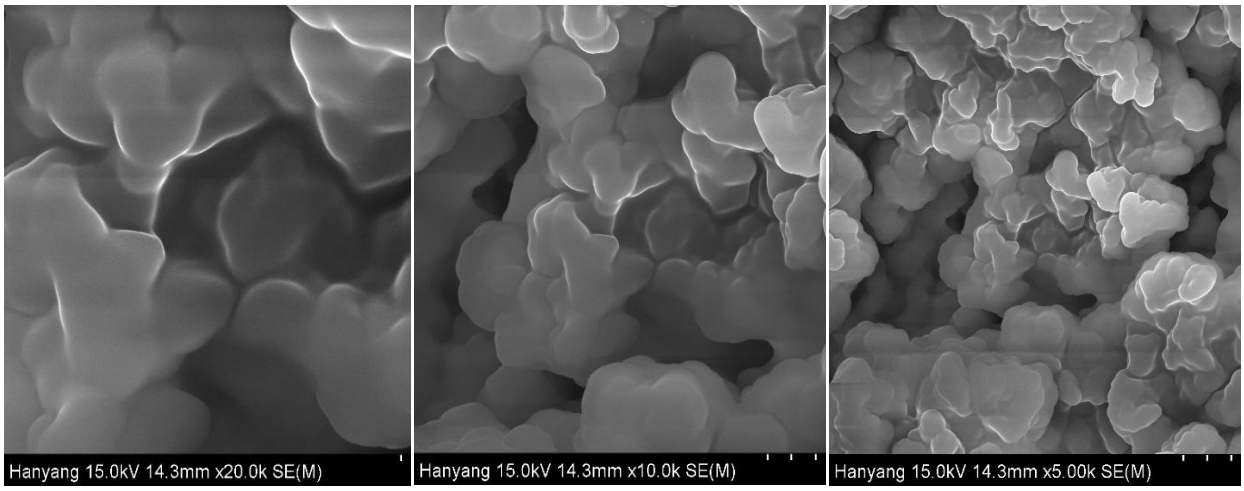

Figure 7.3. SEM micrographs for AU_4

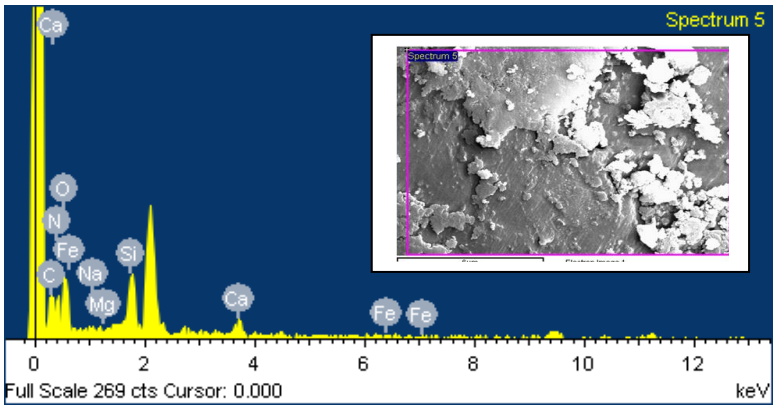

Figure 7.4. EDX Analysis for AU_0

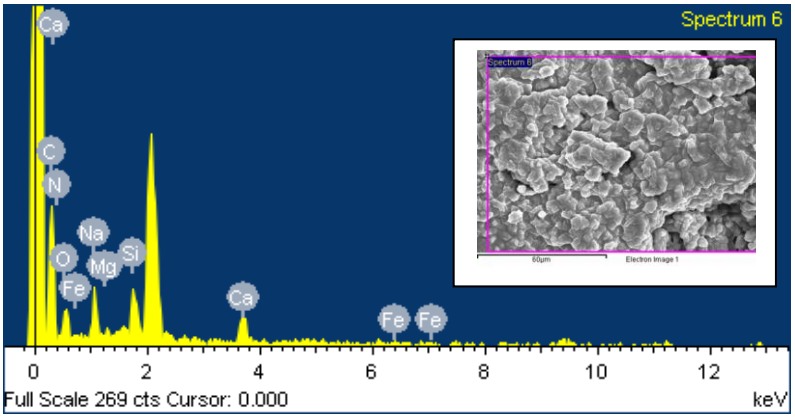

Figure 7.5. EDX Analysis for AU_4

7.4 Discussion

The nanocomposites prepared in order to investigate the ability of urea fertilizer to produce reinforced volcanic ashes were characterized for their morphology, particle sizes and chemical composition. The following observations were made on the Figures 7.1-7.3:

Volcanic ashes after washing were characterized with disorganized particles thereby creating rough surfaces with mixed sizes and shapes of the particles (Figure 7.1). Urea fertilizer was observed to reinforce the particles as seen in Figure 7.2 where, urea uniquely formed a new phase of nanoropes interwoven into a crosslinked pattern. Figure 7.2(d) clearly showed that the tubular reinforcement nanoropes were fibrous. With the introduction of sodium hexametaphosphate (SHMP) into the paraffin treated urea-ashes nanocomposites, the morphology observed in (ii) above changed into the pattern observed in Figure 7.3. The particles were observed to resemble the "hammer and anvil" of the middle ear and so we have termed them as the "nano anvil-hammer". These observations were attributed to the following facts:

a) The AU_0 prepared at 40 °C ensured an effective urea interaction with the decomposing soil organisms in the washed samples observed in Figure 7.1. Biocementation process (which we had thought that it could be associated with $CaCO_3$ formation) led the formation of the nanoropes which in turn acted as reinforcing agents. The formation of the reinforcing nanoropes marked the distinctive structural difference between raw washed samples (Figure 7.1) and the samples treated with urea fertilizer (Figure 7.2). In that way, it may be said that urea fertilizer was highly linked to the formation of the ash-nanoropes which acted to reinforce the volcanic ashes particles to give a pattern observed in Figure 7.2. We have anticipated that, the strength of the urea reinforced nanocomposite could be higher than that of the raw washed volcanic ash particles.

b) The impact of both polymeric paraffin as well as the deflocculating SHMP was noticed to be significant. The transformation of the highly reinforced urea-ash nanocomposites (Figure 7.1) into the pattern seen in the Figure 7.2 revealed the fact that: the polymeric liquid paraffin mobilized the urea-ash reinforced nanocomposites via encapsulation to form masses of "nano-hammer and anvil" structures. On the other hand, the introduction of a dispersing agent SHMP caused a disintegration of the interwoven encapsulated fibrous reinforced urea-ash nanocomposites into the agglomerated particles observed in Figure 7.2. Principally, this

phenomenon was attributed to the fact that: SHMP hexamer acted to prevent the combining of the ash aggregates by decelerating their setting out.

Our observation on the Table 7.1 along with Figure 7.4 and 7.5 confirmed what we have observed in the Figure 7.1-7.3 above. As can be clearly seen, except for the nitrogen, the atomic and weight percentages of the elements were observed to be high in AU_4 and lower in the AU_0 while for the nitrogen it was opposite in that both the atomic and weight percentages of the elements were observed to be high in the AU_0 and lower in the AU_4. The implications behind is: (i) mobilization of atoms led to the formation of precipitated and fibrous nanoropes (Figure 7.2) which in turn acted as reinforcing agents, a process which was associated with the elemental depletion since they acted as raw materials for the formations of calcite and other precipitated particles involved, (ii) Biocementation process actually took place towards the formation of the reinforced urea-ash nanocomposites observed in Figure 7.2. This again was confirmed by the decrease in the atomic and weight percentages of the elements which may be associated with bacteria feeding on the urea leading to the depletion of N, (iii) the framework of the nanoropes or rather the urea-ash nanocomposite was organic backbone and not inorganic due to the high amount of C, N, and O and low amount of in organic species. The particle sizes were in average 0.27 and 0.89 μm for the AU_0 and AU_4 respectively (Table 7.2-7.3). In addition, the two sample test for variance revealed that there is a clear evidence that at the 5% level of significance to suggest that there is a difference in the mean particle sizes exhibited by the AU_0 and AU_4 nanocomposites since $variance_1/variance_2 <> 1$.

Conclusion

Urea reinforced volcanic ash nanocomposites can be made. The process was made possible with the aid of the Biocementation process which utilizes unseen but available soil microbes acting on the urea fertilizer. This study has therefore revealed that, urea although it has been used as fertilizer it may also be used in the Biocementation process. The fibrous nanoropes were observed to reinforce the ash particles following urea Biocementation process. Liquid paraffin was seen to exhibit the ability to transform the reinforced urea-ash nanocomposites into the nano anvil-hammer structures. SHMP was noted to interfere with the Biocementation process by disrupting the reinforced particles into the masses of ash aggregated agglomerates indicating that

the process could be reversible when SHMP and heat are consecutively used. Elemental analysis indicated an antagonistic atomic and weight percentages of nitrogen as compared to other elements of the reinforced nanocomposites in that: the nitrogen's the atomic and weight percentages was observed to be high in the nano anvil-hammer structures and lower in the reinforced urea-ash nanocomposites and vice versa for the atomic and weight percentages of the other elements found in the prepared nanocomposites. In average the particles ranged from 0.27 μm for the reinforced urea-ash nanocomposites and 0.89 μm for the nano anvil-hammer structures; similarly, analysis of variance demonstrated that there is a difference in the mean particle sizes exhibited by the compared two nanocomposites at the 5% level of significance. Concisely, this study has established that reinforced urea-volcanic ash nanocomposites can be made and that the findings obtained can be used in the future design of biomaterials and related nanostructures which requires reinforcement for improved strength.

CHAPTER EIGHT

Silicone Doped Chitosan-acrylamide Co-encapsulated Urea Fertilizer: An Approach to Controlled Release Fertilizers

Summary

Despite being used in the agricultural industry as animal feed additive and fertilizer due to its high nitrogen (*N*) content (≈ 46%), urea is known to undergo unique chemical transformation when field applied resulting into severe losses (of about 60-70%) of total fertilizer applied) in efficiency may result in the absence of special management practices. This paper seeks to describe how to counter balance the 60-70% urea loss through co-encapsulation with biodegradable chitosan-acrylamide polymeric blend along with silicone doping in attempt to design urea controlled release fertilizers (CRFs). Urea was crosslinked with chitosan and acrylamide under refluxed *in situ* co-polymerization technique; the procedures were repeated with silicone doping prior crosslinking with MBA. The nanoparticles were characterized for: molecular vibrations with FTIR/ATR, elemental composition with EDX, crystallinity with X-ray indexing, thermo-performances with TG/DTG, particle size and morphology with SEM and DLS. The IR bands observed within 3426-409 cm^{-1} revealed the formation of new bands after co-encapsulation for the ν_{γ}N-H, ν_{β}N-H, νOH, $\nu_s NH_2$, νCH_2, νC=O, $\delta' NH_2$, νC=C, δNH_2, νC-N, βCH_3, $C-N, γNH_2, νC=O and CH_2. Crystallinity indices for urea with and without silicone doping were found to be 50.9% and 72.1% and their crystalline exhibited wave number and parabolic patterns respectively. Elemental analysis revealed that *N* can be effectively leached from the polymeric excipients following 90 days of diurnal exposure in an open air. The formation of wrinkled Nanodunes as well as Nanoballs 3D network with particle size of about 0.64 μm was observed for the urea CRFs encapsulated with and without silicone doping respectively. Thermogravimetry indicated that the engineered CRFs can decompose between 48 and 570 °C. Empirically, the findings demonstrated that it is possible to design urea CRF formulation with varying particle sizes, and morphologies/shapes along with suitable biodegrability by using chitosan-acrylamide co-encapsulation. The essence is to enhance urea' fertilizer use efficiency (FUE) thereby increasing crop yield and lessen the world food crisis.

Keywords: Encapsulation, *In situ* copolymerization, CRFs, CCFs, Crystallinity Index, Nanoballs, Nanodunes

8.1 Introduction and Literature Review

Owing to its being a low cost nitrogen fertilizer with a high nitrogen content of about 46%, urea fertilizer has been used (within Tanzania in particular) to supplement crop plants of nitrogen (Curtis J. Overdahl, Rehm, & Meredith, 2015; James, 1993; Shaviv, 2001). Urea has been useful in horticultural practices, enrichment of lawns or sods, meadows, prairies and road-side protective grasses necessary to control erosion by the road sides, orchards, in cereals plantation *etc.*, such that it's advanced research is vital for the economic growth of any country like Tanzania whose economy depends on agriculture (Glibert, Harrison, Heil, & Seitzinger, 2006; Jones, Koenig, Ellsworth, Brown, & Jackson, 2007; Kamhabwa, 2014; Minot, 2009; Premarathna et al., 2012).

On the contrary, despite being such an economically and agronomically useful chemical material urea is limited for the reason that: its availability to crop plants is less than 50% with up to 60-70% loss of the sum applied in the soil due to vaporization, hydrolysis, and quick leaching rendering its FUE low (Sempeho, Mubofu, Pogrebnoi, & Shao; Shaviv, 2001). As a consequence, attempts involving the use of excipients molecules to obtain controlled release urea formulations have been done to maximize the efficiency and availability to crop plants to about 70% or more. These include the synthesis of urea-aldehyde condensation products, such as urea-formaldehyde (UF), urea triazone (UT), crotonylidene diurea (CDU), and chemically decomposing compounds, such as isobutylidene-diurea (IBDU) (Sempeho, et al., 2014); urea granules coated by hydrophobic polymers or as matrices such as polyolefins and rubber and gel-forming polymers (hydrogels) which are hydrophilic in nature and sulphur-coated urea (SCU) *etc.*

Essentially, several polymers and polymer resins are known to be used in the designing of urea CRF formulations including: acrylamide, urethane resin, epoxy resin, alkyd resin, unsaturated polyester resin, phenol resin, urea resin, melamine resin, phenol resin, and silicon resin along with a good number of natural bio-polymeric materials such as chitosan which has been used in this study (Sempeho, et al., 2014). For the best our knowledge, no attempts have ever been done to design urea CRF formulations by using co-polymerization of chitosan and acrylamide along with silicone doping. In that case, we have described in this paper the preparation of urea-CRF

formulation as an approach to control release systems (CRSs) using simple and inexpensive starting materials including, silicone oil, chitosan biopolymer, acrylamide and urea synthetic fertilizer.

Chitosan was used in this study owing to its inherent properties such as high swelling ratio (Jamnongkan & Kaewpirom, 2010b), water-retention (CFCW) capacity (Wu & Liu, 2008) antimicrobial activity, availability, low toxicity, biodegrability, capability for high crosslinking, and low processing cost (Bhuvaneshwari, Sruthi, Sivasubramanian, Niranjana, & Sugunabai, 2011; Leceta, Guerrero, & De La Caba, 2013; Leceta, Guerrero, Ibarburu, Dueñas, & De la Caba, 2013). Also, the nanoparticles resulting from chitosan are known to exhibit spherical shapes and uniform sizes (Corradini, De Moura, & Mattoso, 2010a); similarly, the complexes formed between chitosan with other bioactive species (urea in our context) along with other polymers are known in modifying the release characteristics of the named CRSs formulated (Singh, et al., 2011). On the other hand, we have stated elsewhere (Sempeho, et al., 2014) that: "polyacrylamide is known to reduce soil erosion" and also it is biodegradable (K. Nwankwo, 2001; Subbarao, et al., 2013); thus polyacrylamide was chosen to be used along with chitosan in the urea co-polymerization process.

In due course, the synthesized urea CRF formulation is expected to augment crops grain yield and straw yield, as well as enrich soil with nitrogen thereby increasing its nutritional status and also the efficacy of Conventional Chemical Fertilizers (CCFs) such as urea (Sanjeev Kumar, Bauddh, Barman, & Singh, 2013). In fact, the efficacy of CRFs is known to be more than four times higher than CCFs which indicates that even $1/4^{th}$ of chemical fertilizers can be made more effective with organic blending into CRSs (Sanjeev Kumar, et al., 2013).

8.2 Materials and Methods

8.2.1 Materials

Urea (ACS reagent, 99.0-100.5%) was supplied by Sigma Aldrich, deionized distilled water (D.I was supplied by Prof. Kim's lab, chitosan powder was supplied by Sigma Aldrich, acetic acid glacial (99.7%) was supplied by Duksan pure chemicals, Ansan city Kyungkido-Korea, 2,2'-Azobisisobutyronitrile (AIBN) (≥ 98.0%) was supplied by Samchun pure chemicals Co. Ltd, Gyonggi-do, Korea, CCl_3 (≥ 99.0%) was supplied by Junsei Chemical Co., Ltd, Japan, N,N'-

Methylenebisacrylamide (MBA) (≥ 98.0%) was supplied by Samchun pure chemicals Co. Ltd, Gyonggi-do, Korea, acrylamide (≥ 9 8.5%) was supplied by Samchun pure chemicals Co. Ltd, Gyonggi-do, Korea, *n*hexane was supplied by was supplied by Sigma Aldrich, and silicone oil was supplied by Sigma Aldrich.

8.2.2 Methods

a) Preparation of chitosan solution

A chitosan solution (2%) was prepared by dissolving 10 g chitosan powder into 500 ml of 10% glacial acetic acid to get the pH of the solution in a range of 4-5. The solution was stirred for 40 hours at RT until a gold colour was obtained.

b) Preparation of chitosan-acrylamide encapsulated urea

AIBN (0.2 g) was agitated with 30 ml of CCl_3 in the 3-necked round bottomed flask (RBF) containing 0.4 g of MBA and the apparatus was set under hood and was run for 20 minutes under N_2 atmosphere at 60 °C. Thereafter, a chitosan solution prepared which contained 7 g of acrylamide and 0.8 g of urea was introduced and stirred under reflux overnight. The product was washed with n-hexane and dried at 60 °C with a vacuum oven; it was then labelled as CPAM-1. The ability of CPAM-1 to hold urea was tested with EDX for the presence of nitrogen after exposing it under open surroundings for 90 days.

c) Preparation of chitosan-acrylamide encapsulated urea with silicone oil doping

The procedures for the preparation of chitosan-acrylamide encapsulated urea (described above) were repeated with the following modifications. Stirring under reflux was done for six hours after which 1 ml of silicone oil was spiked with a syringe as dopant and then continued stirring overnight. The product was washed with *n*-hexane, dried under vacuum oven and it was then labelled as CPAM.

d) Characterization

Infrared Spectroscopy: FTIR-ATR analysis was carried out in the near infrared region at wavelength between 7500 and 360 cm^{-1} using a Bruker Optic GmbH (alpha model, Laser class

1) Spectrometer with attenuated total reflectance. *X-ray Diffraction:* the XRD analysis was carried out using Rigaku Coorp. D/Max-2500/PC X-ray Diffractometer equipped with a back monochromator operating at 40 kV and 100 mA at the scanning range of 5° – 80° with a step size of 0.1° and a time/step of 1 s using copper cathode (Cu Kα1) as the X-ray source (λ = 1.54056 Å). *Scanning Electron Microscopy (SEM):* the samples surfaces morphology was investigated by using Field Emission Scanning Electron Microscopy (Hitachi S-4800, Japan. The accelerated voltage was 15 kV. *Elemental Analysis:* the chemical composition of the samples was determined by using EDX facility attached into Field Emission Scanning Electron Microscopy (Hitachi S-4800, Japan) accelerated at 15 kV. *Particle Size Analysis:* image Tool software was used to analyse the size of particles from the SEM images. The plot for the average particles sizes was performed thereafter using Origin Pro 8 software.

8.3 Results and Discussion

8.3.1 Vibrational spectra

The infrared spectra of urea as well as of the samples CPAM and CPAM-1 are shown in Figure 8.1 whereas that of chitosan is given away in Figure 8.2. A summary of band assignments for urea, CPAM and CPAM-1 samples is given in the Table 8.1. Detailed band assignments for chitosan can be found elsewhere (Kunjachan, Jose, & Lammers, 2010). Typically, silicones have strong characteristics absorption bands in the mid infrared spectra range at: 3000-2900, 1500-1490, 1260-1250, 1100, 1080-1000, 770, 751-750 and 600 cm $^{-1}$ (Dupont et al., 2007; Groza, Surmeian, Ganciu, & Popescu, 2005; Kim et al., 2012). The characteristics absorption peaks for the acrylamide are known to exist around: 3365, 3352, 3180, 3030, 3011, 1675, 1654-1650, 1612, 1451, 1430, 1353, 1325, 1282, 1138, 1053, 991, 963, 831, 816, 708, 660, 634-626, 490, and 225 cm $^{-1}$ (Magalhães, Almeida Neto, Bezerra, Ricardo, & Feitosa, 2012; Murugan, Mohan, & Bigotto, 1998; Ray, Mohanta, Manavalan, & Sahoo, 2009) whereas those of chitosan biopolymer (Figure 8.2) occur around: 3750, 3367, 3350, 2927-2900, 2875, 1680, 1662, 1605, 1559, 1480, 1426, 1393, 1375, 1333, 1320, 1164-1150, 1092-1080, 1042, 1025, and 896-890 cm $^{-1}$ (Anicuta, Dobre, Stroescu, & Jipa, 2010; Brugnerotto et al., 2001; Kunjachan, et al., 2010; Magalhães, et al., 2012; Silva et al., 2012). For pure urea fertilizer, the absorption bands are clearly seen in the Table 8.1 which is approximately around the values we reported in (Sempeho, et al.).

As indicated in Table 8.1, there were variations in the characteristic absorption bands observed relative to their original starting materials; this has revealed the fact that new bonds have might been formed as a result of co-polymerization between chitosan-acrylamide with urea fertilizer and later with silicone oil used as dopant. The silicone doping was observed to be successful due to disappearance of typical silicone bands; however, the backbone of silicone structure was noticed due to the presence of its characteristics peaks around: 1258, 1081 and 1013 cm $^{-1}$. As seen in Figure 8.1, these characteristics bands were only seen in the CPAM; and they were absent in the CPAM-1 as a result of silicone doping.

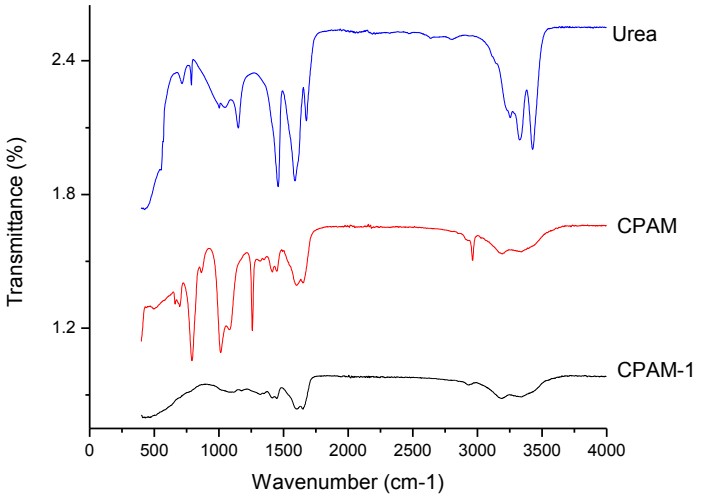

Figure 8.1. FTIR/ATR absorption band for urea fertilizer, urea encapsulated with chitosan-acrylamide co-polymer (CPAM-1) and urea encapsulated with chitosan-acrylamide co-polymer with silicone doping (CPAM)

The FTIR/ATR analysis also revealed success in the encapsulation of urea fertilizer with co-polymerization of chitosan and acrylamide. Upon deducing peaks observed in Figure 8.1, it can easily be said that among all characteristics urea absorption bands, only bands at: 3326 and 1458 cm $^{-1}$ were unaltered after encapsulation. Besides, there were observable variations to these bands that; the absorption band at 3326 cm $^{-1}$ got transformed to 3339 cm $^{-1}$ (for CPAM) and 3337 cm $^{-1}$ (for CPAM-1) after encapsulation. This pointed out that the N-H in phase bond stretching as well as the in phase CH_3 bending vibrations were present but the outer N-H bonds

were completely covered with encapsulant such that the N-H out phase bond stretching were absent after encapsulation. It was thus alleged that, silicone caused a slight band shift from 3337 to 3339 cm $^{-1}$ and from 1447 to 1448 cm $^{-1}$ for CPAM-1 and CPAM respectively.

Table 8.1. Band assignment for CPAM, Urea, and CPAM-1

Urea	CPAM	CPAM-1	Assignment	Reference
			v_{γ}N-H	(Fischer & McDowell, 1960; Larkin,
3426				2011)
			v_{β}N-H	(Fischer & McDowell, 1960; Horvath,
3326	3339	3337		et al., 2010)
			vOH(for H bonding	(Almuslet, et al., 2012; Padil, Nguyen,
3253			associated with urea)	Ševců, & Černík, 2015)
			v_sNH$_2$	(Magalhães, et al., 2012; Murugan, et
	3192	3187		al., 1998; Silva, et al., 2012)
			vCH$_2$	(Anicuta, et al., 2010; Brugnerotto, et al., 2001; Corporation, 2005; Gaylord, 2005b; Ray, et al., 2009; Silva, et al.,
	2962	2935		2012)
			vC=O & δ'NH$_2$	(H Becher, 1956; Magalhães, et al., 2012; Murugan, et al., 1998; Piasek &
1676				Urbanski, 1962a; Silva, et al., 2012)
			vC=C	(Murugan, et al., 1998; Ray, et al.,
	1648	1650		2009)
	1601	1602	δNH$_2$	
			vC-N	(Anicuta, et al., 2010; H Becher, 1956;
1588				Piasek & Urbanski, 1962a)
			βCH$_3$ & $C-N	(H Becher, 1956; Piasek & Urbanski,
1458	1448	1447		1962a)
	1412	1414	v *of* newly formed bonds	
			v *of* newly formed bonds (N-acetylglucosamine-	
		1319	acrylate)	
	1258		γNH$_2$	
			vC=O & CH_2$	(Murugan, et al., 1998; Silva, et al.,
1149		1174		2012)
	1081	1097		(Soleimani, et al., 2012)
	1013			(Aroke & El-Nafaty, 2014; Dawley, et al., 2012; Heah, Kamarudin, Al Bakri, et al., 2012; Mgbemena, et al., 2013b)
	863			
	791			(Aroke & El-Nafaty, 2014; Dawley, et al., 2012; Heah, Kamarudin, Al Bakri, et al., 2012; Liew, Kamarudin, Al Bakri, et al., 2012; Mgbemena, et al., 2013b)

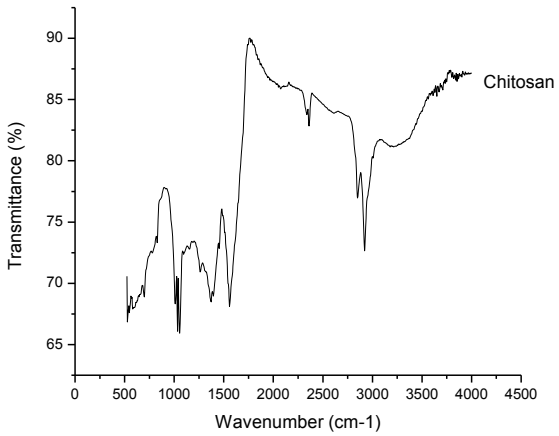

Figure 8.2. FTIR/ATR absorption band for chitosan biopolymer

8.3.2 EDX and X-ray Indexing

The XRD patterns for the CPAM and CPAM-1 were studied in the 2θ range of 5° to 50°. The findings as shown in Figure 8.3 indicated that all the samples were more or less amorphous whereas the level of crystallinity was low. Basing on the methods described by (Park, Baker, Himmel, Parilla, & Johnson, 2010) crystallinity index (CI) was calculated from the ratio of the height of the 002 peak (I_{002}) and the height of the minimum. That said, the CI was calculated for both CPAM and CPAM-1; the results indicated that CPAM-1 was more crystalline than CPAM; their respective crystallinity indices were 72.1% and 50.9%. The peaks observed for CPAM were at 12.30° (d) and 22.5° (s); both were broad and distinct. For CPAM-1, one high intensity peak was observed at 19.0° (d) and another broad peak at 22.5°. The pattern of these broad peaks illustrated that the peak for CPAM-1 had a wider shoulder as compared to CPAM.

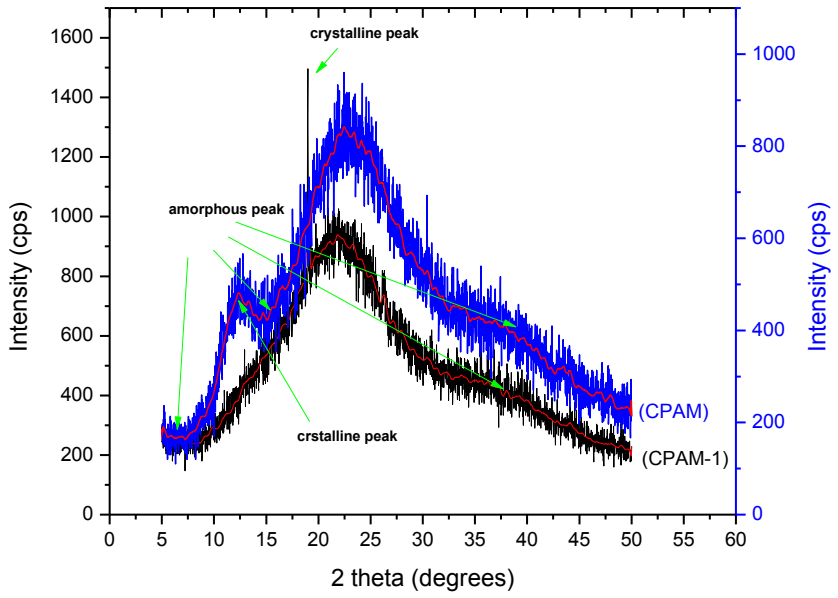

Figure 8.3. The X-ray diffraction pattern for CPAM-1 and CPAM

Quintessentially the following facts were derived from the observations made in the Figure 8.3:

a) Shape of the curve: CPAM-1 exhibited a slightly parabolic curve while the CPAM exhibited a waveband pattern. Reflecting on the findings by (Islam et al., 2011), the waveband pattern observed for the CPAM' curve revealed that: chitosan structure acted as a co-polymer framework during the co-encapsulation process such that its original known structure (Islam, et al., 2011) got modified into the waveband pattern observed in Figure 8.3.

b) Typical crystalline peak (fairly doublet) was observed at 19° in the CPAM-1 curve wherein the peak was of very high intensity; this peak (d) at 19° was considered as a characteristic peak for the CPAM-1 relative to CPAM. In the CPAM the crystalline peaks were also observed but as can be seen the amorphous phase seem to dominate the crystalline phase thereby showing the impact of silicone on the crystallinity of the prepared nanocomposite CPAM-1. The split peak (d) at 12.30° was considered to be distinctive for the CPAM and that; it can be used to identify CPAM from CPAM-1. Basically, the appearance of the split peak (d) at 12.30° for the CPAM was ascribed to the presence of OH^- and NH_2 groups from the chitosan which form stronger intermolecular hydrogen bonds upon co-polymerization. The presence of silicone dopant which covered these functional groups caused a

disappearance of this peak such that it was completely absent in the CPAM. This suggested the fact that the backbone structure of chitosan was not deformed during co-polymerization process but with silicone doping the backbone structure disappeared indicating the existence of a strong interaction between chitosan-acrylamide-urea and silicone. This proves what was mentioned in the IR results.

c) CPAM-1 curve at 30 to 50° portrayed rather smooth pattern as compared to CPAM.

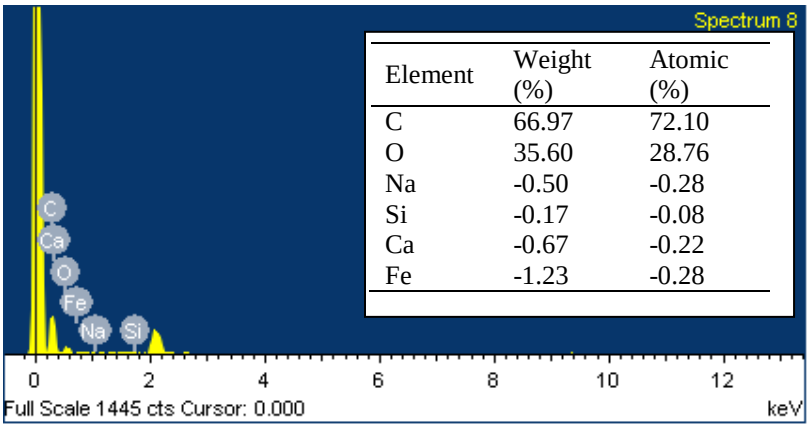

Element	Weight (%)	Atomic (%)
C	66.97	72.10
O	35.60	28.76
Na	-0.50	-0.28
Si	-0.17	-0.08
Ca	-0.67	-0.22
Fe	-1.23	-0.28

Figure 8.4. The EDX spectrum for CPAM-1 after 90 days of exposure to open air showing the depletion of nitrogen from the composite

Furthermore, EDX analysis (Figure 8.4) was carried out for the ability of CPAM-1 to hold urea after exposing it under open surroundings for 90 days. The empirical findings revealed the following facts:

a) CPAM was biodegradable excipient; when it was exposed to atmospheric conditions the urea contents contained was successfully leached to the ground completely. This was verified by the absolute absence of nitrogen after 90 days of testing via EDX elemental analysis.

b) The high amount of C and O (which can be degraded by soil microbes) indicated that the remaining materials after leaching of urea were user friendly waste. In that way, CPAM exhibited high level of environmental friendness to the soil and plants by producing wastes which can positively modify soil conditions.

c) It was hence scrutinised that the release of urea from the CPAM is a feasible process just under quotidian conditions.

8.3.3 SEM and Particle size Analysis

For the purpose of determining the particle size and sample morphology SEM images were taken and analyzed (Figure 8.5-8.7). The following truths were obtained basing on our observations:

a) When urea fertilizer was crosslinked through co-polymerization of acrylamide and chitosan biopolymer under the specified experimental conditions, the resulting composite materials exhibited what we have termed as the "Nanoball" appearance. As can be seen in the Figure 8.5, the Nanoballs were observed to be highly crosslinked and that each particle was strongly bonded to the other in a 3D-network to form a beautiful sheet of numerous Nanoballs.

b) When silicone was doped into the matrices of nanoballs 3D-network, a complete structural transformation was observed. As can be seen in the Figure 8.6, a new phase was formed and we have named it the "Nanodunes". A very beautiful wrinkled sheet of Nanodunes developed at the expense of the Nanoballs thereby indicating the impact of silicone doping on the framework of CPAM-1 composite materials.

Comparatively, the surfaces of the Nanoballs were seen to be smooth while those of the Nanodunes were seen to be rough or rather wrinkled. By instinct, this observation revealed that the surface area of the Nanodunes could be higher than that of the Nanoballs. Besides, the Nanoballs were observed to be highly crosslinked and interconnected than the Nanodunes. That is to say, for the purpose of designing CRF formulations with roundish particles along with maximum crosslinking, the CPAM-1 architecture could be more favourable whereas, if a need is to achieve a maximum surface area, CPAM structural pattern could be more favourable. Owing to that, the choice of a synthetic method will depend on the desired CRF formulation as per the intended usage. On top of that, we have anticipated that the Nanoballs could be more apposite for CRFs formulations engineering designs as the roundish particles could be translocated within the plant tissues with ease due to the nature of their "particle sizes together with morphology" (Sempeho, et al., 2014). Particle size analysis of the anticipated Nanoballs indicated that the average particles sizes as described in the mean region (Figure 8.7) were about $0.64 \pm 0.14\ \mu m$.

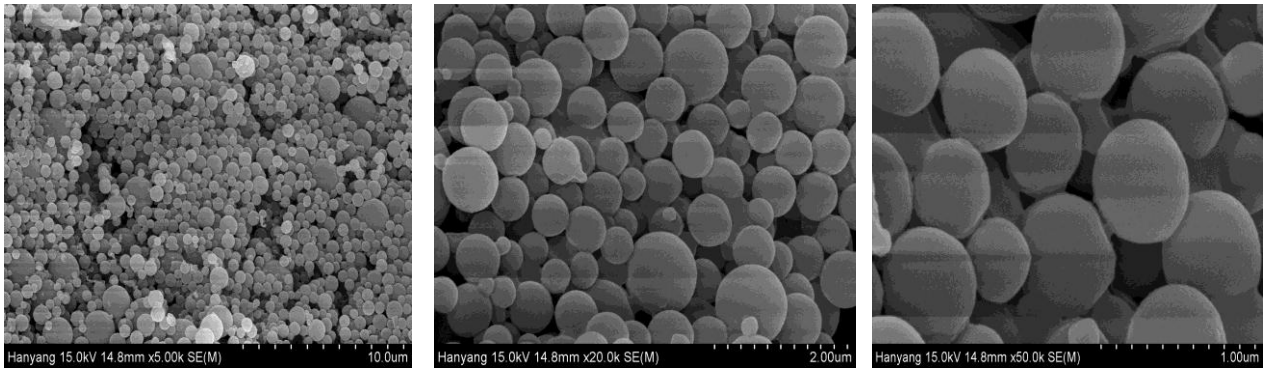

Figure 8.5. The SEM micrograms for the CPAM-1 showing the Nanoballs architecture

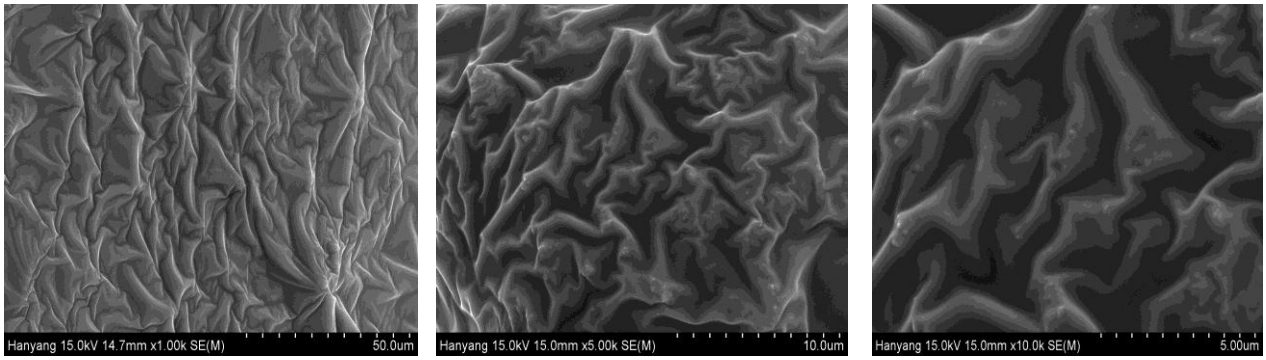

Figure 8.6. The SEM micrograms for the CPAM showing highly wrinkled surfaces: The Nanodunes

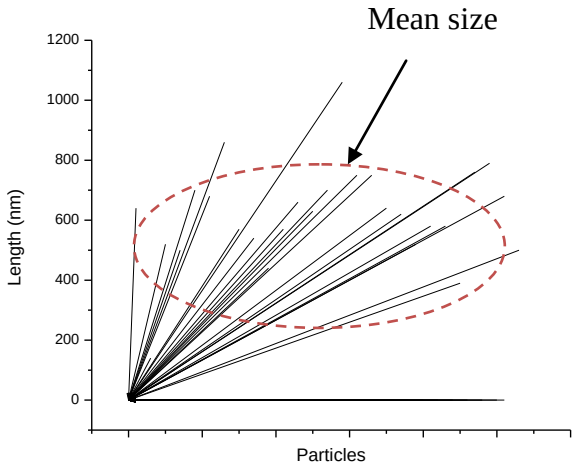

Figure 8.7. The average particle size of CRFs Nanoballs

Conclusion

Pragmatically, a clear discussion on the urea CRF formulation prepared by using chitosan, acrylamide and urea co-polymerization along with silicone doping was given. It was observed that the CRFs exhibit superior characteristics over the CCFs and so, the amendments of the conventional urea fertilizer via co-polymerization of chitosan and acrylamide was a key step toward its commercialization as well as enhanced FUE. Significant morphological variations were observed between the properties of urea crosslinked with and without silicone doping thereby indicating the possibility of designing the urea fertilizer forms as per intended usage basing on the climatic differences and the type of field application. The sizes which were observed to be within the range of 0.64 μm shows that the nanoparticles can be translocated within plants tissues with easy thereby enhancing the availability of N for the plant uptake and improve crop yield due to superior agronomic properties exhibited by the tailored urea CRF formulation.

CHAPTER NINE

9.1 GENERAL DISCUSSION

The study was set out to investigate the preparation, characterization and release profiles of urea controlled release fertilizer synthesized mainly through intercalation and encapsulation reactions utilizing Pugu kaolinite and polymeric materials with the emphasis on the natural polymeric resins. In addition to that, an investigation to explore the reinforced composite solid dispersions of urea fertilizer with volcanic ashes was also carried as a pilot study for the advanced use of volcanic ashes in the Nano-CRF industry. Furthermore, a study on the silicone doped chitosan-acrylamide co-encapsulated urea fertilizer: an approach to controlled release fertilizers was also conducted and the empirical results have been discussed at length in the respective chapters.

The study has unveiled the likelihood of diversifying kaolinite usage from mechanical studies (as seen in chapter 3) to advanced application in the controlled release systems. Correspondingly, the study has sought to know the role of intermediate intercalation steps in the preparation of Urea CRFs as well as the effects of encapsulation and coarcervation on the urea intercalated kaolinite. By the same token, the effect of changing the intercalants in the urea intercalation was also investigated. In essence, despite the differences observed in the properties of Urea CRF formulations (as described in the specific chapters) upon varying the intercalants, the study has indicated that urea CRFs can be formulated by using kaolinite intercalation as well as encapsulation and so concluding the fact that agronomically suitable urea CRFs can be prepared using kaolinite and polymeric materials as stated in the hypothesis of the study. Nevertheless, the efficiency and the effectiveness of the prepared formulations are yet to be studied. As far as the objectives of this study are concerned, the study has demonstrated that it is possible:-

1. To prepare the nanocomposite excipients using polymers and nanoclays.
2. To intercalate urea into the prepared nanocomposite excipients.
3. To characterize the prepared urea CRF formulations basing on the physicochemical, morphological and release profiles

4. To evaluate the release profiles from CRFs experiments in water except that, the possibility of attempting to establish release profiles in the simulated soil condition was not carried out since it was straying important objectives of the study.

Typically, due to volatility of urea fertilizers, most reactions were merely one-pot reactions. Correspondingly, several issues in relation to the objectives of the study have been raised upon careful reflection on the empirical results of the study. Therefore, this section seeks to concentrate on an in-depth discussion of all issues unveiled from the findings. In doing that, a background study was carried out to study the chemo-mechanical properties of Pugu kaolinite to lay down the basics for the characterization techniques used during the main study (Siafu & Lugwisha, 2014). For a better discussion, this section has been framed in small subsections where each subsection was set to answer a particular objective of the proposed study and the descriptions provided are just a critical reflection from the general chapters of this work. The scope of this section will be limited to the following:

- Context and background of the study
- Preparation and characterization of nanocomposite excipients
- Intercalation of urea into the nanocomposite excipients and characterization of the CRFs formulation
- Characterization and evaluation of the release profiles
- A pilot preparation and characterization of urea-volcanic ash composites
- The impact of silicone doping on the properties of chitosan-acrylamide co-encapsulated urea CRFs.
- Policy implications of the study

9.1.1 Context and background of the study

As mentioned elsewhere, CRFs and SRFs belong to the larger group of enhanced-efficiency fertilizers, which also include nitrogen stabilizers, nitrification inhibitors, urease inhibitors, and stabilized fertilizers. Controlled-release fertilizers are generally coated products. Slow-release fertilizers are non-coated products in which the nutrient release is uncontrolled but slow (CEH, 2015). The current trend as revealed in the following pie chart shows the consumption of

controlled- and slow-release fertilizers by major region; the United States and China are seen to be the most significant market for CRFs and SRFs formulations. However, the global market is expected to grow at a rate of over 5% per year during the forecast years, helped by increases in efficiency, reduced quantities of waste due to runoff, and also by increases in food demand by the growing population, especially among the third-world nations that are shifting to a more protein-based diet and away from traditional carbohydrate-based diets. For instance, from 2009 to 2014, CRF and SRF consumption in China grew at an average annual rate of about 30% thereby making China to be the world's largest producer and consumer of CRFs and SRFs (CEH, 2015).

Chart 9.1. Consumption of CRFs and SRFs by major regions-2014

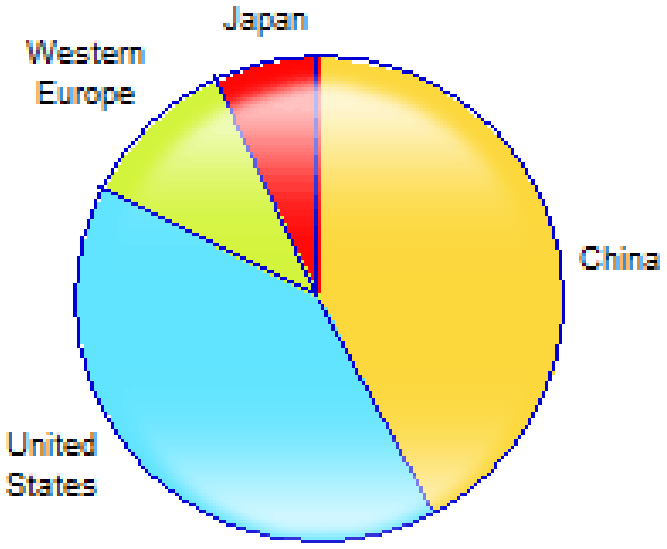

The fact that the overall, global demand for CRFs will continue to increase at around 10% annually during 2014-19 for horticultural and turf applications, including agricultural crop applications, the need for more research on the CRFs formulations is obvious and that describes the reason why this study is crucial and need to be promulgated. Correspondingly, it was said that, "CRFs and SRFs are an efficient alternative to conventional fertilizers (CFs) because of their environmentally friendly, resource-saving, and labour-saving characteristics. Conversely, because of their high price relative to CFs, their use is still limited primarily to ornamental, horticultural, and turf applications. As larger production scales of these materials are achieved,

the costs will continue to decline from current values, making them more attractive for commodity/open-field/broad-acre crops such as corn, wheat, and potatoes. Another factor that will drive CRFs demand in the future is the regulations and penalties that encourage growers to minimize fertilizer runoff in water streams" (CEH, 2015).

On account of that fact, the use of CRFs formulations is seen to be not a plainly new thing in the developed world; yet, the question of whether its use in crop production can be economically worthwhile is still an enigma. Consequently, this study was delimited or rather delineated within the CRFs context focusing on the application of locally available layered phyllosilicates and natural bio-polymeric materials for encapsulation in attempt to design urea based CRFs at relatively low cost. The anticipated increased demand for CRFs to a growing rate of over 5% per annum was and is a motive behind our decision to research on the urea based nanocomposites excipients for the production of urea CRFs formulations. To be more precise, the details other than laboratory synthesis basing on layered aluminosilicates, synthetic polymers, natural biopolymers and the volcanic ashes are beyond the demarcations of rather the scope of the this study. This calls for more researches in the context of this topic, *i.e.*, urea based CRFs.

The background of this study can be traced from our preliminary study (Siafu & Lugwisha, 2014) done in order to investigate the properties of Pugu kaolin for the production of dental porcelains where apart from what was found as per the objectives of the study, there were several observations made on the ability of Pugu kaolinite to intercalate organic species. This created a desire for further searching on the kaolinite intercalation reactions which in turn led to the inception of the idea through which this study was developed. Our main interest at the beginning was to transform Minjingu phosphatic fertilizer (MPF) from SRFs to CRFs but that idea was not sound enough since MPF slow release rate is currently enough for economical field operations; consequently, urea was chosen to be included in this study because it is one of the most widely and regularly used nitrogenous fertilizer in East Africa despite the associated shortcomings which we have described earlier.

9.1.2 Preparation and characterization of nanocomposite excipients

In this section, a discussion pertaining to the experimental findings obtained from the study with respect to the research objectives is provided in attempt to converge the objectives of the study

with the empirical findings. Essentially, the main empirical findings are chapter specific; thus the details of methodology on how laboratory preparations were carried out can be found in the respective chapters. That said, this section will synthesize the empirical findings to answer the following objective of the study: to prepare the nanocomposite excipients using polymers and nanoclays and then characterize them. The best question to be answered could therefore be: is it possible to prepare kaolinite based nanocomposite excipients for urea CRFs? Consider the descriptions hereunder.

i) Sampling, beneficiation and preliminary characterization

Kaolinite reactions depend on the purity of the samples which is the result of beneficiation process (Bloodworth, Highley, & Mitchell, 1993). Throughout the study, the sampling technique employed was quartering technique which involved a series of steps as described below:

Sampling spot was carefully selected as seen Figure 9.1. The surface litter at the sampling spot were removed using shovel and hand hoe followed by a 'V' shaped cut to a depth of 15 cm in the sampling spot. By using Auger the kaolinite sample was drawn from a depth of about 15 cm below the ground. The sample was then scooped on the plastic container, washed and sieved after drying. The fine wet sieved but dried samples were then mixed thoroughly and then spread on a clean nylon sheet in a confined chamber. Thereafter, quartering was carried out by dividing the thoroughly mixed sample into four equal parts as shown in Figure 9.2. Two opposite quarters were discarded and the remaining two were mixed and collected in a plastic bag.

As can be seen from Figure 9.1 (raw kaolinite image), it is possible to clearly see the colourings on the raw kaolinite sample indicating the presence of impurities which must be rid-off before its use. The impurities were removed during beneficiation as described earlier to say that after beneficiation there was a significant reduction of most impurities. That said, the procedures and the wet beneficiation technique used (Figure 9.3) were found to be suitable for the purification of the Pugu kaolinite under study such that it was possible to raise the amount of the kaolinite clay portion and reduce the non-clay portion after beneficiation. In practice, kaolinite manipulation follows beneficiation and in most cases purification is essential for an effective intercalation reaction as described in the specific chapters; for instance natural ferrous impurities were observed to influence intercalation reaction thereby affecting the assessment of the lab synthetic

routes and so the need for beneficiation before the application of Pugu kaolinite in the preparation of release systems couldn't be underestimated.

Figure 9.1 Raw Pugu Kaolinite

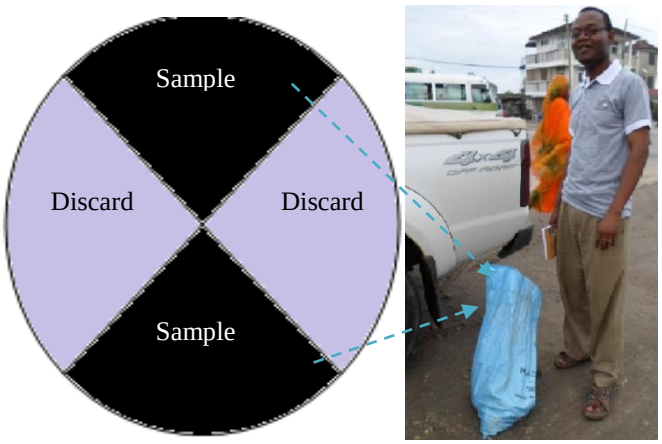

Figure 9.2. Quartering sampling procedure

The results from beneficiation trials had some theoretical implications: the raw kaolin contained kaolinite [$Al_2Si_2O_5(OH)_4$] as a major phase and two minor phases namely quartz (SiO_2) and microcline [$KAlSi_3O_8$] whereas after beneficiation there was an appearance of two new phases namely clinochlore and illite [$KAl_2(Si_3AlO_{10})(OH)_2$] while kaolinite remained to be the major phase. The current theoretical standpoint hold that: weathering of silicate type of minerals do occur during wet beneficiation process and thereafter, the weathered particles reacts with water leading to chemical transformations (Thair Al-Ani & Sarapää, 2008). In view of that the observation made for the appearance of illite following kaolinite wet beneficiation trials was attributed to the reactions of Al and K from the microcline and water thereby contributing to the transformations observed. In that way, the theoretical base for kaolinite wet-beneficiation need to be revisited in order to further an understanding of the likelihood of kaolinite modification as a result of wet beneficiation process. Primarily, characterization of the raw sample followed this order: sampling, mechanical treatment, purification, activation, and beneficiation.

Figure 9.3. Wet beneficiation process

As has been generally accepted, in order to obtain suitable sorbents' characteristics of layered aluminosilicates the need for modifications with acids, salts etc are inevitable (Bel'chinskaya et al., 2011; Lyudmila Novikova, Belchinskaya, Roessner, & Alsawalha, 2013; LA Novikova, Strelnikova, Khodosova, Belchinskaya, & Roessner). In this study, NaCl was used to activate kaolinite under salt conditions and KHP was used for acidic conditions; the results portrayed the effect of NaCl on the order of arrangement of kaolinite layer to vermicular morphology as compared to raw kaolinite. Besides, the effect of salt treatment on the calcined kaolinite was significant; there were noticeable transformations on the kaolinite morphology. This signifies that the reactivity of calcined salt treated kaolinite was high as compared to the raw one. As observed before, the morphology of the kaolinite following salt treatment and then calcination had its structure of urea intercalated nanocomposites completely transformed. Our observation on the improved reactivity of kaolinite upon salt treatment agrees with (Heller-Kallai, 1978; Heller-Kallai & Frenkel, 1979) who found an increased reactivity of clay following dehydroxylation and salt water interaction.

Despite the fact that mineral acids are known to be good in modifying kaolinite structure and also catalyze its reactivity (Lyudmila Novikova, et al., 2013; LA Novikova, et al.), this study has shown that kaolinite reactivity following activation with organic acids like KHP leads to minor reactivity (reactive kaolinite in attenuated form). This was confirmed by the decreasing intercalation of urea into the kaolinite in the KHP activated kaolinite as compared to the salt activated kaolinite. Accordingly, a simple generalization from this observation could be: the reactivity of kaolinite mineral towards urea intercalation depends on/is catalyzed by salt activation along with partial dehydroxylation of layers following mild calcination.

Plate 4. Kazimzumbwi forest where sampling was done

ii) Synthesis and characterization of kaolinite based nanocomposite excipients

Empirically, the results have revealed that it is possible to prepare nanocomposite excipients for use in the designing of urea CRFs formulations by means of Pugu kaolinite mineral found in the Kazimzumbwi forest at Kisarawe Tanzania Plate 4 and 5. The forest containing the Pugu kaolin hills is found at around 43.9 km from the Dar es Salaam city centre; it is historically known for kaolinite mining since the period of German colonialism in Tanganyika as seen in plate 6 where the ruins of old German kaolinite miners are found. In practice mobilization of suspended colloidal particles from a mist of kaolinite solution follows flocculation theory (Dobias, 1993; Moss & Dymond, 1978). The precipitation of colloidal particles was achieved by applying HCl after 7 days of allowing heavy particles to settle leaving behind the suspended particles needed

for intercalation reactions. The presence of excess chloride after flocculation was at first seem to limit the monitoring of subsequent intercalation reactions, however excess washing and testing with $AgNO_3$ was enough to overcome that limitation.

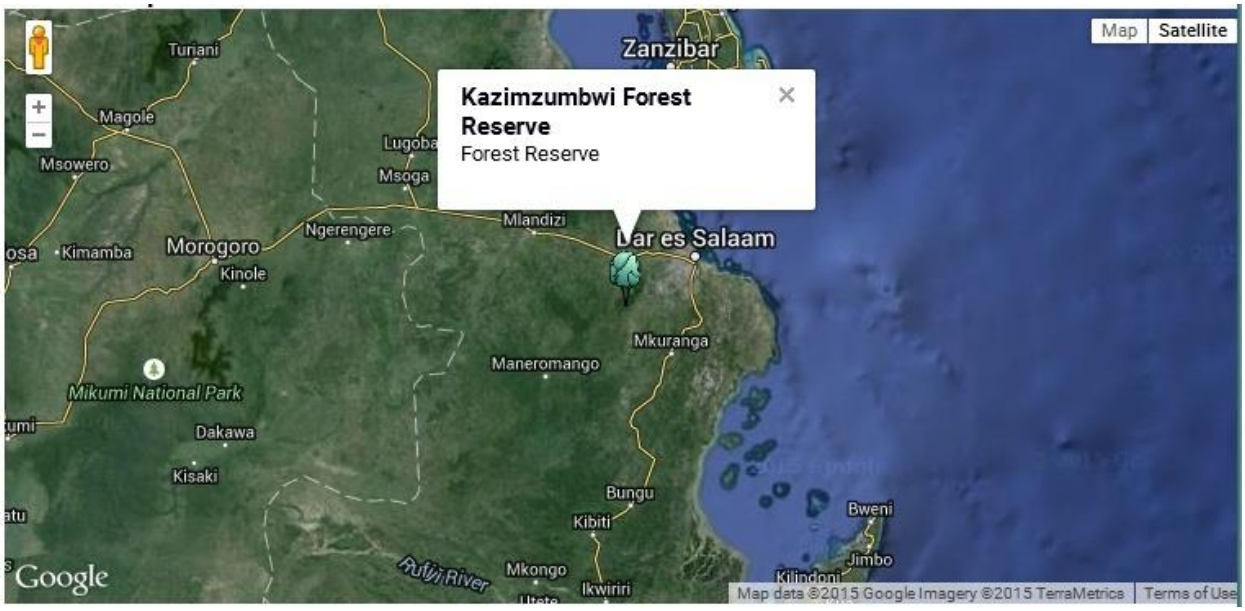

Plate 5. Satellite map around Kazimzumbwi forest reserve where Pugu hills are found

Source: (Google-maps, 2015)

Principally, intercalation reactions were conducted in order to prepare the kaolinite based excipients; as demonstrated in empirical findings chapters that the cation exchangeable region in the kaolinite interlayer spaces can accept the introduced species by way of isomorphous substitution reaction and that process results in the expansion of the interlayer distance between the kaolinite layers (Figure 9.5); this was illustrated in (Sempeho, et al., 2014).

Tentatively, kaolinite is reluctant to most reaction; it was stated elsewhere to say: "Kaolinite is a 1:1 layered silicate with a chemical formula $Al_2Si_2O_5(OH)_4$ consisting of one gibbsite-like dioctahedral sheet and one tetrahedral sheet layer. The ultimate structure is an asymmetric configuration with very little substitution in the structural lattice; thus it has a minimal layer charge and a low exchange capacity (3–15 meq per 100 g). This asymmetric structure allows the formation of hydrogen bonds between consecutive layers, providing a large cohesive energy. In turn, this makes intercalation of polymers more difficult, which is probably the main reason for

the fewer occurrences of kaolin in the preparation of nanocomposite polymer materials, despite it being inexpensive, abundant, readily available, and environmental friendly" (Unalan, Cerri, Marcuzzo, Cozzolino, & Farris, 2014). That is to say, kaolinite being a 1:1 layered phyllosilicate is larger in size than the other types of layered minerals (Figure 9.4) and so it has a fixed structure with no internal surfaces and little isomorphous substitution. As a result kaolinites have relatively low surface area and low capacity to attract ions. In fact, they do not swell when wetted or shrink when dried (Soils, 2015).

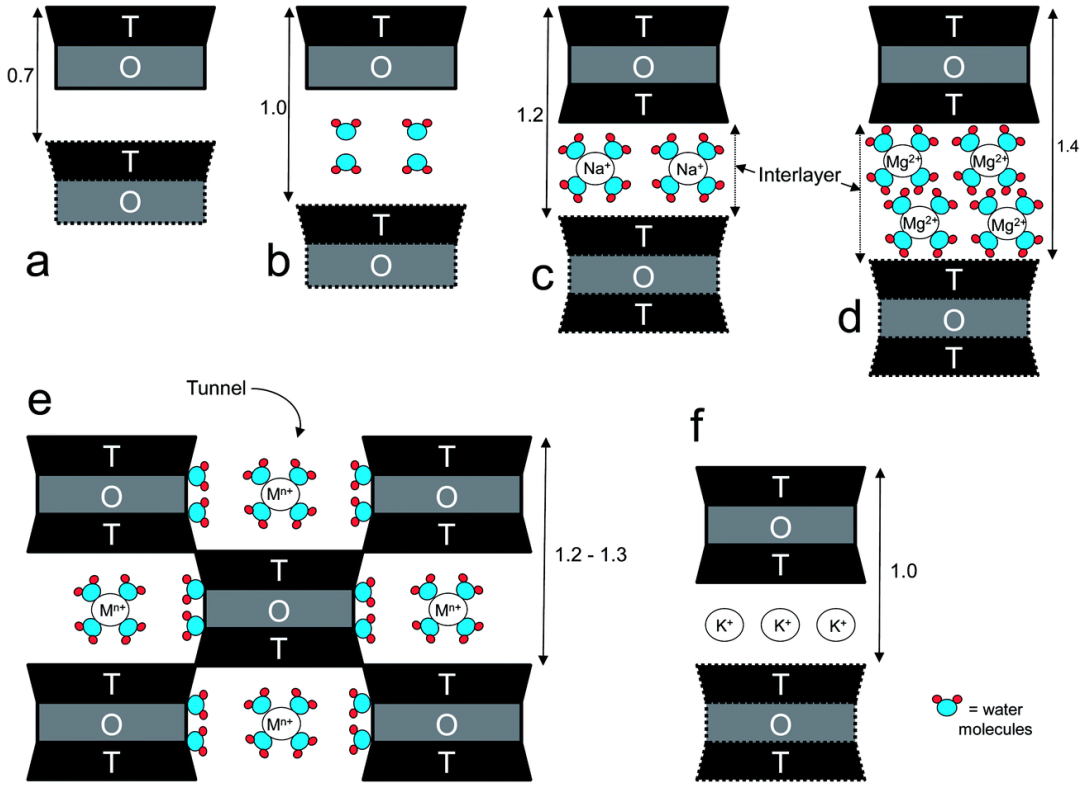

Figure 9.4. Schematic representation of some phyllosilicates viewed perpendicularly to the tetrahedral (T) and octahedral (O) sheets: (a) kaolinite; (b) halloysite; (c) Na^{+}-montmorillonite (a smectite) partially hydrated; (d) Mg-vermiculite fully hydrated; (e) palygorskite–sepiolite structure; (f) muscovite (a flexible mica). Spacing in nm. M^{n+} stands for a generic cation

Source: (Unalan, et al., 2014). Used under CC licensing

In essence, despite this theoretical standpoint stated above, this study has demonstrated that kaolinite interlayer spaces can be expanded and be used for urea intercalation-release reactions by employing intermediate intercalation compounds as pointed out in the empirical findings in

depth. The synthetic routes have already been discussed in the respective empirical chapters, but a comparative evaluation is provided in this segment basing on the following subsections:

- Preparation of kaolinite based nanocomposite excipients using natural iron-rich clay
- Preparation of kaolinite based nanocomposite excipients using laboratory synthesized Fe^{3+} oligomers
- Preparation of kaolinite based nanocomposite excipients using laboratory synthesized hydroxyaluminate oligomers
- Preparation of kaolinite based nanocomposite excipients using DMSO
- Preparation of kaolinite based nanocomposite excipients using methanol
- Preparation of kaolinite based nanocomposite excipients using coupled DMSO-hydroxylaluminate intercalants

In all the cases, the empirical findings have revealed that it is possible to prepare kaolinite based nanocomposite excipients for use in the intercalation and release of urea fertilizer. However, we had observed the variations in the capacity of each intercalant to expand the interlayer spaces; this section will provide detailed theoretical implications behind the observations made.

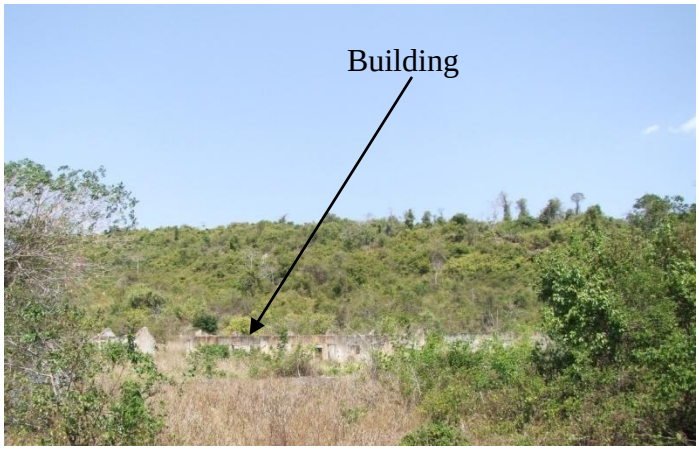

Plate 6. Building ruins of former (German) mining activity at Pugu Hills, Tanzania.

Source: (P. Han, 2009). Location: 6° 52′ 58.43″ S, 39° 4′ 34.93″ E

NB: Licensed under CC BY 3.0 via Wikimedia Commons

a) Preparation of kaolinite based nanocomposite excipients using laboratory synthesized Fe $^{3+}$ oligomers and natural iron-rich clay

Attempts to study the mineralogy of both raw and the beneficiated kaolinite was a breakpoint which opened further investigation on the ability of natural iron-rich clay to expand the kaolinite layers. To the best of our knowledge, this observation has never been made before. We had observed the existence of natural tendency of expansion of kaolinite interlayer distances in the areas where kaolinite samples were heavily contaminated with ferrous impurities as seen in plate

Plate 7. Kaolinite contaminated with ferrous impurities

In search for scientific fact behind this phenomenon, a series of experiments were carried out as described in the specific chapters and the observation made was that: it was possible to attain an intercalation ratio of about 15.3% to 76.8% (depending on the procedure as described in main empirical chapters) just by reacting kaolinite samples with the contaminated samples rich in Fe^{3+} impurities (Plate 7).

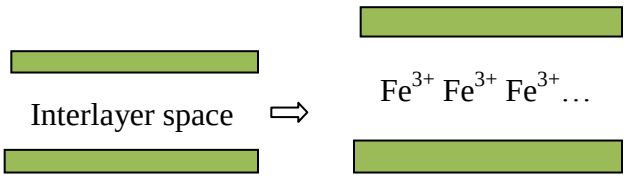

Illustration 9.1. Fe^{3+} replacement in the kaolinite interlayer spaces after treatment with contaminated ferrous impurities

That is to say, the Fe^{3+} contained in the iron-rich clay replaced the exchangeable water and filled the exchangeable position as pointed in the illustration 9.1; this affected the interlayer distances between the functional kaolinite layers. Basically, oligomerization was thought to be the next step in order to investigate the extent of kaolinite' expansion of interlayer distance as a result of insertion of macromolecular ironic complexes through a finite degree of polymerization. As described in the specific chapter ferrihydrite oligomeric cations were prepared and used to expand the interlayer spaces to make it suitable carrier for urea intercalation. As a matter of fact, studies regarding the oligomerization on iron oxide surfaces indicated an interesting interplay between electrostatic and chemical forces of silicic acid (H_4SiO_4) and the surfaces iron oxides (Dol Hamid, Swedlund, Song, & Miskelly, 2011; Hayes, Papelis, & Leckie, 1988). Certain research results such as the ones obtained by (Dol Hamid, et al., 2011) revealed the formation of monomeric silicate complexes with Fe-O-Si linkages and that as the concentration of Si increased Si-O-Si linkages became prevalent. Consider Figure 9.5 showing the schematic description and a quote from (Dol Hamid, et al., 2011):

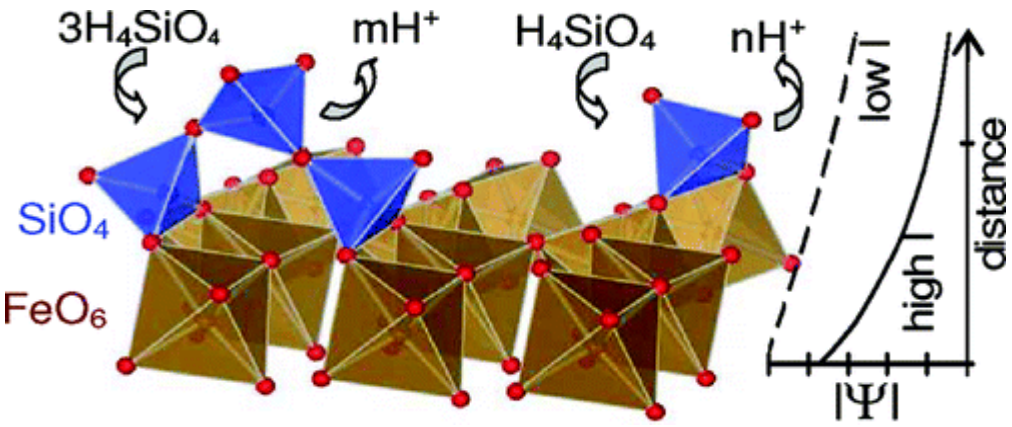

Figure 9.5. H_4SiO_4 Sorption and Oligomerization on an Iron Oxide Surface

Quote: *"The effect of ionic strength on reactions at aqueous interfaces can provide insights into the nature of the chemistry involved. The adsorption of H_4SiO_4 on iron oxides at low surface silicate concentration (Γ_{Si}) forms monomeric silicate complexes with Fe–O–Si linkages, but as Γ_{Si} increases silicate oligomers with Si–O–Si linkages become increasingly prevalent. In this paper, the effect of ionic strength (I) on both Γ_{Si} and the extent of silicate oligomerization on the ferrihydrite surface is determined at pH 4, 7, and 10, where the surface is, respectively, positive, nearly neutral, and negatively charged. At pH 4, an increase in ionic strength causes Γ_{Si} to*

decrease at a given H_4SiO_4 solution concentration, while the proportion of oligomers on the surface at a given Γ_{Si} increases. At pH 10, the opposite is observed; Γ_{Si} increases as I increases, while the proportion of surface oligomers at a given Γ_{Si} decreases. Ionic strength has only a small effect on the surface chemistry of H_4SiO_4 at pH 7, but at low Γ_{Si} this effect is in the direction observed at pH 4 while at high Γ_{Si} the effect is in the direction observed at pH 10. The pH where the surface has zero charge decreases from ≈8 to 6 as Γ_{Si} increases so that the surface potential (Ψ) is positive at pH 4 for all Γ_{Si} and at pH 7 with low Γ_{Si}. Likewise, $\Psi < 0$ at pH 10 for all Γ_{Si} and at pH 7 with high Γ_{Si}. The diffuse layer model is used to unravel the complex and subtle interactions between surface potential (Ψ) and chemical parameters that influence interfacial silicate chemistry. This analysis reveals that the decrease in the absolute value of Ψ as I increases causes Γ_{Si} to decrease or increase where Ψ is, respectively, positive or negative. Therefore, at a given Γ_{Si}, the solution H_4SiO_4 concentration changes with I, and because oligomerization has a higher H_4SiO_4 stoichiometry coefficient than monomer adsorption, this results in the observed dependence of the extent of silicate oligomerization on I". [© 2015 Copyright Clearance Center, Inc.]

NB: Reused under "*American Chemical Society Copyright Clearance Center's Rightslink service for reusing for thesis/dissertation*".

In that view point, we propose the fact that, oligomerization of ferrihydrite (as explained in the empirical findings) followed the formation of the monomeric [Fe-O-Si] linkages which in turn was oligomerized *in-situ* within the interlayer spaces leading to an observed expansion of 3.61 Å to 3.62 Å from the kaolinite intercalated with natural iron rich clays and oligomeric Fe^{3+} respectively. Concisely, the principle implications to our observations are:

- Kaolinite nanocomposite excipients for use in the intercalation of urea fertilizer can be prepared via intermediate intercalation step utilizing oligomeric ferrihydrite complexes.
- There is always a naturally occurring intercalation process resulting from a naturally induced oligomerization of ferrous species present as impurities in the kaolin group of minerals. Nevertheless, statistical significance of this phenomenon has not yet been established considering the fact that there are variations in the kaolinite mineralogy and chemical compositions as per diversity in the seasonal and geographical factors.

b) Preparation of kaolinite based nanocomposite excipients using laboratory synthesized hydroxyaluminate oligomers

On the other hand, oligomerization of Al^{3+} cations was also carried out as explained in the empirical findings. Preparation of these kaolinite excipients for the intercalation of urea was carried out as described before; nevertheless, despite the known synthetic route for oligomerization of hydroxylaluminum aqueous cations, the synthetic route given in this study is unique in itself due to an enhanced emphasis on the aging and maturation during the growth of the oligomers. The following questions were reflected in this section:

- What are the differences between un-aged and aged-matured oligomers in their capacity to intercalate kaolinite interlayer region?
- Does temperature influence intercalation of hydroxylaluminum oligomers?
- What pattern can be observed when comparing hydroxylaluminum cationic vis-à-vis ferrihydrite cationic oligomers in the intercalation capacity?

The findings basing on the laboratory experiments have revealed almost negligible intercalation when un-aged hydroxylaluminum solution was used as an intercalation agent. On the other hand, for the aged and matured hydroxylaluminum oligomers, the rate of intercalation of the hydroxyaluminum species into the kaolinite interlayer spaces was seen to rise with aging time (Figure 9.6)

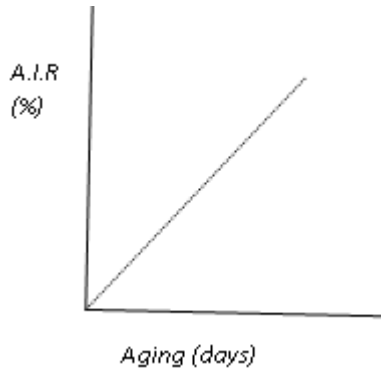

Figure 9.6. Relationship between the apparent intercalation ratio (A.I.R) and aging time

In addition to that, temperature was found to influence intercalation process for the reason that: the reactivity of kaolinite is known to increases following the dehydroxylation of salt treated kaolinite along with concurrent encounter with water which catalyses the intercalation, an observation which was noted elsewhere (Heller-Kallai, 1978; Heller-Kallai & Frenkel, 1979) basing on the equation below:

$$2SiO_2 \cdot Al_2O_3 \cdot 2H_2O + 2nMx \rightarrow 2SiO_2 \cdot Al_2O_3 \cdot nM_2O + 2nHx + (2\text{-}n)H_2O$$

Hitherto, what can be said about the findings obtained is that: oligomerization of Al^{3+} and Fe^{3+} cations has led to the following generalizations:-

- ► Ferrihydrite oligomers have a more capacity to intercalate into the kaolinite interlayer spaces as compared to the hydroxylaluminum cationic oligomers.
- ► Fe^{3+} impurities in the kaolin do have a natural tendency to intercalate kaolinite interlayer spaces due to natural simultaneous oligomerization process taking place
- ► Hydroxylaluminum intercalant has a big capacity to attain smaller particles of kaolinite nanocomposite excipients than the ferrihydrite oligomers. Thus, when intercalation capacity is needed then, ferrihydrite oligomerization intercalations reactions could be more relevant; when size of the particles matters the most, then, hydroxylaluminum oligomerization intercalations reactions should be counted. These conclusions are limited to the reaction conditions stipulated in the empirical results which are chapter specific.
- ► Intercalation ratio is proportionally dependent on the size of the oligomer used for intercalation. This fact can be comprehended by considering Figure 9.7 which depicts an analysis between the cationic oligomers intercalated into the kaolinite interlayer spaces. However, the trend was not regular when results for intercalation compound prepared from the kaolinite and natural Fe^{3+} contaminated clays were plotted as seen in Figure 9.8; an irregular trend of impure intercalant was recorded. Thus, our observation on the fact that *intercalation ratio is proportionally dependent on the size of the oligomer used for intercalation* is limited to the kaolinite minerals intercalated with laboratory synthesized oligomers (that is, the pure oligomeric cations).

Our generalization on the proportionality between intercalation ratio and the size of cationic oligomer was also found to hold true in the anionic intercalants used namely DMSO and methanol. This has been given in details in the coming section.

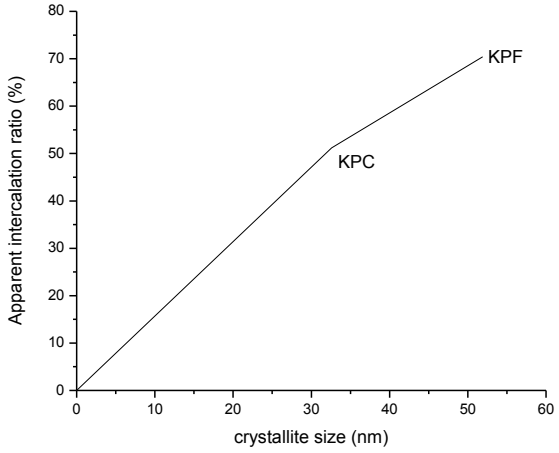

Figure 9.7. Relationship between apparent intercalation ratio and crystallite sizes in the oligomeric intercalated kaolinite compounds

c) Preparation of kaolinite based nanocomposite excipients using DMSO, methanol and coupled DMSO- hydroxylaluminate intercalants

DMSO (78.13 g/mol) is known to exist in resonant structure and it has the ability to associate with hydrogen bonds to form a more stable and compact structure due to its ability to "lock in" the hexameric water clusters (Szmant, 1975) thereby inducing a more intensive structuring of water which in our case, an intensive structuring of water in the exchangeable region of the kaolinite interlayer spaces means a more expansion and thus a greater ability of kaolinite to accept DMSO to intercalate. Besides, it has been found elsewhere that those hydrogen bonds between DMSO and the water molecules are longer lived than water-water hydrogen bonds (A Luzar & D Chandler, 1993; Alenka Luzar & David Chandler, 1993). Comparatively, methanol (MF 32.04 g.mol) which was also used to intercalate kaolinite can associate via hydrogen bonding but the ability to form compact and stable long lived hydrogen bonds between itself and water is not known but it is expected to be low as compared to that of DMSO.

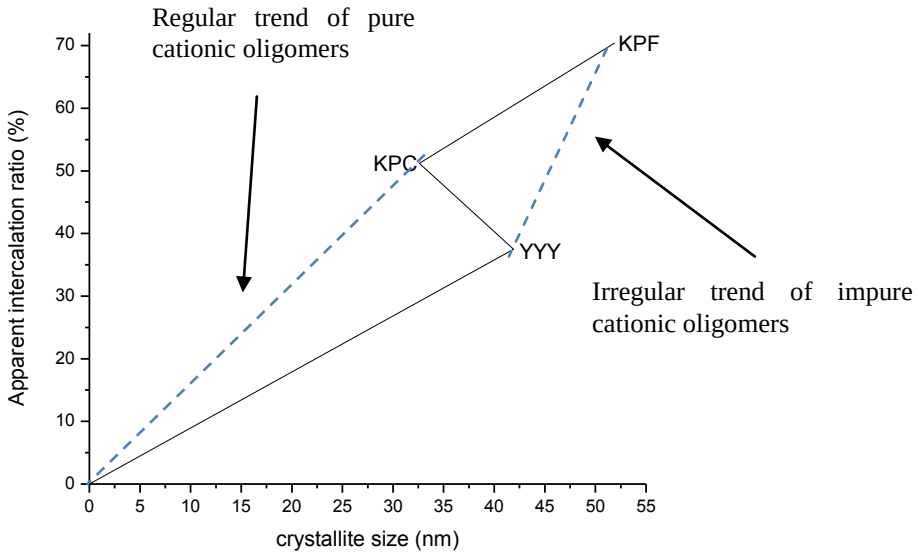

Figure 9.8. The effect of natural Fe^{3+}-clay oligomer on the relationship between apparent intercalation ratio and crystallite sizes in the oligomeric intercalated kaolinite compounds

The reason behind the ability of DMSO molecules to create strong structural effect than methanol lies on the fact that DMSO being a strong hydrogen acceptor than methanol (owing to the presence of resonance) has the capacity to bond with water more strongly (A Luzar & D Chandler, 1993; Alenka Luzar & David Chandler, 1993); consequently the solvated DMSO molecules during the interaction with exchangeable water is likely to bond to two waters in order to form an average angle between the two hydrogen bonds in the DMSO:$2H_2O$ aggregate nearly tetrahedral thereby exhibiting far more ability to expand the interlayer spaces. This phenomenon is known to strengthen the attractive potential of mean force between pairs of water in the presence of DMSO(A Luzar & D Chandler, 1993; Alenka Luzar & David Chandler, 1993).

In view of that, a comparative analysis of the pattern observed for the intercalation ratios and the size of DMSO intercalated kaolinite as well as the methanol intercalated kaolinite revealed that: DMSO did intercalate more into the kaolinite interlayer spaces than methanol did thereby giving similar trends observed in Figure 9.9 (which closely agree with Figure 9.7) thereby giving rise to the following fact to say: intercalation ratio and the size of the intercalant are directly proportional regardless of whether the intercalant is anionic or cationic oligomer.

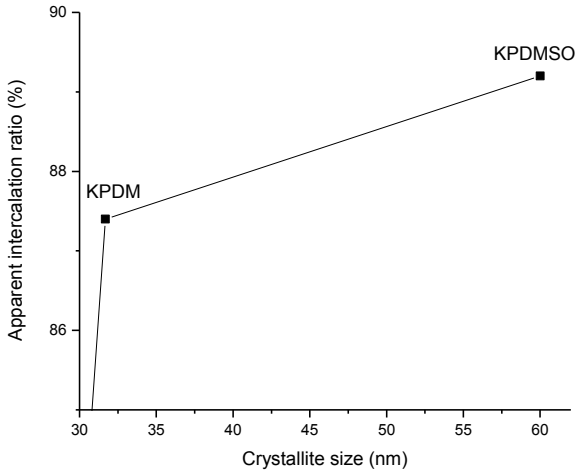

Figure 9.9. Relationship between apparent intercalation ratio and crystallite sizes in the methanol and DMSO intercalated kaolinite compounds

However, a close view of Figure 9.10 would indicate the limitation to this observation which we've just made before to say: the trend for the interdependence between intercalation ratio and the size of a named intercalant only hold true if the intercalating species (intercalant) are of the same chemical nature *i.e.* either all are cationic oligomers or all are anionic species. In that case, the following statement can be drawn to say: intercalation ratio is directly proportional to the size of the intercalant provided that the intercalants under consideration are of the same chemical nature. This concept we have named it as the *order of kaolinite intercalation interaction*. Figure 9.10 shows the limitations to this concept which occur when intercalants of different chemical nature are tested. But, Figure 9.10 has revealed the possibility of the occurrence of a conceptual point that deviates from the *order of kaolinite intercalation interaction.* This conceptual point has been termed as the *stable intercalation state* (SIS point) and it will be described more in the coming sections.

Therefore, if we recall our basic question from the research objectives which was stated as follows: is it possible to prepare the kaolinite based nanocomposite excipients for use in preparing the urea controlled release fertilizers? Certainly as the answer may be, it was demonstrated that kaolinite nanocomposite excipients or rather carriers of urea have been successfully prepared by varying intercalating species namely, hydroxyaluminum oligomers and ferrihydrite cationic oligomers as well as DMSO and methanol anionic intercalants where the

empirical findings indicated that the anionic intercalating species intercalated more than cationic oligomers and also, the order observed for the stability along with intercalation strength in the kaolinite interlayer spaces was hydroxyaluminum oligomers < ferrihydrite oligomers < methanol < DMSO. Similarly it was observed that the size of the intercalant counts on the capacity to intercalate within the kaolinite interlayer spaces.

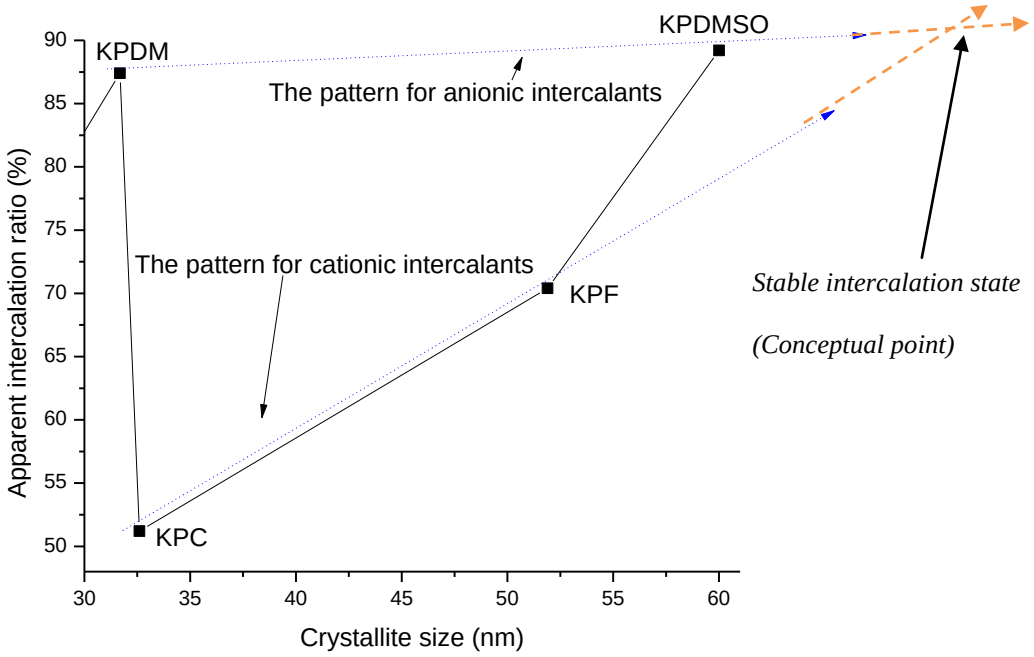

Figure 9.10. Deviation to the order of kaolinite intercalation interaction and conceptual stable intercalation state

9.1.3 Intercalation of urea into the nanocomposite excipients and characterization of the CRFs formulation

In this section our discussion is dual faceted: (i) a description of a trial experiment done to intercalate urea directly into the kaolinite is given and (ii) a convergence between empirical findings basing on the urea intercalated kaolinite in each nanocomposite excipients with respect to the objectives of the study is given along with comparative study between urea intercalated kaolinite prepared via direct intercalation and via nanocomposite excipients is given.

i) Urea-kaolinite direct intercalation

A simple pilot experiment was carried out to investigate whether urea can intercalate directly into the kaolinite interlayer spaces without the intermediate step which involved the use of the prepared nanocomposite excipients. In a nut shell, the procedure for this experiment was as follows: 20 g were taken from a 5% beneficiated kaolinite colloidal solution (KU_0) and agitated for 30 minutes with urea fertilizer in a ratio of 4:3 following mechanical blending. The sample was washed and made into powder for analysis using vacuum oven set to 60 °C; the sample was labeled KU_1. The procedure was repeated for 12 hours and 72 hours and the samples obtained were named KU_2 and KU_3 respectively. Characterization was preliminarily done with XRD and SEM alone. The results for the X-ray indexing were summarized in Table 9.1.

Table 9.1. X-ray indexing for the pilot experiment

Sample	A.I.R (%)	Expansion (nm)	
KU_1	27.100	0.425	
KU_2	25.800	0.397	*Stable intercalation state*
KU_3	31.000	0.397	

The pattern seen in Table 9.1 revealed that, urea fertilizer can directly be intercalated into the kaolinite interlayer spaces however, the intercalation ratio was very low (between 27.1-31-0%) signifying that the rate of forward reaction towards urea direct intercalation was not favoured under the specified reaction conditions. Figure 9.11 confirmed the fact that urea was intercalated though poorly for the reason that the pattern for kaolinite decomposition (NaKP) has a very minor change after urea intercalation (KU) and also the pattern of urea decomposition and that of urea in the intercalated state are on the same temperature regimes while differing in intensity only. That may suppose that when urea was directly intercalated, the favoured reaction was merely adsorption and not intercalation. That said, these result showed that urea direct intercalation was not a favoured reaction and the yield was poor.

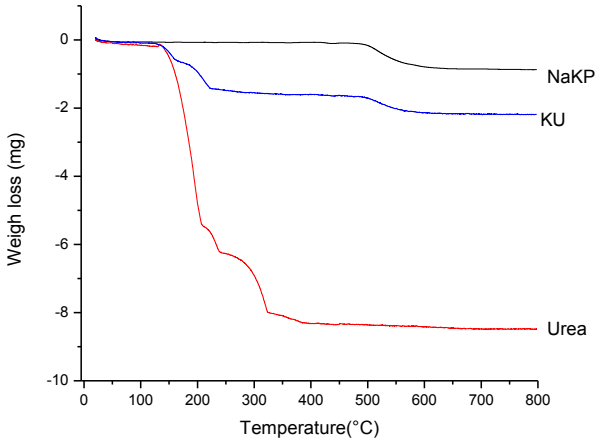

Figure 9.11 Thermogravimetry for the pilot experiment

To further confirm that fact, SEM images of the urea-kaolinite direct intercalation material (KU) were analyzed and findings showed the existence of compact layers, adsorbed urea particles on the layers as well as the formation of vermiform morphology (Figure 9.12).

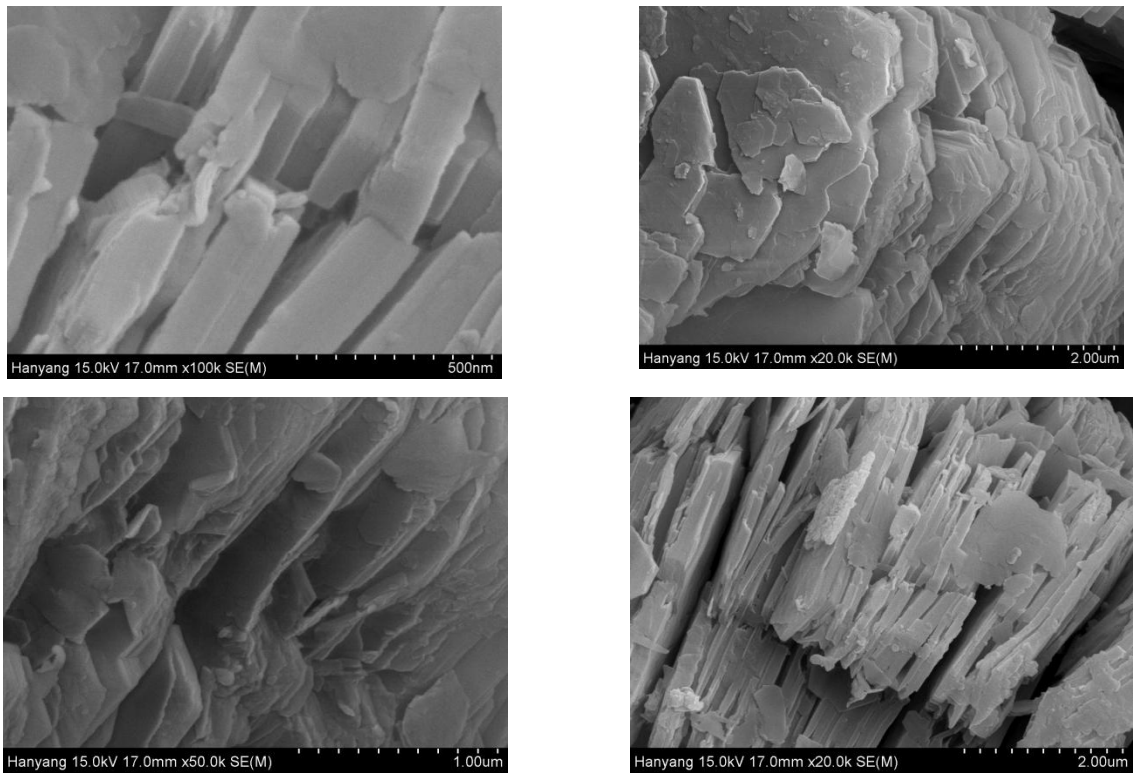

Figure 9.12. SEM images for the urea-kaolinite direct intercalation compound; pilot study

The ATR-FTIR spectrum of the sample as seen in Figure 9.13 showed that: the structures of both urea and kaolinite before and after intercalation was associated with a very small changes, however the changes seen in the IR peaks are significant enough to confirm that there was an intercalation to formulate urea intercalated kaolinite but the reaction was poor and less favoured.

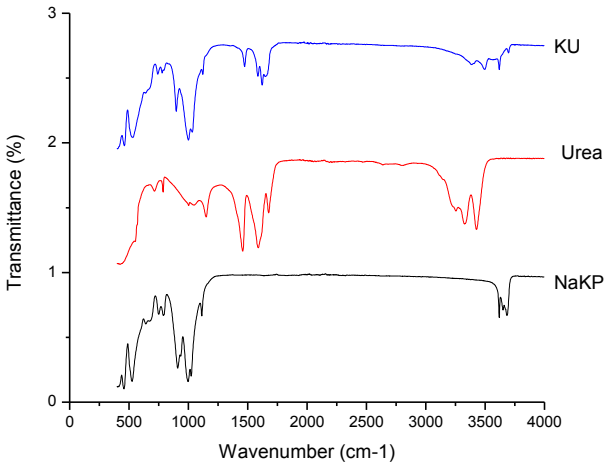

Figure 9.13. The FTIR/ATR spectra for urea-kaolinite direct intercalation compound; pilot study

Now that we know urea can be intercalated directly into the kaolinite interlayer spaces but with poor intercalation ratio it is necessary to look at the pattern observed between the intercalation with the expansion of the kaolinite layers. As reflected in Table 9.1 that there is a point where though intercalation ratios keep on changing, the *d*-spacing remains constant or rather the expansion of layers no longer takes place. This observation yields to the following two arguments:

One. The first intercalation force (during urea direct intercalation) was marked by a sharp increase in the expansion of layers giving a big expansion diameter of about 0.425 nm. This first intercalation force was just short lived; but the condition which we have named "stable intercalation state" is the most favoured state attained during the intercalation process.

Two. Existence of the stable intercalation state: this state was marked by the stability and uniformity in the expanded diameter of *d*-spacings despite an extended maturation time, and it is represented as 0.3967 nm at 25.8% and 31.0% intercalation ratios. The findings have revealed that at the stable intercalation state intercalation ratios are not static rather they're dynamic due

to the arrangement of intercalated species within the interlayer species as will be described in the coming sections. Figure 9.14 was then established to illustrate this phenomenon. Fundamentally, it is now clear that urea-kaolinite direct intercalation reaction is not favoured; therefore, preparation of urea intercalated kaolinite to make the needed urea CRF formulations was alternatively carried out by way of substitution reaction using the nanocomposites excipients as intermediate intercalation compounds.

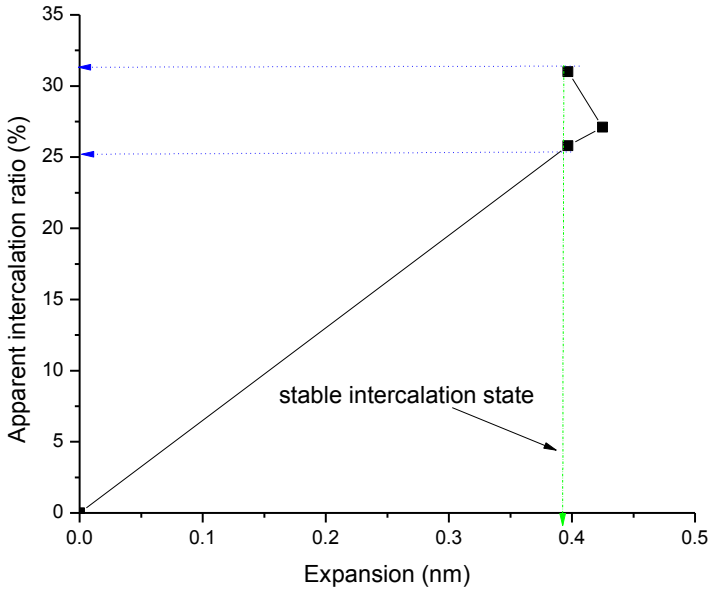

Figure 9.14. Describing the existence of the stable intercalation state

ii) Urea-kaolinite intercalation via intermediate nanocomposite excipients

In view of the fact that urea-kaolinite direct intercalation reaction was not favoured, this section provide a comparative critical analysis in order to evaluate the convergence between the empirical findings and the objectives of the study that require intercalation of urea fertilizer into the prepared nanocomposite excipients and then do the characterization. An important reminder here is that: four nanocomposite excipients were prepared as explained before and these were KPDMSO, KPDM, KPC, and KPF; their intercalation orders were described before in their respective chapters. Urea fertilizer was intercalated in each of the four nanocomposite excipients and the results have been described in the specific chapters, however, a critical analysis of the four urea CRF formulations obtained from the four nanocomposites excipients namely, KPDMU,

KPDMU, KPCU, KPFU respectively as well as the KU prepared from the urea-kaolinite direct intercalation reaction has unveiled the following facts:

a) The concept of the "order of kaolinite intercalation interaction"

The order of the average intercalation of urea intercalated kaolinite compounds was observed to follow similar trend as the order of intercalation of their respective nanocomposite excipients, *i.e.* KU < KPCU < KPFU < KPDMU. In view of that a simple hypothesis was stated to say: the order of intercalation of urea intercalated kaolinite molecules is dependent on the intercalation order of their corresponding nanocomposite excipients.

b) Existence of the stable intercalation state

As described before in the evaluation of the pilot study pertaining to the direct intercalation of urea into the interlayer spaces that: there is an existence of what we have named "stable intercalation state".

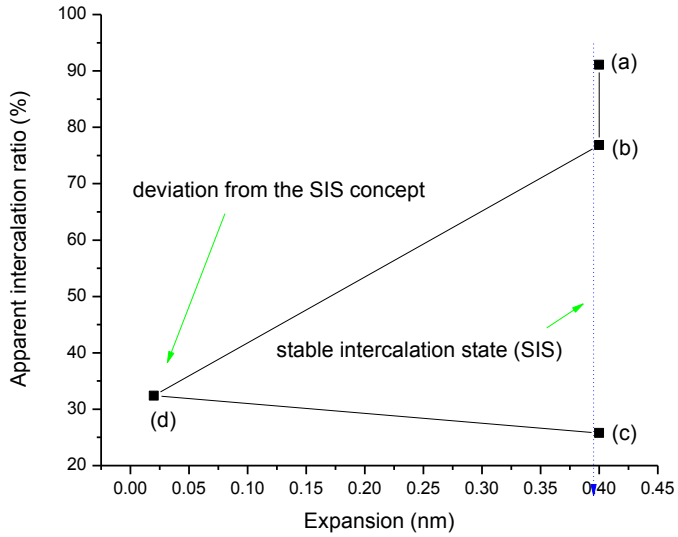

Figure 9.15. Rationalizing the stable intercalation state for the approximated expansion values for (a) KPDMU, (b) KPFU, (c) KU, and (d) KPCU

A comparative analysis on the urea CRF formulations prepared from chemically different nanocomposite excipients (Figure 9.15) has confirmed that observation. Consider Figure 9.15;

there is something in common seen and that is an existence of stable or rather uniformity in the lattice expansion of about 0.4 nm despite the variation in the (i) excipients used as precursors for urea intercalation to make urea CRFs, (ii) crystallite size and (iii) intercalation ratio. This phenomenon is what we have named "stable intercalation state" which occurred when there was a stable and uniform lattice expansion [$\Delta d_{(001)}$] of interlayer spaces in the $d_{(001)}$ direction despite the variation in the intercalation ratio. Considering illustration 9.2; an account of the urea intercalation process can be described as follows:

- When urea is directly reacted with kaolinite, adsorption reaction is the most favoured reaction rather than intercalation. This has been exhibited when we examined the outcomes of urea direct intercalation which was associated with very low intercalation ratio. This step was named as the *pseudo intercalation process*.

- When urea was intercalated by a way of replacing the intercalating species or rather through an intermediate intercalation step involving the use of excipients, intercalation is favoured over adsorption. This has been demonstrated in the role of intercalants namely, KPDMSO, KPDM, KPC, and KPF as described in the empirical findings. As seen in the illustration, this step was marked by the onset of intercalation of urea into the interlayer spaces.

- Expansion of *d*-spacing follows after the first intercalation process; however the intercalated urea is not well packed as seen in the illustration 9.2. This step is short-lived and it was marked by *unstable intercalation state i.e.* a state where both lattice expansions keeps on changing with the change in the intercalation ratio.

- Stable intercalation state follows aging time or rather maturation period. Maturation or rather aging effect observed allows particles or rather intercalated species to have a maximum interaction time within the interlayer spaces where they tend to "reorganize so that their surfaces become better defined and their sizes turn out to be more uniform (analogous to the Ostwald ripening) (IUPAC, 1997; Vetter, Iggland, Ochsenbein, Hänseler, & Mazzotti, 2013). That is to say, stable intercalation state is reached when lattice expansion is constant but the intercalation process and hence intercalation ratio keeps on changing due to reorganization of particles in attempt to attain size uniformity, well defined surface interaction as well as orientation of layers relative to the intercalating species.

Principally, the existence of the stable intercalation state distinguishes the urea-kaolinite intercalation reaction from just a mere adsorption reaction as seen in the illustration 9.2 we have just described. That is to say, in order to confirm whether urea-kaolinite intercalation has taken place and not just a mere adsorption of urea particles on the kaolinite surfaces, the stable intercalation state must be attained from the critical analysis of the X-ray diffraction patterns of the intercalation compounds.

c) Dynamic nature of the intercalated kaolinite

Evaluation of the structure of kaolinite obtained in the empirical findings has revealed the diversity of kaolinite morphology during urea intercalation. We have demonstrated the existence of varying structural features of the urea intercalated kaolinite following coupling of intercalants as well as application of calcination conditions prior to re-intercalation. Apart from the molecular diversity exhibited by kaolinite dynamic properties (as described in the empirical findings), several physical changes associated with this phenomenon were also noticed including colour change, textural changes and crystallinity of the nanocomposites synthesized.

In the DMSO experimental set up the colour, texture and crystallinity properties observed were noted and given in Figure 9.16 where, the original white colour of the salt treated kaolinite was observed to change from white crystalline (NaKP), milky colour with semi-dry sticky in texture (KPDMSO), whiter colour with semi-dry in texture (KPDM), white-brownish colour with agglomerated sticky texture (KPDMU) and finally to white-brownish in colour with jelly texture (KPDMUG). The milky colour with semi-dry sticky in texture of KPDMSO was observed to

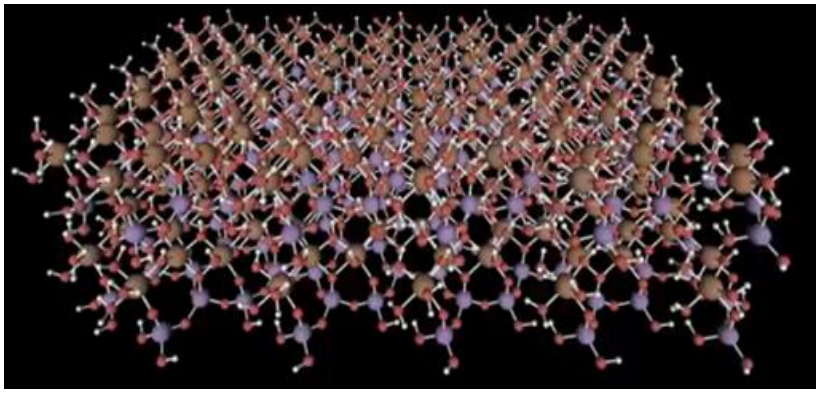

Kaolinite

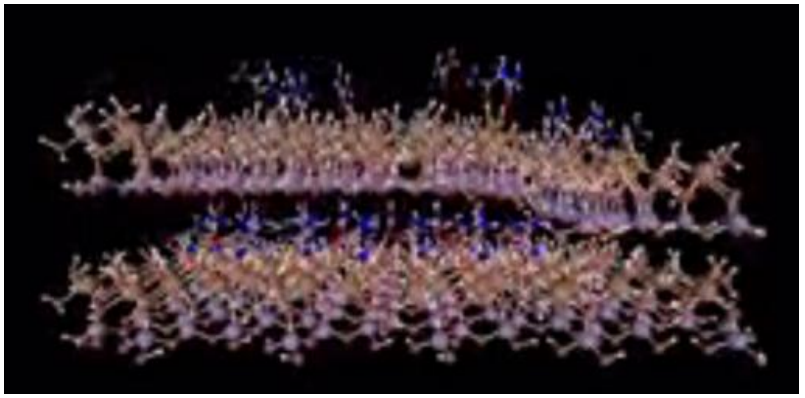

Expansion of d-spacing before aging

Urea direct intercalation

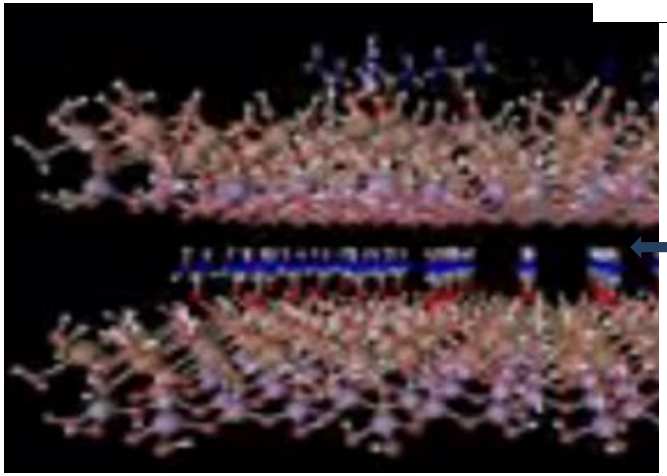

Lattice expansion after maturation: ready for release. It is a *stable intercalation state*

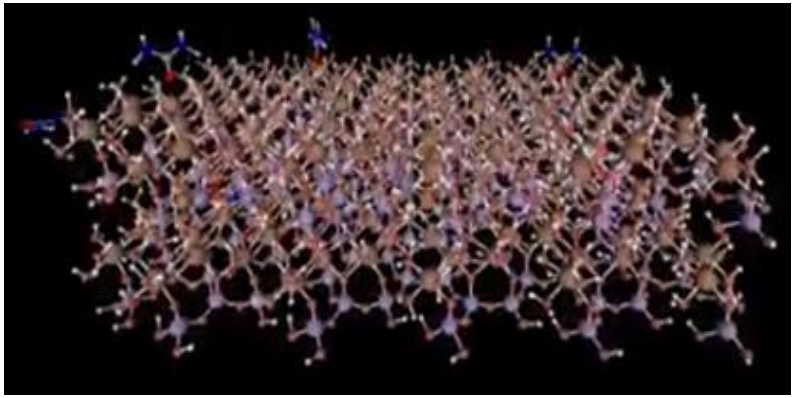

Urea pseudo intercalation

Intermediate step: via intercalant

Then urea substitution

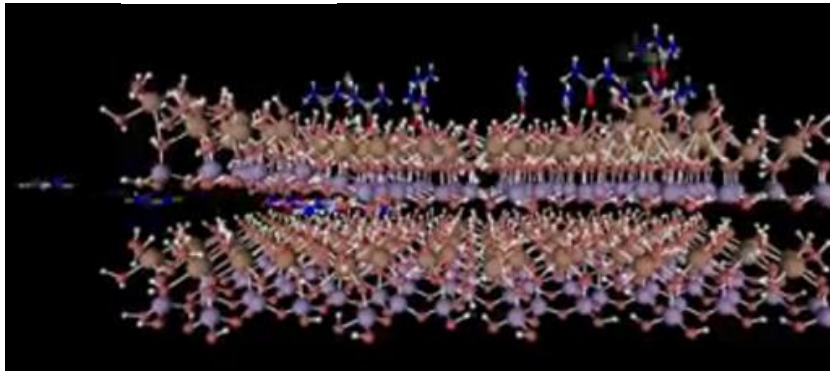

Intercalation begins

Illustration 9.2. Stable intercalation state

change to dark-greying colour when calcined to 400 °C (KPDMSO-400) and then to milky-whitish crystals upon calcination to 850 °C (FKPPDMSO).

Figure 9.16. Variation in colour of NaKP, KPDMSO, KPDM, KPDMU, KPDMUG, KPDMSO-400 and FKPPDMSO.

For the hydroxyaluminum experimental set up the colour, texture and crystallinity properties observed were noted and given in Figure 9.17 where, the original white colour of the salt treated kaolinite was observed to change from white crystalline (NaKP as seen in Figure 9.16), gold-milkish colour with semi-sticky texture (KPC), light-gold colour with semi-dry in texture (KPCU); and that the light-gold colour was observed to change to grey when calcined to 400 °C (KPC-400) and then to white colour crystals upon calcination to 850 °C (FKPC).

For the Ferrihydrite experimental set up the colour, texture and crystallinity properties observed were noted and given in Figure 9.18 where, the original white colour of the salt treated kaolinite was observed to change from white crystalline (NaKP), to wheat or pale goldenrod colour, orange, orange red, dark orange, saddle brown and dark red for the Fy, KPF, KPFU, Y, YDMSO, and Q_1 respectively.

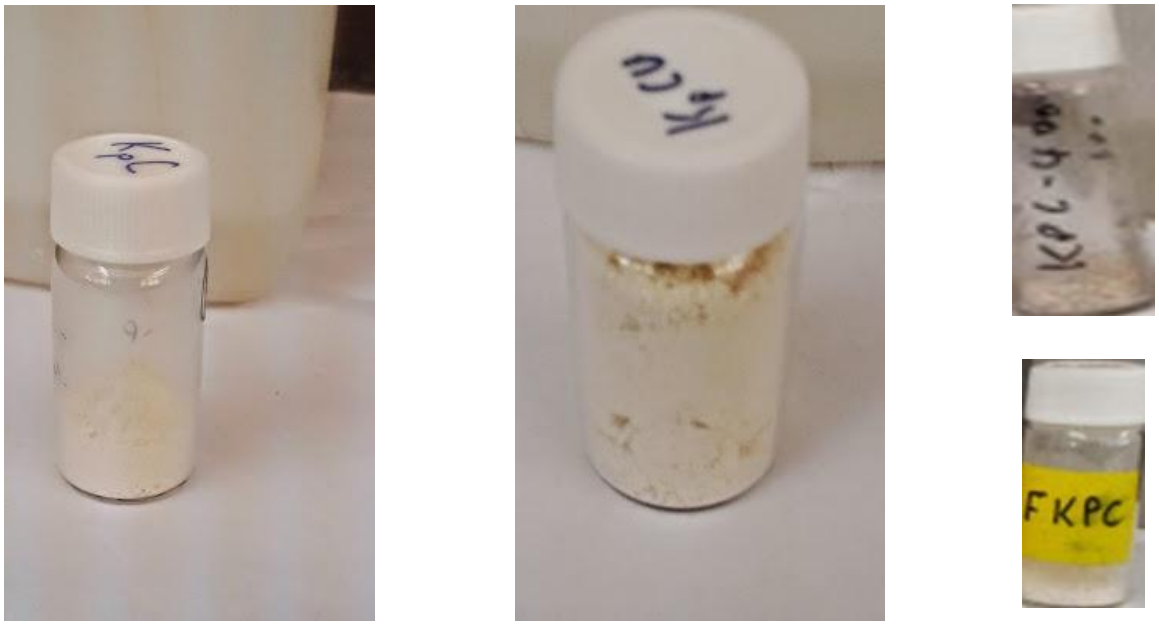

Figure 9.17. Variation in colour of KPC, KPCU, KPC-400, and FKPC

For the urea direct intercalation experimental set up (Figure 9.19) there were no significant change in colour that was observed; besides, only texture and crystallinity properties were noticed to change from dry crystalline NaKP to semi-dry with little sticky texture upon treatment with urea to form KU.

Figure 9.18. Variation in colour of NaKP, Fy, KPF, KPFU, Y, YDMSO, and Q1

Figure 9.19. Variation in colour of NaKP and KU

9.1.4 Characterization and evaluation of the release profiles

This objective was fulfilled only in part due to the nature of the experimental set-up needed for release trials. The release procedures for one CRF formulation took about 90 days to attain a stable release profile. Thus, it was only possible to perform release experiments for three systems only which were pure urea fertilizer, KPDMU and KPDMUG. As indicated in (Sempeho, Kim, Mubofu, Pogrebnoi, & Shao, 2015) that each CRS was tested for urea release in a period of 150 hours only and it was observed that 100% of the total urea was released instantly within a very short time for pure urea fertilizer whereas 100% of the total urea was released in a period of 97 hours for urea intercalated into the kaolinite interlayer spaces and only 87% of the total urea was released in a period of 150 hours from the encapsulated urea CRF prepared. The details on the release profiles for the three systems were given in the empirical results. In this section we have included an analysis basing on the one Way Anova which was performed to study whether at 0.05 level of significance, the means of urea release are significantly different or not. Consider Table 9.2 below:

Table 9.2. ANOVA of mean urea release of pure urea, KPDMU and KPDMUG

	DF	Sum of Squares	Mean Square	F Value	Prob > F
Model	1	7348.79	7348.79	6.15	0.02
Error	60	71677.42	1194.62		
Total	61	79026.21			

Determination of the existence of significant difference at α = 0.05 significance level between the mean urea release for the pure urea fertilizer, KPDMU, and KPDMUG using the one way analysis of variance (ANOVA) was carried out; the results as seen in Table 9.2 indicated that, a significant difference existed in the mean urea release of the three tested samples where P_{value} (0.02) < 0.05. Likewise, since the F_{value} (calculated) 6.15 is larger than the $F_{0.05}$ (critical) value of 0.02, then the null hypothesis H_0 was rejected and the alternative hypothesis H_α was accepted. As far as this objective is concerned, the characterization and evaluation of the release profiles was only performed on the three systems stated above. The limitation of time and resources restricted the fulfillment of this objective to the anticipated level; however, what was done was enough to conclude on the suitability of the CRFs formulations designed.

9.1.5 Characterization of urea-volcanic ash composites and chitosan-acrylamide co-encapsulated urea CRFs

The ability of urea fertilizer to crosslink and produce the reinforced nanocomposites of urea volcanic ashes named as the Nanoropes along with its ability to produce the Nanodunes and Nanoballs upon chitosan-acrylamide co-encapsulation was investigated and described in details within respective empirical chapters. The Nanoropes were observed to reinforce the ash particles and produced a high strength nanocomposites; SHMP was seen to cause a disintegration of the reinforced particles into what was called "Nano anvil-hammer" structures. The likelihood that Biocementation process could take place between urea and ash particles was demonstrated. Nevertheless, the question on whether the findings do tally with the first objectives of the research is the main theme of this section. Our reflection on the first objective of this study revealed that both reinforced urea-volcanic ash nanocomposites as well as the chitosan-acrylamide con-encapsulated urea nanocomposites prepared as described in chapters 7 and 8 can be used as excipients for urea CRF formulation thereby accomplishing the first objectives of the research. This could be rationalized as follows:

- Elemental N-composition: It was found that weight and atomic percent for the nitrogen contained in the nanocomposite excipients were 37.44 and 40.13% for AU_0 and 9.94 and 10.35% for the AU_4 of the reinforced urea-ash nanocomposite excipients. However the N-content in the nanocomposite based on the chitosan-acrylamide co-encapsulated urea was

almost insignificant as described in the empirical findings. The rationale behind the amount of nitrogen contained in the prepared nanocomposite excipients could be that both reinforced nanocomposites of urea volcanic ashes as well as chitosan-acrylamide con-encapsulated urea nanocomposites can be used as carriers or rather excipients for the purpose of preparing urea CRF formulations and therefore fulfilling the first objective of this study to say: the preparation of nanocomposite excipients using polymers and volcanic ashes is a feasible process.

- The patterns and varying surface features as well as variation in the chemical properties observed in both reinforced nanocomposites of urea volcanic ashes as well as chitosan-acrylamide con-encapsulated urea nanocomposites revealed that characterization of nanocomposite excipients using polymers and volcanic ashes is realistic and it was the third objective of this study. Hitherward, the question of relevance as per the relationship between the findings and the research objectives has been made clear.

Furthermore, both pathways namely, the Biocementation route (via reinforced nanocomposites of urea volcanic ashes) and the Co-encapsulation route (via chitosan-acrylamide con-encapsulated urea nanocomposites) indicated that they can be employed in the engineering design of urea CRFs nanocomposite excipients. Nonetheless, Biocementation pathway was seen to be more effective than the Co-encapsulation pathway for the reason than the nature of interactions between participating species was physisorption in the Biocementation and chemisorptions in the Co-encapsulation since the chitosan biopolymer was noticed to chemically modify the urea fertilizer. In that case, for the Co-encapsulation route, the amount of N-contained was very inconsequential thereby impairing the likelihood of N-release and its availability to plants tissues. The high amount of N-contained following Biocementation particularly in the urea reinforced volcanic ashes without polymeric paraffin and deflocculating SHMP showed that release profiles can be established with this pathway. Beside, this pathway was associated with the formation of highly reinforced nanocomposite excipients which signified an improved strength and so superior properties of the resulting nanocomposite excipients and their subsequent CRF formulations.

Comparatively, the pattern of particle sizes observed of 0.27, 0.89, 0.64 for the AU_0, AU_4 and $CPAM^{-1}$ respectively portrayed that the easy of translocation of CRF particles within the plant tissues could follow the following order: $AU_0 > CPAM^{-1} > AU_4$. The raison d'être behind this pattern could be that: the pathway towards AU_0 CRF design is more favourable in the formation of fine sized CRFs formulation. But, all the synthetic pathways revealed a very dynamic nature in the morphology of the prepared urea CRFs formulations.

9.1.6 Policy implications of the study

a. The 2012 Draft National Agriculture Policy in Tanzania

According to the 2012 Draft National Agriculture Policy in Tanzania (Chiza & MAFC, 2012) the following policy statements were analysed:

- Low productivity of factors of production

Statement: *One of the critical weaknesses in agriculture is low productivity of land, labour and capital. This is caused mainly by inadequate finance to obtain productivity enhancing inputs, low returns to labour due to inadequate knowledge and skills; low use of labour saving technologies and low use of improved farm inputs such as quality seeds, fertilizers, chemicals and pesticides (Pg 1).*

- Agricultural Inputs

Statement: *Tanzania acknowledges that increased use of modern inputs (fertilizers, agrochemicals, seeds, farm implements etc) is a pre-requisite for achieving sufficient agricultural productivity and growth to meet economic development, poverty reduction and food security goals (pg 17).*

- Objective: *Utilization of productivity enhancing inputs increased in a cost-effective, financially sustainable and environmentally sound manner*.

- Policy Statements from the Objective above

i) *The Government shall enforce laws and regulations to safeguard farmers from the supply of substandard inputs;*

ii) *Input production, procurement and distribution shall be promoted;*

iii) *Private sector participation in multiplication of pre-basic and basic seeds shall be promoted;*

iv) *The domestic production multiplication and distribution of agricultural inputs shall be promoted to involve both public and private sector;*

v) *Farmers shall be supported to access modern inputs; and*

vi) *Agro-chemical and fertilizer manufacturing industry shall be developed*.

"*The National Agriculture Policy is indeed a tool for facilitating the attainment of NSGRP objectives, Tanzania Development Vision 2025 that envisages raising the general standards of living of Tanzanians to the level of a typical medium-income developing country by 2025 and meeting the Millennium Development Goals*."

b. The sustainable industries development policy SIDP of 1996-2020

In addition, the sustainable industries development policy SIDP of 1996-2020 (Kigoda & MIT-TZ, 1996) regarding the utilization of local resources contained the following information:

- *Tanzania has abundant raw materials which can be exploited for use in local industries. However, most existing industries have relied heavily on imported raw materials and inputs. In order to encourage utilization of local resources endowment, the government will:*
    - *Encourage investment in industries utilizing local raw materials and inputs… and*
    - *Establish and effective inter-sectoral mechanism for procurement of locally produced raw materials by domestic industries.*

c. The NM-AIST Motto, Vision and Mission

Moreover, the NM-AIST vision and mission statement describe that:

The Vision of NM-AIST: *to become a world-class institution of higher learning dedicated to the pursuit and promotion of excellence in science, engineering and technology, and their applications for economic growth and sustainable development in Africa*.

The Mission of NM-AIST: *to deliver and promote high quality and internationally competitive teaching and learning, research and innovation, and public service in science, engineering and technology for enhanced value addition to people and natural resources, emphasizing entrepreneurship* (NM-AIST, 2009).

The NM-AIST motto state that: *Academia for Society and Industry*.

Generally, this section seeks to reflect on the implications of this study on these policy issues as described below:

- CRFs usage in agriculture: the application of CRFs in the agriculture sector will mark an advanced stage of crop production in Tanzania. The designed CRFs formulations have been anticipated to be able to improve FUE for urea fertilizer and so, increase crop production. This address the policy statement regarding the low productivity factors of production stated above.

- Modernization of agriculture inputs: it was said in the policy that, "*increased use of modern inputs (*fertilizers in our context*) is a pre-requisite for achieving sufficient agricultural productivity and growth*". Thus, with urea CRFs usage the possibilities of an increased use of modern agriculture inputs (which here now we refer to urea fertilizer) will materialize thereby increasing the pace of developing a modern agriculture practices in Tanzania.

- Environmental sustainability: as reflected on the objectives to say "*enhancing inputs increased in a … sustainable and environmentally sound manner*". As described in the empirical findings, most of the urea nanocomposite excipients were prepared using biodegradable locally available materials such as gum arabic and chitosan biopolymers. Besides, the acrylamide synthetic polymer used despite being synthetic materials has been associated with the ability to modify the soil conditions as explained before. In that case, our CRFs designs comply with the policy statement regarding agriculture inputs and

environmental soundness since biodegradable materials pause no environmental threat. Even though our argument regarding biodegrability and environmental soundness is till controversial (EU, 2015; Gunther, 2015), we still hold that they are far more suitable to use than non-biodegradable in the CRF engineering.

- Value addition to Tanzanian raw materials: as mentioned in the sustainable industries development policy, the government policy encourages the utilization of local resources in the industrial productions via inter-sectoral mechanism. The design involved the use of locally available Pugu kaolinite mineral, gum arabic and chitosan biopolymers and Oldoinyo Lengai volcanic ashes. In that way, the study has demonstrated the likelihood of value addition of Tanzania local resources in the urea CRF production. This also has an implication to the country's economy and scientific-technological employment regimes.

- Economic growth: the policy statement indicated in the Tanzania Development Vision 2025 that, the general standards of living of Tanzanians to the level of a typical medium-income developing country will be attained by 2025 thereby meeting the Millennium Development Goals. Our CRF formulation design revealed the fact that it is possible to locally industrialize urea CRF production process which in turn will fulfill the "…*procurement of locally produced raw materials by domestic industries*" and reduce fertilizer importation, increase exports and provide employment to both industrialists and farmers which in turn contribute to the economic growth.

- The integration of lab design to the production of urea CRFs formulation into the field practices of course following a period of incubation, will justify the fact that academia can be used to initiate and develop CRF formulation based industries and improve people's welfare via advanced agricultural practices.

9.2 CONCLUSION

Empirically, we have demonstrated that nanocomposite excipients for use in the engineering of CRF formulations, particularly in the release of urea fertilizer can be synthesized by using simple starting materials including, Pugu kaolinite, DMSO, hydroxyaluminum oligomers, methanol, gum arabic biopolymer, cationic ferrous oligomers, Oldoinyo Lengai volcanic ashes, polymeric liquid paraffin, and chitosan biopolymer. As has been generally accepted, urea CRFs do exhibit grandeur properties than the conventional urea fertilizer due to an extended nutrient release which in turn (i) synchronizes availability of nutrients with plants' demands, (ii) reduces localized toxicity due to elimination of bursting effect, (iii) reduces the tailing effect, and (iv) enhances NUE. In that way, the essence of carrying out this study is obviously substantial. In addition, the fact that CRFs supply nutrients to the crops at an extended period of time (up to several seasons) through a single application justifies the economic merit of carrying out this study in that: significant amount of cost can be saved (i) through minimization of short-seasonal fertilization which in turn saves the manual labour and fertilizer inputs required for top dressing operations, and (ii) by engaging in CRFs production industries using available local resources which in turn reduces importation expenditures.

Similarly, the findings presented endeavoured to cover certain dual faceted theoretical gaps and that is (i) the question of how to reduce the 60-70% loss of the total urea'-N applied to the crop field as a result of vaporization and hydrolysis by soil urease into ammonia, and (ii) the question of whether the 1:1 layered phyllosilicate kaolinite by virtues of being hard to undergo intercalation reactions can be successfully utilized to intercalate urea to formulate the urea CRFs. In the same line, there was a question of whether encapsulation using natural biopolymers and the urea release therein can be attained on the urea-kaolinite as well as urea-ash nanocomposite compounds.

Divergently from our expectations, the findings have revealed that the kaolinite-urea nanocomposites are very dynamic than what is known in the literature; it was possible to clearly lay bare in the main findings that the known euhedral pseudo hexagonal platelets can be vigilantly manoeuvred to synthesize particles of diverse morphologies from stacked vermiform, blocky vermiform, pustulated form, curled-glomeruli, desert cactus forms, brain form

agglomerations *etc.*, as indicated in the main results. Besides, the study on the urea-ash nanocomposite exhibited unique reinforced-nanoparticles which offer an added strength of the resulting materials. Along with that, silicone oil dopant defied the known theoretical stance that chitosan is associated with the formation of roundish nanoparticles; this was proven to be correct in some ways and wrong in other ways as a result of silicone doping on the prepared round chitosan based nanocomposite excipients.

Several new phenomena were recorded in this study including the following: (i) the occurrence of natural but moderate intercalation reactions due to simultaneous oligomerization of ferrous cations in the ferrous contaminated kaolins, (ii) the proportionality in the relationship between intercalation ratio and the size of the intermediate intercalation anionic or cationic species, (iii) the concept of the order of kaolinite intercalation interactions, (iv) the existence of the stable intercalation state, (v) the pseudo intercalation process, (vi) unstable intercalation state, and (vii) the breakpoint between Biocementation and co-encapsulation processes. The study has therefore indicated the possibilities of introducing new theoretical concepts arising from the critical analysis and reflections on the main findings. Notwithstanding what is often reported about the applications of Pugu kaolinite in particular (of course and other natural materials used in this study), the benefits of using the same for CFRs industry cannot be underrated as per the diversity of their chemistry, availability and the new theoretical perspectives which this study has brought forth. We have come to a point of utter attempt to say, the studies on the nanocomposite excipients for controlled release fertilizer formulations utilizing kaolinite, volcanic ashes along with the associated bio-polymeric materials have not being all-inclusive or rather not yet fully exhausted and hence, there are more rooms to research and exhaust all such possibilities such that sustained CRFs technologies apt for this resource limited era can be designed and commercialized.

9.3 RECOMMENDATIONS

As far as the subject of CRFs is concerned, attempts to facilitate the substantial extensive application of CRF formulation in agriculture will be limited to the cost associated with CRFs production. In most cases polymer encapsulated CRF formulations are sold at relatively higher rates despite the benefits. Consider Table 9.3 adopted from work done by (Zhang, et al., 2009), it is evident that most farmers would not afford the CRFs let alone the CCFs and this was the reason behind this study that is to develop CRFs using inexpensive locally available materials to cut down the production cost so that many farmers can afford the price.

Table 9.3. Price of some CRF products

Fertilizer Variety	Time of Release in Months	Selling Price/ (RMB10,000/ tonne)	As a Multiple of the Price of Urea
Osmocote 5	5-6	1.36	8
Osmocote 301	3-4	1.80	11
Osmocote 801	8-9	2.08	12
Multicote 1	3-4	1.16	7
Multicote 2	5-6	1.52	9
Multicote 3	8-9	1.68	10
Cau-A10	3-4	0.50	3
Urea	-	0.17	1

Source: (Zhang, et al., 2009)

Owing to that viewpoint the following are some recommendations necessary for future studies:

- The use of locally available materials is inevitable when it comes to cut cost of CRFs production. Thus, it is recommended more studies to explore the suitability of several other layered phyllosilicates as well as biopolymeric materials for use in the engineering of apt nanocomposite excipients for controlled release fertilizers.

- Similarly, research on the inexpensive locally available materials should tally researches on the designing of suitable low cost equipment for use in the CRFs production. That is

to say, there should be a way to link materials engineering aspect of formulations and mechanizations when it comes to cost reduction.

- Release profiles. Very few release profiles were analyzed in this study basing on simulated lab water conditions. Thus, there is a need that field crops should be the major target for future CRFs design and release profile analysis involving actual field crops. This will facilitate the development of CRFs prototypes with easy.

- Also, we have not evaluated the relationship between the sizes of the CRFs particles with the release rate. This calls for more studies to investigate how particle sizes influence the nutrients release.

- Furthermore, there is need to clearly indicate the effects caused by variations in the thickness of the each prepared CRFs in the release rate. This should be done hand to hand with the evaluation of likelihood of whether bursting and/or tailing effect might occur during both, the field operation and during the release phases.

- Lastly, is the need to incubate the synthetic schemes so as to see how best the prepared CRFs can be commercialized after adequate laboratory and field testing.

REFERENCES

AAPFCO. (1997). Official Publication No. 50. West Lafayette, Indiana, USA.

Abeysinghe, S. (2012). *Keggin-type aluminum nanoclusters: synthesis, structural characterization and environmental implications.* M.Sc., University of Iowa

Iowa City, Iowa.

Agnihotri, S. A., & Aminabhavi, T. M. (2004). Controlled release of clozapine through chitosan microparticles prepared by a novel method. *Journal of Controlled Release*, *96*(2), 245-259.

Agric, J. (2014). Meister: Advanced Coated Fertilizer for the New Agriculture, from http://www.jcam-agri.co.jp/en/product/meister.html

Agric., J. (2014). MEISTER: Advanced Coated Fertilizer for the new agriculture. Tokyo, Japan: JCAM AGRI. CO., LTD: http://www.jcam-agri.co.jp/en/product/meister.html.

Aguzzi, C., Cerezo, P., Viseras, C., & Caramella, C. (2007). Use of clays as drug delivery systems: possibilities and limitations. *Applied Clay Science*, *36*(1), 22-36.

Akwilapo, L. D. (1999). *Utilisation of Pugu kaolin clay in porcelain and aluminosilicate refractories focusing on mechanisms for strength development.* PhD, Institutt for kjemi.

Akwilapo, L. D., & Wiik, K. (2003). Ceramic properties of Pugu kaolin clays. Part I: Porosity and modulus of rupture. *Bulletin of the Chemical Society of Ethiopia*, *17*(2).

Akwilapo, L. D., & Wiik, K. (2004). Ceramic properties of pugu kaolin clays. Part 2: Effect of phase composition on flexural strength. *Bulletin of the Chemical Society of Ethiopia*, *18*(1).

Al-Ani, T., & Sarapaa, O. (2008). Clay and clay mineralogy: Physical-chemical properties and industrial uses. *GTK, M*(19), 3232/3241.

Al-Ani, T., & Sarapää, O. (2008). Clay and Clay Mineralogy. *Physical-chemical Properties and Industrial Uses*.

Al-Thawadi, S. M. (2013). Consolidation of Sand Particles by Aggregates of Calcite Nanoparticles Synthesized by Ureolytic Bacteria under Non-Sterile Conditions. *Journal of Chemical Science and Technology Jul*, *2*(3), 141-146.

Almuslet, N., Elfatih, A., Al Sayed, A., & Mohamed, G. (2012). Diode Laser (532 nm) Induced Grafting of Polyacrylamide onto Gum Arabic. *Journal of Physical Science*, *23*(2), 43-53.

Ameena, K., Dilip, C., Saraswathi, R., Krishnan, P., Sankar, C., & Simi, S. (2010). Isolation of the mucilages from< i> Hibiscus rosasinensis</i> linn. and Okra (< i> Abelmoschus

esculentus</i> linn.) and studies of the binding effects of the mucilages. *Asian Pacific Journal of Tropical Medicine, 3*(7), 539-543.

Anicuta, S.-G., Dobre, L., Stroescu, M., & Jipa, I. (2010). Fourier transform infrared (FTIR) spectroscopy for characterization of antimicrobial films containing chitosan. *Analele Universitatii din Oradea fascicula: Ecotoxicologie, Zootehniesitehnologii de Industrie Alimentara*, 1234-1240.

Aroke, U., & El-Nafaty, U. XRF, XRD and FTIR Properties and Characterization of HDTMA-Br Surface Modified Organo-Kaolinite Clay.

Aroke, U., & El-Nafaty, U. (2014). XRF, XRD and FTIR Properties and Characterization of HDTMA-Br Surface Modified Organo-Kaolinite Clay. *International Journal of Emerging Technology and Advanced Engineering, 4*(4).

Association, I. F. I. (2000). *Fertilizers and their use: a pocket guide for the extension officers*: FAO.

Auerbach, S. M., Carrado, K. A., & Dutta, P. K. (2004). Handbook of Layered Materials: CRC Press: New York, NY, USA.

Bajaj, H. C., & Jasra, R. V. (2007). Synthesis and characterization of organic bentonite using Gujarat and Rajasthan clays. *Current Science, 92*(7), 1005.

Balan, E., Saitta, A. M., Mauri, F., & Calas, G. (2001). First-principles modeling of the infrared spectrum of kaolinite. *American Mineralogist, 86*(11-12), 1321-1330.

Bang, S. C., Bang, S. S., Choi, S. R., Lee, S. J., Lee, J. H., & Kim, J. S. (2014). Method of manufacturing soil reinforced by microbe-based bio-binders and soil produced by the method: Google Patents.

Banwell, C. N., & McCash, E. M. (1994). *Fundamentals of Molecular Spectroscopy* (4 ed.): McGraw-Hill.

Barlow, G., & Corish, P. (1959a). 337. Infrared absorption spectra of some urea complexes. *J. Chem. Soc.*, 1706-1710.

Barlow, G., & Corish, P. (1959b). Infrared absorption spectra of some urea complexes. *J. Chem. Soc.*, 1706-1710.

Barzegar-Jalali, M. (2008). Kinetic analysis of drug release from nanoparticles. *Journal of Pharmacy & Pharmaceutical Sciences, 11*(1), 167-177.

Basak, B., Pal, S., & Datta, S. (2012). Use of modified clays for retention and supply of water and nutrients. *Current Science(Bangalore), 102*(9), 1272-1278.

Beaton, J. D. (2005). History of fertilizers *In Efficient Fertiliser Use Manual* (pp. 1-17): Mosaic Co.

Beaufort, D., Cassagnabere, A., Petit, S., Lanson, B., Berger, G., Lacharpagne, J., & Johansen, H. (1998). Kaolinite-to-dickite reaction in sandstone reservoirs. *Clay Minerals, 33*(2), 297-316.

Becher, H. (1956). Infrared spectroscopic examination of the reaction products of urea and formaldehyde. I. Methylene ureas. *Chem. Ber 89*, 1593-1601.

Becher, H. (1956). Infrared spectroscopic examination of the reaction products of urea and formaldehyde. I. Methylene ureas. *Chem. Ber, 89*, 1593-1601.

Bel'chinskaya, L. I., Voishcheva, O. V., Petukhova, G. A., Ien, L., Khokhlov, V. Y., & Selemenev, V. F. (2011). Effect of the acidic treatment on the adsorption and structural properties of the natural mineral sorbent M45C20. *Russian Chemical Bulletin, 60*(9), 1820-1826. doi: 10.1007/s11172-011-0275-8

Bhattacharyya, K. G., & Gupta, S. S. (2006). Kaolinite, montmorillonite, and their modified derivatives as adsorbents for removal of Cu (II) from aqueous solution. *Separation and Purification Technology, 50*(3), 388-397.

Bhuvaneshwari, S., Sruthi, D., Sivasubramanian, V., Niranjana, K., & Sugunabai, J. (2011). Development and characterization of chitosan films. *IJERA, 1*(2), 292-299.

Bloodworth, A. J., Highley, D. E., & Mitchell, C. J. (1993). Industrial Minerals Laboratory Manual: KAOLIN Nottingham, UK: British Geological Survey.

Bowman, B. T. (1973). The effect of saturating cations on the adsorption of Dasanit®, O, O-diethyl O-[p-(methyl sulfinyl) phenyl] phosphorothioate, by montmorillonite suspensions. *Soil Science Society of America Journal, 37*(2), 200-207.

Bremner, J. M., & Krogmeier, M. J. (1988). Elimination of the adverse effects of urea fertilizer on seed germination, seedling growth, and early plant growth in soil. *Proceedings of the National Academy of Sciences, 85*(13), 4601-4604.

Brown, G., & Brindley, G. (1980). X-ray diffraction procedures for clay mineral identification. *Crystal structures of clay minerals and their X-ray identification, 5*, 305-359.

Brugnerotto, J., Lizardi, J., Goycoolea, F., Argüelles-Monal, W., Desbrieres, J., & Rinaudo, M. (2001). An infrared investigation in relation with chitin and chitosan characterization. *Polymer, 42*(8), 3569-3580.

Carradó, A. (2001). *Contribution to the characterisation of the mechanical and microstructural properties of metalceramic bounds used in dental applications.* PhD Université De Reims, Champagne, Ardenne.

CEH. (2015). Chemical Economics Handbook: Controlled- and Slow-Release Fertilizers Retrieved July 4th, 2015, from https://www.ihs.com/products/controlled-and-slow-release-chemical-economics-handbook.html

Chakraborty, C., Sukul, P. K., Dana, K., & Malik, S. (2013). Suppression of Keto Defects and Thermal Stabilities of Polyfluorene–Kaolinite Clay Nanocomposites. *Industrial & Engineering Chemistry Research, 52*(20), 6722-6730.

Chatzoudis, G., & Rigas, F. (1998). Macroreticular hydrogel effects on dissolution rate of controlled-release fertilizers. *Journal of Agricultural and Food Chemistry, 46*(7), 2830-2833.

Chen, G., D'Auria, M., Beecher, J., Mansfield, M., Godfrey, R., Tanner, T., . . . Dunaway, D. (2010). Identification of the Properties of Gum Arabic Used as a Binder in 7.62-mm Ammunition Primers: DTIC Document.

Cheung, K., & Darvell, B. (2002). Sintering of dental porcelain: effect of time and temperature on appearance and porosity. *Dental Materials, 18*(2), 163-173.

Chime Salome, A., Onunkwo Godswill, C., & Onyishi Ikechukwu, I. (2013). Kinetics and Mechanisms of Drug Release from Swellable and Non Swellable Matrices: A Review. *Research Journal of Pharmaceutical, Biological and Chemical Sciences, 4*(2), 97.

Chiza, C. K., & MAFC. (2012). *National Agriculture Policy: Draft*. URT: MAFC Retrieved from http://www.google.co.tz/url?sa=t&rct=j&q=&esrc=s&source=web&cd=1&cad=rja&uact=8&ved=0CCEQFjAAahUKEwij7qiGqYfGAhWD8XIKHY87ANY&url=http%3A%2F%2Fxa.yimg.com%2Fkq%2Fgroups%2F20674633%2F899875644%2Fname%2FNATIONAL%2BAGRICULTURAL%2BPOLICY-%2BFINAL%2B09%2B%2BJune-%2B2012.pdf&ei=61N5VePMNoPjywOP94CwDQ&usg=AFQjCNGsuKy1IyPt94NGS_nYsGgdhcXpZw&bvm=bv.95277229,d.ZGU.

Chloé, B., & Fabien, S. (2013). Preparation of microcapsules by complex coacervation of gum Arabic and chitosan. *Carbohydrate Polymers, 99* (2014), 608– 616.

Chowdary, K., Mohapatra, P., & Krishna, M. (2006). Evaluation of olibanum and its resin as rate controlling matrix for controlled release of diclofenac. *Indian journal of pharmaceutical sciences, 68*(4), 497.

Chu, F., Sham, A., Luk, H., Andersson, B., Chai, J., & Chow, T. W. (2003). Threshold contrast ratio and masking ability of porcelain veneers with high-density alumina cores. *The International journal of prosthodontics, 17*(1), 24-28.

Church, R. J. (1964). Chemistry and processing of urea and ureaform. . In I. S. V(Ed). (Ed.), *Fertiliser Nitrogen – Its Chemistry and Technology.* (Vol. ICS Monograph No 161. , pp. 247-279). USA: Reinhold Publishing.

Ciros Co., L. (2013). ball clay beneficiation technology Retrieved March 9 2015, from http://en.2xarmed.com/miningother/2617-ball-clay-beneficiation-technology.html

Clark, R. (1989). *Marine Pollution*. Oxford: Clarendon Press.

Cnenr-ns, E. Clays and Clay Minerals Retrieved January 26th, 2015, from http://www.sgtk.ch/rkuendig/dokumente/FS10_Clay_handout.pdf

Colin, S. (2011). Sand could help us reach for stars, from http://www.thenational.ae/news/uae-news/technology/sand-could-help-us-reach-for-stars

Corporation, G. C. (2005). Technical Bulletin Reaction Solvent Dimethyl Sulfoxide (DMSO), January 2005, from www.gaylordchemical.com

Corradini, E., De Moura, M., & Mattoso, L. (2010a). A preliminary study of the incorporation of NPK fertilizer into chitosan nanoparticles. *Express. Polymer Lett., 4*, 509-515.

Corradini, E., De Moura, M., & Mattoso, L. (2010b). A preliminary study of the incorporation of NPK fertilizer into chitosan nanoparticles. *Express Polym. Lett, 4*(8), 509-515.

Costa, M. M., Cabral-Albuquerque, E. C., Alves, T. L., Pinto, J. C., & Fialho, R. L. (2013). Use of polyhydroxybutyrate and ethyl cellulose for coating of urea granules. *Journal of agricultural and food chemistry, 61*(42), 9984-9991.

Costa, P., & Sousa Lobo, J. M. (2001). Modeling and comparison of dissolution profiles. *European journal of pharmaceutical sciences, 13*(2), 123-133.

Craig, R. G., Peyton, F. A., & Asgar, K. (1975). *Restorative dental materials*. St.Louis: Mosby.

Crank, J. (1975). *The mathematics of diffusion*. New York: Oxford University Press.

Curtis J. Overdahl, Rehm, G. W., & Meredith, H. L. (2015). Nutrient Management: Fertilizer Urea Retrieved May 27th, 2015, from http://www.transpakmarine.com/static/pdf/research/ag-chemistry/UreaDescribed.pdf

Czarnecka, A. (2013). *Preparation and characterization of kaolinite-based nanocomposite materials.* University of Ottawa.

Dang, T. H., Chen, B.-H., & Lee, D.-J. (2013). Application of kaolin-based catalysts in biodiesel production via transesterification of vegetable oils in excess methanol. *Bioresource technology, 145*, 175-181.

Das, S., Reddy, G. S., Sharma, K., Vittal, K., Venkateswarlu, B., Reddy, M. N., & Reddy, Y. (1993). Prediction of nitrogen availability in soil after crop residue incorporation. *Fertilizer research, 34*(3), 209-215.

Dawley, M. M., Scott, A. M., Hill, F. C., Leszczynski, J., & Orlando, T. M. (2012). Adsorption of formamide on kaolinite surfaces: a combined infrared experimental and theoretical study. *The Journal of Physical Chemistry C, 116*(45), 23981-23991.

Dawson, J. (1998). Peralkaline nephelinite–natrocarbonatite relationships at Oldoinyo Lengai, Tanzania. *Journal of Petrology, 39*(11-12), 2077-2094.

Deshmukh, V., Singh, S., & Sakarkar, D. (2009). Formulation and evaluation of sustained release metoprolol succinate tablet using hydrophilic gums as release modifiers. *Int j Pharm tech res, 1*(2), 159-163.

Dionísio, M., & Grenha, A. (2012). Locust bean gum: exploring its potential for biopharmaceutical applications. *Journal of pharmacy & bioallied sciences, 4*(3), 175.

Dixit, V. (2014). Dissolution and Dissolution Models: authorSTREAM: http://www.authorstream.com/Presentation/aSGuest106867-1122372-dissolution-and-its-models/.

Dobias, B. (1993). *Coagulation and Flocculation: Theory and Applications*: CRC Press.

Dol Hamid, R., Swedlund, P. J., Song, Y., & Miskelly, G. M. (2011). Ionic strength effects on silicic acid (H4SiO4) sorption and oligomerization on an iron oxide surface: An interesting interplay between electrostatic and chemical forces. *Langmuir, 27*(21), 12930-12937.

Du, C.-w., Zhou, J.-m., & Shaviv, A. (2006). Release characteristics of nutrients from polymer-coated compound controlled release fertilizers. *Journal of Polymers and the Environment, 14*(3), 223-230.

Dupont, A., Andriot, M., Chao, S. H., Colas, A., Cray, S., De Buyl, F., . . . Wolf, A. T. (2007). Silicones in Industrial Applications. In D. J. Roger & G. Mario (Eds.), *Inorganic Polymers* (pp. 61-161): Nova Science Publishers.

Ekebafe, L., Ogbeifun, D., & Okieimen, F. (2011). Polymer applications in agriculture. *Biokemistri, 23*(2).

Emmet, R. T. (1969). SPECTROPHOTOMETRIC DETERMINATION OF UREA IN NATURAL WATERS WITH HYPOCHLORITE AND PHENOL (Vol. AD 686 387). Annapolis, Maryland: Naval Ship Research and Development Laboratory.

England, K. M., Camberato, D. M., & Lopez, R. G. Commercial Greenhouse and Nursery Production.

Eswaran, K., Ghosh, P. K., Mehta, A. S., Mody, K. H., Pandya, J. B., Patolia, J. S., . . . Ramavat, B. K. (2005). Integrated method for production of carrageenan and liquid fertilizer from fresh seaweeds: Google Patents.

EU. (2015). Biodegradable Waste Retrieved June 12th, 2015, from http://ec.europa.eu/environment/waste/compost/

Fan, X. (2009). *Research and development of controlled-release fertilizers as high efficient nutrient management materials in China.* Paper presented at the The Proceedings of the International Plant Nutrition Colloquium XVI.

Fink, J. K. (2013). *Reactive polymers fundamentals and applications: a concise guide to industrial polymers*: William Andrew.

Fischer, P., & McDowell, C. (1960). THE INFRARED ABSORPTION SPECTRA OF UREA-HYDROCARBON ADDUCTS. *Canadian Journal of Chemistry, 38*(2), 187-193.

Fraunhofer, J. A. (2009). *Dental materials at a glance. .* UK: John Wiley & Sons.

Frost, R. L., Kristof, J., Paroz, G. N., & Kloprogge, J. T. (1998). Molecular structure of dimethyl sulfoxide intercalated kaolinites. *The Journal of Physical Chemistry B, 102*(43), 8519-8532.

Fu, G., Nazar, L., & Bain, A. (1991). Aging processes of alumina sol-gels: Characterization of new aluminum polyoxycations by aluminum-27 NMR spectroscopy. *Chemistry of Materials, 3*(4), 602-610.

Fujita, T. (1996). Reply to the request on controlled-release fertilizers. *Personal communication*.

Gardolinsky, J. (2005). Interlayer grafting and delamination of kaolinite. *Christian-Albrechts-University, Kiel, Germany*, 67-69.

Gary, C., Marc, D. A., Charles, R. F., James, B., Mark, M., Reed, G., . . . Dave, D. (2010). Identification of the Properties of Gum Arabic used as Binder in 7.62-mm Ammunition Primers (pp. 1-68). Picatinny Arsenal, New Jersey: U.S. Army Armament Research, Development and Engineering Center.

Gaylord, C. C. (2005a). Dimethyl Sulfoxide (DMSO) Physical Properties. Slidell, USA: Gaylord Chemical Corporation.

Gaylord, C. C. (2005b). Dimethyl Sulfoxide (DMSO) Physical Properties. Slidell, USA Gaylord Chemical Corporation.

Giannelis, E. P. (1996). Polymer layered silicate nanocomposites. *Advanced materials, 8*(1), 29-35.

Gill, P., Moghadam, T. T., & Ranjbar, B. (2010). Differential scanning calorimetry techniques: applications in biology and nanoscience. *Journal of biomolecular techniques: JBT, 21*(4), 167.

Glaser, V., Stajer, P., & Vidensky, J. (1987). Simulace prubehu rozpousteni obalovanych prumyslovych hnojiv ve vode-II. *Chemicky Prumysl, 37*(62), 353-355.

Glibert, P. M., Harrison, J., Heil, C., & Seitzinger, S. (2006). Escalating worldwide use of urea–a global change contributing to coastal eutrophication. *Biogeochemistry, 77*(3), 441-463.

Gobi, R., Rajamannan, B., & Viruthagiri, G. (2009). Mechanical properties related to use of glass waste as a raw material in porcelain stoneware tile mixtures. *Recent Research in Science and Technology, 1*(2), 52-57.

Goertz, H. M. (1993). *Technology developments in coated fertilizers.* Paper presented at the Proceedings: Dahlia Greidinger Memorial International Workshop on Controlled/Slow Release Fertilizers, Technion-Israel Institute of Technology, Haifa.

Google-maps. (2015). Kazimzumbwi forest reserve: directions, from http://travelingluck.com/Africa/Tanzania/Tanzania+%28general%29/_158109_Kazimzumbwi+Forest+Reserve.html

Grim, R. E. (1968). Clay mineralogy. International series in the earth and planetary sciences. *McGraw-Hill, New York.*

Groza, A., Surmeian, A., Ganciu, M., & Popescu, I. (2005). Infrared spectral investigation of organosilicon compounds under corona charge injection in air at atmospheric pressure. *Journal of optoelectronics and advanced materials, 7*(5), 2545-2548.

Guilherme, M. R., Reis, A. V., Paulino, A. T., Moia, T. A., Mattoso, L. H., & Tambourgi, E. B. (2010). Pectin-based polymer hydrogel as a carrier for release of agricultural nutrients and removal of heavy metals from wastewater. *Journal of applied polymer science, 117*(6), 3146-3154.

Gunther, M. (2015). Biodegradable and Non-biodegradable materials Retrieved June 12th, 2015, from http://wwf.panda.org/about_our_earth/teacher_resources/webfieldtrips/bio_nonbio_materials/

Guo, M., Liu, M., Liang, R., & Niu, A. (2006). Granular urea-formaldehyde slow-release fertilizer with superabsorbent and moisture preservation. *Journal of applied polymer science, 99*(6), 3230-3235.

Han, P. (2009). Former buildings of German kaolitine miners at Pugu Hills, Pwani, Tanzania Retrieved June 13th, 2015, from https://en.wikipedia.org/wiki/Pugu_Hills_Forest_Reserve#/media/File:Building_ruins_of_former_%28German%29_mining_activity_at_Pugu_Hills,_Tanzania.jpg

Han, X., Chen, S., & Hu, X. (2009). Controlled-release fertilizer encapsulated by starch/polyvinyl alcohol coating. *Desalination, 240*(1), 21-26.

Hanafi, M., Eltaib, S., & Ahmad, M. (2000). Physical and chemical characteristics of controlled release compound fertiliser. *European polymer journal, 36*(10), 2081-2088.

Hayes, K., Papelis, C., & Leckie, J. (1988). Ionic strength effects on silicic acid (H 4 SiO 4) sorption and oligomerization on an iron oxide surface: an interesting interplay between electrostatic and chemical forces. *J. Colloid Interface Sci, 125*(717), 90039-90032.

Heah, C., Kamarudin, H., Al Bakri, A. M., Bnhussain, M., Luqman, M., Nizar, I. K., . . . Liew, Y. M. (2012). Study on solids-to-liquid and alkaline activator ratios on kaolin-based geopolymers. *Construction and Building Materials, 35*, 912-922.

Heah, C., Kamarudin, H., Mustafa Al Bakri, A., Bnhussain, M., Luqman, M., Khairul Nizar, I., . . . Liew, Y. M. (2012). Study on solids-to-liquid and alkaline activator ratios on kaolin-based geopolymers. *Construction and Building Materials, 35*, 912-922.

Heller-Kallai, L. (1978). Reactions of salts with kaolinite at elevated temperatures: I. *Clay Minerals, 13*(2), 221-235.

Heller-Kallai, L., & Frenkel, M. (1979). Reactions of Salts with Kaolinite at Elevated Temperatures-Part 2. *Developments in Sedimentology, 27*, 629-637.

Hezaveh, H., & Muhamad, I. I. (2013). Controlled drug release via minimization of burst release in pH-response kappa-carrageenan/polyvinyl alcohol hydrogels. *Chemical Engineering Research and Design, 91*(3), 508-519.

Hillier, S., 2003, Clay Mineralogy, in GV Middleton, MJ Church, M Coniglio, LA Hardie, and FJ Longstaffe eds., Encyclopaedia of sediments and sedimentary rocks: Kluwer Academic Publishers, Dordrecht., p. 139-142.

Horvath, E., Kristof, J., & Frost, R. L. (2010). Vibrational Spectroscopy of Intercalated Kaolinites. Part I. *Applied Spectroscopy Reviews, 45*(2), 130-147.

Hosseinzadeh, H. (2010). Controlled release of diclofenac sodium from pH-responsive carrageenan-g-poly (acrylic acid) superabsorbent hydrogel. *Journal of chemical sciences, 122*(4), 651-659.

Il'ina, V. (2007). Glass crystal materials made from mineral and technogenic feedstock from Karelia. *Glass and Ceramics, 64*(9-10), 318-321.

Ilić, B. R., Mitrović, A. A., & Miličić, L. R. (2010). Thermal treatment of kaolin clay to obtain metakaolin. *Hemijska industrija, 64*(4), 351-356.

IPNI. (2013). Coated Fertilizer. Nutrient Source Specifics 2013 Retrieved August 08, 2013 from http://www.ipni.net/publication/nss.nsf/0/33C6A283CC38EE26852579AF007682E3/$FILE/N SS-20%20Coated%20Fertilizer.pdf.

Islam, M., Masum, S. M., Rahman, M. M., Molla, M., Islam, A., Shaikh, A., & Roy, S. (2011). Preparation of Chitosan from Shrimp Shell and Investigation of Its Properties. *International Journal of Basic & Applied Sciences, 11*(1).

IUPAC. (1997). Compendium of Chemical Terminology, 2nd ed. (the "Gold Book"). Compiled by A. D. McNaught and A. Wilkinson. Blackwell Scientific Publications, Oxford (1997). XML on-line corrected version: http://goldbook.iupac.org (2006-) created by M. Nic, J. Jirat, B. Kosata; updates compiled by A. Jenkins. ISBN 0-9678550-9-8. doi:10.1351/goldbook.

Jablonski, S. (Ed.) (2008). Elsevier Health Sciences.

Jacobson, A. J., & Nazar, L. F. (2006). Intercalation Chemistry *Encyclopedia of Inorganic Chemistry*: John Wiley & Sons, Ltd.

James, D. W. (1993). Urea: A Low Cost Nitrogen Fertilizer with Special Management Requirements (Vol. AG/283,1993). USA: Utah State University.

Jamnongkan, T., & Kaewpirom, S. (2010a). Controlled-release fertilizer based on chitosan hydrogel: phosphorus release kinetics. *Sci J UBU, 1*, 43-50.

Jamnongkan, T., & Kaewpirom, S. (2010b). Controlled-release fertilizer based on chitosan hydrogel: phosphorus release kinetics. *Sci J UBU, 1*(1), 43-50.

Janet, F. (2014). For a better concrete, mix sand with bacteria and urea: A new method explores low energy biological processes Retrieved June 4th, 2015, from http://www.zdnet.com/article/for-a-better-concrete-mix-sand-with-bacteria-and-urea/

Jani, G. K., & Shah, D. P. (2008). Evaluation of mucilage of Hibiscus rosasinensis Linn as rate controlling matrix for sustained release of diclofenac. *Drug development and industrial pharmacy, 34*(8), 807-816.

Jarrell, W., & Boersma, L. (1979). Model for the release of urea by granules of sulfur-coated urea applied to soil. *Soil Science Society of America Journal, 43*(5), 1044-1050.

Jarrell, W., & Boersma, L. (1980). Release of urea by granules of sulfur-coated urea. *Soil Science Society of America Journal, 44*(2), 418-422.

Jaynes, W., & Boyd, S. (1991). Hydrophobicity of siloxane surfaces in smectites as revealed by aromatic hydrocarbon adsorption from water. *Clays Clay Miner, 39*(4), 428-436.

Johnston, C. T., de Oliveira, M. F., Teppen, B. J., Sheng, G., & Boyd, S. A. (2001). Spectroscopic study of nitroaromatic-smectite sorption mechanisms. *Environmental science & technology, 35*(24), 4767-4772.

Johnston, C. T., Sposito, G., Bocian, D. F., & Birge, R. R. (1984). Vibrational spectroscopic study of the interlamellar kaolinite-dimethyl sulfoxide complex. *The Journal of Physical Chemistry, 88*(24), 5959-5964.

Jones, C. A., Koenig, R. T., Ellsworth, J. W., Brown, B. D., & Jackson, G. D. (2007). *Management of urea fertilizer to minimize volatilization*: Montana State University Extension.

Joshi, G. V., Kevadiya, B. D., Patel, H. A., Bajaj, H. C., & Jasra, R. V. (2009). Montmorillonite as a drug delivery system: intercalation and in vitro release of timolol maleate. *International Journal of Pharmaceutics, 374*(1), 53-57.

Jovanović, M., & Mujkanović, A. (2013). Characterization, beneficiation and utilization of the clay from cental Bosnia, B&H.

Jovanović, M., & Volkov-Husović, T. (2012). Influence of sintering temperature on raw and beneficiated clay "Klokoti". *Science of Sintering, 44*(2), 161-168.

Kalu, V., Odeniyi, M., & Jaiyeoba, K. (2007). Matrix properties of a new plant gum in controlled drug delivery. *Archives of pharmacal research, 30*(7), 884-889.

Kamhabwa, F. (2014). Consumption of Fertilizers and Fertilizer Use by Crop in Tanzani Retrieved 27th May, 2015, from http://www.amitsa.org/wp-content/uploads/bsk-pdf-manager/196_IFDC-AFO-TANZANIA-FERTILIZER-COMSUMPTION-AND-FUBC-%28JANUARY-2014%29-AFO.PDF

Kanno, H. (2013). USE OF CONTROLLED-RELEASE FERTILIZERS (CRF) FOR SUSTAINABLE CROP PRODUCTION IN ASIA. Ohwashi-Tsukuba Japan: Japan International Research Center for Agricultural Sciences: http://jircas-d.job.affrc.go.jp/Ver-1/english/files/2014/03/fanglei/2013-session-22.pdf.

Katya A. Bazilevskaya, Douglas Archibald, & Martínez, C. E. (2006). *An ATR-FTIR and EXAFS Study of Mixed Fe-Al (oxy) Hydroxides.* Paper presented at the The 18th World Congress of Soil Science (July 9-15, 2006), Philadelphia, Pennsylvania, USA.

Kevadiya, B., Patel, H., Joshi, G., Abdi, S., & Bajaj, H. (2010). Montmorillonite-alginate composites as a drug delivery system: Intercalation and In vitro release of diclofenac sodium. *Indian journal of pharmaceutical sciences, 72*(6), 732.

Kevadiya, B. D., Patel, T. A., Jhala, D. D., Thumbar, R. P., Brahmbhatt, H., Pandya, M. P., . . . Gadhia, P. K. (2012). Layered inorganic nanocomposites: a promising carrier for 5-fluorouracil (5-FU). *European Journal of Pharmaceutics and Biopharmaceutics, 81*(1), 91-101.

Khabas, T., Kulinich, E., Vereshchagin, V., & Babushkin, E. (2003). Development of an undercoat layer for dental porcelain. *Glass and Ceramics, 60*(3-4), 123-126.

Khazaeli, P., Pardakhty, A., & Hassanzadeh, F. (2010). Formulation of Ibuprofen beads by ionotropic gelation. *Iranian journal of pharmaceutical research*, 163-170.

Kielmann, U., Jeschke, G., & García-Rubio, I. (2014). Structural Characterization of Polymer-Clay Nanocomposites Prepared by Co-Precipitation Using EPR Techniques. *Materials, 7*(2), 1384-1408.

Kigoda, A. O., & MIT-TZ. (1996). *Sustainable Industries Development Policy SIDP (1996-2020).* URT: MIT-TZ Retrieved from http://www.tzonline.org/pdf/sustainableindustrial.pdf.

Kim, C. H., Joo, C.-K., Chun, H. J., Yoo, B. R., Noh, D. I., & Shim, Y. B. (2012). Instrumental studies on silicone oil adsorption to the surface of intraocular lenses. *Applied Surface Science, 262*, 146-152.

Kloprogge, J. T. (2004). Handbook of Layered Materials edited by Scott M. Auerbach, Kathleen A. Carrado and Prabir K. Dutta. Marcel Dekker Inc, New York, Basel, 2004, 646 pp.[ISBN 0-8247-5349-6]. Price $195. *Clays and Clay Minerals, 52*(6), 795-797.

Kloth, B. (1996). Aglukon Spezialdünger GmbH: Reply to the request on controlled-release fertilizers. *Personal communication*.

Kobayashi, Y., Ohira, O., Ohashi, Y., & Katoh, E. (1991). Bending strength and sicrostructure of sommercial sorcelains for table wares. *J. Ceram. Soc. Jpn, 99*(6), 495 – 502.

Kulik, A., Shergill, I., Novikov, P., Malé-Alemany, M., Portell, J., & Lloveras, M. (2012). Stone Spray Robot Retrieved June 4th, 2015, from http://www.dezeen.com/2012/08/22/stone-spray-robot-by-anna-kulik-inder-shergill-and-petr-novikov/

Kumar, S., Bauddh, K., Barman, S., & Singh, R. P. (2013). Evaluation of conventional and organic matrix entrapped urea and di-ammonium phosphate for growth and productivity of Triticum aestivum L. and mobilization of NO 3−, NO 2−, NH 4+ and PO 4− 3 from soil to plant leaves. *Int. J. Agro. Plant Prod, 4*(6), 1357-1368.

Kumar, S., & Gupta, S. K. (2012). Natural polymers, gums and mucilages as excipients in drug delivery. *Polim. Med, 42*(3-4), 191-197.

Kumar, S., & Gupta, S. K. (2013). Rosin: A naturally derived excipient in drug delivery systems. *Polim. Med, 43*(1), 45-48.

Kumar, S. V., Sasmal, D., & Pal, S. C. (2008). Rheological characterization and drug release studies of gum exudates of Terminalia catappa Linn. *Aaps Pharmscitech, 9*(3), 885-890.

Kunjachan, S., Jose, S., & Lammers, T. (2010). Understanding the mechanism of ionic gelation for synthesis of chitosan nanoparticles using qualitative techniques. *Asian journal of pharmaceutics, 4*(2), 148.

Laird, D. A., & Fleming, P. D. (1999). Mechanisms for adsorption of organic bases on hydrated smectite surfaces. *Environmental toxicology and chemistry, 18*(8), 1668-1672.

Lajos, P. B. (2008). Soil science: Sources of negative charge. Debreceni Egyetem a TÁMOP 4.1.2 pályázat keretein belül: Fejezet - World Reference Base for Soil Resources.

Landels, S. (1994). Controlled-Release Fertilizers: Supply and Demand Trends in US Nonfarm Markets. *Publisher: SRI International. Menlo Park, CA, USA*.

Landels, S. (2010). Controlled release fertilizers: Expanding their use beyond traditional markets *In New Ag International* (Vol. March issue, pp. 42-49).

Larkin, P. (2011). *Infrared and Raman spectroscopy; principles and spectral interpretation*: Elsevier.

Leceta, I., Guerrero, P., & De La Caba, K. (2013). Functional properties of chitosan-based films. *Carbohydrate polymers, 93*(1), 339-346.

Leceta, I., Guerrero, P., Ibarburu, I., Dueñas, M., & De la Caba, K. (2013). Characterization and antimicrobial analysis of chitosan-based films. *Journal of Food Engineering, 116*(4), 889-899.

Letaief, S., & Detellier, C. (2009). Clay− polymer nanocomposite material from the delamination of kaolinite in the presence of sodium polyacrylate. *Langmuir, 25*(18), 10975-10979.

Li, B., He, J., Evans, D. G., & Duan, X. (2004). Inorganic layered double hydroxides as a drug delivery system—intercalation and in vitro release of fenbufen. *Applied clay science, 27*(3), 199-207.

Li, H., Sheng, G., Teppen, B. J., Johnston, C. T., & Boyd, S. A. (2003). Sorption and desorption of pesticides by clay minerals and humic acid-clay complexes. *Soil Science Society of America Journal, 67*(1), 122-131.

Li, W., Zhang, L., Liu, C., & Liang, Z. (2012). Preparation and Property o f Poly (acrylamide-co-acrylic acid) Macromolecule Slow-releasing Fertilizer. *Int. J. Electrochem. Sci, 7*, 11470-11476.

Liang, R., Yuan, H., Xi, G., & Zhou, Q. (2009). Synthesis of wheat straw-g-poly (acrylic acid) superabsorbent composites and release of urea from it. *Carbohydrate Polymers, 77*(2), 181-187.

Liew, Y. M., Kamarudin, H., Al Bakri, A. M., Luqman, M., Nizar, I. K., Ruzaidi, C., & Heah, C. (2012). Processing and characterization of calcined kaolin cement powder. *Construction and Building Materials, 30*, 794-802.

Liew, Y. M., Kamarudin, H., Mustafa Al Bakri, A., Luqman, M., Khairul Nizar, I., Ruzaidi, C., & Heah, C. (2012). Processing and characterization of calcined kaolin cement powder. *Construction and Building Materials, 30*, 794-802.

Liu, G., Zotarelli, L., Li, Y., Dinkins, D., Wang, Q., & Ozores-Hampton, M. (2014). Controlled-Release and Slow-Release Fertilizers as Nutrient Management Tools. USA: U.S. Department of Agriculture, UF/IFAS Extension Service, University of Florida, IFAS.

Liu, M., Liang, R., Zhan, F., Liu, Z., & Niu, A. (2007). Preparation of superabsorbent slow release nitrogen fertilizer by inverse suspension polymerization. *Polymer international, 56*(6), 729-737.

Lobitzer, H., Giacomini, R., Muller, H. W., Notstaller, R., & Schwaighofer, B. (1982). Geology and Utilisation of the Pugu Hills Kaolin Deposit. . Tanzania: Institute for Geologie Inc.

Loux, M. M., Liebl, R. A., & Slife, F. W. (1989). Adsorption of clomazone on soils, sediments, and clays. *Weed Science*, 440-444.

Ltd, E. (2013). Zeta Potential – Electrophoresis Retrieved 5 September, 2013, from http://www.escubed.co.uk/sites/default/files/zeta_potential_(an011)_elecrophoresis.pdf

Lu, D., Xiao, C., & Xu, S. (2009). Starch-based completely biodegradable polymer materials. *Express Polymer Letters, 3*(6), 366-375.

Lu, E.-X., Jiang, Z.-Q., Zhang, Q.-Z., & Jiang, X.-G. (2003). A water-insoluble drug monolithic osmotic tablet system utilizing gum arabic as an osmotic, suspending and expanding agent. *Journal of controlled release, 92*(3), 375-382.

Lugwisha, E. (2009a). Properties of fired bodies made from Tanzanian talc-clay mixes for ceramic applications. *Tanzania Journal of Science, 32*(2), 69-79.

Lugwisha, E. (2009b). Thermal and x-ray investigations of kowak clay in northwestern Tanzania and its possible industrial use. *Tanzania Journal of Science, 32*(2), 81-89.

Lugwisha, E. H. J. (2011). Identification of clay minerals of the eastern southern region of Lake Victoria by ethylene glycol and heat: X-ray diffraction and infrared spectroscopy studies. *Tanz. J. Sci., 37*, 167-178.

Lugwisha, E. H. J., & Siafu, S. I. (2014). THE PROPERTIES OF FELDSPATHIC DENTAL PORCELAIN FROM TANZANIAN ALUMINOSILICATE MATERIALS. *International Journal of Development Research, 4*(11), 2260-2265.

Luzar, A., & Chandler, D. (1993). Structure and hydrogen bond dynamics of water-dimethyl sulfoxide mixtures by computer simulations. Interim report, April 1992-October 1993: California Univ., Berkeley, CA (United States). Dept. of Chemistry.

Luzar, A., & Chandler, D. (1993). Structure and hydrogen bond dynamics of water–dimethyl sulfoxide mixtures by computer simulations. *The Journal of chemical physics, 98*(10), 8160-8173.

Lynne, H., Strand, G., & Lyng, S. (1980). Investigation of ceramic raw materials from Tanzania. (Vol. Project No. 79 10 03). Oslo: Sentralinstitute for Industriell Forskning.

Ma, Z.-y., Jia, X., Zhang, G.-x., Hu, J.-m., Zhang, X.-l., Liu, Z.-y., . . . Zhou, F. (2013). pH-Responsive Controlled-Release Fertilizer with Water Retention via Atom Transfer Radical Polymerization of Acrylic Acid on Mussel-Inspired Initiator. *Journal of agricultural and food chemistry, 61*(23), 5474-5482.

Macewan, D. M. (1947). The nomenclature of the halloysite minerals. *Mineral. Mag, 28*, 36-44.

Madejova, J. (2003). FTIR techniques in clay mineral studies. *Vibrational spectroscopy, 31*(1), 1-10.

Magalhães, A. S. G., Almeida Neto, M. P., Bezerra, M. N., Ricardo, N. M., & Feitosa, J. (2012). Application of ftir in the determination of acrylate content in poly (sodium acrylate-co-acrylamide) superabsorbent hydrogels. *Química Nova, 35*(7), 1464-1467.

Mahat, B. S. (2010). *Mathematical Models used in Drug Release Studies.* KATHMANDU UNIVERSITY: http://www.scribd.com/doc/54516124/MATHEMATICAL-MODELS-USED-IN-THE-DRUG-RELEASE-STUDIES, DHULIKHEL, NEPAL. Retrieved from http://www.scribd.com/doc/54516124/MATHEMATICAL-MODELS-USED-IN-THE-DRUG-RELEASE-STUDIES

Malik, K., Arora, G., & Singh, I. (2011). Locust bean gum as superdisintegrant–Formulation and evaluation of nimesulide orodispersible tablets. *Polimery w medycynie, 41*(1), 17-28.

Martin, R. T. (1984). Process for mineral beneficiation: Google Patents.

Martínez Rus, F., Pradíes Ramiro, G., Suárez García, M. J., & Rivera Gómez, B. (2007). Cerámicas Dentales: Clasificación y Criterios de Selección. *RCOE 12*, 253-263.

Matusik, J., Scholtzová, E., & Tunega, D. (2012). Influence of synthesis conditions on the formation of a kaolinite-methanol complex and simulation of its vibrational spectra. *Clays and Clay Minerals, 60*(3), 227-239.

Mauro, M., Italo, F., Anna, M., Andrea, A., Elisabetta, R., Maria, C., . . . Carla, C. (2014). MeOx/SBA-15 (Me = Zn, Fe): highly efficient nanosorbents for mid-temperature H_2S removal. *J. Mater. Chem. A, , 2*, 19396-19406. doi: 10.1039/C4TA03540B

Mayer, H. (2010). *Nutrient release patterns of controlled release fertilizers used in the ornamental horticulture industry of south Florida.* M.Sc., University of Florida.

McColm, I. J., & O'Bannon, L. S. (1994). *Dictionary of ceramic science and engineering*: Springer.

McLean, J. W., & Hughes, T. (1965). The reinforcement of dental porcelain with ceramic oxides. *British dental journal, 119*(6), 251.

Meybeck, A., & Gitz, V. (2012). GREENING THE ECONOMY WITH CLIMATE-SMART AGRICULTURE FOOD Hanoi, Vietnam,: FAO.

Meybeck, A., & Gitz, V. (2012). Greening the economy with climate-smart agriculture food. Hanoi, Vietnam: FAO.

Mgbemena, C. O., Ibekwe, N. O., Sukumar, R., & Menon, A. (2013a). Characterization of kaolin intercalates of oleochemicals derived from rubber seed (< i> Hevea brasiliensis</i>) and tea seed (< i> Camelia sinensis</i>) oils. *Journal of King Saud University-Science, 25*(2), 149-155.

Mgbemena, C. O., Ibekwe, N. O., Sukumar, R., & Menon, A. R. (2013b). Characterization of kaolin intercalates of oleochemicals derived from rubber seed (Hevea brasiliensis) and tea seed (Camelia sinensis) oils. *Journal of King Saud University-Science, 25*(2), 149-155.

Min, Z., Yuechao, Y., Fupeng, S., & Yanxi, S. (2005). Study and Industrialized Development of Coated Controlled Release Fertilizers [J]. *Journal of Chemical Fertilizer Industry, 2*, 001.

Minot, N. (2009). Fertilizer policy and use in Tanzania Retrieved 27th May, 2015, from http://fsg.afre.msu.edu/aamp/seminar_2/seminar_3_tanzania.pdf

Miyata, Y. (1989). *Coated fertilizers: focus on sulphur coated compound fertilizers.* Paper presented at the Proc. Symp. on Fertilisers - Present and Future, Japan.

Moffa, J. (1988). Porcelain materials. *Advances in dental research, 2*(1), 3-6.

Moore, W. J. (1972). Physical chemistry. Engelwood Cliffs, NJ: Prentice-Hall.

Morkhade, D., Fulzele, S., Satturwar, P., & Joshi, S. (2006). Gum copal and gum damar: Novel matrix forming materials for sustained drug delivery. *Indian journal of pharmaceutical sciences, 68*(1), 53.

Moss, N., & Dymond, B. (1978). Flocculation: theory and application. *Mine and Quarry Journal, 5*, 1-8.

Murugan, R., Mohan, S., & Bigotto, A. (1998). FTIR and polarised Raman spectra of acrylamide and polyacrylamide. *Journal of the Korean Physical Society, 32*(4), 505-512.

Mwakarukwa, G. M. (1988). Geologic and Economic Aspect of Clays in Tanzania. In R. H. Kimambo (Ed.), *Developmnent of the Non-metallic Minerals and the Silicate Industry in Tanzania*. Dar es Salaam: East African Publication Ltd.

Nakagaki, S., Machado, G. S., Halma, M., dos Santos Marangon, A. A., de Freitas Castro, K. A. D., Mattoso, N., & Wypych, F. (2006). Immobilization of iron porphyrins in tubular kaolinite obtained by an intercalation/delamination procedure. *Journal of Catalysis, 242*(1), 110-117.

Nakamoto, K. (1986). *Infrared and Raman Spectra of Inorganic and Coordination Compounds* New York: John Wiley and Sons.

Nakamoto, K. (1997). *Infrared and Raman Spectra of Inorganic and Coordination Compounds* (5 ed.): Wiley, Publishers.

Nandi, B., Goswami, A., & Purkait, M. (2009). Removal of cationic dyes from aqueous solutions by kaolin: kinetic and equilibrium studies. *Applied Clay Science, 42*(3), 583-590.

Nanjwade, B. K. (2013). FUNDAMENTALS OF MODIFIED RELEASE FORMULATIONS. KLE University College of Pharmac- INDIA: Department of Pharmaceutics: https://www.google.com/url?sa=t&rct=j&q=&esrc=s&source=web&cd=1&cad=rja&uact=8&ved=0CCMQFjAA&url=http%3A%2F%2Fapi.ning.com%2Ffiles%2Fn5OxHQ0ab5xtv8QP-Fp3eJlZdWEcLnrQ2yWWZ1LWPoC3bly9iOzib*Hi5lW8hWaM-D9AY5nAbRwuThr-inRne0FGH1zxO*T5%2FFundamentalsofModifiedReleaseFormulations.pptx&ei=LdnF

U5TMDIb-8QXQqYCoBQ&usg=AFQjCNFKcgCsWACXkE5xjyrhL9GFPONE0Q&sig2=bQ-ZXrTWW29RjXMHmyknDw.

NanoComposix. (2012). Zeta Potential Analysis of Nanoparticles, from http://cdn.shopify.com/s/files/1/0257/8237/files/nanoComposix_Guidelines_for_Zeta_Potential_Analysis_of_Nanoparticles.pdf

Narender, D. (2014). THEORIES AND MECHANISMS OF DISSOLUTION TESTING. KAKATIYA UNIVERSITY: Pharmawiki: pharmawiki.in/ppt-theories-and-mechanisms-of-dissolution-testing/.

NM-AIST. (2009). The Nelson Mandela African Institution of Science and Technology: Mission And Vision Retrieved June 12th, 2015, from http://www.nm-aist.ac.tz/about_us.html

Nokhodchi, A., Nazemiyeh, H., Khodaparast, A., Sorkh-Shahan, T., Valizadeh, H., & Ford, J. (2008). An in vitro evaluation of fenugreek mucilage as a potential excipient for oral controlled-release matrix tablet. *Drug development and industrial pharmacy, 34*(3), 323-329.

Novikova, L., Belchinskaya, L., Roessner, F., & Alsawalha, M. (2013). Characterization of surface acidity and catalytic ability of natural clay minerals by means of test catalytic reaction. *Acta Geodynamica et Geomaterialia, 10*(4), 172.

Novikova, L., Strelnikova, O. Y., Khodosova, N., Belchinskaya, L., & Roessner, F. Comparison of surface acidity/basicity of natural and modified aluminosilicates by conversion of 2-methylbut-3-yn-2-ol.

Nwankwo, K. (2001). Polyacrylamide as a Soil Stabilizer for Erosion Control, Wisconsin Department of Transportation. *Madison. Report*.

Nwankwo, K. N. (2001). Polyacrylamide as a soil stabilizer for erosion control.

Occelli, M., & Tindwa, R. (1983). Physicochemical properties of montmorillonite interlayered with cationic oxyaluminum pillars. *Clays Clay Miner, 31*(1), 22.

Odeku, O., & Itiola, O. (2002). Characterization of khaya gum as a binder in a paracetamol tablet formulation. *Drug development and industrial pharmacy, 28*(3), 329-337.

Odeku, O. A., & Fell, J. T. (2004). Evaluation of khaya gum as a directly compressible matrix system for controlled release. *Journal of pharmacy and pharmacology, 56*(11), 1365-1370.

Odeku, O. A., & Fell, J. T. (2005). In-vitro evaluation of khaya and albizia gums as compression coatings for drug targeting to the colon. *Journal of pharmacy and pharmacology, 57*(2), 163-168.

Odeku, O. A., & Patani, B. O. (2005). Evaluation of dika nut mucilage (Irvingia gabonensis) as binding agent in metronidazole tablet formulations. *Pharmaceutical development and technology*, *10*(3), 439-446.

Oder, R. (1976). High gradient magnetic separation theory and applications. *Magnetics, IEEE Transactions on*, *12*(5), 428-435.

Olejnik, S., Aylmore, L., Posner, A., & Quirk, J. P. (1968). Infrared spectra of kaolin mineral-dimethyl sulfoxide complexes. *The Journal of Physical Chemistry*, *72*(1), 241-249.

Organization, U. I. D., & Center, I. F. D. (1998). *Fertilizer Manual*: Springer.

Padil, V. V. T., Nguyen, N. H., Ševců, A., & Černík, M. Fabrication, Characterization and Antibacterial Properties of Electrospun Membrane Composed of Gum Karaya, Polyvinyl Alcohol and Silver Nanoparticles.

Padil, V. V. T., Nguyen, N. H., Ševců, A., & Černík, M. (2015). Fabrication, Characterization and Antibacterial Properties of Electrospun Membrane Composed of Gum Karaya, Polyvinyl Alcohol and Silver Nanoparticles. *Journal of Nanomaterials*, *501*, 750726.

Park, S., Baker, J. O., Himmel, M. E., Parilla, P. A., & Johnson, D. K. (2010). Research cellulose crystallinity index: measurement techniques and their impact on interpreting cellulase performance. *Biotechnol Biofuels*, *3*(10).

Parolo, M., Fernández, L., Zajonkovsky, I., Sánchez, M., & Bastion, M. (2011a). Antibacterial activity of materials synthesized from clay minerals. *Science against microbial pathogens: communicating current research and technological advances. Formatex, Microbiology series*, *3*, 144-151.

Parolo, M., Fernández, L., Zajonkovsky, I., Sánchez, M., & Bastion, M. (2011b). Antibacterial activity of materials synthesized from clay minerals. *Science against microbial pathogens: communicating current research and technological advances. Formatex, Microbiology series*(3), 144-151.

Patel, H. A., Joshi, G. V., Pawar, R. R., Bajaj, H. C., & Jasra, R. V. (2010). Mechanical and thermal properties of polypropylene nanocomposites using organically modified Indian bentonite. *Polymer Composites*, *31*(3), 399-404.

Peak, D., Ford, R. G., & Sparks, D. L. (1999). An in situ ATR-FTR investigation of sulfate bonding mechanisms on goethite *J. Colloid Interface Sci. , 218*, 289-299.

Peak, D., Luther III, G. W., & Sparks, D. L. (2003). Boric acid and borate adsorption mechanisms on amorphous iron oxides: An in situ ATR-FTIR spectroscopic study. *Geochimica et Cosmochimica Acta 67*(14), 2551-2560.

Pendyala, V., Baburao, C., & Chandrasekhar, K. (2010). Studies on some physicochemical properties of Leucaena Leucocephala bark gum. *Journal of advanced pharmaceutical technology & research*, *1*(2), 253.

Pereira, E. I., Minussi, F. B., da Cruz, C. C., Bernardi, A. C., & Ribeiro, C. (2012). Urea–Montmorillonite-Extruded Nanocomposites: A Novel Slow-Release Material. *Journal of agricultural and food chemistry, 60*(21), 5267-5272.

Peter, T. (2014). Stool made of Sand and Urine Retrieved June 4th, 2015, from http://www.dezeen.com/2014/02/08/stools-made-of-sand-and-urine-by-peter-trimble/

Piasek, Z., & Urbanski, T. (1962a). The Infrared Absorption Spectrum and Structure of Urea. *Bull. Acad. Polon. Sci., Ser. Sci. Chim, 10*, 113-120.

Piasek, Z., & Urbanski, T. (1962b). INFRARED ABSORPTION SPECTRUM AND STRUCTURE OF UREA. *BULLETIN DE L ACADEMIE POLONAISE DES SCIENCES-SERIE DES SCIENCES CHIMIQUES, 10*(3), 113-&.

Pinto, F. C. H., Silva-Cunha, A., Pianetti, G. A., Ayres, E., Oréfice, R. L., & Da Silva, G. R. (2011). Montmorillonite clay-based polyurethane nanocomposite as local triamcinolone acetonide delivery system. *Journal of Nanomaterials, 2011*, 15.

Pope, R. M., & Fry, E. S. (1997). Absorption spectrum (380-700 nm) of pure water. II. Intergrating Cavity Measurements. *Applied Optics (Optical Society of America), 36*(33), 8710-8723. doi: 10.1364/AO.36.008710

Premarathna, L., McLaughlin, M. J., Kirby, J. K., Hettiarachchi, G. M., Stacey, S., & Chittleborough, D. J. (2012). Selenate-enriched urea granules are a highly effective fertilizer for selenium biofortification of paddy rice grain. *Journal of agricultural and food chemistry, 60*(23), 6037-6044.

Raban, S. (1994). Release mechanisms of membrane coated fertilizers. In A. Shaviv (Ed.), *Advances in Agronomy* (pp. 1-49). Faculty of Agricultural Engineering, Technion, IIT-Israel. .

Raban, S., Zeidel, E., & Shaviv, A. (1997). Release mechanisms controlled release fertilizers in practical use. *Third Int. Dahlia Greidinger Sym. on Fertilisation and The Environment"(JJ Mortwedt, and A. Shaviv, Eds.)*, 287-295.

Ray, D., Mohanta, G. P., Manavalan, R., & Sahoo, P. K. (2009). Synthesis and characterization of acrylic based copolymeric hydrogel nanoparticles: an approach to drug delivery. *International Journal of ChemTech Research, 1*(3).

Rosenblum, M. A., & Schulman, A. (1997). A Review of all-ceramic Restoration. . *The Journal of the American Dental Association, 128*, 297-307.

Rutkai, G., Makó, É., & Kristóf, T. (2009). Simulation and experimental study of intercalation of urea in kaolinite. *Journal of colloid and interface science, 334*(1), 65-69.

Saikia, N., Bharali, D., Sengupta, P., Bordoloi, D., Goswamee, R., Saikia, P., & Borthakur, P. (2003). Characterization, beneficiation and utilization of a kaolinite clay from Assam, India. *Applied Clay Science, 24*(1), 93-103.

Santos, P. (1989). Ciência e Tecnologia de Argilas, Vol. 1, 2 a edição, Edgard Blücher Ltda, S: Paulo.

Satyanarayana, K. G., & Wypych, F. (2004). *Clay surfaces: fundamentals and applications* (Vol. 1): Academic Press.

Sawhney, B., & Singh, S. (1997). Sorption of atrazine by A1-and Ca-saturated smectite. *Clay. Clay Miner., 45*, 333-338.

Sempeho, S. I., Esther, H. J. L., & Leonard, D. A. (2012). *Suitability of kaolin and quartz from Pugu and feldspar from Morogoro as raw materials for the production of dental porcelain.* M.Sc., University of Dar es Salaam, Dar es Salaam.

Sempeho, S. I., Kim, H. T., Mubofu, E., & Hilonga, A. (2014). Meticulous Overview on the Controlled Release Fertilizers. *Advances in Chemistry, 2014*.

Sempeho, S. I., Kim, H. T., Mubofu, E., Pogrebnoi, A., & Shao, G. (2015). Encapsulated Urea-Kaolinite Nanocomposite for Controlled Release Fertilizer Formulations. *Journal of Chemistry, 2015*(Article ID 237397), 17.

Sempeho, S. I., Kim, H. T., Mubofu, E., Pogrebnoi, A., Shao, G., & Hilonga, A. (2015a). *Encapsulated Urea-Kaolinite Nanocomposite for Controlled Release Fertilizer Formulations*. Materials Science and Engineering. Nelson Mandela African Institution of Science and Technology.

Sempeho, S. I., Kim, H. T., Mubofu, E., Pogrebnoi, A., Shao, G., & Hilonga, A. (2015b). Encapsulated Urea-Kaolinite Nanocomposite for Controlled Release Fertilizer Formulations. *Journal of Chemistry, 2015*, 17. doi: 10.1155/2015/237397

Sempeho, S. I., Lugwisha, E. H. J., & Akwilapo, L. D. (2012). *Suitability of kaolin and quartz from Pugu and feldspar from Morogoro as raw materials for the production of dental porcelain.* M.Sc., University of Dar es Salaam, Dar es Salaam

Sempeho, S. I., Mubofu, H. T. K. E., Pogrebnoi, A., & Shao, G. Encapsulated Urea-Kaolinite Nanocomposite for Controlled Release Fertilizer Formulations.

Sharpley, A., & Menzel, R. (1987). The impact of soil and fertilizer phosphorus on the environment. *Adv. Agron, 41*, 297-324.

Shavit, U., Shaviv, A., Shalit, G., & Zaslavsky, D. (1997). Release characteristics of a new controlled release fertilizer. *Journal of Controlled Release 43*(2), 131-138.

Shaviv, A. (1996). Plant response and environmental aspects as affected by rate and pattern of nitrogen release from controlled release N fertilizers *Progress in nitrogen cycling studies* (pp. 285-291): Springer.

Shaviv, A. (2001). Advances in controlled-release fertilizers. *Advances in agronomy, 71*, 1-49.

Shaviv, A. (2005). *Controlled release fertilizers.* Paper presented at the IFA International Workshop on Enhanced-Efficiency Fertilizers.

Shaviv, A., Raban, S., & Zaidel, E. (2003a). Modeling controlled nutrient release from a population of polymer coated fertilizers: Statistically based model for diffusion release. *Environmental science & technology, 37*(10), 2257-2261.

Shaviv, A., Raban, S., & Zaidel, E. (2003b). Modeling controlled nutrient release from polymer coated fertilizers: Diffusion release from single granules. *Environmental science & technology, 37*(10), 2251-2256.

Shaviv, A., Zlotnikov, E., & Zaidel, E. (1995). *Mechanisms of nutrient release from controlled release fertilizers.* Paper presented at the Proceedings, Dahlia Gredinger Memorial International Workshop on Controlled Release Fertilizers. Hagin, J. and Mortvedt, J.(eds). Technion, Israel Institute of Technology, Haifa. Israel.

Sher, F. (2010). Crystal Structure Determination I. Pakistan Institute of Engineering and Applied Sciences: National Workshop on Crystal Structure Determination using Powder XRD, organized by the Khwarzimic Science Society, 15 –17 August 2007.

Shoji, S., & Gandeza, A. T. (1992). *Controlled release fertilizers with polyolefin resin coating*. Sendai, Japan: Kanno Printing Co. Ltd.

Siafu, S. I., & Lugwisha, E. H. J. (2014). The Properties of Feldspathic Dental Porcelain from Tanzanian Aluminosilicate Materials. *International Journal of Development Research, 4*(11), 2260-2265.

Siepmann, J., & Peppas, N. (2001). Modeling of drug release from delivery systems based on hydroxypropyl methylcellulose (HPMC). *Advanced drug delivery reviews, 48*(2), 139-157.

Silva, S. M., Braga, C. R., Fook, M. V., Raposo, C. M., Carvalho, L. H., & Canedo, E. L. (2012). Application of infrared spectroscopy to analysis of chitosan/clay nanocomposites. *Infrared spectroscopy-materials science, engineering and technology. Croatia: InTech*, 43-62.

Singh, A., Sharma, P. K., & Malviya, R. (2011). Release behavior of drugs from various natural gums and polymers. *Polimery w medycynie, 41*(4), 73-80.

Soils, A. (2015). Soil Colloids and the Surface Chemistry of Soils Retrieved June 13th, 2015, from http://faculty.yc.edu/ycfaculty/ags105/week08/soil_colloids/soil_colloids_print.html

Soleimani, M., Naghizadeh, R., Mirhabibi, A., & Golestanifard, F. (2012). Effect of calcination temperature of the kaolin and molar Na2O/SiO2 activator ratio on physical and microstructural properties of metakaolin based geopolymers. *Iranian Journal of Materials Science & Engineering, 9*(4).

Southan, D. E. (1968). *The physical properties of modern dental porcelain.* PhD, Sydney University.

Southern Agricultural Insecticides, I. (1998). SA-50 Controlled-Release Fertilizer 14-14-14: OSMOCOTER Retrieved August 08, 2013 from http://www.southernag.com/docs/labels_msds/contrl.pdf

Speakman, S. A. (2014). *Estimating Crystallite Size Using XRD*. MIT Center for Materials Science and Engineering. MIT. Retrieved from http://prism.mit.edu/xray

Stein, H., & Cheremisinoff, N. (1986). Encyclopedia of Fluid Mechanics: slurry flow technology. *Encyclopedia of Fluid Mechanics: slurry flow technology, 5*.

STEPHEN, R., & WAID, J. (1964). TOXICITY AS A CAUSE OF THE INEFFICIENCY OF UREA AS A FERTILIZER. *Journal of Soil Science, 15*(1), 49-65.

Subbarao, C. V., Kartheek, G., & Sirisha, D. (2013). Slow release of potash fertilizer through polymer coating. *International Journal of Applied Science and Engineering*, *11*(1), 25-30.

Sunardi, S., Irawati, U., Arryanto, Y., & Sutarno, S. (2011). Modified kaolin with cationic surfactant for gibberellic acid carrier materials. *Indonesian Journal of Chemistry, 11*(1), 96-102.

Suresh, R., Borkar, S., Sawant, V., Shende, V., & Dimble, S. (2010). Nanoclay drug delivery system. *Int J Pharm Sci Nanotechnol, 3*, 901-905.

Szmant, H. H. (1975). Physical properties of dimethyl sulfoxide and its function in biological systems. *Annals of the New York Academy of Sciences, 243*(1), 20-23.

Talaat, H., Sorour, M., Aboulnour, A., Shaalan, H., Ahmed, E. M., Awad, A., & Ahmed, M. (2008). Development of a multi-component fertilizing hydrogel with relevant techno-economic indicators. *Am Eurasian J Agric Environ Sci, 3*(5), 764-770.

Talukdar, M. M., Vinckier, I., Moldenaers, P., & Kinget, R. (1996). Rheological characterization of xanthan gum and hydroxypropylmethyl cellulose with respect to controlled-release drug delivery. *Journal of pharmaceutical sciences, 85*(5), 537-540.

Tandon, H. L. S. (2010). A Short History of Fertilisers. New Delhi-INDIA: Fertiliser Development and Consultation Organisation.

Teagarden, D. L., Hem, S. L., & White, J. L. (1982). Conversion of aluminum chlorohydrate to aluminum hydroxide. *J. Soc. Cosmet. Chem, 33*, 281-295.

Thomas, S., & Occelli, M. (2000). Effects of synthesis conditions on the thermal stability of a Texas montmorillonite expanded with [Al13O4 (OH) 24 (H2O) 12] 7+ cations. *Clays and clay minerals, 48*(2), 304-308.

Thompson, J., & Cuff, C. (1985). Crystal structure of kaolinite: dimethylsulfoxide intercalate. *Clays and Clay Minerals, 33*(5), 490-500.

Timm, B., & Danz, W. (1964). History of nitrogen fixation processes. In V. E. In Sauchelli (Ed.), *Fertiliser Nitrogen – Its Chemistry and Technology* (Vol. ICS Monograph No 161, pp. 40-57). USA: Reinhold Publishing.

Tironi, A., Trezza, M., Irassar, E., & Scian, A. (2012). Thermal treatment of kaolin: effect on the pozzolanic activity. *Procedia Materials Science, 1*, 343-350.

Trenkel, M. E. (2010). *Slow-and controlled-release and stabilized fertilizers: An option for enhancing nutrient use efficiency in agriculture*: IFA, International fertilizer industry association.

Trenkel, M. E., & Association, I. F. I. (1997). *Controlled-release and stabilized fertilizers in agriculture* (Vol. 11): International Fertilizer Industry Association Paris.

Tunney, J. J., & Detellier, C. (1996). Chemically modified kaolinite. Grafting of methoxy groups on the interlamellar aluminol surface of kaolinite. *Journal of Materials Chemistry, 6*(10), 1679-1685.

Ukessays.com. (2013a). Controlled Release Fertilizers and Nanotechnology Traces Biology Essay Retrieved April, 2015, from http://www.ukessays.com/essays/biology/controlled-release-fertilizers-and-nanotechnology-traces-biology-essay.php

ukessays.com. (2013b). Controlled Release Fertilizers And Nanotechnology Traces Biology Essay Retrieved August 2013, 2013, from http://www.ukessays.com/essays/biology/controlled-release-fertilizers-and-nanotechnology-traces-biology-essay.php

Ukessays.com. (2013c). Controlled Release Fertilizers and Nanotechnology Traces Biology Essay, August 2013, from http://www.ukessays.com/essays/biology/controlled-release-fertilizers-and-nanotechnology-traces-biology-essay.php

Unalan, I. U., Cerri, G., Marcuzzo, E., Cozzolino, C. A., & Farris, S. (2014). Nanocomposite films and coatings using inorganic nanobuilding blocks (NBB): current applications and future opportunities in the food packaging sector. *RSC advances, 4*(56), 29393-29428.

UNIDO-IFDC. (1979). Fertiliser Manual: Kluwer Academic Publishers.

Uwins, P. J., Mackinnon, I. D., Thompson, J. G., & Yago, A. J. (1993). Kaolinite-NMF intercalates. *Clays and Clay Minerals, 41*(6), 707-717.

Vahur, S. (2014). IR Spectra of Carbohydrates: Gum Arabic Retrieved November 10, 2014, from http://tera.chem.ut.ee/IR_spectra/index.php?option=com_content&view=article&id=107&Itemid=77

Vaughan, F. (1955). Energy changes when kaolin minerals are heated. *Clay Mineral Bull, 2*(13), 265-274.

Vellora Thekkae Padil, V., Nguyen, N. H., Ševců, A., & Černík, M. (2014). Fabrication, Characterization, and Antibacterial Properties of Electrospun Membrane Composed of Gum Karaya, Polyvinyl Alcohol, and Silver Nanoparticles. *Journal of Nanomaterials, Article ID: 750726*.

Venyaminov, S. Y., & Prendergast, F. G. (1997). Water (H_2O and D_2O) Molar Absorptivity in the 1000-4000 cm $^{-1}$ Range and Quantitative Infrared Spectroscopy of Aqueous Solutions. *Analytical Biochemistry, 248*(AB972136), 234-245.

Vetter, T., Iggland, M., Ochsenbein, D. R., Hänseler, F. S., & Mazzotti, M. (2013). Modeling nucleation, growth, and Ostwald ripening in crystallization processes: a comparison between population balance and kinetic rate equation. *Crystal Growth & Design, 13*(11), 4890-4905.

Vijayaraghavan, C., Vasanthakumar, S., & Ramakrishnan, A. (2008). In vitro and in vivo evaluation of locust bean gum and chitosan combination as a carrier for buccal drug delivery. *Die Pharmazie-An International Journal of Pharmaceutical Sciences, 63*(5), 342-347.

Von Fraunhofer, J. A. (2013). *Dental materials at a glance*: John Wiley & Sons.

Weaver, C. E. (1956). The distribution and identification of mixed-layer clay in sedimentary rocks. *Am. Mineral, 141*, 202-221.

Weiss, A., Thielepape, W., Going, G., Ritter, W., & Schaer, H. (1963). Kaolinit–Enlager Ungsver bind Ungen. *Int.Clay Conf., 1*, 287–305

Williams, G. J. (1979). Studies on the effect of particle size on some properties of dental stone. *Journal of Materials Science, 14*(8), 1907-1913.

Wu, L., & Liu, M. (2008). Preparation and properties of chitosan-coated NPK compound fertilizer with controlled-release and water-retention. *Carbohydrate Polymers, 72*(2), 240-247.

Yan, C., Chen, J., Zhang, C., & Han, L. (2005). Kaolinite-urea intercalation composites. *American Ceramic Society Bulletin, 84*(12), 9301-9305.

Yan, W., Li, N., Li, Y., Liu, G., Han, B., & Xu, J. (2011). Effect of particle size on microstructure and strength of porous spinel ceramics prepared by pore-forming in situ technique. *Bulletin of Materials Science, 34*(5), 1109-1112.

Yuechao, Y., Yuqing, G., Min, Z., Jianqiu, C., & Haining, C. (2007). Effects of coating properties of controlled-release fertilizers on nutrient release characteristics. *Transactions of the Chinese Society of Agricultural Engineering, 2007*(11).

Yvon, J., & Jean-Maurice, C. (1994). FTIR reflectance vs. EPR studies of structural iron in kaolinites. *Clays and clay minerals*, *42*(3), 308-320.

Zaidel, E. (1996). *Models of controlled release of fertilizers.* Technion-Israel Institute of technology, Faculty of agricultural engineering.

Zhang, F., Zhang, W., & Ma, W. (2009). The Chemical Fertilizer Industry in China: A Review and its Outlook. *International Fertilizer Association, Paris, France.*

APPENDICES

Appendix 1. Whole rock clay analysis for the original kaolin

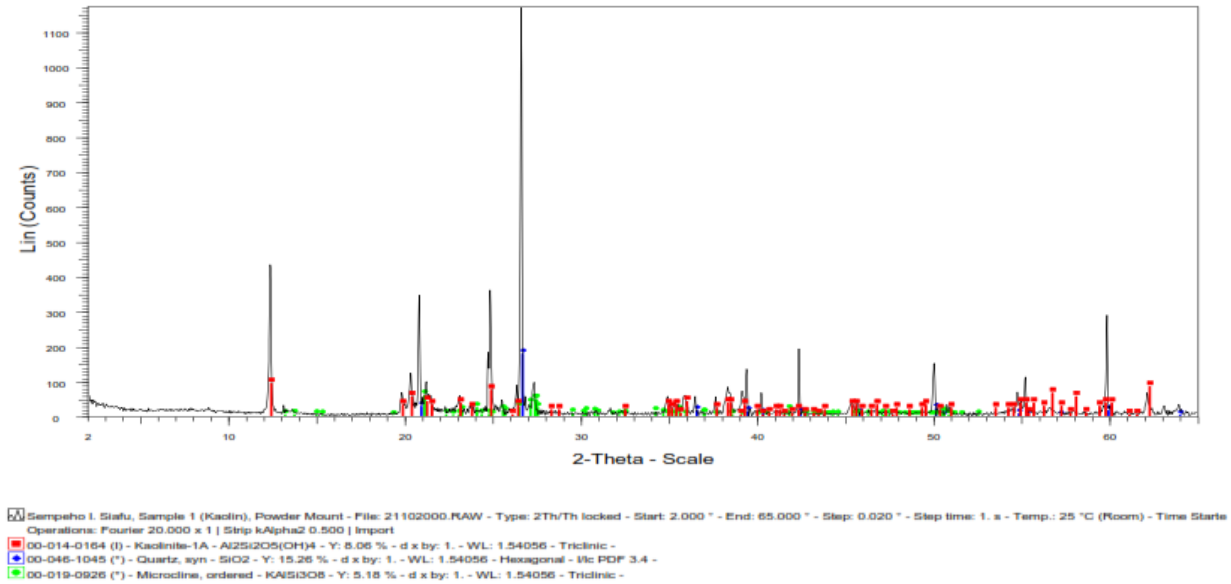

Appendix 2. Whole rock clay analysis for the beneficiated kaolin

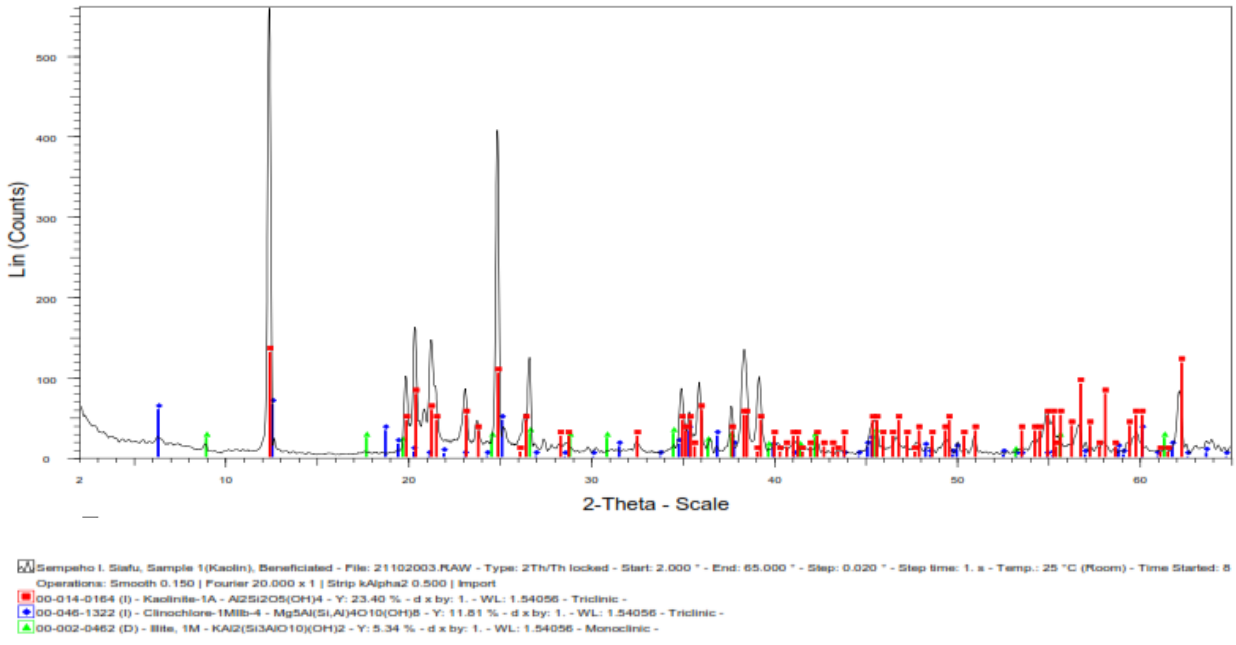

Appendix 3. Oriented clay analysis for the original kaolin

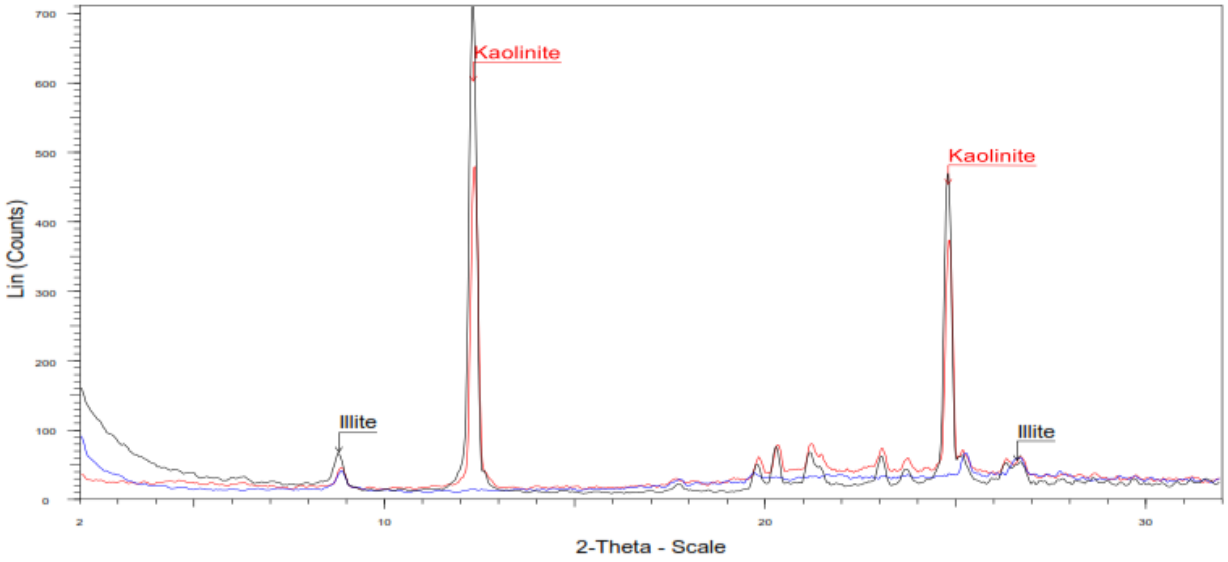

Sempeho I. Siafu, Sample 1, Air Dried - File: 2110200a.RAW - Type: 2Th/Th locked - Start: 2.000 ° - End: 32.000 ° - Step: 0.020 ° - Step time: 1. s - Temp.: 25 °C (Room) - Time Started: 8 s - Operations: Smooth 0.189 | Fourier 20.000 x 1 | Strip kAlpha2 0.500 | Import
Sempeho I. Siafu, Sample 1, Glycolated - File: 2110200b.raw - Type: 2Th/Th locked - Start: 2.000 ° - End: 32.000 ° - Step: 0.020 ° - Step time: 1. s - Temp.: 25 °C (Room) - Time Started: 3 s - Operations: Smooth 0.189 | Fourier 20.000 x 1 | Strip kAlpha2 0.500 | Import
Sempeho I. Siafu, Sample 1(Kaolin), Heated - File: 2110200c.RAW - Type: 2Th/Th locked - Start: 2.000 ° - End: 32.000 ° - Step: 0.020 ° - Step time: 1. s - Temp.: 25 °C (Room) - Time Started: Operations: Smooth 0.189 | Fourier 20.000 x 1 | Strip kAlpha2 0.500 | Import

Appendix 4. Oriented clay analysis for the beneficiated kaolin

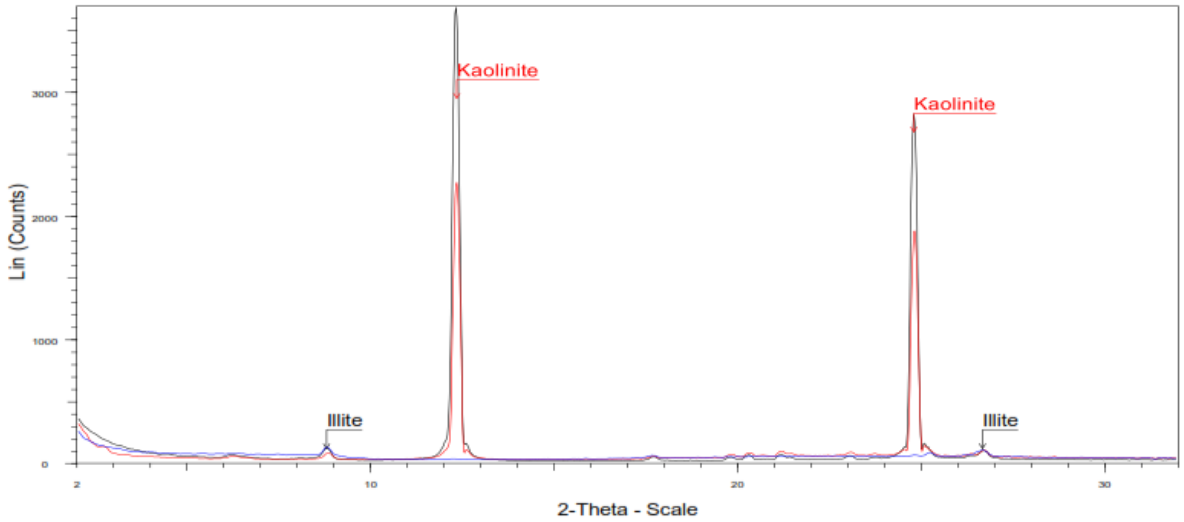

Sempeho I. Siafu, Sample 1 (Kaolin - Beneficiated), Air Dri - File: 2110203a.RAW - Type: 2Th/Th locked - Start: 2.000 ° - End: 32.000 ° - Step: 0.020 ° - Step time: 1. s - Temp.: 25 °C (Room) - Time Operations: Smooth 0.189 | Fourier 20.000 x 1 | Strip kAlpha2 0.500 | Import
Sempeho I. Siafu, Sample 1 (Kaolin - Beneficiated), Glycola - File: 2110203b.RAW - Type: 2Th/Th locked - Start: 2.000 ° - End: 32.000 ° - Step: 0.020 ° - Step time: 1. s - Temp.: 25 °C (Room) - Time Operations: Smooth 0.189 | Fourier 20.000 x 1 | Strip kAlpha2 0.500 | Import
Sempeho I. Siafu, Sample 1 (Kaolin - Beneficiated), Heated - File: 2110203c.RAW - Type: 2Th/Th locked - Start: 2.000 ° - End: 32.000 ° - Step: 0.020 ° - Step time: 1. s - Temp.: 25 °C (Room) - Time Operations: Smooth 0.189 | Fourier 20.000 x 1 | Strip kAlpha2 0.500 | Import

Appendix 5. Evidence showing the altitude climbed for sampling of volcanic ashes

OL DOINYO LENGAI MOUNTAIN TREKKING

CBO

This is to Certify that

Mr / Mrs / Miss SEMPEYO. I. SIAFU

Has successfully climbed Ol Doinyo Lengai an Active Volcanic Mountain height 2,980m, 9,777ft.

Date: 19/3/20[illegible] Time: [illegible] Age: 30YRS.

TOUR GUIDE : KISHILI [illegible] CBO COORDINATOR: MATHAYO KOKANYI

SIGNATURE: [illegible] SIGNATURE: [illegible]

CERTIFICATE No. EECDI/ 0434

Supported By: UNWTO Federal Ministry of Food, Agriculture and Consumer Protection TANZANIA FAO GIAHS